Comparative Study between Nanofiltration and Reverse Osmosis Membranes for the Removal of Heavy Metals from Electroplating Wastewater

Ahmed Faiq Al-Alawy
Assistant Professor
College of Engineering-University of Baghdad
ahmedalalawy@yahoo.com

Miqat Hasan Salih
Researcher
College of Engineering-University of Baghdad
mekat2007me@yahoo.com

ABSTRACT

The present work aimed to study the efficiency of nanofiltration (NF) and reverse osmosis (RO) process for water recovery from electroplating wastewater and study the factors affecting the performance of two membrane processes. Nanofiltration and reverse osmosis membranes are made from polyamide as spiral wound module. The inorganic materials $ZnCl_2$, $CuCl_2.2H_2O$, $NiCl_2.6H_2O$ and $CrCl_3.6H_2O$ were used as feed solutions. The operating parameters studied were: operating time, feed concentrations for heavy metal ions, operating pressure, feed flow rate, feed temperature and feed pH. The experimental results showed, the permeate concentration increased and water flux decreased with increase in time from 0 to 70 min. The permeate concentrations increased and flux decreased with increase in feed concentrations from 10 to 300 mg/l. Raising of pressure from 1 to 4 bar, permeate concentration decreased for RO, for NF decreased and then increased at high pressure and increase the flux. The rises of flow rate from 20 to 50 l/h decreased permeate concentration and the flux increase. The rises of temperature from 26 to 40 °C, increased permeate concentration and increased the flux. The rise in pH from 4 to 7, decreased the flux as the pH goes from acidic side towards alkaline. The polyamide nanofiltration membrane had allowed permeation of chromium and copper ions to lower than permissible limits. Nanofiltration membrane had allowed permeation of nickel and zinc ions at low concentration of these ions. The polyamide RO membrane gave a high efficiency for removal of chromium, copper, nickel and zinc and it had allowed permeation of these ions to the lower than permissible limits. The rejection at first three minutes when the feed concentration approximately was constant for chromium in NF and RO, was 99.7% and 99.93%, for copper was 98.43% and 99.33%, for zinc was 97.96% and 99.49%, and for nickel was 97.18% and 99.49% respectively. The maximum recovery for chromium in NF and RO was 71.75% and 48.5%, for copper was 75.62% and 50.68%, for zinc was 80.87% and 54.56%, for nickel was 60.06% and 46.18% respectively. For a mixture of synthetic electroplating wastewater, nanofiltration and reverse osmosis membranes have a high rejection percentage for heavy metal ions. It was obtained pure water and concentrations of less than allowable limits for heavy metals in the case of the mixture.

Key words: nanofiltration, reverse osmosis, electroplating wastewater.

دراسة مقارنة بين اغشية النانو والتناضح العكسي لإزالة المعادن الثقيلة من مياه الصرف الصحي الناتجة من الطلاء الكهربائي

أحمد فائق العلوي
أستاذ مساعد
كلية الهندسة-جامعة بغداد

ميقات حسن صالح
باحث
كلية الهندسة-جامعة بغداد

الخلاصة

هذا العمل يهدف إلى دراسة كفاءة غشاء النانو وعملية التناضح العكسي لاسترجاع المياه من مياه الصرف الصحي الناتجة من الطلاء الكهربائي، ودراسة العوامل التي تؤثر في أداء الغشائين. اغشية النانو والتناضح العكسي مصنوعة من مادة البولي أميد

على شكل (spiral wound module). المواد غير العضوية كانت كلوريد الزنك، كلوريد النحاس المائي، كلوريد النيكل المائي، و كلوريد الكروم المائي استخدمت ك محلول اللقيم. العوامل التشغيلية التي تم دراستها هي: الزمن، تركيز الداخل، الضغط، التدفق، درجة الحرارة، درجة الحموضة. وأظهرت النتائج التجريبية، تركيز الناتج يزداد و تدفق المياه يقل مع زيادة الوقت (0-70 دقيقة). تركيز الناتج يزداد و تدفق المياه يقل مع زيادة تركيز الداخل (10-300) ملغ/لتر. رفع الضغط (1-4 بار)، تركيز الناتج يقل للتناضح العكسي ويقل ثم يزداد عند الضغط العالي لغشاء النانو ويزداد تدفق المياه. رفع التدفق (20-50 لتر/ساعة)، يقل تركيز الناتج ويزداد الجريان. رفع درجة الحرارة (26-40 درجة مئوية)، يزداد تركيز الناتج ويزداد الجريان. رفع درجة الحموضة (4-7)، يقل الجريان كلما يذهب الرقم الهيدروجيني من الجانب الحمضية نحو القلوية. غشاء بولي أميد NF أتاح تخلل ايونات الكروم والنحاس إلى أقل من الحدود المسموح بها. NF أتاح تخلل أيونات النيكل والزنك إلى أقل من الحدود المسموح بها عندما تتواجد بتراكيز منخفضة. غشاء بولي أميد RO يعطي كفاءة عالية لإزالة الكروم والنحاس والنيكل والزنك، وقد أتاح تخلل هذه الأيونات إلى أقل من الحدود المسموح بها. كان الرفض في ثلاث دقائق الأولى عندما كان تركيز التغذية ثابتا تقريبا للكروم في NF و RO 99.7% و 99.93%، للنحاس هو 98.43% و 99.33%، للزنك هو 97.96% و 99.49%، للنيكل 97.18% و 99.49% على التوالي. وكان الحد الأقصى لاسترداد الماء في حالة الكروم في NF وRO % 48.5 و%، النحاس 75.62% و 50.68%، الزنك 80.87% و 54.56%، النيكل 60.06% و 46.18% على التوالي. لخليط من مياه الطلاء الكهربائي الاصطناعية، أغشية النانو والتناضح العكسي لديها نسبة الرفض عالية لأيونات المعادن الثقيلة. تم الحصول على مياه نقية وبتراكيز أقل من الحدود المسموح بها للمعادن الثقيلة في حالة الخليط.
الكلمات الرئيسية: غشاء النانو، التناضح العكسي، مياه الصرف الصحي الناتجة من الطلاء الكهربائي.

1. INTRODUCTION

As the world's population and the consequent demand for water supply increase, the world is facing a fresh water crisis due to the rapid depletion of the resources of fresh water. Domestic and industrial activities have contaminated the ground water and the surface water to a large extent. Precious resource conservation and the sustainable development of water will require maximal recycling and reuse, **Alzahrani, et al., 2013 and Dannys, et al., 2016**. Due to discharge of big amounts of waste water contaminated with heavy metals, industries containing heavy metals, such as Cu, As, Cd, Ni, Cr, Zn and Pb; are the most dangerous among the chemical intensive industries. Heavy metals can be absorbed by living organisms, due to their high solubility in the aquatic environments. If the heavy metals are found beyond the permitted concentration limits, they can cause health problems, **Barakat, 2011**. Waste water contains the heavy metals originated from tanneries, batteries, pesticides galvanizing plants, fertilizer industries, metal plating facilities, mining operations, paper industries and pigment, stabilizers and thermoplastics manufacture and etc., **Jain, 2013**. The maximum contaminant level (standards) of zinc metal in water is <10 mg/l, **Wahaab, et al., 2010**, copper metal is 4 mg/l, nickel metal is 4 mg/l and chromium metal is 2 mg/l, **Abhang, et al., 2013**.

The wastewater from electroplating industry that is polluted with heavy metals attracted increasing interest due to the development of this industry in last years. The wastewater from electroplating consists of heavy metals such as cadmium, chromium, nickel, zinc and copper. However, the heavy metals and pure water have a great possibility of being reused if the heavy metals from wastewater of electroplating industry can be removed efficiently, **Wei, et al., 2013**. Various technologies have been applied for the removal of heavy metals from water and waste water, such as chemical precipitation, adsorption, coagulation-flocculation, floatation, ion exchange, electrochemical processes, and membrane filtration, **Boricha, and Murthy, 2009**. The techniques involving chemical reactions require the use of large amounts of expensive organic solvents and other polluting chemicals, they are slow and laborious, and the recovery of the components is seldom complete, **Gherasim, and Mikulášek, 2014**.

Membrane processes with different type of membranes give a good promise for removal of heavy metals for their space saving, easy operation and high efficiency. The membrane technologies utilized to remove heavy metals from the waste water are nanofiltration (NF), reverse osmosis (RO) and electrodialysis. NF is the intermediate system between ultrafiltration and RO. Nanofiltration is a promising process for the retention of heavy metal ions such as, chromium, arsenic and copper from waste water. Nanofiltration membrane benefits from high efficiency of contaminant removal, comparatively low energy consumption, reliability and ease of operation, **Fu, and Wang, 2011**. In reverse osmosis, a pressure driven membrane, heavy metals is rejected, while water can pass through the membrane. Reverse osmosis membrane has been developed with a pore size down to 10^{-4} µm because of the stringent environmental legislation. Reverse osmosis membrane is more efficient for the removal of heavy metals from inorganic solution compared to nanofiltration, as indicated by the rejection percentage of over 97% with a concentration of heavy metals ranging from 21 to 200 ppm. The advantages of utilizing reverse osmosis involve a high salt rejection, high water flux, chemical stability, mechanical strength, the ability to withstand high temperatures and resistance to biological attack, **Kurniawan, et al., 2006**.

Some researchers investigated the application of nanofiltration and reverse osmosis processes for the treatment of waste water containing heavy metals such as copper and cadmium ions. Synthetic wastewater containing Cd^{+2} and Cu^{+2} ions at different concentrations were prepared and subjected to treatment by reverse osmosis and nanofiltration membranes in the laboratory. The results showed that high removal efficiency of the heavy metals could be achieved by reverse osmosis membranes which are 98 and 99% for copper and cadmium. Nanofiltration was able for removal of more than 90% of the copper ions existing in the feed water. The results showed that the reverse osmosis membranes was able for treating wastewater with an initial concentration of 500 mg/l and decreasing the concentration of ion to about 3 mg/l (removal of 99.4%), while the average removal efficiency of nanofiltration membranes was 97%, **Abu Qdais, and Moussa, 2004**.

In this study, the effect of time, feed concentration, pressure, flow rate, temperature and pH on flux and permeate concentration have been studied for polyamide spiral wound NF and RO membranes to remove heavy metals from electroplating wastewater. The concentration of heavy metal ions was measured by an atomic absorption spectrometry.

2. THEORETICAL BACKGROUND

The flux of solvent, which is generally water through the membrane is linearly proportional to the pressure difference and osmotic pressure difference across the membrane, **Kucera, 2010**:

$$J_w = k_w\ (\Delta P - \Delta\pi) \qquad (1)$$

Where: J_w is the flux of water (l/m^2.h), k_w is the permeability coefficient of pure water (l/m^2.h.bar), ΔP is the applied pressure driving force (bar) and $\Delta\pi$ is the osmotic pressure of the solution (bar).

Solution osmotic pressure is related to its dissolved solute concentration and is predicted from Van't Hoff equation as:

$$\pi = (\varphi\ i\ R_g\ T\ C)/M.wt \qquad (2)$$

Where: φ is the osmotic coefficient (dimensionless), i is the number of dissociated ions per molecule (Van’t Hoff factor) (dimensionless), T is the temperature (K), R_g is the universal gas constant (l.bar/mole.K), C is the concentration of solute (mg/l) and $M.wt$ is the molecular weight of solute.

The Van't Hoff factor is inserted to express the deviation from ideal solution behavior that implicates finite volume occupied by molecules of solute and their mutual attraction as in Vander Waals attraction, **Khudair, 2011**.

By measuring the solute concentrations in feed solution (C_F) and also in permeate solution (C_P), the rejection is calculated as follows, **Gherasim, and Mikulášek, 2014**:

$$R\% = \left(1 - \frac{C_P}{C_F}\right) * 100\% \tag{3}$$

Where: R is the solute rejection (percentage), C_P is the concentration in permeate (mg/l) and C_F is the concentration in feed solution.

Recovery can be expressed as the volume of permeate divided by the initial volume of feed. This expression applied in batch concentrating mode. For the overall system, the expression is, **Absar, et al., 2008**:

$$Y\% = \frac{V_P}{V_F^o} * 100\% \tag{4}$$

Where: $Y\%$ is the recovery (percentage), V_P is the volume of permeate (l) and V_F^o is the initial feed volume (l).

3. EXPERIMENTAL WORK

Four types of feed solutions were used for the membrane process zinc chloride ($ZnCl_2$), copper chloride dihydrate ($CuCl_2.2H_2O$), nickel chloride hexahydrate ($NiCl_2.6H_2O$) and chromic chloride ($CrCl_3.6H_2O$). Synthetic wastewater containing the desired concentrations of Zn^{+2}, Cu^{+2}, Ni^{+2} and Cr^{+3} were prepared by dissolving the desired amount of $ZnCl_2$, $CuCl_2.2H_2O$, $NiCl_2.6H_2O$ and $CrCl_3.6H_2O$ in deionized water of 1-2 µs/cm conductivity. Solution pH was adjusted to a desired value by adding 0.5 M citric acid ($C_6H_8O_7.H_2O$) or 1 M sodium hydroxide (NaOH) as required. The total feed solution volume was 8 liters. The chemical analysis of components is given in **Table 1**. The polyamide thin-film composite nanofiltration and reverse osmosis membranes were used in this work. The specifications of NF and RO membranes are given in **Table 2**. Schematic diagrams of lab-scale NF and RO system used in these experiments are shown in **Fig. 1**.

Feed solution was prepared in feed vessel by dissolving the heavy metal compounds in 8 liter of deionized water. Pressure gauge (0-10 bar) was used in the feed line to indicate the operating pressure, the feed solution drawn from the feed vessel by centrifugal pump (Model: 15 GR-18, Rated power: 150 W, Rated voltage: 220-240 V, Rated current: 0.58 A, Rated speed: 2860 r/min, Frequency: 50/60 Hz, Highest head: 15 m, Rated head: 10 m, Max. capacity: 25 l/min, Rated capacity: 10 l/min, Insulation class: B) then the solution is introduced into the spiral-wound nanofiltration or reverse osmosis element by means of a high pressure pump (Model: HF-6050, Max. outlet pressure: 125 psi, Open flow: 1.2 l/min, VOLTS: 24 VDC, AMPS: 0.26 A). The feed temperature was varied by submersible electrical coil (Rated power: 1000 W, Rated voltage: 220V). The feed flow rate was controlled by rotameter (Range: 10-100 l/h). The concentrate stream is recycled to the feed vessel and mixed with the vessel. The water flux was obtained by dividing the permeate volume by the product of effective area of membrane and time. The concentration of heavy metal ions was measured by an atomic absorption spectrometry (Buck 210/211, Variable Slit Band Width 2A, 7A & 20A, Dimensions: 40"L x 12"W x 12"H; Weight: 50 lbs, U.S.A., Perkin Elmer, Sr.Nr:1159 A). After recording the results, the solution was drained by a drain valve and the system was washed by deionized water. After each replacement for inorganic component, the membrane must be clean. For the cleaning of metallic scales low solution pH is used. Cleaning steps:

- Preparing the cleaning solution and adjust the pH.
- Pumping the cleaning solution into NF or RO membranes.
- Recycling the cleaning solution.
- Cleaning the unit with deionized water. The cleaning continues until the conductivity of the product stream reaches approximately those of feed water.

4. RESULTS AND DISCUSSION

4.1 Effect of Operating Conditions

It can be easily observed from **Figs. 2** and **3** that the flux from nanofiltration and reverse osmosis unit decrease with increase in operating time. The continuous decline of the flux was mainly because of the gradual solution viscosity increment and to heavy metal deposition on the surface of the membrane; with the increasing in feed concentration and osmotic pressure gradually, which led to further membrane scaling and concentration polarization. Due to the boundary layer on the surface of the membrane formed by heavy metals the resistance against flux increased. This behavior is in agreement with **Lee, et al., 2006 and Wang, et al., 2007**. For NF membrane the increase in time to 70 min resulted in the decline of flux from 20.667 to 15.405 LMH for zinc, 17 to 14.405 LMH for copper, 12.333 to 11.44 LMH for nickel and 17 to 13.667 LMH for chromium. For RO membrane the increase in time to 70 min resulted in the decline of flux from 11.083 to 10.393 LMH for zinc, 10.583 to 9.655 LMH for copper, 9.083 to 8.798 LMH for nickel and 10.333 to 9.238 LMH for chromium. **Figs. 4 and 5** show the effects of time on recovery percentage of permeate. The recovery percentage increased according to Eq. (4) because the accumulation volume of permeate has been increased as time increased. For NF the increase in time to 70 min resulted in the increase of water recovery from 9.25 to 60.06% for nickel, 12.75 to 71.75% for chromium, 12.75 to 75.62% for copper and 15.5 to 80.87% for zinc. For RO the increase in time to 70 min resulted in the increase of water recovery from 6.81 to 46.18% for nickel, 7.75 to 48.5% for chromium, 7.93 to 50.68% for copper and 8.31 to 54.56% for zinc. **Figs. 6** and **7** show that the heavy metal ions concentration in the product gradually increased with increase in operating time. This behavior can be explained by the increase of the feed concentration with time in the recirculation mode led to increase in concentration polarization and this cause an increase in the salt passage. This behavior is in agreement with **Wei, et al., 2013 (**who studied the changes in the chromium, copper, and nickel ion concentrations in the permeate and rejection rates versus operating time under a continuous concentration process, respectively. Over the course of operation, the heavy metal concentrations in permeate gradually increased. The heavy-metal concentrations in permeate only slightly increased with continued operation). For NF membrane the first 30 minutes resulted in the increase in permeate concentration of 42.79% for zinc, 66.31% for copper, 15.49% for nickel and 33.29% for chromium. The final 40 minutes resulted in the increase in permeate concentration of 26.05% for zinc, 95.17% for copper, 43.96% for nickel and 127.27% for chromium. For RO membrane the first 30 minutes resulted in the increase in permeate concentration of 17.72% for zinc, 70.37% for copper, 54.77% for nickel and 66.72% for chromium. The final 40 minutes resulted in the increase in permeate concentration of 52.58% for zinc, 18.43% for copper, 41.35% for nickel and 14.59% for chromium. The behavior of rejection of heavy metal ions as shown in **Figs. 8 and 9** due to the concentration of heavy metal ions in permeate which has increased with time and the increase in feed concentration (feed concentration has been changed with time) because of the recirculation mode. The rejection at first three minutes when the feed concentration approximately constant for chromium in NF and

RO was 99.7% and 99.93%, for copper was 98.43% and 99.33%, for zinc was 97.96% and 99.49%, for nickel was 97.18% and 99.49% respectively.

Fig. 10 shows that the permeate flux have been decreased with increasing feed concentration of zinc. This behavior is due to increase in osmotic pressure, decrease of the effective pore size of the membrane due to adsorption of solute on the surface of the membrane and the effect of concentration polarization. This behavior is in agreement with **Al-Rashdi, et al., 2013**. The possibility of fouling inside the pores of membrane would be larger in case of the concentrated solution flowing, this fouling could act in blockage a number of bores completely or partly, so the flux would be decreased. The increase in feed concentration of zinc ions from 10 to 300 mg/l resulted in the decline in flux of 24.7% for NF and 20.48% for RO. **Fig. 11** shows that zinc ions concentration in permeate has been increased as the feed concentration increased due to the increase in concentration of feed due to recirculation mode. This behavior is in agreement with **Ahn, et al., 1999**. The increase in feed concentration of zinc ions from 10 to 300 mg/l resulted in the increase of permeate concentration from 1.409 to 13.71 mg/l for NF and 0.19 to 4.63 mg/l for RO.

Fig. 12 shows the permeate flux has been increased with increasing applied pressure, this behavior is due to an increase of the preferential sorption of water at higher pressure, and thus the solvent permeability increases at high pressure compared with the solute permeability. This behavior is in agreement with **Lee, et al., 2006**. The increase in applied pressure from 1 to 4 bar resulted in the increase in flux of 304.06% for NF and 311.98% for RO. **Fig. 13** shows the concentration of zinc ions in permeate has been decreased with increasing applied pressure which can be explained by the following: at low pressure the solute diffusive transport through the membrane is higher than that of convective transport. As the applied pressure increases, the decrease of the concentration of ions in permeate becomes possible due to convective transport becomes more important at high pressure. This behavior was observed for RO membrane, this behavior is in agreement with **Chai, et al., 1997**. For NF membrane the permeate concentration has been decreased and then increased at high pressures, this behavior can be explained as the increase in pressure caused an increase in the flux so that the solution level in the feed tank decreased and the feed became more concentrated (i.e. the concentration of zinc ions in feed solution is higher than that of initial feed concentration) and the concentration polarization has been increased with increasing pressure causing an increase in permeate concentration at high pressures, in this case the effect of both concentration polarization and convective transport play an important role. This behavior is in agreement with **Al-Rashdi, et al., 2013**. The permeate concentration had decreased from 20.85 to 11.01 mg/l at p= 1-3 bar and then increased to 11.45 mg/l at p=4 bar for NF and decreased from 6.89 to 3.45 mg/l for RO.

Fig. 14 shows that the permeate flux increases with increasing in feed flow rate (cross flow velocity). These increment means that there is a boundary layer concentration polarization at the surface of the membrane, as the flow rate or cross flow velocity has been increased this boundary layer has been decreased. This behavior is I agreement with **Murthy, and Chaudhari, 2009**. The increase in feed flow rate from 20 to 50 l/h resulted in the increase in flux of 6.25% for NF and 5.48% for RO. **Fig. 15** shows that the increase in feed flow rate leads to a decrease in the permeate concentration of nickel ions. Similar behavior were found in literature **Frare`s, et al., 2005 and Ahn, et al., 1999**. Mass transfer coefficient increased with increase in feed flow rate which decreased the concentration polarization and decrease the permeate concentration and this behavior is in agreement with **Gherasim, and Mikulášek, 2014, Boricha, and Murthy, 2009 and Murthy, and Chaudhari, 2009**. The increase in feed flow rate from 20 to 50 l/h resulted in the decrease of permeate concentration of 7.13% for NF and 38.27% for RO.

It is clear from **Fig. 16** that the increase in feed temperature leads to an increase in permeates flux. This behavior can be explained as the solvent diffusion coefficient increased, the average pore size of the active layer increased slightly and the solution viscosity decreased with an increase in the temperature of feed, which led to an increase in the permeate flux. This behavior is in agreement with **Wei, et al., 2013 and Wang, et al., 2007**. The increase in feed temperature from 26 to 40 $^{\circ}$C resulted in the increase in flux of 9.64% for NF and 55% for RO. **Fig. 17** shows that the increases in feed temperature leads to an increase in permeate concentration of copper ions. Increasing the temperature influence the heavy metals adsorption by the membranes, more copper ions will be adsorbed on the membrane surface due to the diffusion rate of the molecules has been increased, also the increase of membrane pore size resulting in an increase in the permeate concentration. This behavior is in agreement with **Abd Alameer, 2011**. The increase in feed temperature from 26 to 40 $^{\circ}$C resulted in the increase of permeate concentration of 8.28% for NF and 6.14% for RO.

It is clear from **Fig. 18** that for chromium the flux has been decreased as the pH goes from the acidic side towards the alkaline side. More decrease is shown around the region of pH=5 and pH=7 for NF membrane and at pH=7 for RO membrane. The maximum flux of chromium was at pH=4 for both membrane. It is well known that when the pH of the solution decreases, the solubility of dissolved salts increases. From membrane point of view, this would decrease the rate of fouling on the membrane surface which leads to decrease the osmotic pressure and consequently the permeate flux would increase. On the contrary increasing pH of solution would accelerate the deposition of salt on membrane surface. This agrees with **Abd Alameer, 2011**. **Fig. 19** shows that the increase in pH would lead to an increase in the precipitation of dissolved salts which will foul the membrane surface, hence, increasing the resistance to salt passage through the membrane. Therefore higher removal values are obtained at pH=7 for chromium. The decreasing of pH means the increasing of the concentration of hydrogen ion, H^+, while the increasing of pH is a result of increasing of hydroxide ion OH^-. The molecular weight of hydroxide ion is much larger than H^+. According to the pore side theory for membranes the permeation of hydrogen ion with small molecular weight (i.e. small ions size) is larger than the hydroxide ion, and this can be explain the reason of the high permeability of heavy metal ions in lower pH range. The electrical charge equilibrium will be varied according to the concentration of the ions on both sides of the membrane. This behavior agrees with **Al-Alawy, 2000**.

The flux for nanofiltration is higher than that from reverse osmosis membrane; this is due to the pore size of nanofiltration membrane which is larger than that of reverse osmosis membrane and the RO has higher osmotic pressure than NF membranes as a result the permeability of pure water for nanofiltration is approximately twice that of RO. The flux of NF is higher than that of RO for chromium about 50-82%, copper 30-62%, nickel 22-36% and zinc 50-85%. The concentrations of heavy metal ions in permeate for nanofiltration is higher than that from reverse osmosis membranes. The concentration or rejection has been affected by size exclusion than other mechanisms, and NF has higher MWCO which means larger pore size than RO, but rejection for RO system mainly depends on solution diffusion transport.

4.2 NF and RO Simulated Electroplating Wastewater

Experiments has been made to show the effect of time (0-70 min) on the flux and concentration of heavy metal ions in NF and RO process for a mixture of synthetic electroplating wastewater, **Wei, et al., 2013**. **Figs. 20 to 22** show the effect of time for a mixture of electroplating wastewater on flux and the concentration of heavy metal ions in permeate for NF and RO. The increase in time to 70 min resulted in the decline of flux from 16.83 to 13.48 LMH for NF process and 10.17 to 9.32 LMH for RO process. The increase in time to 70 minutes resulted in the increase in permeate concentration for NF process from 0.042 to 0.568 mg/l for zinc, 1.878 to 7.01 mg/l for copper, 0.696 to 2.654 mg/l for nickel and 0.421 to 2.461 mg/l for chromium. The NF membrane has allowed permeation of chromium, nickel, copper and zinc ions to lower than permissible limits. For RO process the permeate concentration has been increased from 0.0335 to 0.12 mg/l for zinc, 0.848 to 2.442 mg/l for copper, 0.541 to 0.807 mg/l for nickel and 0.13 to 0.643 mg/l for chromium. The RO membrane has allowed permeation of chromium, nickel, copper and zinc ions to lower than permissible limits. The explanation for this behavior for NF and RO is the same as explained in section 4.1.

5. CONCLUSIONS

Nanofiltration and reverse osmosis processes can be used for recovery of water from heavy metal solutions. The polyamide nanofiltration membrane has allowed permeation of chromium and copper ions to lower than permissible limits. Nanofiltration membrane has allowed permeation of nickel and zinc ions at low concentration of these ions. The polyamide reverse osmosis membrane gives a high efficiency for removal of chromium, copper, nickel and zinc ions and it has allowed permeation of these ions to the lower than permissible limits. The rejection at first three minutes when the feed concentration approximately constant for chromium in NF and RO was 99.7% and 99.93%, for copper was 98.43% and 99.33%, for zinc was 97.96% and 99.49%, for nickel was 97.18% and 99.49% respectively. The maximum recovery for chromium in NF and RO was 71.75% and 48.5%, for copper was 75.62% and 50.68%, for zinc was 80.87% and 54.56%, for nickel was 60.06% and 46.18% respectively. For a mixture of synthetic electroplating wastewater, nanofiltration and reverse osmosis membranes have a high rejection percentage for heavy metal ions. Pure water was obtained and with concentration of less than the allowed for heavy metals in the case of the mixture.

6. REFERENCES

- Abd Alameer, A. M., 2011, *Dye Removal from Industrial Wastewater Using Membrane Technology*, M.Sc. thesis, University of Technology.
- Abhang, R. M., Wani , K. S., Patil, V. S., Pangarkar, B. L., and Parjane, S. B., 2013, *Nanofiltration for Recovery of Heavy Metal Ions from Waste Water - A Review*, International Journal of Research in Environmental Science and Technology, Vol. 3, PP. 29-34.
- Absar, B., Kadi, S. E. L., and Belhamiti, O., 2008, *Mathematical Modeling of Reverse Osmosis Process by the Orthogonal Collocation on Finite Element Method*. Asian Journal of Applied Sciences, Vol. 1, PP. 1-18.
- Abu Qdais, H., and Moussa, H., 2004, *Removal of Heavy Metals from Wastewater by Membrane Processes: A Comparative Study*, Desalination, Vol. 164, PP. 105-110.
- Ahn, K. H., Song, K. G., Cha, H. Y., and Yeom, I. T., 1999, *Removal of Ions in Nickel Electroplating Rinse Water Using Low-Pressure Nanofiltration*, Desalination, Vol. 122, PP. 77-84.
- Al-Alawy, A. F., 2000, *Study of the Factors Affecting the Efficiency of Reverse Osmosis Process*, M.Sc. thesis, Baghdad University.
- Al-Rashdi, B. A. M., Johnson, D. J., and Hilal, N., 2013, *Removal of Heavy Metal Ions by Nanofiltration*, Desalination, Vol. 315, PP. 2-17.
- Alzahrani, S., Mohammad, A. W., Hilal, N., Abdullah, P., and Jaafar, O., 2013, *Comparative Study of NF and RO Membranes in the Treatment of Produced Water—Part I: Assessing Water Quality*, Desalination, Vol. 315, PP. 18–26.
- Barakat, M. A., 2011, *New Trends in Removing Heavy Metals from Industrial Wastewater*, Arabian Journal of Chemistry, Vol. 4, PP. 361–377.

- Boricha, A. G., and Murthy, Z. V. P., 2009, *Preparation, Characterization and Performance of Nanofiltration Membranes for the Treatment of Electroplating Industry Effluent*, Separation and Purification Technology, Vol. 65, PP. 282–289.
- Chai, X., Chen, G., Yue, P. L., and Mi, Y., 1997, *Pilot Scale Membrane Separation of Electroplating Waste Water by Reverse Osmosis*, Journal of Membrane Science, Vol. 123, PP. 235-242.
- Dannys, E., Green, T., Wettlaufer, A., Madhurnathakam, C. M. R., and Elkamel A., 2016, *Wastewater Treatment with Microbial Fuel Cells: A Design and Feasibility Study for Scale-up in Microbreweries*, Journal of Bioprocessing & Biotechniques, Vol. 6, PP. 1-6.
- Frare`s, N. B., Taha, S., and Dorange, G., 2005, *Influence of the Operating Conditions on the Elimination of Zinc Ions by Nanofiltration*, Desalination, Vol. 185, PP. 245–253.
- Fu, F., and Wang, Q., 2011, *Removal of Heavy Metal Ions from Wastewaters: A Review*, Journal of Environmental Management, Vol. 92, PP. 407-418.
- Gherasim, C. V., and Mikulášek, P., 2014, *Influence of Operating Variables on the Removal of Heavy Metal Ions from Aqueous Solutions by Nanofiltration*, Desalination, Vol. 343, PP. 67–74.
- Jain, G., 2013, *Removal of Copper and Zinc from Wastewater Using Chitosan*, M.Sc. thesis, National Institute of Technology, Rourkela.
- Khudair, W. N., 2011, *Reduction of Concentrating Poisonous Metallic Radicals from Industrial Wastewater by Forward and Reverse Osmosis*, M.Sc. thesis, Baghdad University.
- Kucera, J., 2010, *Reverse Osmosis Design, Processes, and Applications for Engineers*, John Wiley & Sons, Inc. Hoboken, New Jersey, and Scrivener Publishing LLC, Salem, Massachusetts.
- Kurniawan, T. A., Chan, G. Y. S., Lo, W. H., and Babel, S., 2006, *Physico–Chemical Treatment Techniques for Wastewater Laden with Heavy Metals*, Chemical Engineering Journal, Vol. 118, PP. 83–98.
- Lee, J. W., Kwon, T. O., and Moon, I. S., 2006, *Performance of Polyamide Reverse Osmosis Membranes for Steel Wastewater Reuse*, Desalination, Vol. 189, PP. 309-322.
- Murthy, Z. V. P., and Chaudhari, L. B., 2009, *Separation of Binary Heavy Metals from Aqueous Solutions by Nanofiltration and Characterization of the Membrane Using Spiegler–Kedem Model*, Chemical Engineering Journal, Vol. 150, PP. 181–187.
- Wahaab, R. A., Moawad, A. K., Abou Taleb, E., Ibrahim, H. S., and El-Nazer, H. A. H., 2010, *Combined Photocatalytic Oxidation and Chemical Coagulation for Cyanide and Heavy Metals Removal from Electroplating Wastewater*, World Applied Sciences Journal, Vol. 8, PP. 462-469.
- Wang, Z., Liu, G., Fan, Z., Yang, X., Wang, J., and Wang, S., 2007, *Experimental Study on Treatment of Electroplating Wastewater by Nanofiltration*, Journal of Membrane Science, Vol. 305, PP. 185–195.
- Wei, X., Kong, X., Wang, S., Xiang, H., Wang, J., and Chen, J., 2013, *Removal of Heavy Metals from Electroplating Wastewater by Thin-Film Composite Nanofiltration Hollow-Fiber Membranes*, Industrial & Engineering Chemistry Research, Vol. 52, PP. 17583−17590.

NOMENCLATURE

C	concentration of solute, mg/l
C_F	concentration in feed solution, mg/l
C_P	concentration in permeate, mg/l
i	number of dissociated ions per molecule (Van't Hoff factor), dimensionless
J_w	flux of water, l/m^2.h

k_w	permeability coefficient of pure water, l/m^2.h.bar
Q_F	feed flow rate, l/h
R	solute rejection, percentage
R_g	universal gas constant, l.bar/mole.K
T	temperature, K
t	time, min
V_F^o	initial feed volume, l
V_P	volume of permeate, l
Y	recovery, percentage
ΔP	applied pressure driving force, bar
$\Delta\pi$	osmotic pressure of the solution, bar
φ	osmotic coefficient, dimensionless

ABBREVIATIONS

NF	Nanofiltration
UF	Ultrafiltration
RO	Reverse osmosis
LMH	Liter per square meter per hour
MWCO	Molecular weight cut off

Table 1. Chemical specification of inorganic compounds.

Specification	Zinc Chloride ($ZnCl_2$)	Copper Chloride Dihydrate ($CuCl_2.2H_2O$)	Nickel Chloride Hexahydrate ($NiCl_2.6H_2O$)	Chromic Chloride ($CrCl_3.6H_2O$)
Minimum assay	97.0%	99.0%	98.0%	97.0%
Molecular weight	136.28	170.48	237.69	266.45
CAS-No.	7646-85-7	10125-13-0	13478-00-7	10078
Made in	India	India	India	England

Table 2. Specification of nanofiltration and reverse osmosis element.

Specifications	NF	RO
Type of membrane	Polyamide thin-film composite	Ultra low pressure aromatic polyamide reverse osmosis membrane element
Active membrane area, m^2	0.36	0.36
Average permeated flow	0.57 m^3/d	0.19 m^3/d
Maximum feed water SDI	5	5
Maximum feed water temperature $^\circ$C.	45	45
pH range of feed water during continuous operation	2-11	3-10
pH range of feed water during chemical cleaning	1-12	2-12

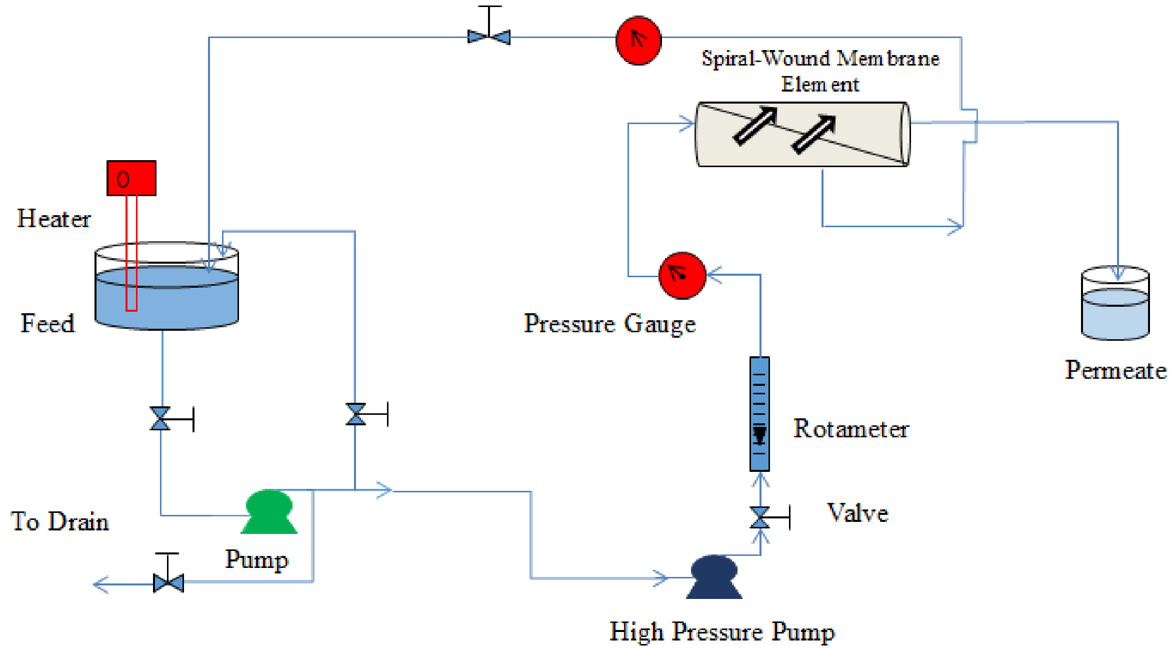

Figure 1. Schematic diagram of lab-scale RO system.

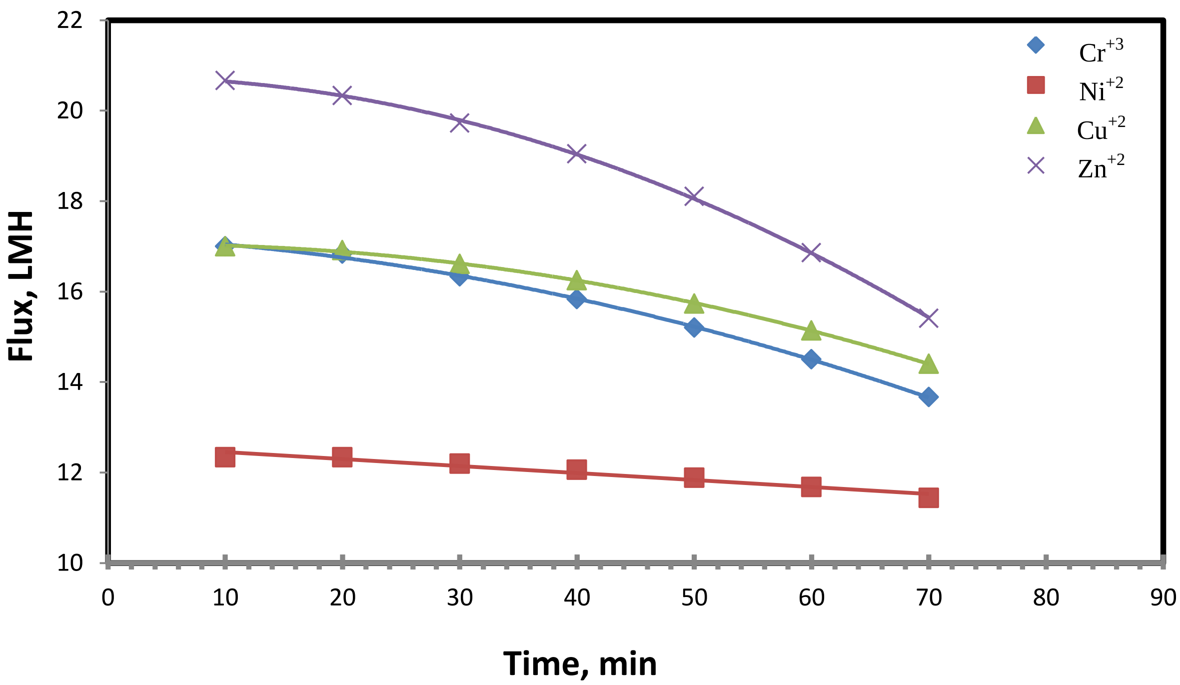

Figure 2. Effect of operating time on flux for NF process (Q_F=40 l/h, T=26 $^{\circ}$C, P=2 bar, $C_{F, ions}$=300 mg/l).

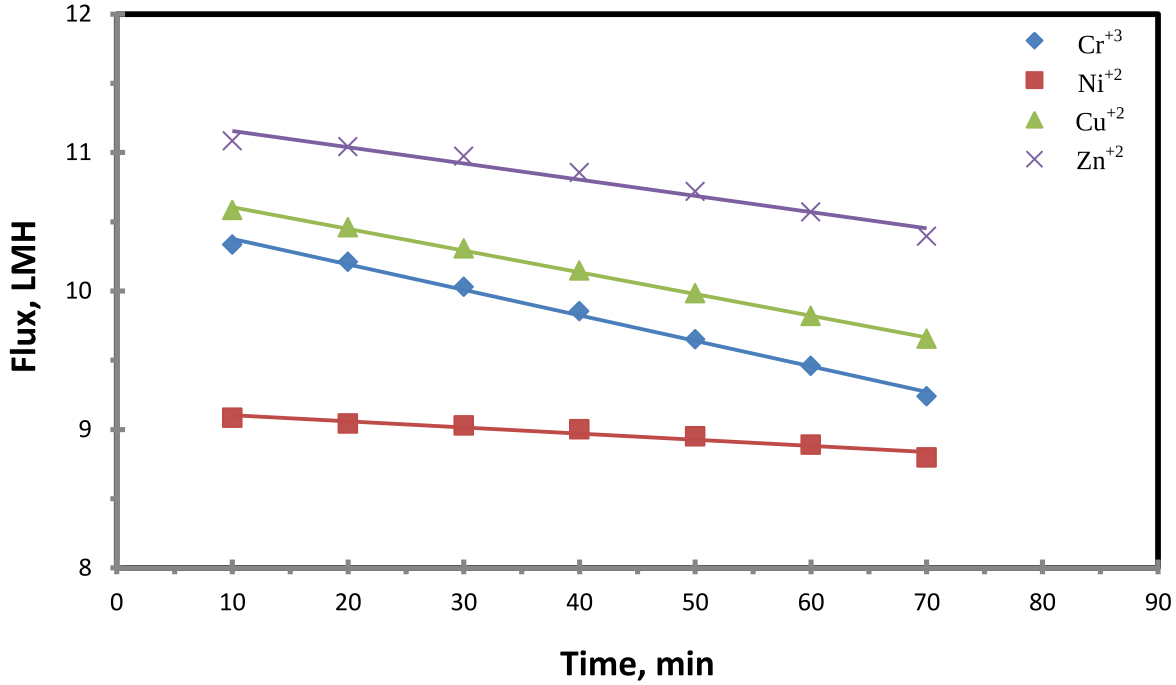

Figure 3. Effect of operating time on flux for RO process (Q_F=40 l/h, T=26 °C, P=2 bar, $C_{F, ions}$=300 mg/l).

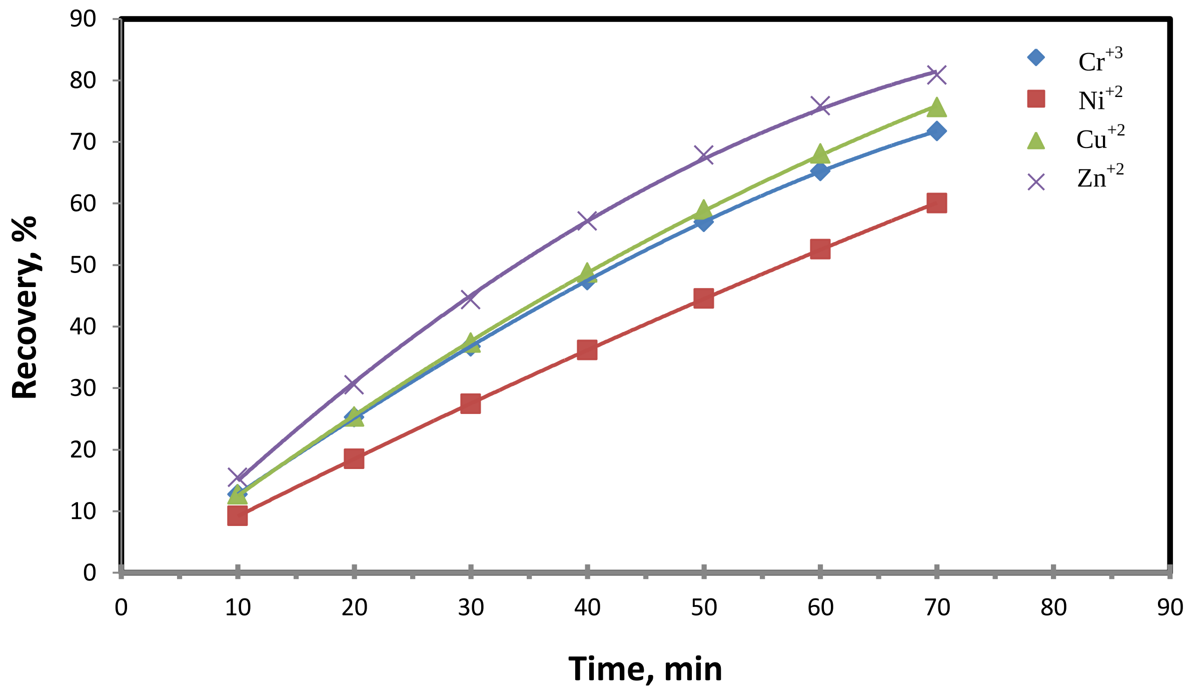

Figure 4. Effect of operating time on recovery percentage for NF process (Q_F = 40 l/h, T = 26 °C, P = 2 bar, $C_{F, ions}$=300 mg/l).

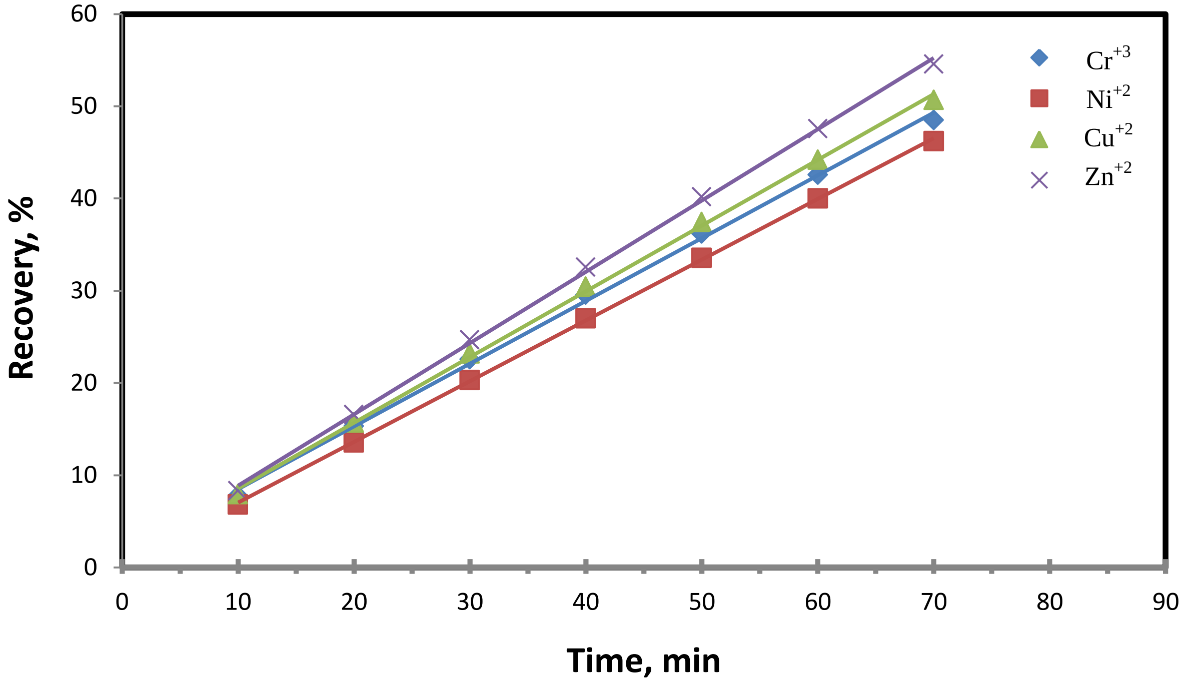

Figure 5. Effect of operating time on recovery percentage for RO process (Q_F = 40 l/h, T = 26 °C, P = 2 bar, $C_{F,\ ions}$=300 mg/l).

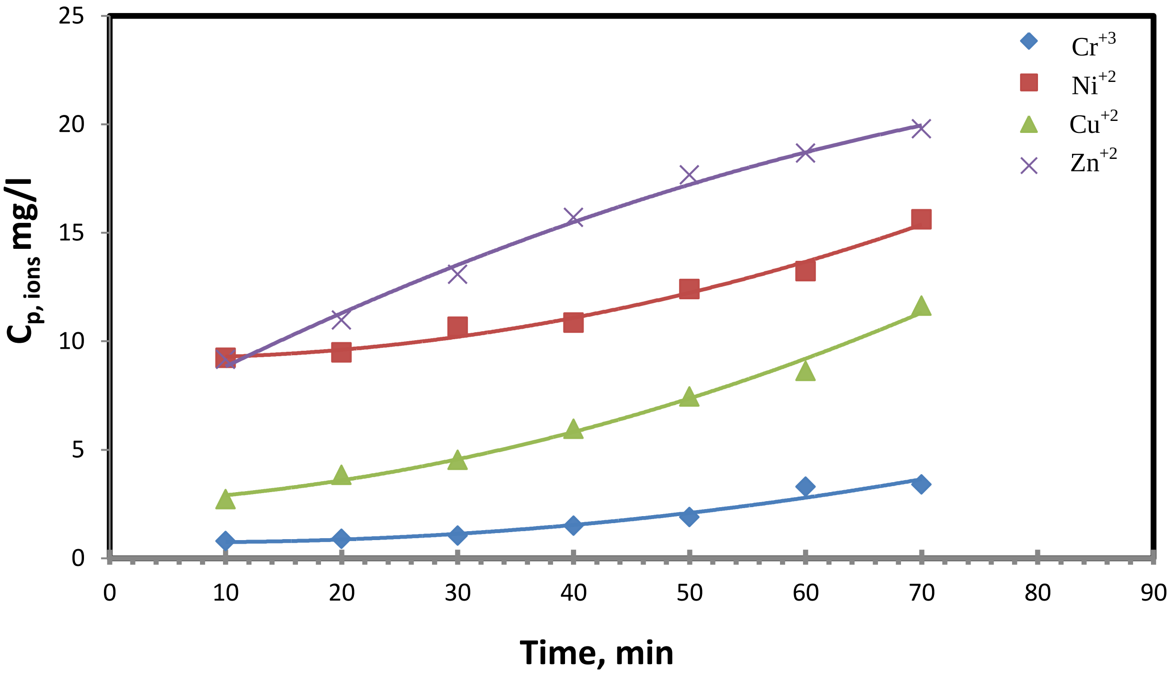

Figure 6. Effect of operating time on permeate concentration of ions for NF process (Q_F=40 l/h, T=26 °C, P=2 bar, $C_{F,\ ions}$=300 mg/l).

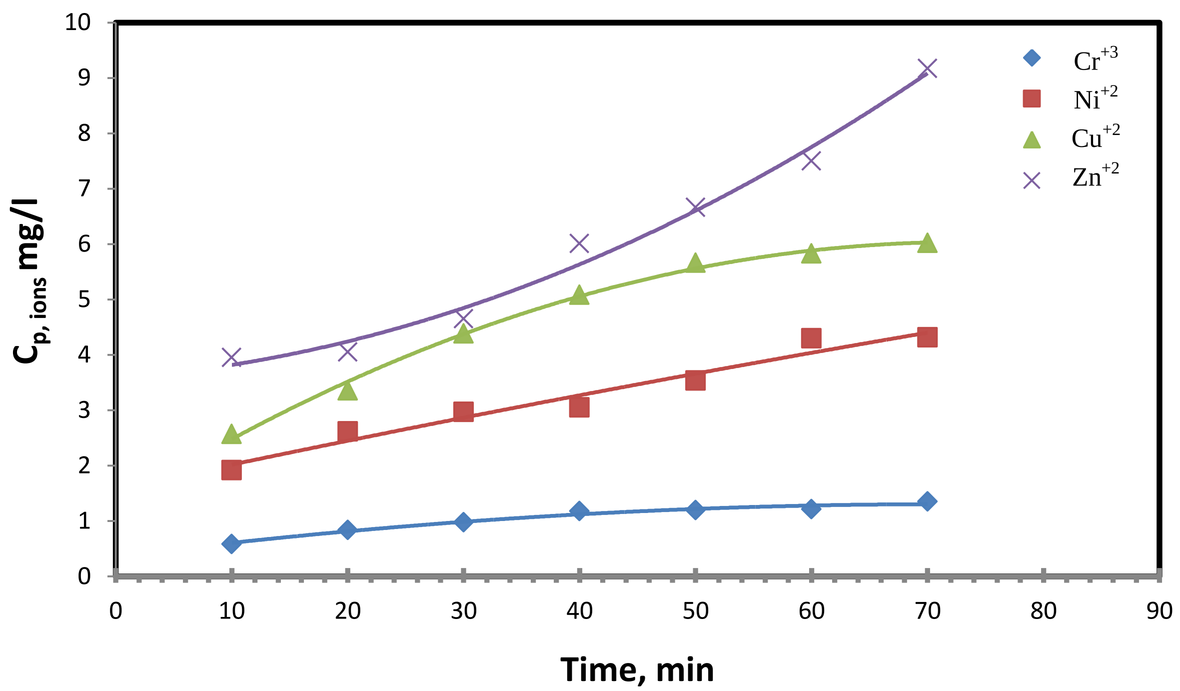

Figure 7. Effect of operating time on permeate concentration of ions for RO process (Q_F=40 l/h, T=26 °C, P=2 bar, $C_{F,\ ions}$=300 mg/l).

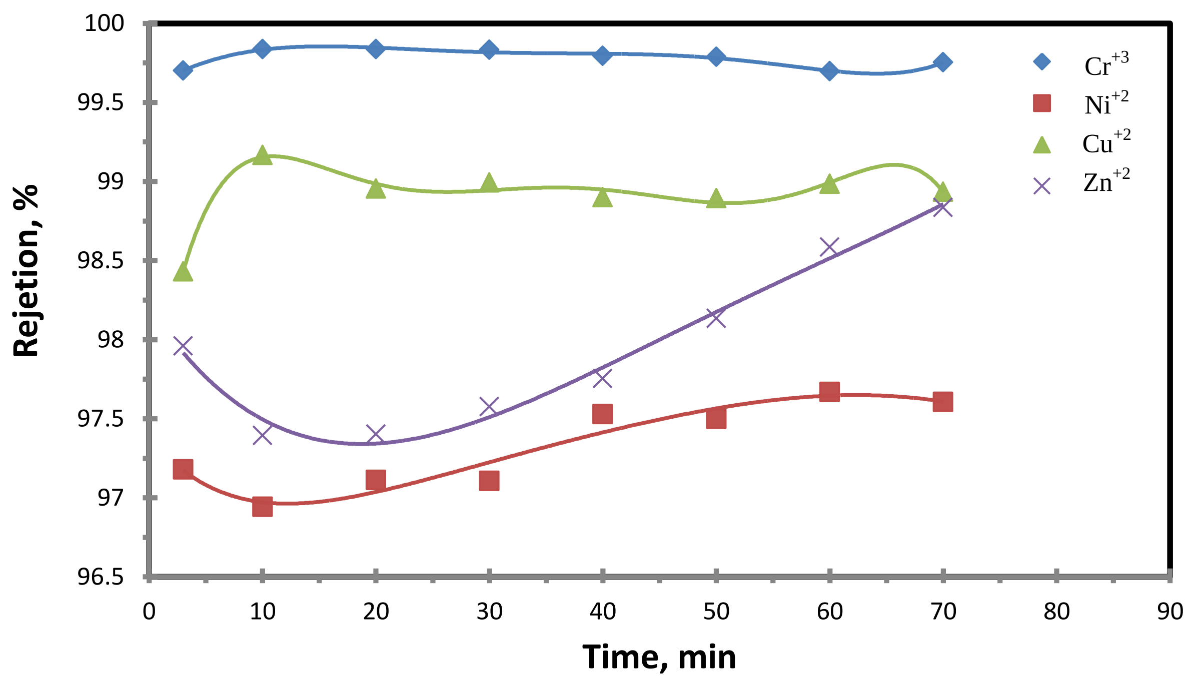

Figure 8. Effect of operating time on rejection percentage of heavy metal ions for NF process (Q_F = 40 l/h, T = 26 °C, P = 2 bar, $C_{F,\ ions}$=300 mg/l).

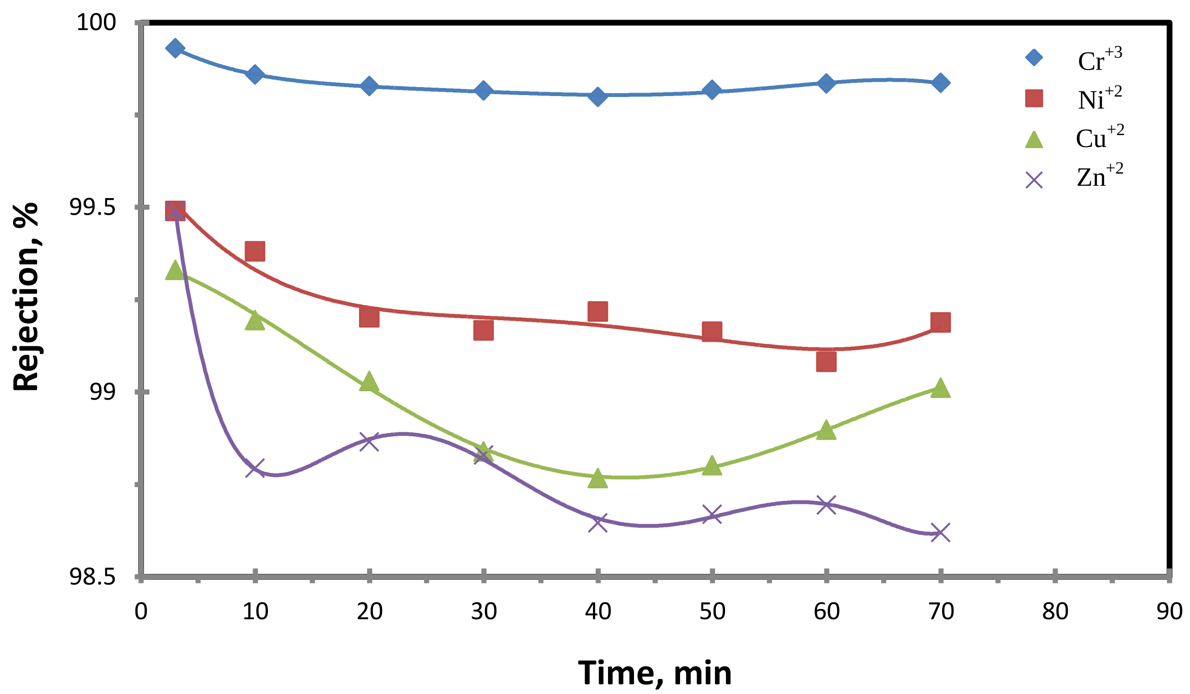

Figure 9. Effect of operating time on rejection percentage of heavy metal ions for RO process (Q_F = 40 l/h, T = 26 °C, P = 2 bar, $C_{F,\ ions}$=300 mg/l).

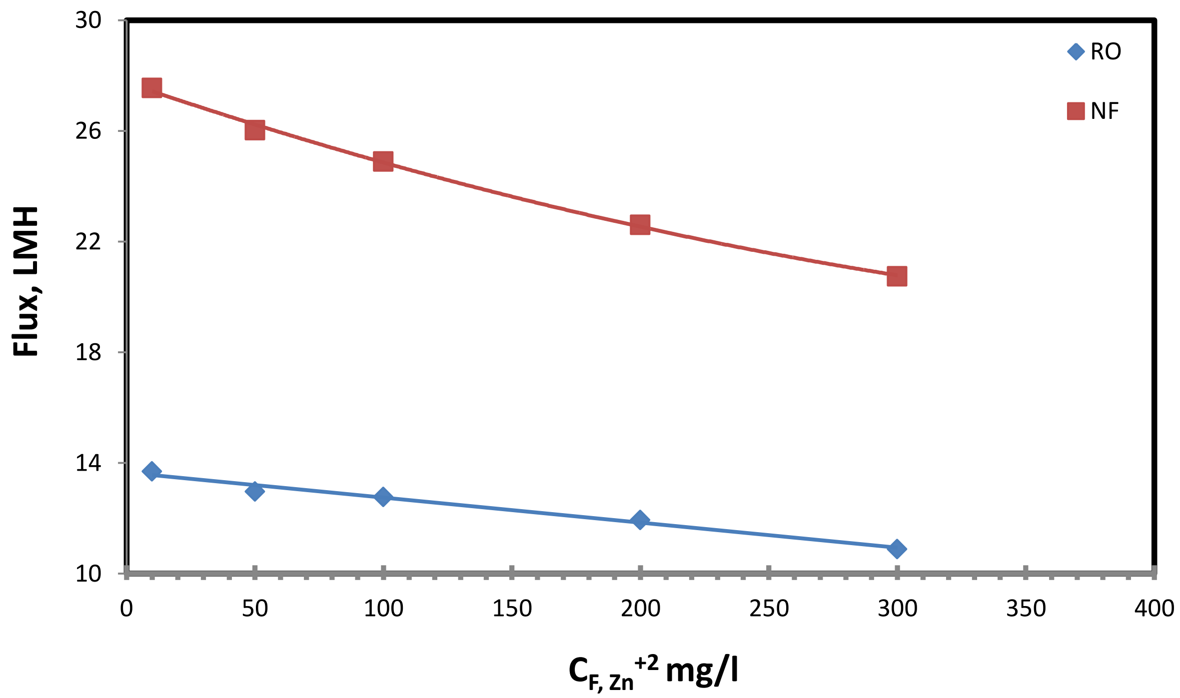

Figure 10. Effect of feed concentration of zinc ions on flux (t=30 min, T=26 °C, P=2 bar, Q_F=40 l/h, pH=6).

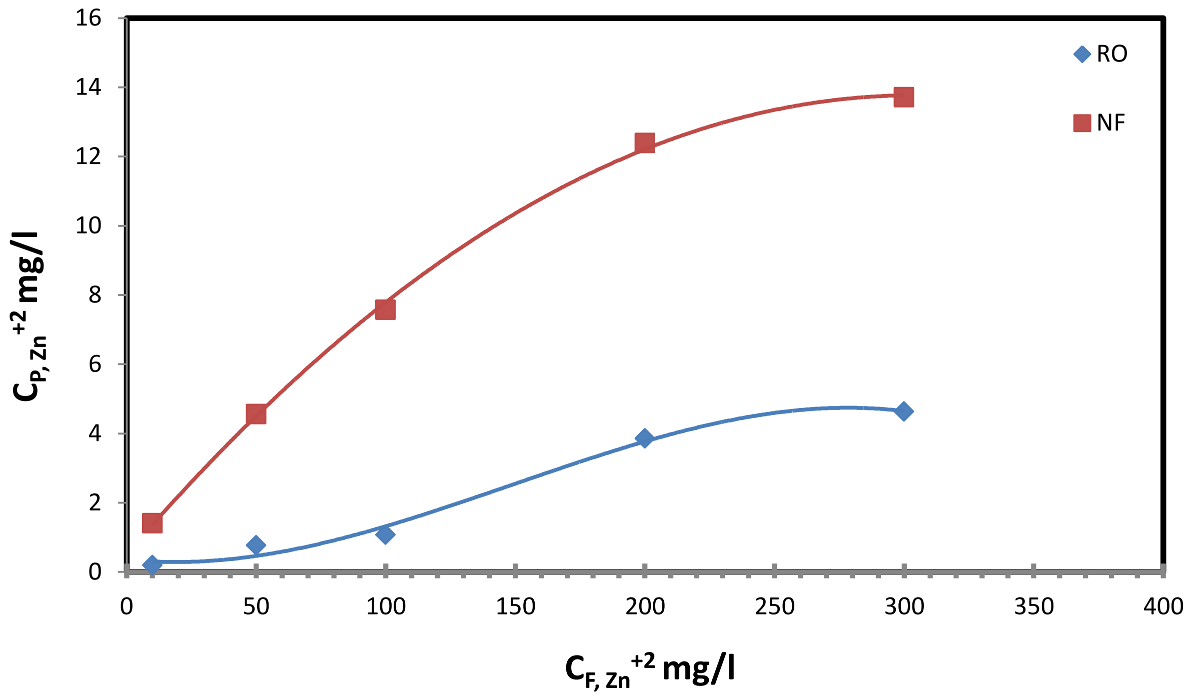

Figure 11. Effect of feed concentration of zinc ions on permeate concentration (t=30 min, T=26 $^{\circ}$C, P=2 bar, Q_F=40 l/h, pH=6).

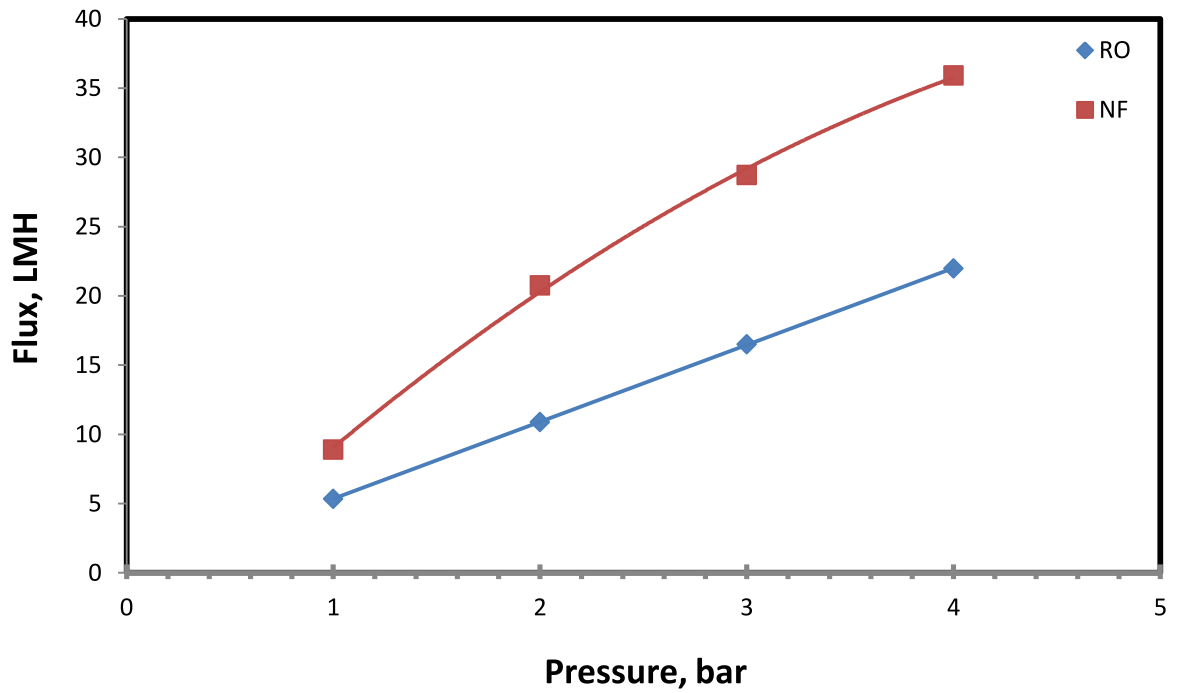

Figure 12. Effect of operating pressure on flux for zinc ions (t=30 min, T=26 $^{\circ}$C, Q_F=40 l/h, $C_{F, Zn}^{+2}$=300 mg/l, pH=6).

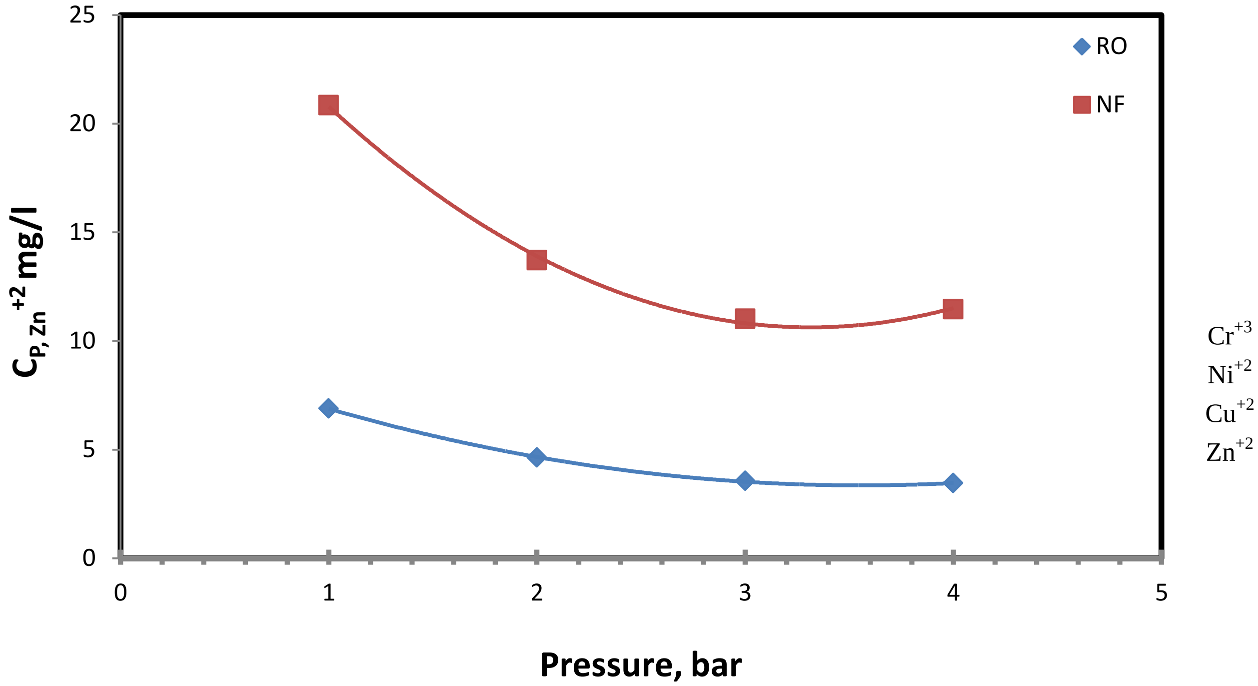

Figure 13. Effect of operating pressure on permeate concentration of zinc ions (t=30 min, T=26 $^{\circ}$C, Q_F=40 l/h, $C_{F, Zn}$ $^{+2}$=300 mg/l, pH=6).

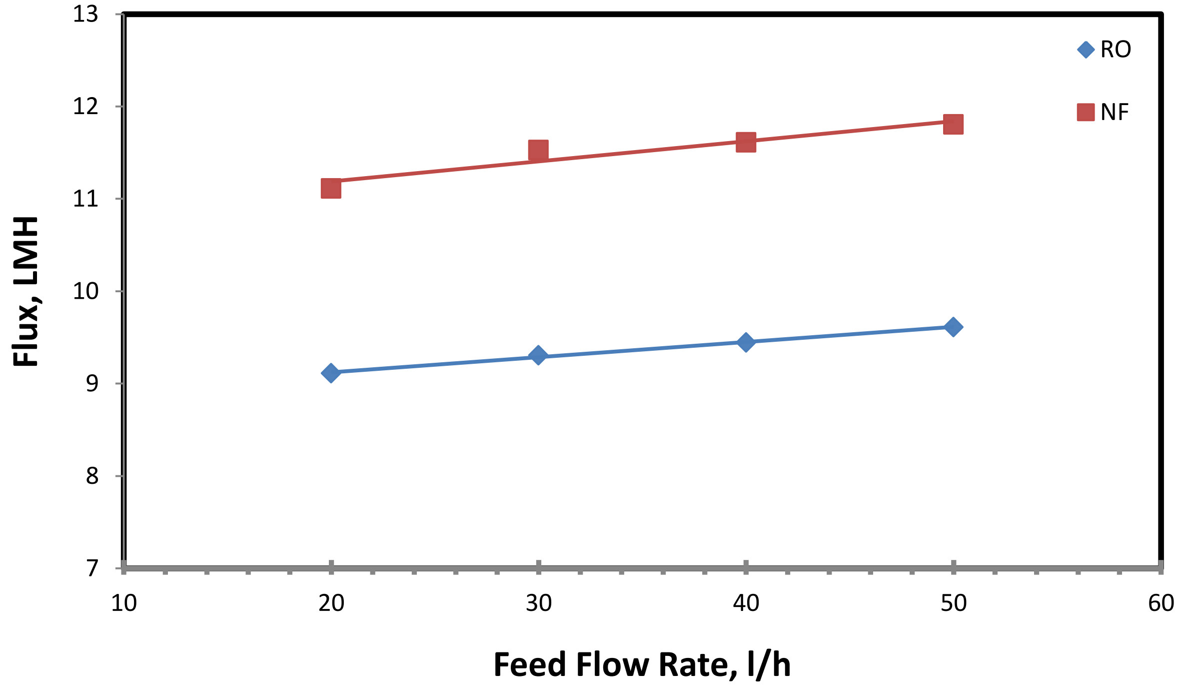

Figure 14. Effect of feed flow rate on flux for nickel ions (t=30 min, T=26 $^{\circ}$C, P=2 bar, $C_{F, Ni}$ $^{+2}$=300 mg/l, pH=6).

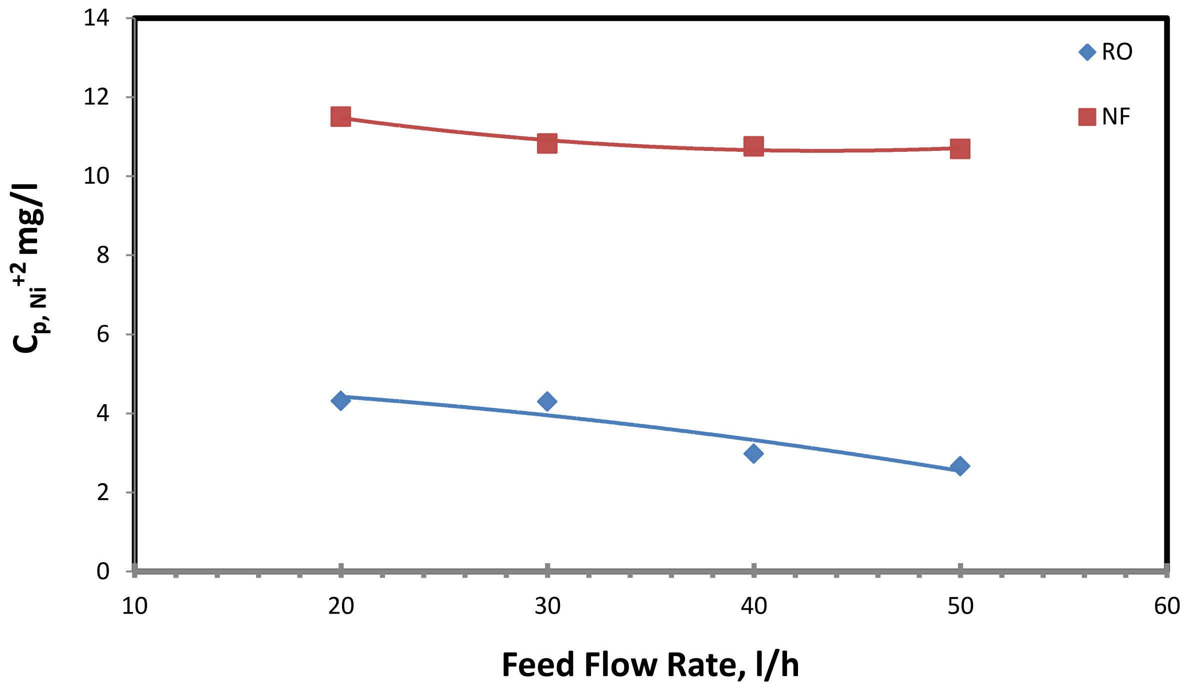

Figure 15. Effect of feed flow rate on permeate concentration of nickel ions (t=30 min, T=26 $^{\circ}$C, P=2 bar, $C_{F, Ni}{}^{+2}$=300 mg/l, pH=6).

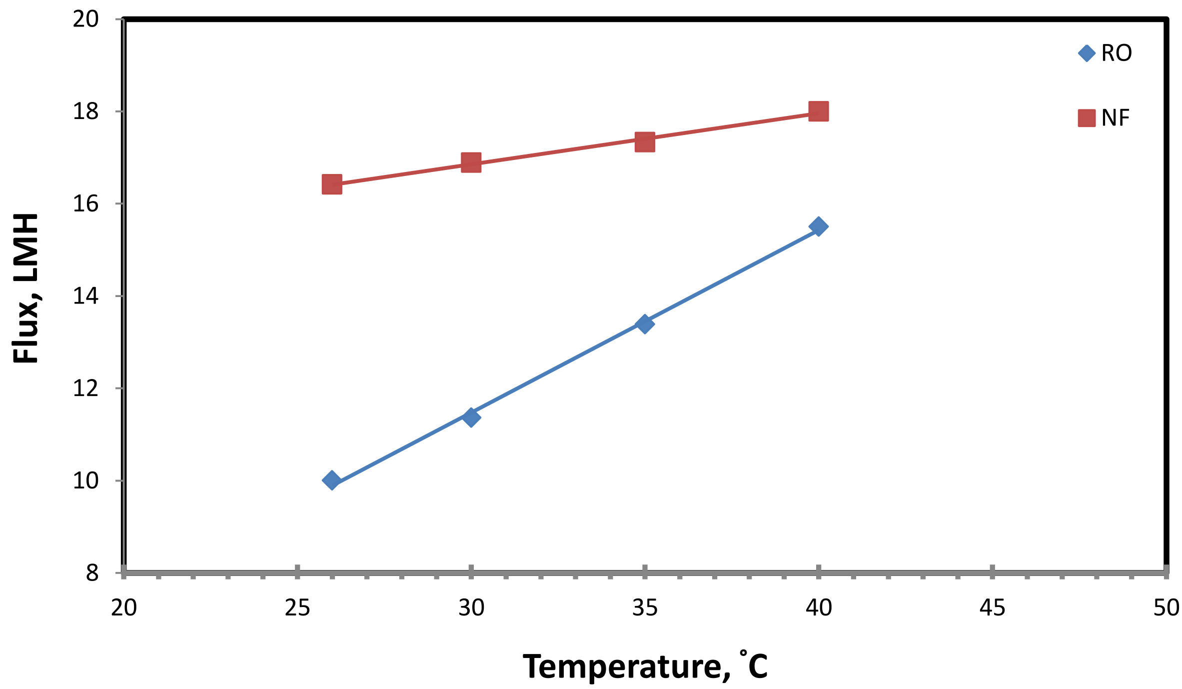

Figure 16. Effect of feed temperature on flux for copper ions (t=30 min, P=2 bar, Q_F=40 l/h, $C_{F, Cu}{}^{+2}$=300 mg/l, pH=5).

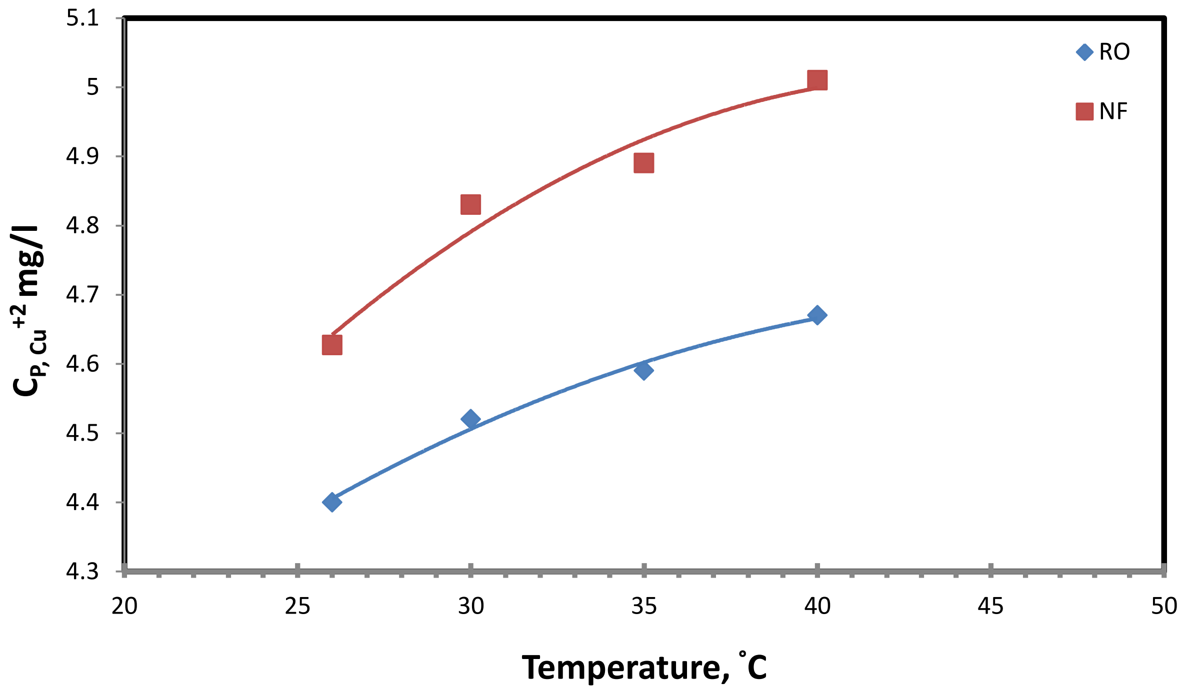

Figure 17. Effect of feed temperature on permeate concentration of copper ions (t=30 min, P=2 bar, Q_F=40 l/h, $C_{F, Cu}{}^{+2}$=300 mg/l, pH=5).

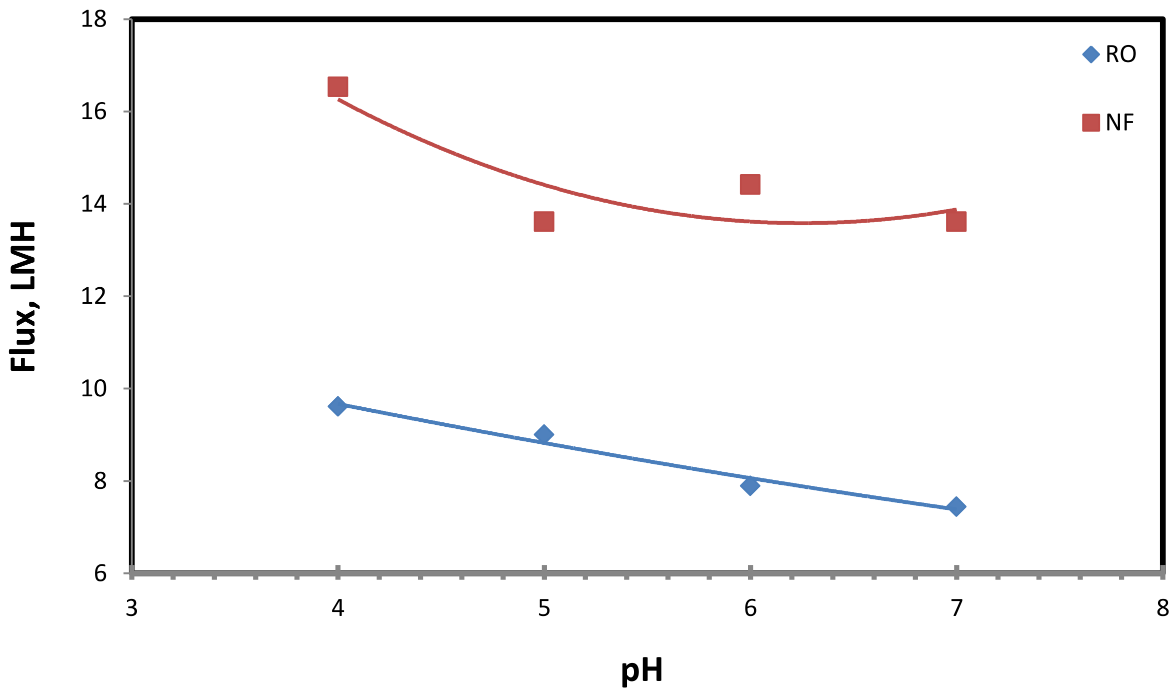

Figure 18. Effect of feed pH on flux for chromium ions (t=30 min, T=26 ˚C, P=2 bar, $C_{F, Cr}{}^{+3}$=300 mg/l, Q_F=40 l/h).

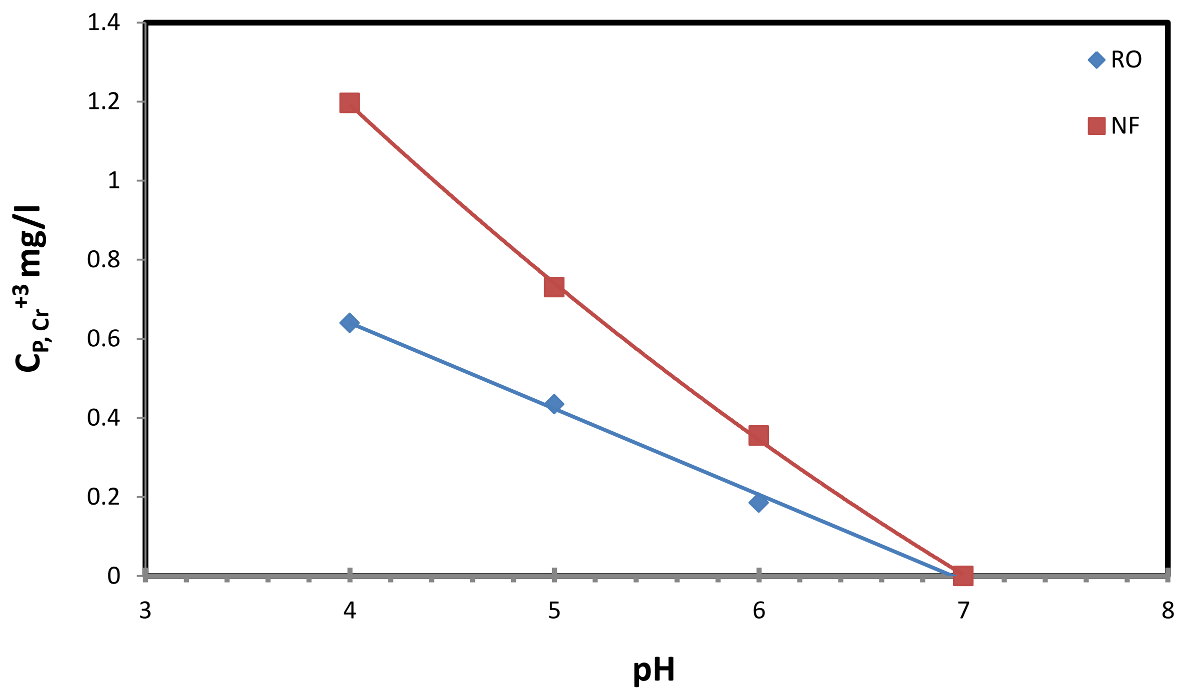

Figure 19. Effect of feed pH on permeate concentration of chromium ions (t=30 min, T=26 °C, P=2 bar, $C_{F,\,Cr}{}^{+3}$=300 mg/l, Q_F=40 l/h).

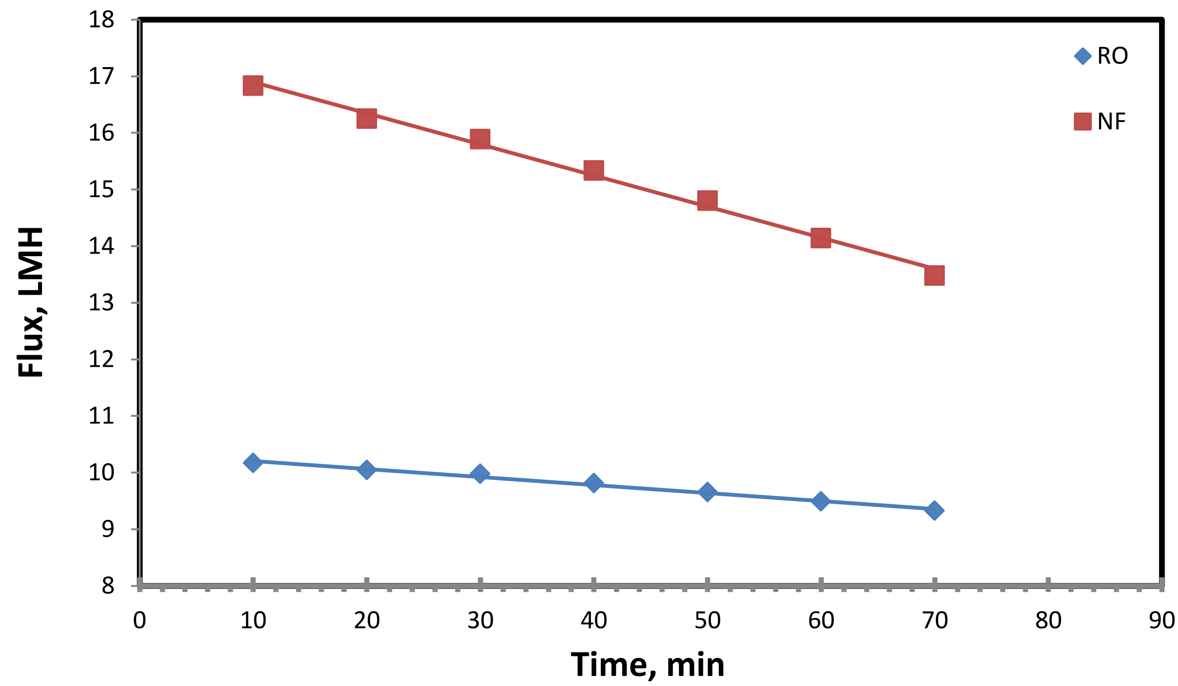

Figure 20. Effect of operating time on flux of a mixture of electroplating wastewater (Q_F=40 l/h, T=26 °C, P=2 bar, pH=3.49, $C_{F,\,Zn}{}^{+2}$=15 mg/l, $C_{F,\,Cu}{}^{+2}$=60 mg/l, $C_{F,\,Cr}{}^{+3}$=125 mg/l, $C_{F,\,Ni}{}^{+2}$=150 mg/l).

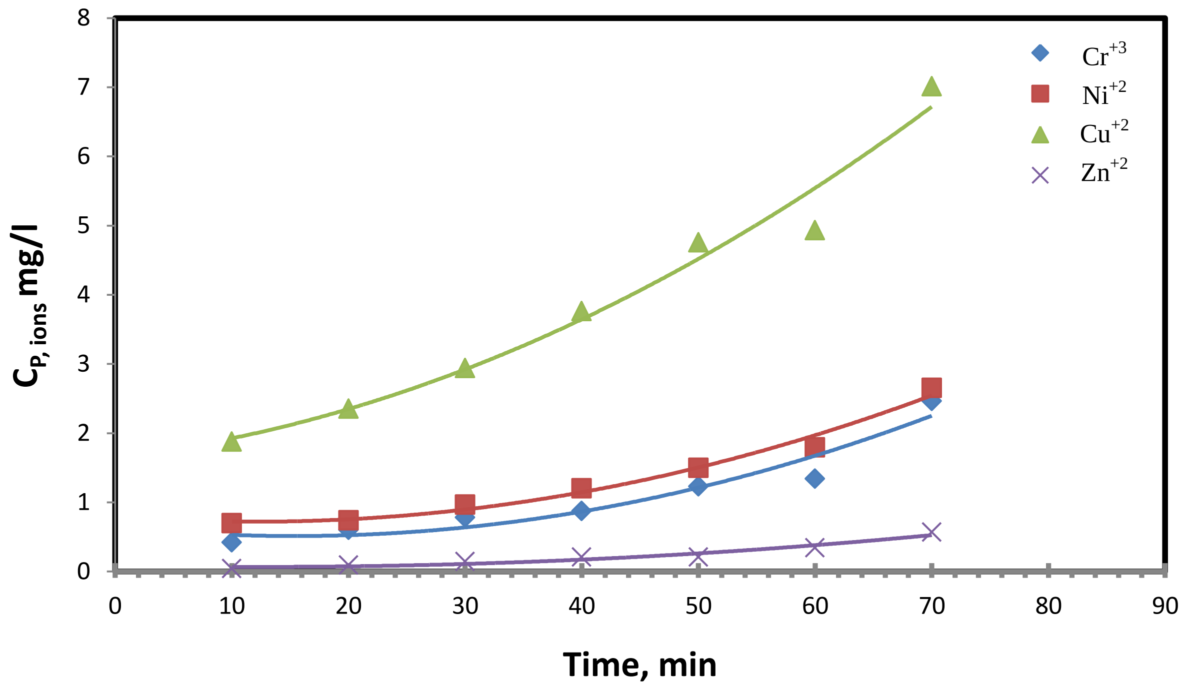

Figure 21. Effect of operating time on permeate concentration of ions in a mixture of electroplating wastewater for NF process (Q_F=40 l/h, T=26 $^{\circ}$C, P=2 bar, pH=3.49, $C_{F,\ Zn}{}^{+2}$=15 mg/l, $C_{F,\ Cu}{}^{+2}$=60 mg/l, $C_{F,\ Cr}{}^{+3}$=125 mg/l, $C_{F,\ Ni}{}^{+2}$=150 mg/l).

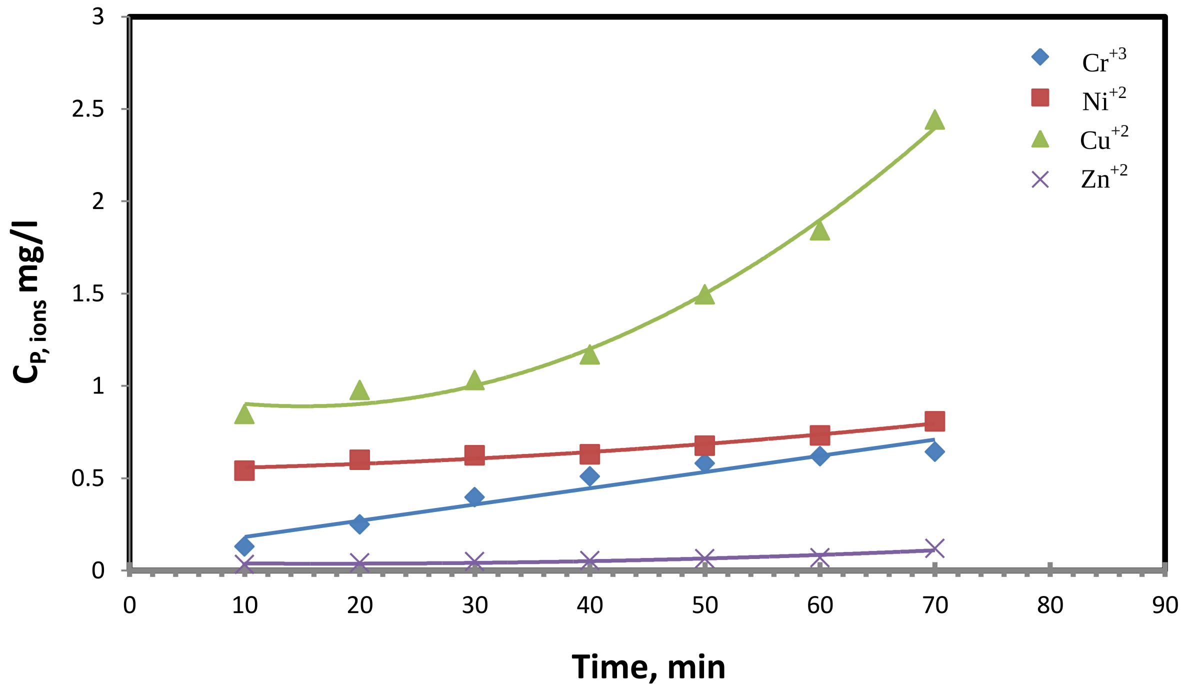

Figure 22. Effect of operating time on permeate concentration of ions in a mixture of electroplating wastewater for RO process (Q_F=40 l/h, T=26 $^{\circ}$C, P=2 bar, pH=3.49, $C_{F,\ Zn}{}^{+2}$=15 mg/l, $C_{F,\ Cu}{}^{+2}$=60 mg/l, $C_{F,\ Cr}{}^{+3}$=125 mg/l, $C_{F,\ Ni}{}^{+2}$=150 mg/l).

Cultivation of *Chlorella Vulgaris* Using Airlift Photobioreactor Sparged with 5%CO_2-Air as a Biofixing Process

Mahmood Khazzal Hummadi AL-Mashhadani
Lecturer
College of engineering- University of Baghdad
Chemical Engineering Department
Email: mkh_control@yahoo.com

Entisar Mohsin Khudhair
College of engineering- University of Baghdad
Chemical Engineering Department
Email: entisar.mohsen@gmail.com

ABSTRACT

The present paper addresses cultivation of *Chlorella vulgaris* microalgae using airlift photobioreactor that sparged with 5% CO_2/air. The experimental data were compared with that obtained from bioreactor aerated with air and unsparged bioreactor. The results showed that the concentration of biomass is 0.36 g l^{-1} in sparged bioreactor with CO_2/air, while, the concentration of biomass reached to 0.069 g l^{-1} in the unsparged bioreactor. They showed also that aerated bioreactor with CO_2/air gives more biomass production even the bioreactor was aerated with air. This study proved that application of sparging system for cultivation of *Chlorella vulgaris* microalgae using either CO_2/air mixture or air has a significant growth rate, since the bioreactors become more thermodynamically favorable and provide impetus for a higher level of production.

Key words: microalgae, *chlorella vulgaris*, airlift photobioreactor, CO_2 biofixing process

زراعة الكلوريلا فيلغارس في مفاعل الايرلفت مع ضخ خليط 5 %CO_2 -هواء كعملية تثبيت بايلوجية

د.محمود خزعل حمادي
مدرس
كلية الهندسة-جامعة بغداد

انتصار محسن خضير
باحث
كلية الهندسة-جامعة بغداد

الخلاصة

البحث الحالي يتناول دراسة زراعة طحالب الكلوريلا فيلغارس باستخدام مفاعل حيوي ضوئي الايرليفت بتهوية خليط من 5٪ CO_2 / الهواء. وتم مقارنة البيانات التجريبية مع التي تم الحصول عليها من مفاعل حيوي ضخ مع الهواء النقي فقط ومفاعل حيوي اخر بدون تهويه. النتائج أظهرت أن تركيز الكتلة الحيوية هو 0.36 g l^{-1} في مفاعل حيوي مع خليط من CO_2 / الهواء، في حين، تركيز الكتلة الحيوية وصلت إلى 0.069 g l^{-1} في مفاعل حيوي بدون تهوية. هذه النتائج اثبتت أن مفاعل حيوي التي ضخ اليه خليط من CO_2 / الهواء يعطي مزيدا من إنتاج الكتلة الحيوية من الزراعة في مفاعل حيوي ضخ اليه الهواء فقط. أثبتت هذه الدراسة أن تطبيق نظام التهوية لتفعيل نمو طحالب الكلوريلا فيلغارس باستخدام خليط من CO_2 / الهواء أو الهواء النقي فقط يعطي معدل نمو كبير، لأن المفاعلات الحيوية تصبح أكثر ملاءمة للديناميكية الحرارية وتوفر حافزا لمستوى أعلى من الإنتاج.

الكلمات الرئيسية: الطحالب، كلوريلا فيلغارس، مفاعل حيوي ضوئي الايرلفت، عملية تثبيت CO_2 بايلوجيا.

1. INTRODUCTION

Until recently, fossil fuel as a main source of energy is considered. However, concern about the depletion of this source is still a big challenge for the researchers. Therefore, the finding convincing alternatives to meet this challenge is necessary. Fossil fuels are also one of the reasons changing the climate by increasing the greenhouse gases (GHGs) such as carbon dioxide, methane, water vapor, nitrogen oxide and sulphur oxide **Amaro et al., 2011; Demirbas, 2011; Lee et al., 2010; Ranjan et al., 2010, Liu, 1994**. Among these gases, carbon dioxide is the most plentiful of gas and represents about 68% of the estimated total (GHG) emission **Harrington and Foster, 1999; Kondili and Kaldellis, 2007; Roman, et al., 2007.** In 1997, more than 170 countries signed the Kyoto agreement to reduce carbon dioxide emissions **Gutierrez et al., 2008.**

In addition, many studies have concerned biological process such as CO_2 mitigation from environment by fixing mechanism **De Morais and Costa, 2007a.** Some studies have used the terrestrial plants as source of biodiesel fuel for example; palm and soybeans **Costa and De Morais, 2011; Demirbas and Demirbas, 2011.** This alternative requires a long time to be ready for use and requires a large areas of farmland that definitely affect the production of food crops and increasing the global food crisis **Ozkurt, 2009; Demirbas 2010 ; Kecebas et al,2009; Demirbas 2011 ; Costa and de Morais, 2011; Demirbas and Demirbas, 2011.** Therefore, with these challenges, the researchers used another biological process which is less expensive and more economic through using the microalgae for CO_2 mitigation and convert it into biomass production **Carvalho et al., 2011**. In general, cultivation of microalgae requires sunlight as a source of energy, nutrients, water, and carbon dioxide as a source of carbon and regulation of pH in the medium **Chisti, 2007; Carvalho et al., 2011.** The microalgae have other advantages over terrestrial plants crops including, higher growth and biomass production rates, and shorter maturity rates. Normally microalgae double their biomass within 24 hours. Also, it required far less land for growing thus which is not compromising food production and supply, and oil content reaches to 20-50% in its biomass **Chisti, 2007; Clarens et al., 2010; Lee et al., 2010; Mercer and Armenta, 2011**. The cultivation of microalgae is obtained in a closed engineering system such as airlift reactor, which has recently gained renewed interest as a promising strategy for carbon dioxide mitigation **Filali et al, 2011.** This system has a great potential productivity due to better control of the environment and harvesting efficiency. Furthermore it has optimized space/volume utilization, therefore, more efficient use of costly land **Pedroni et al., 2001.**

Furthermore, supplying the carbon dioxide represents one of the major limiting factor in scale up the bioreactor design **Richmond, 2008; Morita et al., 2000**. Therefore, using CO_2 as sparging gas in the microalgae cultivation helps to strip oxygen accumulated and prevent toxicity of algae cells **Ying et al., 2013.** The current research represents an objective study which has been carried out to verify the effect of the proportion of carbon dioxide with the air on the growth of *Chlorella vulgaris* microalgae by using airlift photobioreactor that was designed by different working group **Al-Mashhadani et al., 2015.**

2. MATERIAL AND METHOD

2.1 Microalgae Culture and Cultivation Medium

Microalgae strain used in the current experiments is *Chlorella vulgaris*, which was isolated and purified at Plant Laboratory for Graduate Studies, Department of Biology, College of Science, University of Baghdad by using serial dilution and different plating techniques as described by **Abed et al, 2014**. This type of microalgae was collected from three different places in drinking water treatment plant that is located on Tigris River and purified by serial dilution. The stock cultures were propagated and maintained on NPK medium (20:20:20+TE N: P: K) commercial fertilizer. Its advantages are its being low-cost nutrients and high water soluble for biomass culture **Ammar, 2016.** This fertilizer has the following composition as percent concentration (N as urea 2.1% and as ammonia 17.9% , P as phosphorus oxide 20% , K as potassium oxide 20% with trace element consist of Mg 0.1% , Zn 0.05% , Mn 0.05% , Fe 0.1% , Cu 0.05% , B 0.02% and Vitamin B 0.0005%). This medium was prepared by dissolving these salts in RO treated water, the pH (6.23) was adjusted by using (0.1 N) of NaOH and HCl.
The incubation conditions used were continuously illuminated by three cool-white fluorescent light tubes (T5 Led, china), each fluorescent tube was 10 Watt and 2 foot length mounted approximately 10 inches at the surface of the flasks. Agitation was carried out by bubbling continuously sterile and (2.3) filtered air into the stock culture to provide a constant source of CO_2. The weekly subculture of algae cells was made to maintain the inoculum.

2.2 Design of Lab Scale Airlift Loop Photobioreactor

Fig.1 shows the configuration of airlift bioreactor used in the present study. The design of the airlift bioreactor was made according to results obtained from **Al-Mashhadani et al., 2015** using Navier-Stokes equations as main equations in their modeling. However; some modifications have been done to get a suitable environment of microalgae culture. The modified bioreactor was fabricated out of Plexiglass pipe, with dimensions of 350 mm in height and 150 mm in diameter. The airlift loop bioreactor consists of a stone diffuser located in the center of concentric tubes with 80 mm in diameter, fixed at distance 30 mm from the bottom and internal draught tube with dimension 100mm in diameter, 250 mm in height and fixed at 50 mm above the bottom of the reactor, 6 mm above the stone diffuser . Holes were made on the top of the reactor for fixing the props and exhaust gas.

2.3 Experiment Setup and Culture Condition

Fig. 2 illustrates the setup of photobioreactors for *Chlorella vulgaris* cultivation with lab scale airlift loop reactor. Both reactors have the same dimensions and were provided with magnetic stirrers (MRHEI-Tec, Germany) to ensure that all cells are exposed to the light and to prevent microalgae sedimentation. The microalgae cells were continuously illuminated over 24h per day by three fluorescent cool white lights, while the temperature of the culture media was controlled by aquarium heater controller (HK 50, China) at 30°C.

PH meter and dissolved oxygen (DO) props were fixed in downcomer region for daily measurement. The bioreactors were aerated with air that was mixed with 5% CO_2 from a gas cylinder for 28 minutes every day during the cultivation time. The CO_2/air mixture was adjusted in small mixture provided with a gas analyzer (Biogas 5000, G Geotech, UK, England) to achieve a desired concentration of CO_2 in the airstream and the flow rate was regulated by the gas flow meter at 200ml/min. The sparging gas mixture was filtered and sterile through inline air filtered 20 mm in diameter which was inserted in the bottom of the reactor as can be seen in **Fig. 2**. The air was supplied by air pump (HX-106A, China) and mixed with CO_2 when it is required. The second rector culture was operated with no additional CO_2, except that already existed in the air supplied.

The pre-cultured of *Chlorella vulgaris* was inoculated into the reactors with an inoculum size 250ml that was fed to the reactor and completed with 5L of NPK, as working volume and operating in a batch mode under 30°C. During this time, the airlift photobioreactor was sterilized by filled with a solution of about 200 ppm of odium Meta bisulfide (Na_2SO_4) as a decontamination agent hold in the airlift bioreactor for about 20 minutes before inoculation.

In this work, two sets of experiments were conducted. In the first experiment, one of the airlift bioreactor cultures was dosed with 5% CO_2 enriched with air. The dosing was periodically for about 28 min per day at a rate 200 ml /min, the dosing was carried out until pH reached 6. While the second bioreactor was unaerated (control) for comparison purpose with the cultures aerated.

The second experiment was conducted to represent a comparison between one aerated with mixture of air and 5% CO_2 and another aerated with only air at the same aeration time. After gas dosing, 5ml of samples of each culture was taken to evaluate kinetic parameter. PH and dissolved oxygen were measured before and after dosing.

2.4 Analytical Determination

Chlorella cultivation in the airlift reactors was tested for up 11days and during this time, sampling process was carried out every 24h intervals. Microalgae growth rate was estimated by two different methods. The first method measures the optical density (OD) at wavelength 680 nm (i.e., OD_{680}). This wavelength was chosen on preliminary tests for estimation the maximum absorbance (optical density) at wide range of wavelength. Researchers used similar wavelength **Mohd et al., 2011** and

Jeong et al., 2003 by using UV spectrophotometer (GENESYS 10UV, USA) to ensure maintaining an exponential phase of growth. The second method was measuring the dry weight of microalgae (g l^{-1}) by filtering the samples after centrifuged it in (Centrifuge PLC- 03, Taiwan) with 3000 r/min for 20 min then dried at 60 ^{0}C for 1h. A linear regression equation was derived to describe the relationship between biomass dry weight (g l^{-1}) and corresponding OD at 680 nm wavelengths.
The pH value for each culture was measured daily before and after gas dosing using pH meter (CRISON, Basic 20, USA). The dissolved oxygen (DO) level of the cultures was also measured before and after gas using (CRISON, OXI 45+, Spin).

3. KINETIC PARAMETER

Growth curve of density with time was accomplished by the biomass concentration (X, g l^{-1}) that can be used to estimate maximum specific growth rates (μ, d^{-1}), biomass doubling time (td, d), maximum biomass concentration (X_{max} , g l^{-1}) and volumetric biomass productivities (P, g l^{-1} d^{-1}) for each cultures.
Specific growth rate, μ (day^{-1}) was estimated from Eq.(1) **Chiu et al., 2009.**

$$\mu = \frac{Ln\frac{X_t}{X_o}}{\Delta t} \tag{1}$$

Where X_t and X_0 are dry biomass concentrations (g l^{-1}) respectively during the exponential logarithmic growth phase, and Δt is the cultivation time in the day during the exponential logarithmic growth phase **Ketheesan and Nirmalakhandan, 2012.**

Doubling time (td, d) was calculated from Eq. (2)

$$t_d = \frac{Ln\,2}{\mu} \tag{2}$$

Biomass productivity, P (dry g l^{-1} day^{-1}) in batch mode was estimated from the variation in biomass concentration within the cultivation time (day) according to Eq. (3) **Ryu et al, 2009.**

$$P = \frac{(X_t - X_o)}{t} \tag{3}$$

Where X_t is the dry biomass concentration (g l^{-1}) at t (day) and X_0 is the dry biomass concentrations at inoculation **De Morais and costa, 2007a**.

According to the method described by **Ketheesan and Nirmalakhandan, 2012,** the carbon dioxide biofixation rate F_{CO2}, (g_{CO2} day^{-1}) can be estimated from Eq. (4)

$$F_{CO2} = a\ P\ V_C \qquad (4)$$

Where P is the biomass productivity of the culture (g l^{-1} d^{-1}), V_C is the culture volume in liter and (a) is the mass of CO_2 fixed in unit biomass which calculated by Eq. (5)

$$a = Cc\ (M_{CO2}/\ M_C) \qquad (5)$$

Where Cc is the carbon content of the dried microalgae biomass (g carbon (g biomass)$^{-1}$), since 50% of carbon content in the dry biomass **Becker, 1994**, M_{CO2} is the molecular weight of CO_2 and M_C is the molecular weight of Carbon.

4. RESULTS AND DISCUSSION

Chlorella vulgaris growth was investigated in airlift bioreactor to determine the photosynthetic efficiency in this reactor. According to the suggested experimental design, two experiments were carried out to estimate the aeration effect on *Chlorella* growth at constant temperature and illumination.

Effect of aeration on growth of microalgae

In the first experiment, *Chlorella* was cultivated in batch airlift bioreactors. The sparging system was carried out using ambient air enriched with 5% pure CO_2 and the results were compared with no aeration culture (unsparged bioreactor). **Fig.4** shows the growth curves for *Chlorella vulgaris* cultivation. From this figure, it can be seen that the algae cells have a close biomass concentration during the first day (lag phase) in reactor sparging with CO_2. After adaption, cells began good growth during the experiment culture. Whilst, cells cultivated in control reactor took a long period for adoption. The maximum biomass concentration was obtained from a culture aerated with 5% CO_2. The cell concentration recorded about 0.36 (g l^{-1}) after 11 days. While, the growth rate with absence of aeration (control) has no significant increase, and maximum concentration of the cells was about 0.069 (g l^{-1}) at 10^{th} day then began inhibited.

In the second experiment, *Chlorella* was also cultivated in batch airlift bioreactors. But, one of the bioreactors was sparged with ambient air enriched with 5% pure CO_2, while the other bioreactor was sparged with ambient air only for the same period of sparging (28 min) in both reactors.

Fig.5 shows the growth curve of *Chlorella* cells aerated with air enriched with 5% CO_2. It has the same behaviour of that in the first experiment except the adaption period, although the experiments were carried out at a different time. This gives a kind of credibility the results of those experiments.

However, in the first experiment culture, the microalgae cells require one day for adaption, while in the second experiment, the response displayed no adoption (lag phase). This behaviour was because the stock cultures already were maintained under 5% CO_2. **Schimidell et al., 2001** demonstrated that when the inoculums culture are maintained under different conditions from those used in the cultivation runs, the adaptation (lag) phase probably will be long. But it absents when the conditions are similar. **Yun et al., 1997** also checked that acclimatization of the inoculum is important and found that when stock cultures of *Chlorella vulgaris* were maintained under air, it grew less well in media containing 15% (v/v) additional CO_2, but when the inoculum was grown under air supplemented with 5% CO_2, it grew better in culture media containing 15% additional CO_2 than it did in media containing 5% CO_2.

As can be seen from the **Fig. 5**, *Chlorella* cells also reached to the 0.359 g l^{-1} as maximum biomass concentration in 11 day under aeration with 5% CO_2, which is approximately the same result obtained in the first experiment. While the growth rate without any addition of CO_2 only atmospheric air, the growth rate was slow. The microalgae biomass concentration reached to 0.056 g l^{-1} at 3rd day and remained stable at this value for few days then increased slowly to reach maximum concentration (X_{max}) 0.083 g l^{-1} at 11th day to be double concentration compared with its inoculum. The important kinetic parameter for *Chlorella* cultivate in both experiment are summarized in **Table (1).**

The experimental data showed higher maximum specific growth rate, maximum biomass concentration, maximum biomass productivity and minimum doubling time under culture with CO_2 enrichment with 5% CO_2 for both experiments. The highest value of specific growth rate was (0.39 day^{-1}) while the lowest value of specific growth rate was (0.17 day^{-1}) for *Chlorella* species cultivated with 0.036% of CO_2 in ambient air. Whereas, no significant value in specific growth for control because of the very slow growth and unobtainable exponential phase. In addition, the shortest biomass doubling time (td, day) was 1.7 day at 5% CO_2 aerated, while the longest td was 3.9 days at ambient air aerated as a notice in **Table 1.** Therefore, as maximum growth rate increased, biomass doubling time decreases and cultivation becomes more economically sustainable. So microalgae can duplicate their biomass in less than 7 days, whereas higher plants take many months or years **Vonshak et al., 1982**. In this study, the doubling time was equal to or less than 4 days.

The productivity (g l^{-1} per day) of *Chlorella* species cultivated under 5% CO_2 for both experiments reached to the maximum value of 0.031 (g l^{-1} per day), while 0.0077 (g l^{-1} per day) was obtained for culture aerated with air only. The 0.0036 (g l^{-1} per day) which is the maximum value was obtained per day for control.

Fig.6 shows the photographic view of algae cultivation in the two experiments. It can be seen that there is significant difference between the cultures using high concentration of CO_2 and the ambient air or control in the present study.

The results in this study are approximately similar to other studies that cultivated *Chlorella* species in photobioreactor under aeration of 5% CO_2, for example; **Chiu et al., 2008** found when *Chlorella* sp. cultivate under 5% CO_2 with continuous aeration and illumination the specific growth rate was (μ_{max}= 0.34 day^{-1}) and cell dry weight was (X_{max}= 0.899 g l^{-1}) for high density inoculum about ($8x10^6$cells ml^{-1}). While, he obtained (X_{max}= 0.062 g l^{-1}) as cell dry weight and (μ_{max}= 0.127 day^{-1}) for low-density inoculum about ($8x10^5$cells ml^{-1}). **De Morais and Costa, 2007a, b** found that the best kinetics of *Chlorella* is (μ_{max}= 0.31 day^{-1}) and doubling time is (td=2.27 day). The maximum productivity was (P_{max}= 0.14 g l^{-1} per day) for *Chlorella* cultivated under 6% CO_2 for 15 min in every hour during the illumination with 12 hr light / 12 hr dark photoperiod.

Effect of aeration on carbon dioxide biofixation

Dissolved carbon dioxide and fixation by microalgae through the photobioreactor was detected during each experiment. From the previous studies it depended on the law of material conservation. It allows for calculating carbon dioxide biofixation rate from estimation the microalgae biomass production rate (g l^{-1} d^{-1}). In which, the carbon content of the biomass (g_{CO2} /g biomass) approximately ranges from (0.5 - 0.57). Some of calculations were conducted using a report biomass molecular formula ($CO_{0.48}$ $H_{1.83}N_{0.11}P_{0.01}$) **Chisti, 2007.** These calculations were used when direct biofixation rate of CO_2 was not available, which is based on the assumption that biofixation rate of CO_2 in the form of extracellular products was negligible.

In this study, CO_2 biofixation rate was determined according to the method described in **Becker, 1994** that is similar to use by other researchers i.e., **Ho et al., 2010 and Tang et al., 2011.** It was found that the fixation rate of CO_2 resulted in high value when CO_2 concentration increased in air. As shown in **Table 1.**, the maximum biofixation rate of CO_2 was (0.28 g_{CO2}/day) observed at 5% CO_2 when 5L culture sparged with 28 min per day at a rate of 200 ml/min. While it was (0.069 g_{CO2}/day) when the ambient air was contained approximately 0.036% of CO_2.

A good similarity was noticed between the values obtained from this study and the values from the following researchers; **Tang et al., 2011** found that CO_2 fixation rate was (0.244 g_{CO2}/day) for *Chlorella* cultivated in 1L Erlenmeyer flask when continuously aerated with 5% CO_2 enriched air. Whereas, he found the fixation rate was (0.134 g_{CO2}/day) for culture continuously aerated with 0.036% CO_2., **Sydney et al., 2010** found CO_2 fixation rate was (0.251 g_{CO2} /day) for *Chlorella vulgaris* cultivated in 8 L working volume continuously aerated with 5% CO_2.

Some researchers had other results of CO_2 fixation rate for *Chlorella* cultivated such as; **Ryu et at., 2009** who found CO_2 fixation rate was (0.35 g_{CO2}/day) for *Chlorella* species cultivated with 5% CO_2 concentration in 600 ml bioreactor under continues aeration, **Lv et al., 2010** recorded CO_2 fixation rate (0.6 - 1.2) at maximum value in 5L photobioreactor aerated with hollow fiber membrane sparging with 0.5% CO_2; And **Scragg et al., 2002** who found the biofixation of CO_2 for *Chlorella* aerated at ambient air at 25 ^{0}C was (0.04 g l^{-1} per day) and (0.024 g l^{-1} per day) in Wayamba's media and Low N medium respectively.

Photosynthetic activity of the culture medium containing *Chlorella* cells was determined by pH and dissolved oxygen (DO) monitoring. Both of measurements were carried out daily before and after dosing of air enriched with 5% CO_2 or with air only (without bubbling).

Effect of aeration on pH of the culture

As can be seen in **Fig. 7** and **Fig. 8**, the behaviour of culture curves aerated with 5% CO_2 are the same. The periodical supplement of CO_2 to the culture resulted in almost steady pH level in the target region (6.18 – 9.02) without the use of expensive buffer and the periodic dosing made pH controlled in the expected range. So this results in a potential for both energy and economic saving. While for the culture aerated by air only a gradual increase in PH was noticed and this increased caused algae inhabitation as noticed in **Fig. 8**. Commonly, as microalgae growth, the pH in the culture increased due to cellular metabolism which converted CO_2 uptake through photosynthesis to the carbonic acid (H_2CO_3), then the last was dissociated into bicarbonate (HCO_3^{-1}) of the medium. CO_2 is uptake by microalgae metabolism at a rate depending on the activity of the photosynthesis, which itself depended on the light activity. This causes increasing in associate to H^+ ion and increasing in pH, but as a consequence of pH increasing (CO_3^{-2}) increased also. When HCO_3^{-1} and CO_2 decreased causes photosynthetic reaction inhabitation and the approximately of the algae trichomes and (OH^-) ion are formed making pH become more alkaline which improves the rate of algae respiration **Steenman, 1975; Fox, 1996.** Therefore the many algae cultures need to use buffer or acid added when pH of culture increased over the suitable level via an auto-controlled culture.

In this study neither acid nor buffer was added because it was expected that the increasing pH could be neutralized by daily CO_2 supply by dosing technique. While noticing the pH of control culture also increased very slowly continually until the 10^{th} day with its dry weight increased from 0.03g l^{-1} to only 0.06 g l^{-1} as a record in **Fig. 4** .Corresponding , its pH also increased slowly and rising from (7 - 8.32) as shown in **Fig. 7**. Then, when pH values not changes, this means the algae began died. The culture aerated only air also grew slowly to reaches a maximum value at 9^{th} day with its dry weight increased from (0.03 g l^{-1} to 0.074 g l^{-1}) as seen in **Fig. 4**. Correspondingly, its pH increased slowly from (7- 9.2) as shown in **Fig. 8**. However, after 9 days the pH barely increased and was maintained at (9.21 - 9.25). Whilst the algae almost stopped growing as well, with the cell dry weight (0.07 - 0.083 g l^{-1}) because of absence CO_2 supplied and O_2 accumulation in the culture can cause adverse effects on the growth of alga. The reasons are that; after pH went above 9 value, the culture of microalgae was inhibited because for most type of microalgae the suitable pH ranges from 6 to 9 **Coutteau, 1996.** And over this ranges inhabitation in growth occurs.

In the culture aerated by air enrichment with 5% CO_2, the cell dry weight increased dramatically from a range (0.03 – 0.36) g l^{-1} during the experiment culture, the corresponding pH was assumed to rise even faster than the culture aerated with air only or the control culture. However, due to dosing daily so the pH of the culture maintained in a suitable range. As can be seen from **Fig. 7** and **Fig. 8**, the pH values from a range (7.89 - 9.02) as heights value before dosing to the range (6.16 - 6.18) as low value after 28 min of CO_2 dosing daily. Because of the desirable culture condition (CO_2 unlimited and O_2 free), the pH value reduced to this range then returned to increase back to about (7.89 - 8.34) within only one day ago. The next day, another 28 min of dosing dragged it back to around the range (6.16 - 6.18) again. Such a virtuous cycle kept pH within a desirable range, making the culture also not limited by pH. Therefore these results indicate that the increasing CO_2 concentration led to improving algae biomass productivity.

Effect of aeration on DO of the culture

Dissolved oxygen (DO) also was determined through the experiments culture in airlift photobioreactor. It is a point to photosynthesis activity. During the lighting process, microalgae metabolism occurs as a result of photosynthetic generation, in which the oxygen concentration increases steadily. While carbon dioxide disbursed by microalgae and reached to saturation state with culture medium, this causes dissolving level dropped steadily and DO rejected through metabolism. In addition, the initial O_2 value was generated in the culture through which air bubbled.

Fig. 9 and **Fig. 10** show the daily values of DO measurement for both experiments. As noticed from **Fig. 9** there is no change for control culture curve and the DO stay stable through the run. This refers to low photosynthesis activity as a result of no aeration occurs. While in another culture when air aerated which made mixing in the reactor and decreases in the DO value. Through the culture runs, air enriched with 5% CO_2 dosing periodically at 28 min per day found decreases of DO in a suitable range from (20.1 – 22.9 mg l^{-1}) as highest value before dosing to (8.24 – 8. 9 mg l^{-1}) as low value after dosing daily. This process kept the DO in the culture safety. Increasing the microalgae biomass through the culture aerated with 5% CO_2, resulted of consequently increased accumulation of the DO in culture, as shown in **Fig 9** and **Fig 10**. Whilst, the reactor culture when aerated with air only, DO values range from (12.2 -15.6 mg l^{-1}) as highest value before dosing to (8.35 – 8.76 mg l^{-1}) as low value after dosing daily. Whereas, DO of the control culture recorded as increased from (12.4 to 13.9 mg l^{-1}) during the cultivation experiment. This slowly increased occur due to the low growth of the cells without aeration. In addition, the mixing of culture efficiently by bubbling air is very important for microalgae cultivation in a closed reactor, because the high elevated dissolved oxygen concentration level can lead to severe photo-oxidation which damage microalgae cells and causes decreasing the treatment efficiency **Oswald, 1988; Lee and Lee, 2003; Richmond, 1991.** For instance, oxygen level above air saturation (0.2247 mole O_2 m^{-3}) could inhibit photosynthesis in many microalgae species, even if carbon dioxide concentration is maintained at elevated levels **Aiba, 1982.** Generally, the mixing not only reduces the DO in microalgae cultures but also ensures good mass transfer of carbon dioxide and oxygen in the culture system **Ugwu et al., 2007.**

5. CONCLUSIONS

The present article studied the behavior of *Chlorella vulgaris* microalgae in airlift photobioreactor. The growth rate and biomass production was experimentally achieved with *Chlorella vulgaris* culture in airlift photobioreactor. The airlift bioreactor as draft tube proved promising technology for obtained optimal mixing. Moreover, the designed system has successfully shown ability to sequester CO_2 from airstream containing 5% CO_2 concentration. As well, the *Chlorella vulgaris* has very effective to quantitatively remove CO_2 from an elevated CO_2 airstream in laboratory bioreactor. The main results showed higher growth rate and biomass production can be achieved if the sparging system was 5% CO_2/Air compare with air only. For example, maximum growth rate was (0.39 d^{-1}) and maximum cell concentration was (0.36 g l^{-1}). While with sparging air, the maximum growth is (0.17 d^{-1}) with (0.038 g l^{-1}) cell concentration.

In addition, this study showed the high CO_2 biofixation potential by *Chlorella vulgaris* microalgae was 0.28 g_{CO2} per day. The periodic dosing strategy of CO_2 is proposed for *Chlorella* cultivation as well. Daily 28 minutes of 5% CO_2 enriched with airstream supplement to the culture maintained pH at a suitable level (6.18 - 8.3) without using any expensive buffer for adjustment the pH value. Removal of oxygen from the culture was investigated in the current study. The aeration system decreases the DO concentration of the culture in a suitable range from (22 mg l^{-1} to 8.29 mg l^{-1}) after periodically dosing daily.

6. ACKNOWLEDGEMENT

The authors like to express sincere gratitude to Prof. William Zimmerman in University of Sheffield, UK; Dr. Stephen J. Wilkinson (Chester University, UK), and Dr. Hemaka Bandalusena (Loughborough University, UK) for their invaluable academic guidance. The authors are also grateful to College of Science / Department of biology, for their scientific support for this research work. In addition, they also thankful to the department of chemical engineering in Baghdad University.

7. REFERENCES

- Abed, I.J., AL-Hussieny, A.A., Kamel, R.F., and Jawad, A.M., 2014, *Environmental and Identification study of algae present in three drinking water plants located on Tigris River in Baghdad*. International Journal of Advanced Research, Vol. 2, PP.895-900.
- Aiba, S., 1982, *Growth kinetics of photosynthetic microorganisms*, Journal Advance Biochemical Engineering, Vol. 23, PP.85–156.
- AL-Mashhadani, M. K.H., Wilkinson, S. J., and Zimmerman, W.B., 2015, *Airlift bioreactor for biological applications with microbubble mediated transport processes*, Chemical Engineering Science, 137, PP. 243–253.

- Ammar, S.H., 2016, *Cultivation of microalgae chlorella vulgaris in Airlift photo- bioreactor for Biomass Production using commercial NPK Nutrient*, Al-Khwarizmi Engineering Journal, Vol. 12, No. 1, PP. 90-99.
- Amaro, H.M., Guedes, A.C., and Malcata, F.X., 2011, *Advances and perspectives in using microalgae to produce biodiesel*, Applied Energy 88, PP. 3402-3410.
- Becker, E.W., 1994, *Microalgae: Biotechnology and Microbiology*, first ed. Cambridge University Press, New York.
- Carvalho, J. R.M., Vargas, J.V.C., Ramos, L.P., Marino, C.E.B., and Torres, J.C.L., 2011, *Microalgae biodiesel via in situ methanolysis*, Journal of Chemical Technology and Biotechnology 86, PP.1418-1427.
- Chisti, Y., 2007, *Biodiesel from microalgae*, Biotechnology Advances 25, PP.294-306.
- Chiu, S.Y., Kao, C.Y., Chen, C.H., Kuan, T.C., Ong, S.C., and Lin, C.S., 2008, *Reduction of CO2 by a high-density culture of Chlorella sp. in a semicontinuous photobioreactor*, Bioresour Technology 99, PP. 3389–3396.
- Chiu, S.Y., Kao, C.Y., Tsai, M.T., Ong, S.C., Chen, C.H., and Lin, C.S., 2009, *Lipid accumulation and CO2 utilization of Nannochloropsis occult in response to CO_2 aeration*. Bioresour Technology 100, PP.833–838.
- Clarens, A.F., Resurrection, E.P., White, M.A., and Colosi, L.M., 2010, *Environmental life cycles comparison of algae to other bioenergy feedstock*. Environmental Science and Technology 44, PP.1813-1819
- Coutteau, P., 1996, *Micro-Algae," In: P. Lavens and P. Sorge- loos, Eds., Manual on the Production and Use of Live Food for Aquaculture*, FAO Fisheries Technical Paper No. 361, Laboratory of Aquaculture and Artemia Reference Center, University of Gent, Belgium.
- Costa, J.A.V., and De Morais, M.G., 2011, *The role of biochemical engineering in the production of biofuels from microalgae*, Bioresource Technology 102, PP.2-9.
- De Morais, M.G., and Costa, J.A., 2007a, *Isolation and selection of microalgae from coal fired thermoelectric power plant for biofixation of carbon dioxide*, Energy Conversion Management 48, PP. 2169–2173.
- De Morais, M.G., and Costa, J.A., 2007b, *Carbon dioxide fixation by Chlorella kessleri, C. vulgaris, Scenedesmus obliquus and Spirulina sp. cultivated in flasks and vertical tubular photobioreactors*, Biotechnology Lett. 29, PP.1349–1352.
- Demirbas, H.A., 2010, *Biofuels for future transportation necessity*, Energy Education Science Technology, Part A; 26, PP. 13-23.
- Demirbas, A., and Demirbas, M.F., 2011, *Importance of algae oil as a source of biodiesel*, Energy Conversion and Management 52, PP. 163-170.
- Demirbas, A., 2011, *Biodiesel from oilgae, biofixation of carbon dioxide by microalgae: a solution to pollution problems*, Applied Energy 88, PP.3541-3547.
- Filali, R., Tebbani, S., Dumur, D., Diop, S., Isambert, A., Pareau, D., and Lopes, F., 2011, *Estimation of Chlorella vulgaris growth rate in a continuous photobioreactor*, Preprints of the 18th IFAC World Congress Milano (Italy) August 28-September 2.
- Fox, R.D. 1996, *Spirulina production and potential. France: Edisud* .; ISBN 2-84744-883.
- Gutierrez, R., Gutierrez, S. R., and Nafidi, A., 2008, *Trend analysis using nonhomogeneous stochastic diffusion processes*. *Emission of CO_2*, Kyoto protocol in Spain. Stoch. Environment Resource Risk Assess. 22, PP. 57-66.

- Ho, S.H., Chen, W.M., and Chang, J.S., 2010, *Scenedesmus obliquus CNW-N as a potential candidate for CO2 mitigation and biodiesel production*. Bioresource Technology 101, PP.8725 8730.
- Harrington, L., and Foster, R.,1999, *Australian residential building sector greenhouse gas emissions 1990–2010*. Final Report, Energy Efficient Strategies. Australian Greenhouse Office.
- Jeong, M.L., Gillis, M.J. and Hawng, J.Y., 2003, *Carbon dioxide mitigation by microalgae photosynthesis* . Bull. Korean Chem.Sco.24, 12, PP. 1763-1766.
- Kecebac, A., and Alkane , MA., 2009, *Educational and consciousness-raising movements for renewable energy in Turkey* . Energy Education Science Technology Part B,1 , PP. 157-170 .
- Ketheesan, B., and Nirmalakhandan, N., 2012, *Feasibility of microalgal cultivation in a pilot-scale airlift- driven raceway reactor*, Bioresource technology 108, PP.196 - 202.
- Kondili, E.M., Kaldellis, J.K., 2007, *Biofuel implementation in East Europe: Current status and future prospects. Renew*, Sust. Energy. Rev. 11, PP.2137-2151.
- Lee, J.S. and Lee, J.P., 2003, *Review of advances in biological CO2 mitigation technology, Biotechnol*. Bioproc. E 8 , PP. 259–354
- Lee, J.-Y., Yoo, C., Jun, S.-Y., Ahn, C.-Y., and Oh, H.-M., 2010, *Comparison of several methods for effective lipid extraction from microalgae*, Bioresource Technology 101, PP. S75-S77.
- Liu, L. U., 1994, *The net environmental Effects of Carbon Dioxide Reduction polices*, Master of Science Thesis in Technology and Policy at the Massachusetts Institutes of Technology.
- Lv, J.M., Cheng, L.H., Xu, X.H., Zhang, L., and Chen, H.L., 2010, *Enhanced lipid production of Chlorella vulgaris by adjustment of cultivation conditions*, Bioresource Technology 101, PP.6797–6804.
- Mercer, P., Armenta, R.E., 2011. Developments in oil extraction from microalgae. European Journal of Lipid Science and Technology 113, 539-547.
- Mohd, Y.A.Y., Hassan, J.M.B., Ashikeen, N. M., Sabuddin, R., Muda, R. A., Sulaiman, S., Makpol, S. and Wan, W.Z.N., 2011, *Fatty acids composition of microalgae Chlorella vulgaris can be modulated by varying carbon dioxide concentration in outdoor culture*. African Journal of Biotechnology Vol. 10, No. 62, PP. 13536-13542
- Morita, M., Watanabe Y., and Saiki H., 2000, *Investigation of photobioreactor design for enhancing the photosynthetic productivity of microalgae*. Biotechnology Bioenergy, 69, PP,693-698.
- Oswald, W.J., 1988, *Micro-algae and waste-water treatment. In: M.B.L. Borowitzka, Editor, Micro-algal Biotechnology*, Cambridge University Press, Cambridge , pp. 305–328.
- Ozkurt, I., 2009. *Qualifying of safflower and algae for energy*. Energy Educ. Sci. Technol. Part A;23, PP.145-151 .
- Pedroni, P., Davison, J., Beckert, H., Bergman, P., and Benemann, J., 2001, *A proposal to establish an international network on bio-fixation of CO_2 and greenhouse gas abatement with microalgae*. Journal of energy and environmental research 1(1), PP.136-150.
- Ranjan, A., Patil, C., Moholkar, V.S., 2010. *Mechanistic assessment of microalgal lipid extraction*. Industrial and Engineering Chemistry Research 49, PP. 2979-2985.

- Richmond A., 1991, *Large scale microalgal culture and applications*. In: Round FE and D.J. Chapman DJ, editor. Progress in phycological research. Bristol: Biopress. Ltd., Bristol.Vol.7. PP 269–330.
- Richmond, A., 2008 , *Handbook of Microalgal Culture technology and Applied Phycology*, Wiley-Blackwell, New York.
- Ryu, H.J., Oh, K.K., Kim, Y.S., 2009, *Optimization of the influential factors for the improvement of CO_2 utilization efficiency and CO_2 mass transfer rate*. Journal Industrial Engineering Chemical 15, PP.471–475.
- Roman, L.,Y., Barrett, C.J., Liu, Z.Y., and Dumesic, J.A., 2007, *Production of dimethylfuran for liquid fuels from biomass-derived carbohydrates*. Nature. 447, PP.982-985.
- Schmidell, W., Lima, A.U., Aquarone, E., and Borzani W., 2001, *Industrial biotechnology*, vol.2. Sa˜o Paulo: Edgard Blucher LTDA.
- Scragg, A.H., Illman, A.M., Carden A. and Shales, S.W., 2002, *growth of microalgae with increased calorific values in a tubular bioreactor*. Biomass Bioenergy, 23, PP. 67–73.
- Steenman, N. E., 1975, *Marine Photosynthesis with Special Emphasis on the Ecological Aspects*, Elsevier Scientific Publishing Co., New York.
- Sydney, E. B., Sturm, W., De Carvalho J. C., Thomaz, S. V., Larroche, C., Ashok P. D., and Ricardo, C. S., 2010, *Potential carbon dioxide fixation by industrially important microalgae*. Bioresource Technology 101, PP. 5892–5896
- Tang, D., Han, W., Li, P., Miao, X., Zhong, J., 2011, *CO_2 biofixation and fatty acid composition of Scenedesmus obliquus and Chlorella pyrenoidosa in response to different CO2 levels*. Bioresource Technology 102, PP. 3071–3076.
- Ugwu, C.U., Aoyagi, H. and Uchiyama, H., 2007, *Influence of irradiance, dissolved oxygen concentration, and temperature on the growth of Chlorella sorokiniana*. Photosynthetic, Vol. 45, No.2, PP. 309-311.
- Vonshak, A., Abeliovich, A., Boussiba, A., Arad, S, and Richmond, A., 1982, Production of Spirulina Biomass: Effects of Environmental Factors and Population Density, Biomass Journal, Vol. 2, PP.175–85.
- Ying, K., Al- Mashhadani, M., K. H., James, O. H., Daniel, J. G. and Zimmerman ,W. B., 2013, *Enhanced Mass Transfer in Microbubble Driven Airlift Bioreactor for Microalgal Culture*. Engineering, Vol. 5, PP. 735-743.
- Yun, Y.S., Lee, S.B., Park, J.M., Lee, C.I., and Yang, J.W., 1997, *Carbon dioxide fixation by algae cultivation using wastewater nutrients*, Journal Chemical Technical Biotechnology, 69, PP. 451–5.

8. NOMENCLATURE

a	mass of CO_2 fixed in unit biomass
Cc	carbon content of the dried microalgae biomass, (g carbon (g biomass)$^{-1}$)
d	day
F_{CO2}	carbon dioxide biofixation rate, (g_{CO2} day^{-1})
M_{CO2}	molecular weight of CO_2, (g gmol^{-1})
M_C	molecular weight of Carbon, (g gmol^{-1})

P	biomass productivity, (g l^{-1} d^{-1})
P_{max}	maximum volumetric productivity, (g $l^{-1}d^{-1}$)
t	time, (day)
td	doubling time, (day)
V_C	culture volume, (L)
X_t	biomass concentration at any time t, (g l^{-1})
X_0	biomass concentration at the inoculation, (g l^{-1})
X_{max}	maximum biomass concentration, (g l^{-1})
μ_{max}	maximum specific growth rate, (day^{-1})
Δt	the cultivation time in day during the exponential growth phase

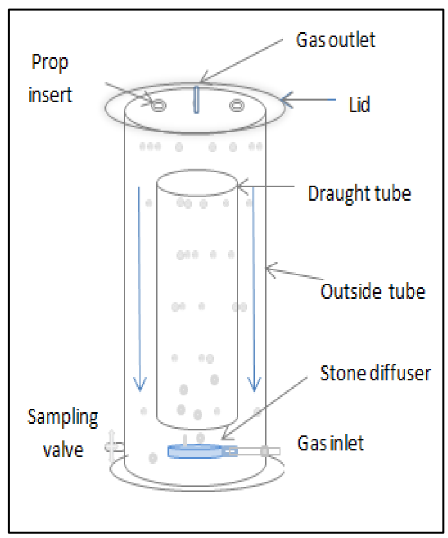

Figure 1. The structure of airlift loop bioreactor**.**

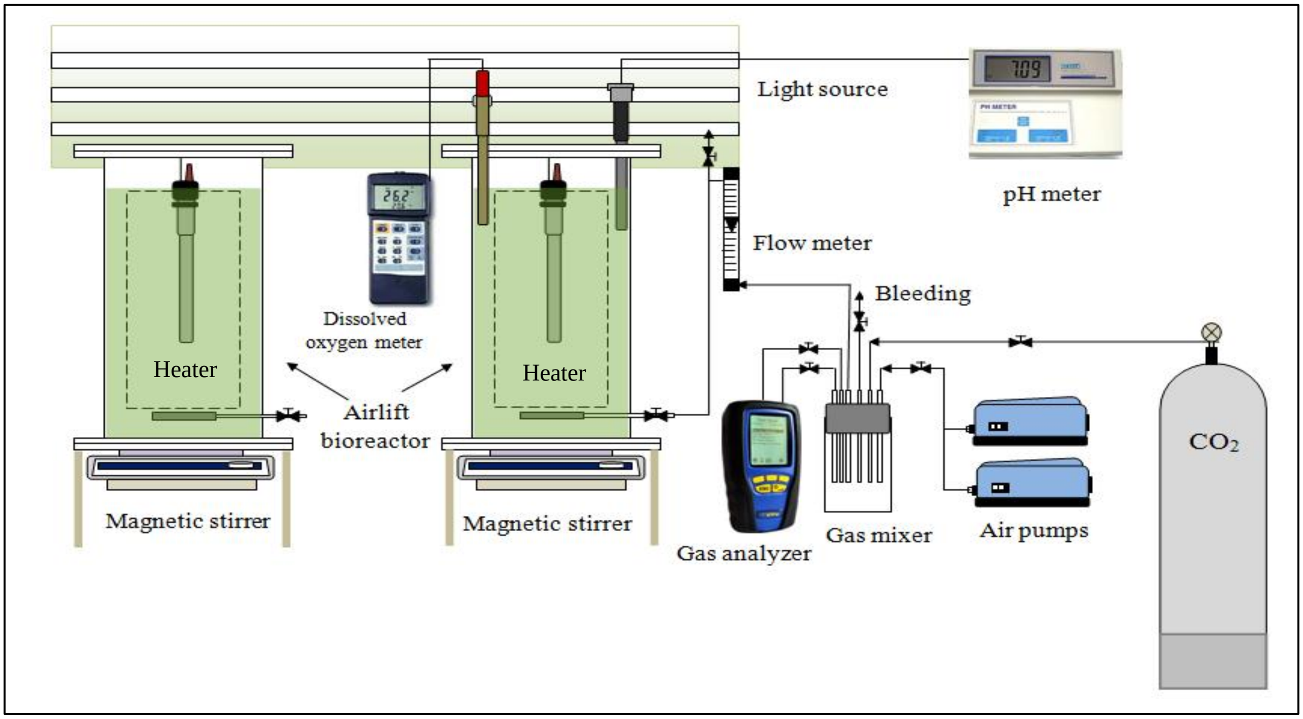

Figure 2. Schematic diagram of the photobioreactor setup.

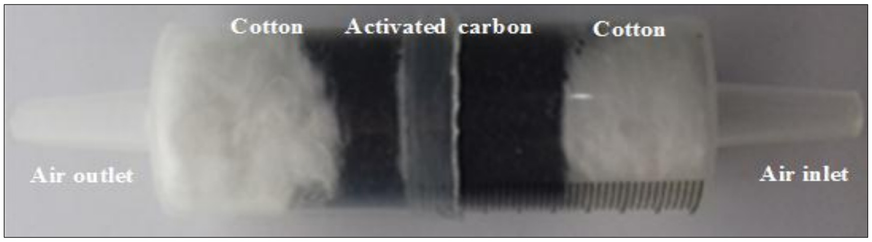

Figure 3. Aeration filter used in avoiding contamination in the airlines.

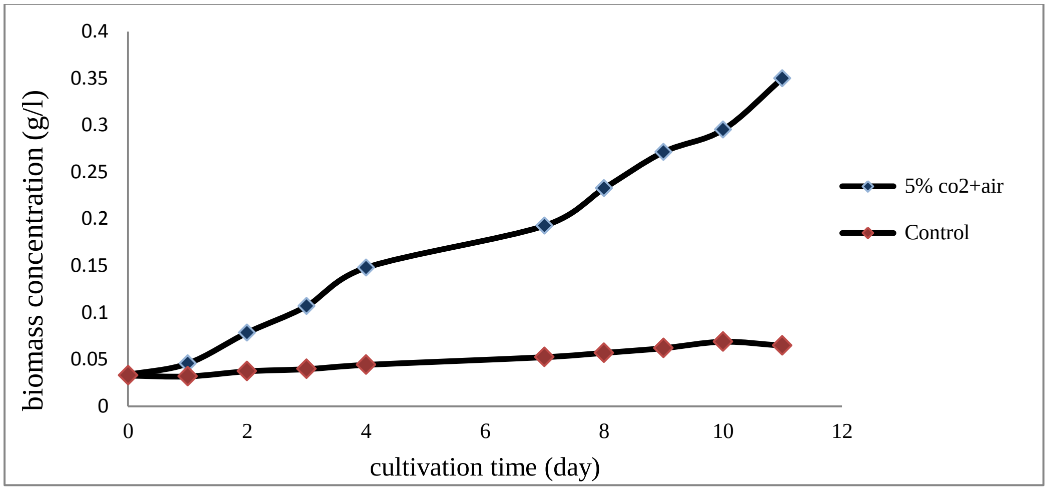

Figure 4. Effect of the concentration of CO_2 sparging on the growth of *Chlorella vulgaris*. The culture was inoculated with 0.033 gl^{-1} of microalgae cell approximately and cultivate without aeration (control), air enriched with 5% CO_2 bubbled at 200 ml/min for 28 min per day under continues illumination and 30 ^{0}C temperature.

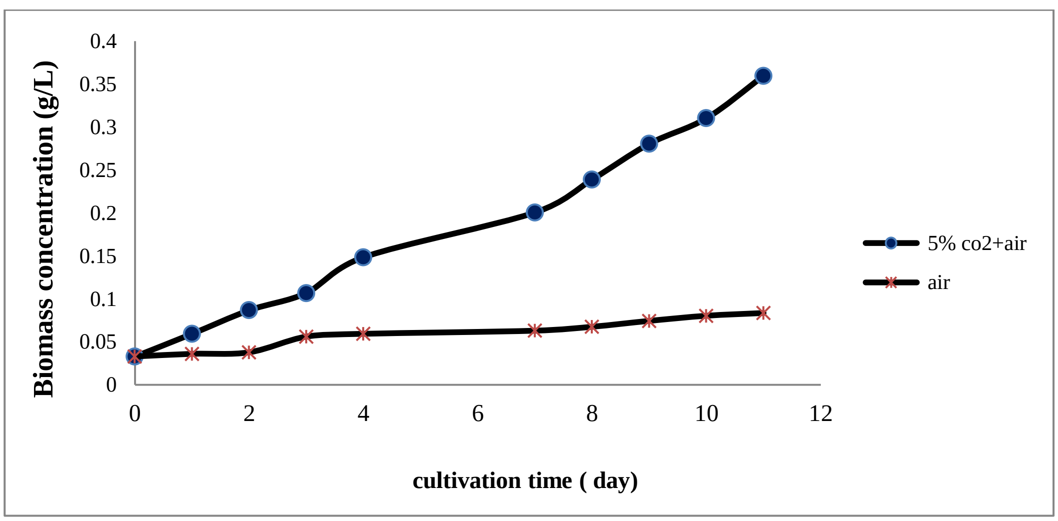

Figure 5. Effect of the concentration of CO_2 aeration on the growth of *Chlorella vulgaris* .In the culture approximate 0.033g l^{-1} of microalgae cell was inoculated and cultivate under atmospheric air, air enriched 5% CO_2 bubbled at 200 ml/min for 28 min per day under continues illumination and 30 ^{0}C temperature.

Table1. Maximum specific growth rate (μmax, d^{-1}), doubling time (td. d), Maximum biomass concentration (g l^{-1}/d) and CO_2 fixation rate (FCO2, g_{CO2} /day) for *Chlorella vulgaris* in airlift photobioreactor.

	CO_2 aeration	μ_{max} (day^{-1})	td(day)	X_{max} (gl^{-1})	P_{max}(gl^{-1}d^{-1})	F_{CO2}(gco$_2$ per day)
Experiment(1)	Control	-	-	0.069	0.0036	-
	Air with5%CO_2	0.39	1.76	0.36	0.031	0.28
Experiment (2)	Air	0.17	3.9	0.083	0.0076	0.07
	Air with5%CO_2	0.39	1.7	0.359	0.031	0.28

(-) means no significant value obtained.

(a) (b)

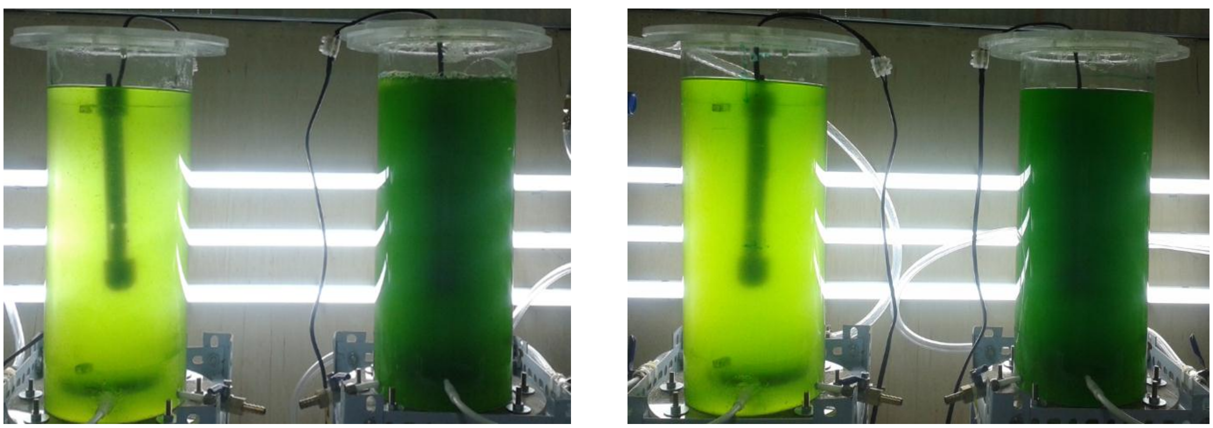

Figure 6. Photograph of cultivation *Chlorella vulgaris* in the two experiments (a) Comparision between cultivation under air enriched with 5% CO_2 and control (no aeration). (b) Exp.2. Comparision between cultivation under air enriched 5% CO_2 and ambient air only.

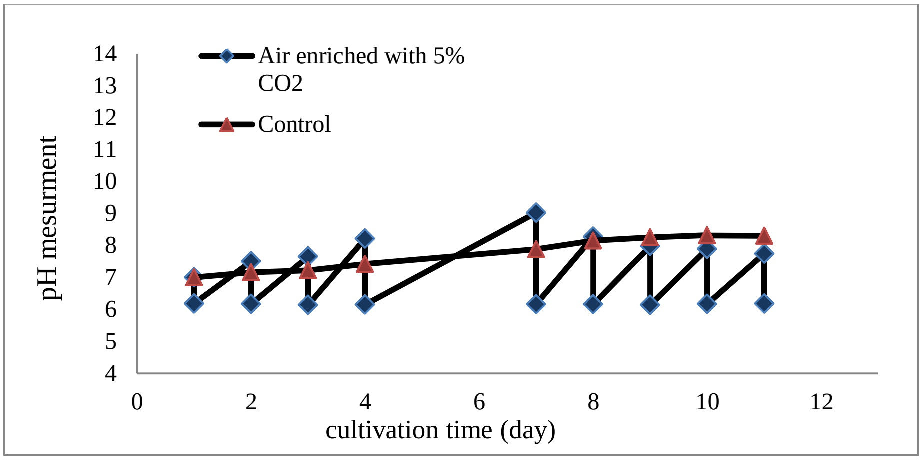

Figure 7. Daily pH values changes with culture time for *Chlorella vulgaris* supplied periodically 5% CO_2 for 28 min per day compare with control. There are two pH values per day, a higher value one and a lower value, representing the pH values before and after dosing, respectively.

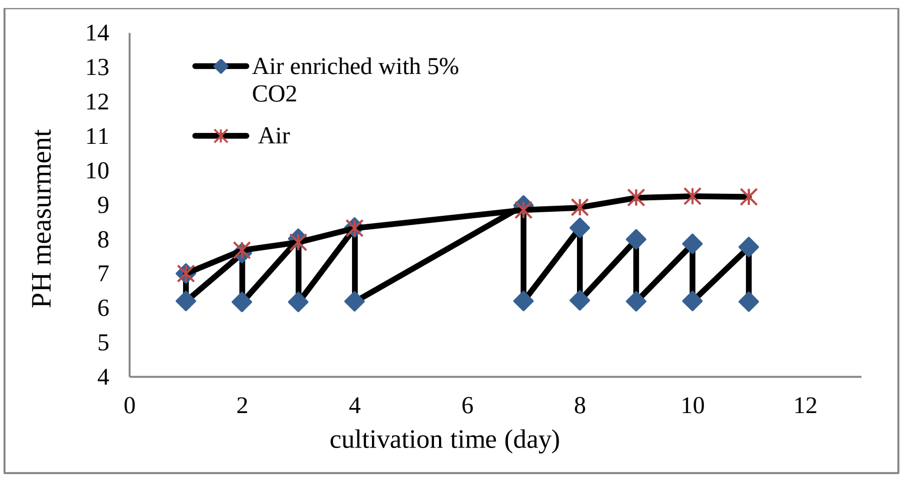

Figure 8. Daily pH values changes with culture time for *Chlorella vulgaris* supplied periodically 5% CO_2, air for 28 min per day. There are two pH values per day, a higher value one and a lower value one, representing the pH values before and after dosing, respectively.

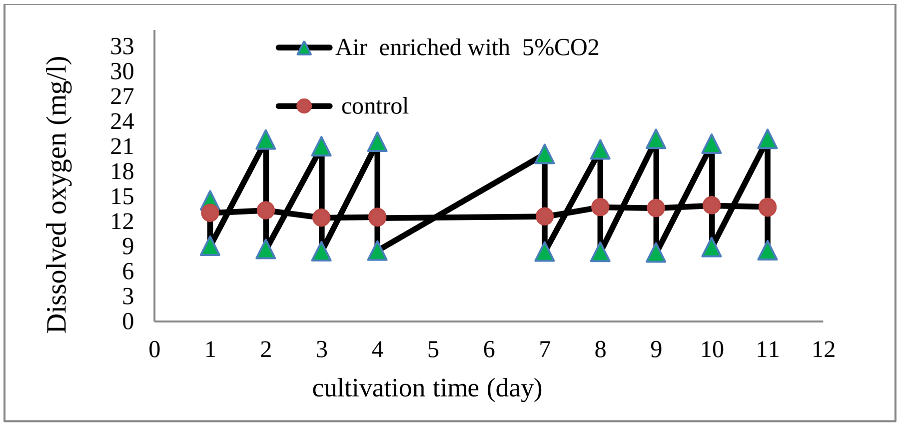

Figure 9. Daily DO values changes with culture time for *Chlorella vulgaris* supplied periodically 5% CO_2 for 28 min per day compare with control. There are two DO values per day, a higher value one and a lower value one, representing the DO values before and after dosing, respectively.

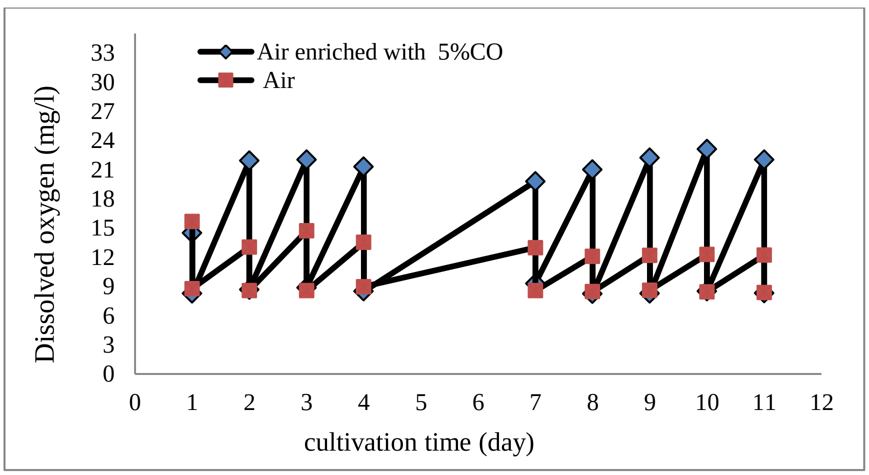

Figure 10. Daily DO values changes with culture time for *Chlorella vulgaris* supplied periodically 5%CO_2, air for 28min per day. There are two DO values per day, a higher value one and a lower value one, representing the DO values before and after dosing, respectively.

Hydraulic Analysis of the Samarra-Al Tharthar System

Mohammed Sadeq Abdulwahid Abdulridha
Ministry of Water Resource /General Commission for Maintaining Irrigation and Drainage Projects
sadikmalak@yahoo.com

Dr. Hayder A. Al Thamiry
College of Engineering \ University of Baghdad /Dept. of Water Resources
dr_hydr@yahoo.com

ABSTRACT

Low incoming discharge upstream of Samarra-Al Tharthar System leads to sediment accumulation and forming islands, especially an island upstream of Al Tharthar Regulator. This island and the sedimentation threaten the stability of the structure and reduce the efficiency of the system. This study aims to hydraulically identify the sedimentation problem mentioned above, to find solutions of how to control the sediment problems, and to develop the capacity of the system for 500 years return period flood of 15060 m^3/s. Surface Water Modeling System (SMS10.1) with two dimensional depth average models (RMA-2) software were used to simulate and analyze the system. The results of analysis showed that the maximum permissible discharge through the system was 8250 m^3/s where the discharge from Samarra Barrage was 2400 m^3/s to avoid flooding in Baghdad city. The water surface level could be lowered during constructing; the new Al Tharthar Regulator expansion capacity of 7000 m^3/s in the case of peak flood (15060 m^3/s) to 68.51 m.a.m.s.l. upstream of Samarra Barrage by dredging the island and channel. On the other hand, during constructing the guide bank, and dredging the island and channel, the water surface elevation was 68.91 m.a.m.s.l. upstream of Samarra Barrage.

Key words: Tigris River, Simulation, Flow analysis, SMS, RMA2

التحليل الهيدروليكي لمنظومة سامراء – الثرثار

الخلاصة

تسبب انخفاض الايرادات المائية مقدم منظومة سامراء- ثرثار في تراكم الترسبات وتكون الجزرات وخصوصا الجزرة المقابلة للناظم وهذه الجزر والترسبات تهدد استقرار هذا الهيكل وتقلل من كفاءة المنظومة. تمت دراسة استيعاب المنظومة وفقا لواقع الحال وكذلك الاعتماد على ثلاثة سيناريوهات اساسية في دراسة المنظومة وهي سنوات الجافة والفيضانية. وتم توظيف برنامج نظام نمذجة المياه السطحية (SMS10.1) والموديل ثنائي البعد RMA2 لإعداد نموذج رياضي ثنائي البعد يحاكي المنظومة من اجل دراسة الاداء الهيدروليكي للمنظومة خلال السنوات الفيضانية والجافة وتحري السعة الفعلية لها وايجاد الحلول اللازمة لتحسين سعة المنظومة وتطويرها لإمرار موجة فيضانية بتصريف 15060 م^3/ ثا لفترة عودة 500 سنة . من نتائج المحاكاة استنتج ان الحد الاقصى المسموح لاستيعاب المنظومة هو 8250 م^3/ ثا حيث ان التصريف المطلق من سدة سامراء 2400 م^3/ ثا لضمان عدم فيضان مدينة بغداد. وأوطأ منسوب ممكن تحققه عند انشاء ناظم توسعة الثرثار الجديد ذو سعة 7000 م^3/ ثا في حالة فيضان 15060م^3/ ثا كان 68.51 م فوق مستوى سطح البحر مقدم سدة سامراء مع كري الجزرة والقناة. وعند انشاء السدة الموجهة وكري الجزرة والقناة تعطي منسوب المياه مقدم سدة سامراء 68.91م فوق مستوى سطح البحر و 66.6م فوق مستوى سطح البحر مقدم ناظم الثرثار.

كلمات مفتاحية: نهر دجلة ، محاكاة ، تحليل الجريان ، SMS ، RMA2

1. INTRODUCTION

Iraqi rivers are considered non regime channels according to the fluctuation in their discharges and the reduction in the inflow, especially in the recent years. Low discharges cause harmful effects on the rivers, morphology through the accumulated sediment in low velocity regions, capacity of the rivers, and changing the flow pattern.

Samarra Barrage and Al Tharthar Regulator system is a multi-purpose barrage on Tigris River adjacent (West) to Samarra City and north of Baghdad, Iraq. Reduced discharges of Tigris River, the draught seasons, and the lack of rainfall with an increased need to water led to serious problems in the river. Problems like sedimentation upstream of the system and formation of islands resulted upstream of system. These islands and the sedimentation threaten the stability of this structure and reduce the efficiency of the system.

The main purpose of the system is to divert floodwater in Tigris River to Lake Tharthar through Al Tharthar Regulator, control irrigation, and power generation of 84 MW.

This system consists of Samarra Barrage, which consists of 17 gates and passes 7000 m^3/s and Al Tharthar Regulator which can divert 9000 m^3/s across 36 gates. The design capacity of the reservoir is 150,000,000 m^3 but most of that is filled with sediment.

It was built in 1956 by the German company "Zeblin" to control 16000 m^3/s peak flood flow rate. During 1969, Tigris witnessed a high flood of 15000 m^3/s at Begi City.

This study aims to identify the problem, find the required solutions, how to control the sediment problems, and also to predict the capacity of the system at 500 years return period flood of 15060 m^3/s.

Outcomes are expected to improve the flow upstream of the system, occupy flood discharge and reduce the accumulation of sediment.

Simulation will be done by using Surface Water Modeling System (SMS) with the two dimensional depth average models (RMA-2) software.

The preparation of a two-dimensional mathematical model simulates the system in order to evaluate the hydraulic performance of the system during flood, dry years, and actual capacity of the system, define the required treatments to improve the capacity of the system, develop capacity of the system to the expected 500 year return period discharge of 15060 m^3/s capacity, and define the best scenario to avoid sedimentation during dry seasons.

2. HYDROLOGY OF TIGRIS RIVER BETWEEN SAMARRA BARRAGE AND BAGHDAD CITY.

Al-Samuraie, 2004, studied the hydraulic behavior of Tigris River between Samarra Barrage Station and Sarai Station in Baghdad City. This study used discharges between 300 and 7000 cumecs. The main results of the study showed that the bank full discharge is 3175 cumecs, when released from Samara Barrage is the maximum possible discharge that could be passed through the river. Recently, the capacity of Tigris River capacity within Baghdad city is limited to 2500 m^3/s (**National Center for Water Resources Management**).

3. STUDY AREA

After the flood of 1954 which, apart from inflicting economic disaster, threatened to be a national tragedy when many cities were subjected to flood, the Ministry of development (at that time) invited consulting engineers in order to make the necessary investigations and studies for a flood control project, **Figure (1-A)**. The work at the first stage of the present Samarra–Al Tharthar scheme was inaugurated in 1956, **Figure (1-B)** with an estimated Al Tharthar lake storage capacity of 73 billion cumecs, comprising of Samarra Barrage, by which the river level can be raised sufficiently to divert flood water over the west bank of the river; a spillway formed by the construction of a dyke to prevent the water from returning to the river through which the water will flow to the depression; and a regulator to control flow onto the spillway. It is the policy of the government of Iraq to develop the water resources to the extent that all water available for irrigation will be actually used for that purpose. After the 1969 flood, Al Tharthar Project has been developed by raising the surrounding embankments in order to hold large quantities of water to prevent flood hazards ,**Ministry of Water Resource, 2003.**

3.1 Samarra-Al Tharthar System

The system is consisting of the following facilities as shown in **Fig. 2** Samarra Barrage, Al Tharthar Regulator, Tigris-Al Tharthar channel and Al Tharthar irrigation project channel. The first facility includes the irrigation gates, fish path, hydroelectric station and Al- Ishaqi regulator. The second facility includes head regulator for Al Tharthar irrigation system and Al Tharthar escape regulator. This system starts from the end of the closing dyke till the middle dyke with 252 m length from the right shoulder to the left of the facility. There are 17 vertical gates, 12*5.5 m dimensions in Samarra Barrage, power gates 14 gates, 10*12 m dimensions. 6 of them are used for the hydro-electric system now and Al Ishaqi 4 gates, 2.5*2.5 m dimensions.

3.2 The Guide Bank

In the original design of SOGREAH, there was a guide bank to direct the flow into hydroelectric station and separate Al Tharthar Regulator from Samarra Barrage. In the basic design of Samarra-Al Tharthar System there supposed to set up a barrage to guide the flow and separate Al Tharthar Regulator from Samarra Barrage. The guide bank closes the small dyke channel and determines the direction of the Tigris and the section that feeds the flow of flood to Al Tharthar Regulator. At that time, the guide bank was not build, as shown in **Fig.3**

3.3 Suggested New Expansion Regulator

It is expected that there will be flood of 500-year return period upstream Samarra Barrage with a discharge of 15060 m^3/s. For this reason, the Ministry of Water Resources decided to expand the capacity of Al Tharthar canal to attain the maximum benefit of this project by controlling flood of Tigris River. Expanding Al Tharthar Regulator is a suggestion made by the Alphurate Center for the Study and Designs Irrigation Facilities/ Ministry of Agriculture and Irrigation in 1988. It was built near Al Tharthar Regulator that exists now. It passes a discharge of 7000 m^3/s. It consists of 28 openings about 396.6 m long and about 392.7 m away from Al-Tharthar. In the case of its execution it would be with the same characteristics, **Fig4.**

4. MESH GENERATIONS

The finite element mesh was generated by using the SMS software package for the case study of Samarra-Al Tharthar System. All regions in the domain were represented by two-dimensional, depth-averaged elements. The mesh was built by using an adaptive tessellation technique for triangular elements and a patch technique for rectangular ones; the mesh consists of nodes, from which elements are generated. Each node in the mesh is described by an XYZ coordinate system. The value of X and Y indicate the position of the node with respect to some point of reference, while the Z value indicates the ground elevation (bathymetry) at that particular node.

The finite element mesh was generated to represent the case of dry year as shown in **figure (5)**. **Figures (6)** and **(7)** represent the finite element mesh for the case of flood year.

5. TOPOGRAPHY

Bathymetry data for the study site was collected in the form of XYZ coordinates by using a Leica TC 600 total station **,Center of Studies and Engineering Designs/ Ministry of Water Resources, 2013.** In order to create a numerical model, information about the topography in the study area is needed. The topography for the area upstream of Samarra-Al Tharthar System was surveyed in advance with a total station by the Ministry of Water Resource. From this survey, around 3583 scatter points were obtained with x, y, and z-coordinates. For the pre-construction situation, these points were simply converted into contour lines by using the scatter module within SMS as can be seen in **Fig.8**

6. INPUT PARAMETERS AND BOUNDARY CONDITIONS

In order to receive reliable results from the RMA2 computations, input parameter values have to be properly assigned. The input parameters in this model include the upstream boundary conditions (flow from river 1, flow from river 2, and flow from river 3), as shown is **Fig.9**, the downstream boundary condition (water surface elevation at Samarra Barrage and outflow at Al Tharthar Regulator), Manning's roughness coefficient, n, and the eddy viscosity, E, as was previously mentioned.

A summary of the boundary condition for dry and flood seasons is shown in **Tables 1.** and **(2)**, respectively. Discharge rates were recorded by the National Center for Water Resources Management in the case of dry season. The water surface elevation was considered as 67.4 m.a.m.s.l. at Al Tharthar Regulator as an operation water level upstream of the control structures in all scenarios for dry year and 69 m.a.m.s.l. for flood year.

7. SCENARIOS OF THE SYSTEM

The study was divided into three main categories according to inflow as:

A- Dry season.
B- Flood season with discharges of 10400 and 11400 m^3/s according to actual situation.
C- Flood season with a discharge of 15060 m^3/s, according to 500-year return period flood.

The adopted treatments for each of the above categories are based on the following items:

1. Dredging of the channel and total or partial dredging of the island upstream of Al Tharthar Regulator to elevation 60 m.a.m.s.l. for the island area and a level of 62 m.a.m.s.l. for Al Tharthar channel, or without dredging.
2. Constructing a Guide Bank.
3. Constructing the expansion of Al Tharthar Regulator.

The first category consists of four cases that were based on the release from the control structures. Then they were identified as Samarra Barrage only, Samarra Barrage with Al Tharthar Regulator, Samarra Barrage with hydroelectric station, and Samarra Barrage with both hydroelectric station and Al Tharthar Regulator.

8. RESULTS AND DISCUSSIONS

In this research, the flow of Tigris River upstream the system was simulated by using a mathematical model RMA2 within SMS10.1 system for dry and flood seasons and because the results of the model are in the form of a digital map it was not possible to present the maps of all scenarios that were used in the mathematical simulation. So, it the result of one of the scenarios will be presented in the dry season and in the case of operating hydroelectric station, Samarra

Barrage and Al Tharthar Regulator, and operating the system in the existing situation with a discharge of 492 m^3/s.

The distribution of the velocities in the study area was identified as a digital contour map as shown in **Fig. 10 and 11**. It is obvious that the flow velocity upstream of Samarra Barrage ranges between 0 and 0.3 m/s while the flow velocity upstream of Al Tharthar Regulator is close to zero because of the lack of discharge that passes from Al Tharthar Regulator. When constructing the guide bank the flow will be directed towards the hydroelectric power station and Samarra Barrage.

On the other hand, the results of the flood season presented to pass the flood peak with a discharge of 15060 m^3/s for a return period of 500 years when constructing the expansion of Al Tharthar Regulator with a capacity of 7000 m^3/s. **Fig. 12.** shows the distribution of velocity for four cases ranging between 0 and 0.75 m/s upstream of Al Tharthar Regulator and 0 to 1.5 m/s upstream of Samarra Barrage in the existing situation. **Table3.** shows that the water depth ranges between 14 and 17 m upstream of Al Tharthar Regulator and reaches 20.4 m upstream of Samarra Barrage.

Fig. 13 shows the water levels for four operational cases; the water surface elevation upstream of Samarra Barrage would be 68.5 and 68.9 in case of island and canal dredging and in case of constructing the guide bank، and island and canal dredging upstream of Al Tharthar Regulator. Thus, flow over will happen and the level of water surface reaches 78.4 and 79.19 m for the two other cases as shown in **Table4**.

9. CONCLUSIONS

The maximum permissible discharge through the system is 8250 m^3/s while the discharge from Samarra Barrage is 2400 m^3/s. Guide bank improves the flow towards the hydroelectric station and Samarra Barrage. When operating the system with a discharge of 15060 m^3/s and constructing new Al Tharthar Regulator expansion capacity of 4000 m^3/s, water surface elevation will be higher than the allowable limit by 1.51, 0.70, 3.70, and 0.60 m upstream Samarra Barrage for all cases overtopping and overtopping will occur. While operating the system with a discharge of 15060 m^3/s and constructing new Al Tharthar Regulator expansion capacity of 7000 m^3/s, water surface elevation will be lower than the allowable limit by 0.50 and 0.10 m upstream Samarra Barrage in case of dredging the island and channel and constructing a guide bank with dredging the island and channel upstream Al Tharthar Regulator consequently. Water surface elevation will be higher than the allowable limit by 9.40 and 4.19 m upstream Samarra Barrage in other cases and overtopping will occur. The expansion regulator of 7000 m^3/s is the solution for the 500-years return period flood since the water level upstream of Samarra Barrage is within the maximum allowable limit of 69 m.a.m.s.l.

REFERENCES

- Al-Samuraie, A.A., 2004, *Hydraulic Performance of Tigris River Flow Between Samarra Barrage Station and Sarai Station in Baghdad City*, M.SC., Thesis Building and Construction Engineering Department University of Technology.

- Ministry of Water Resources,2003. *Tigris River Discharge through Samara, Al-Adhaim*, and Baghdad Gauging Stations, General Establishment of Dams and Reservoirs, Unpublished Report, Baghdad.

- Ministry of Water Resources, National Center for Water Resources Management, 2013, *Data for the levels of the Tigris River for the study area*, unpublished data.

- Ministry of Water Resources,2014. *National Center for Water Resources Management*, Hydrological data records, unpublished data.

A- Layout of Head Works of Samarra Barrage as it was planned.

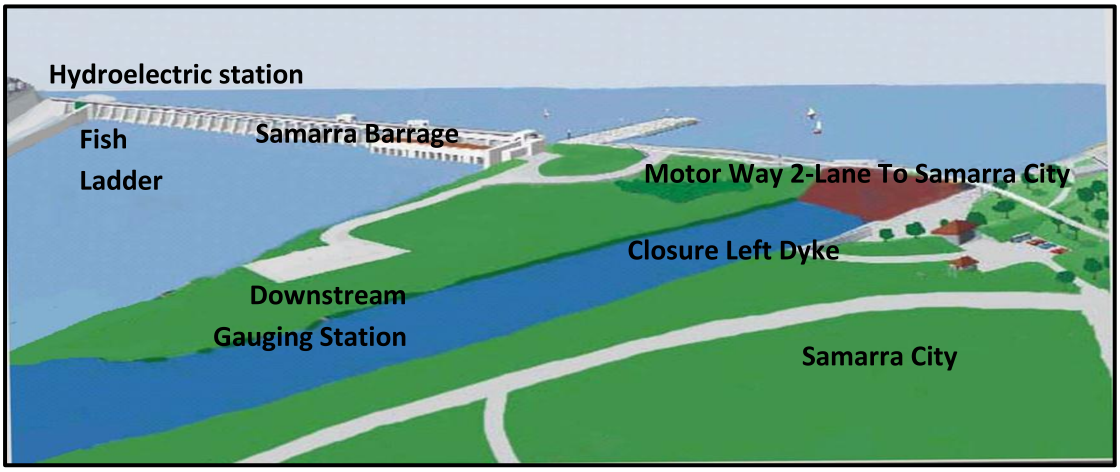

B- Layout of head works of Samarra Barrage as it was built**.**

Figure 1 . Layout of head works of Samarra Barrage, General Establishment of Dams and Reservoirs, Unpublished Report, Baghdad. Ministry of Water Resources,2003.

Figure 2. Satellite image of Samarra-Al Tharthar System**.**

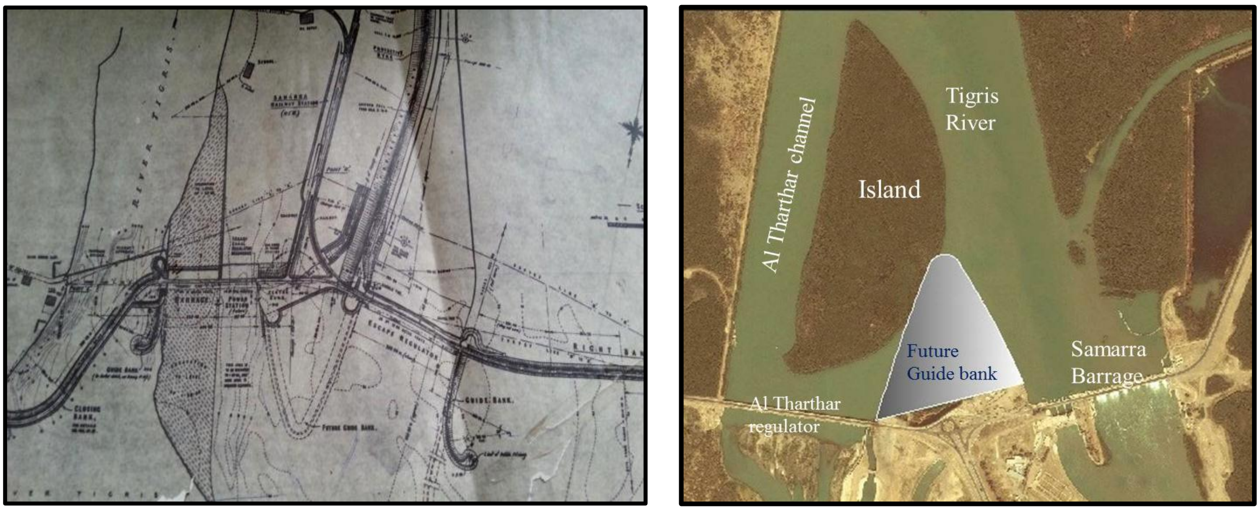

Figure 3. Layout of the future guide bank, Wadi Tharthar Project by Coode and Partners S.W.T, 1954.

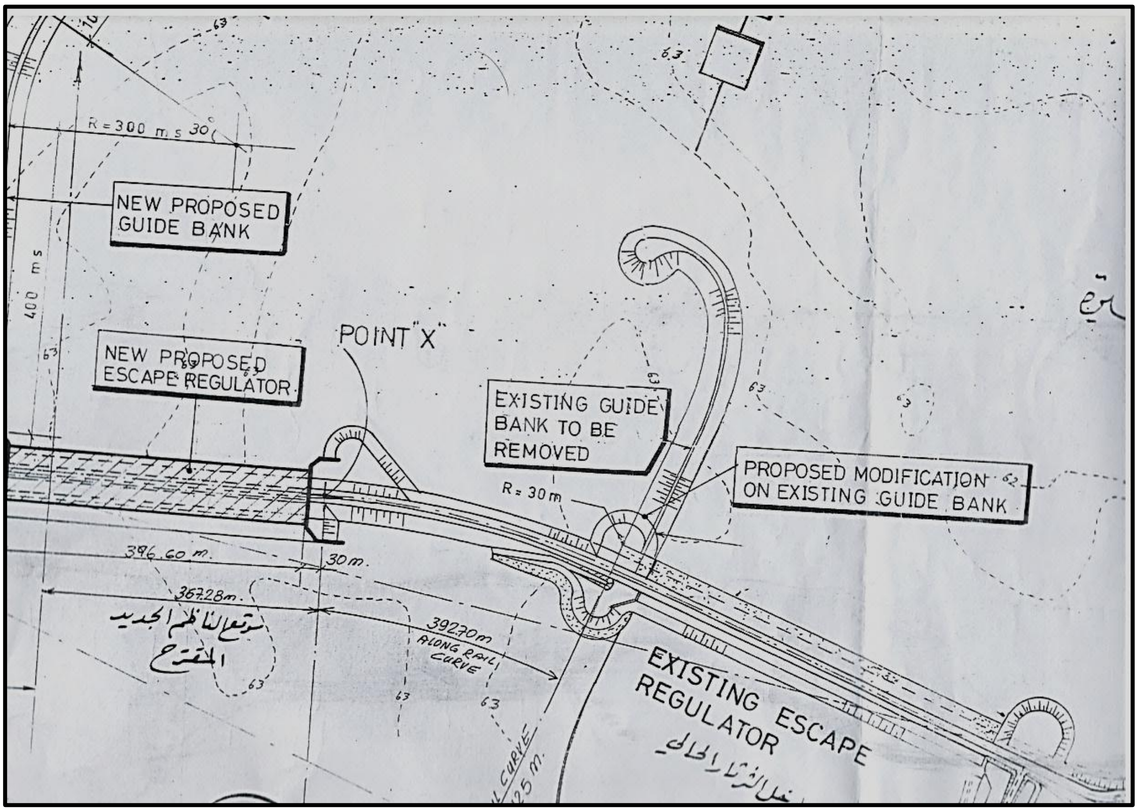

Figure 4. Layout of the expansion of Al Tharthar Regulator. Alphurate Center for the Study and designs irrigation facilities,1988.

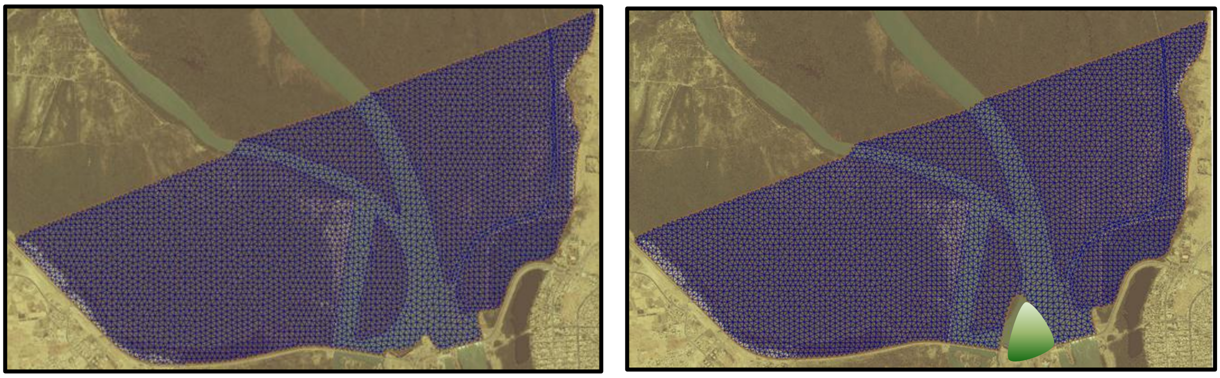

A- Without construction of guide bank . **B-** With construction of guide bank.

Figure 5. Finite elements of the type adaptive tessellation in the mathematical model of the study area for actual situation in dry year.

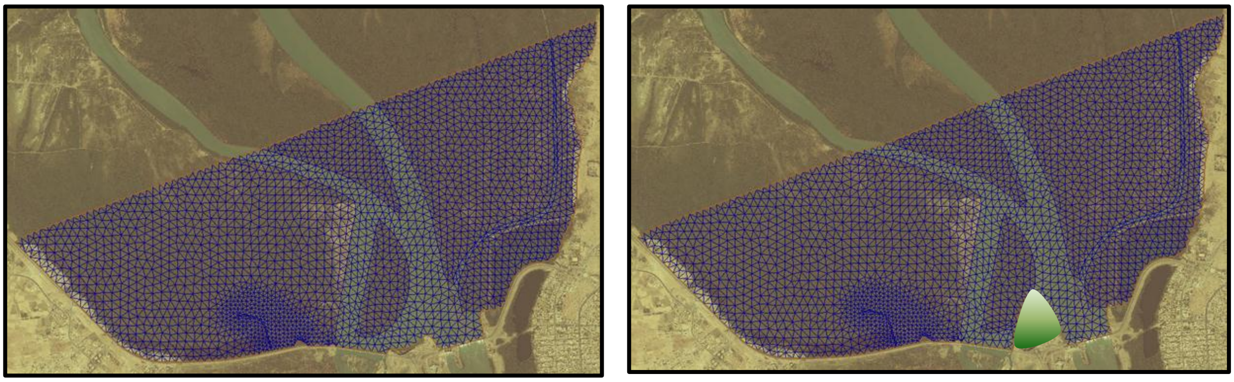

A- Without construction of guide bank **B-** With construction of guide bank

Figure 6. Finite elements of the type adaptive tessellation in the mathematical model of the study area for actual situation with discharge 15060 m^3/s, with new expansion of Al Tharthar Regulator for 4000 m^3/s.

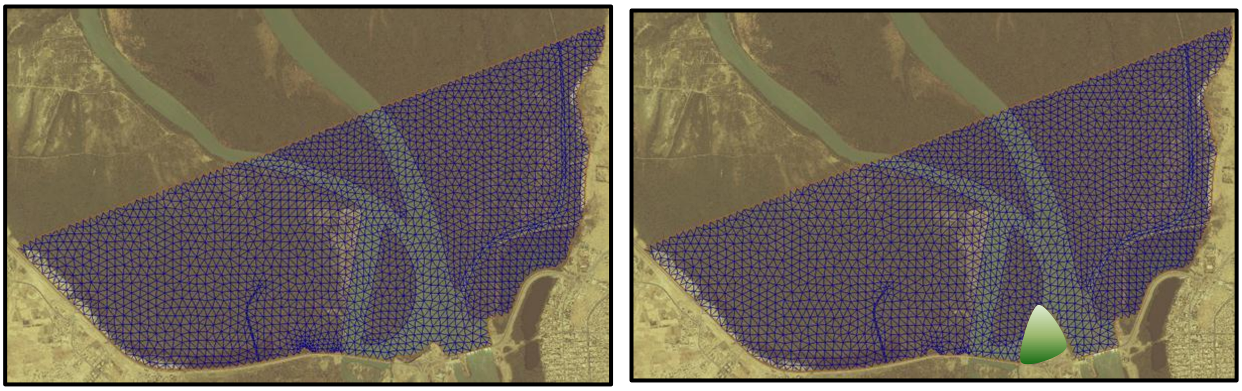

A- Without construction of guide bank **B-** With construction of guide bank

Figure 7. Finite elements of the type adaptive tessellation in the mathematical model of the study area for actual situation with discharge 15060 m^3/s, with new expansion of Al Tharthar Regulator for 7000 m^3/s.

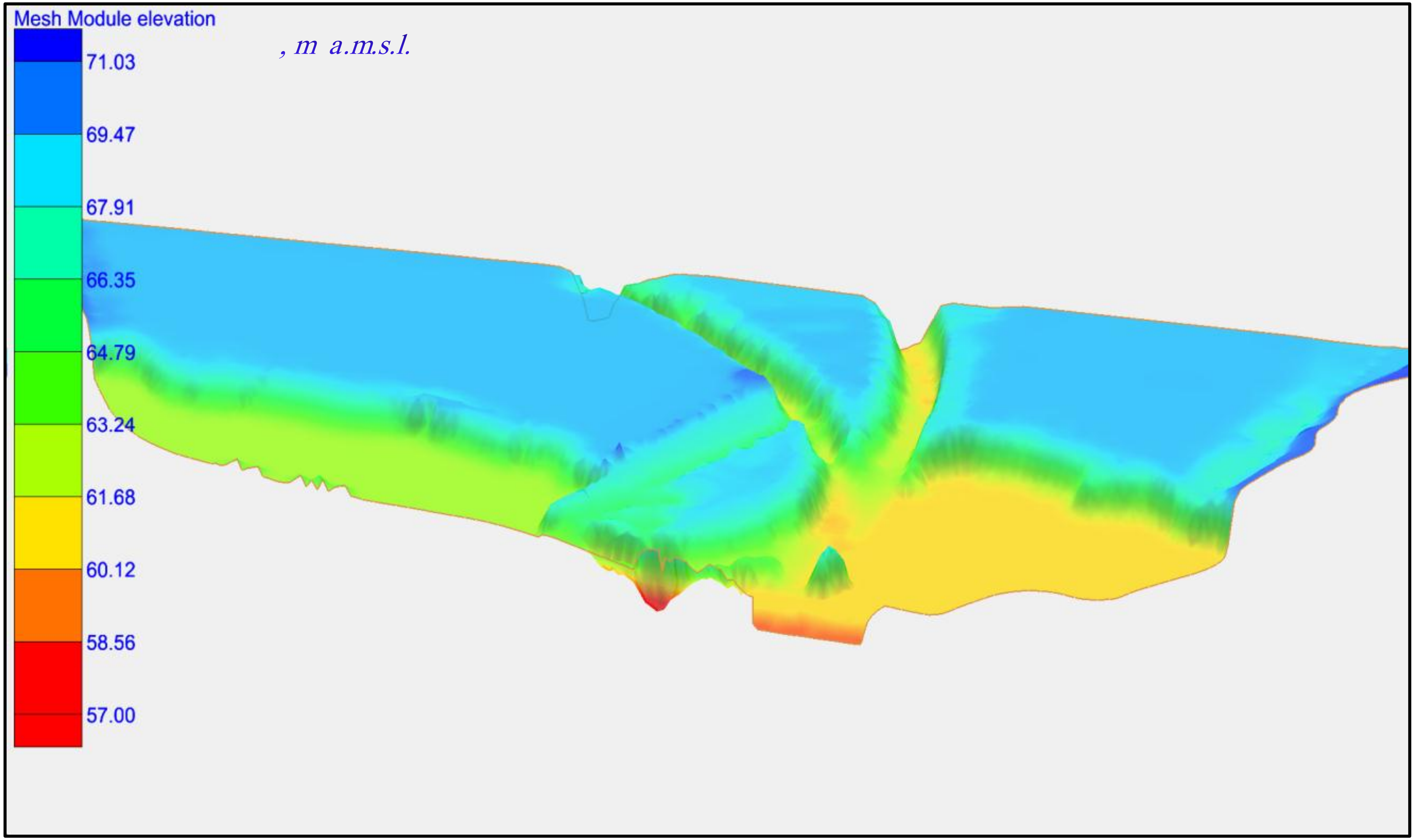

Figure8. Digital elevation model (DEM) of Samarra Tharthar system, Center of studies and Engineering Designs/ Ministry of Water Resources(2013).

A. Layout input parameters at dry year

B. Layout input parameters at flood year

Figure 9. Layout of boundary conditions for the study area.

Table 1. Input parameters and boundary conditions for dry year.

Operation case	River 1, (m^3/s)	River 2, (m^3/s)	River 3, (m^3/s)	Al Tharthar Regulator, (m^3/s)	Water level at Samarra Barrage, (m)
Samarra Barrage	193	289	10	---	67.4
Samarra Barrage with hydroelectric station	193	289	10	---	
Samarra Barrage with Al Tharthar Regulator	193	289	10	72	
Samarra Barrage with hydroelectric station and Al Tharthar Regulator	193	289	10	72	

Table 2. Input parameters and boundary conditions for flood year.

Discharge combination	Inlet Discharge, (m^3/s)	Water level at Al Tharthar Regulator, (m)	New Al Tharthar Regulator, (m^3/s)	Water level at Samarra Barrage, (m^3/s)
10400	10400	W.L	---	2400
11400	11400	W.L	---	
15060	15060		3660	

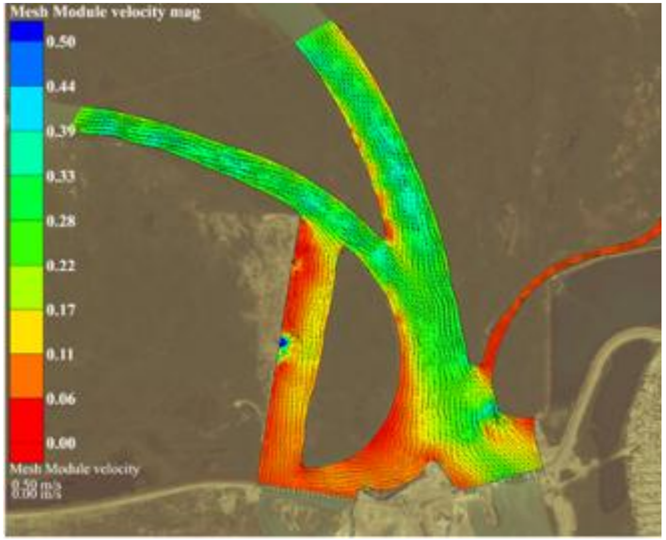

Operation of Samarra Barrage only

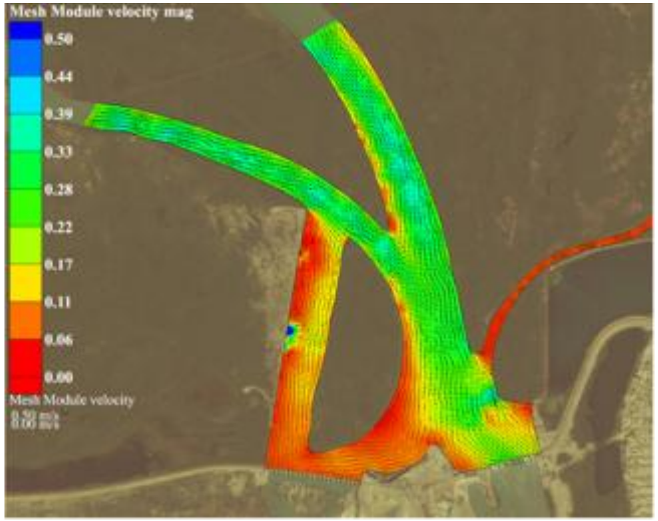

Operation of Samarra Barrage and Al Tharthar Regulator

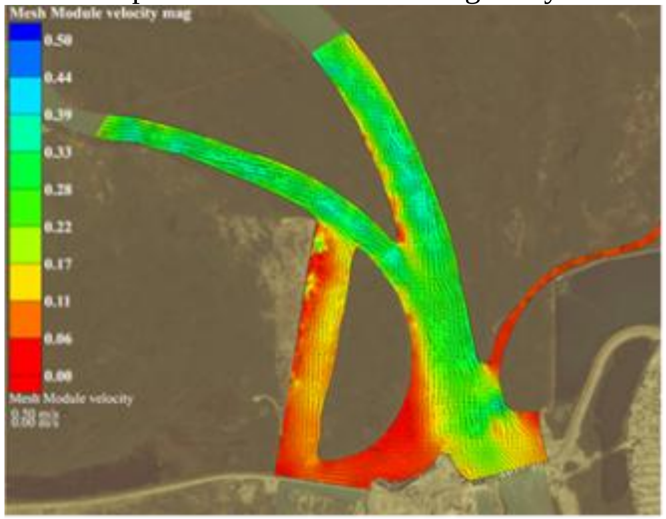

Operation of Samarra Barrage with Hydroelectric station

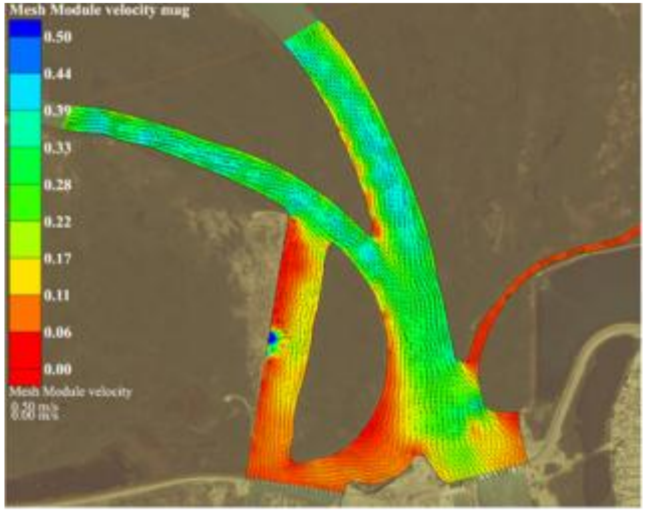

Operation of Samarra Barrage with Al Tharthar Regulator with Hydroelectric station

Figure 10. Velocity distribution upstream of Samarra-Al Tharthar system for first scenario in case existing situation.

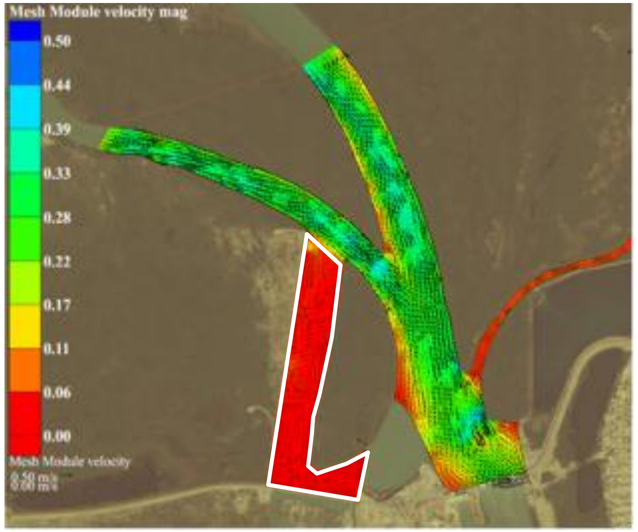

Operation of Samarra Barrage only

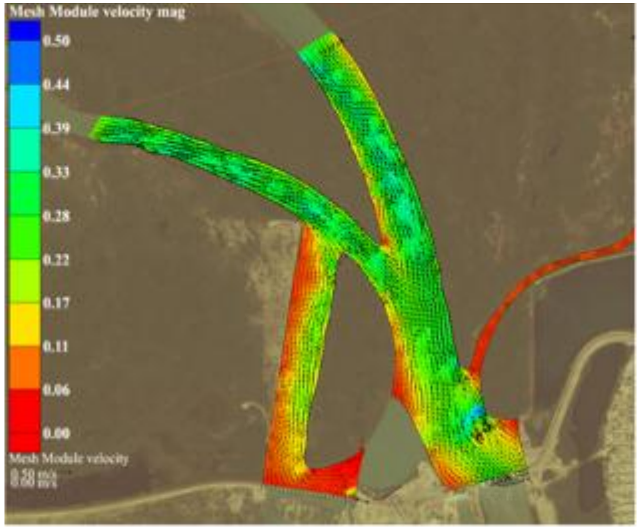

Operation of Samarra Barrage with Al Tharthar Regulator

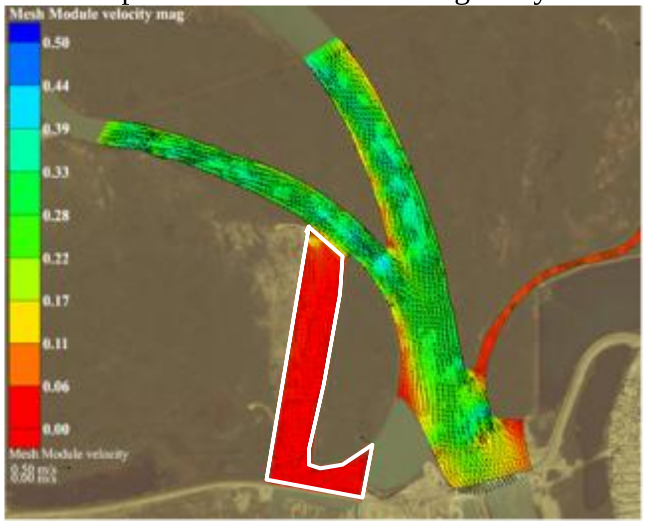

Operation of Samarra Barrage with Hydroelectric station

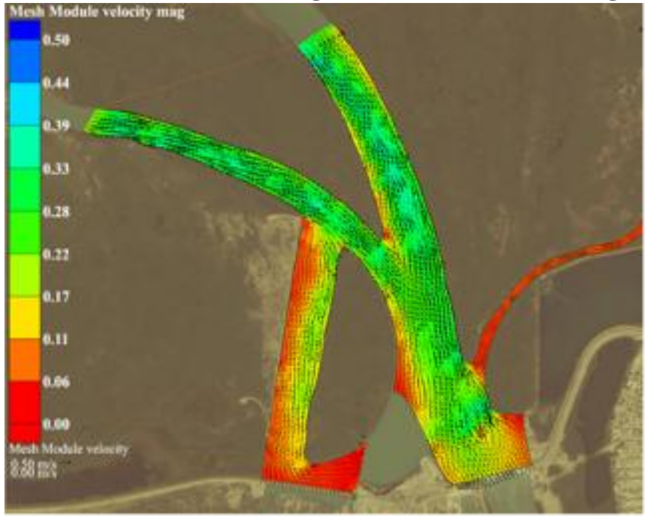

Operation of Samarra Barrage with Al Tharthar Regulator with Hydroelectric station

Figure 11. Velocity distribution upstream of Samarra-Al Tharthar system for first scenario in case existing situation with guide bank.

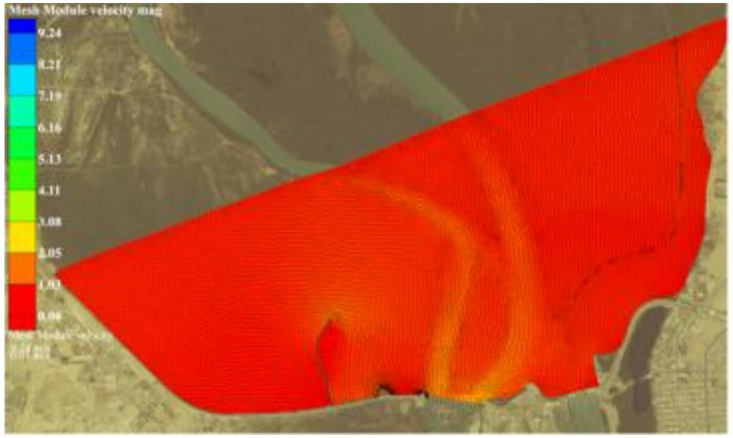

1- Existing situation

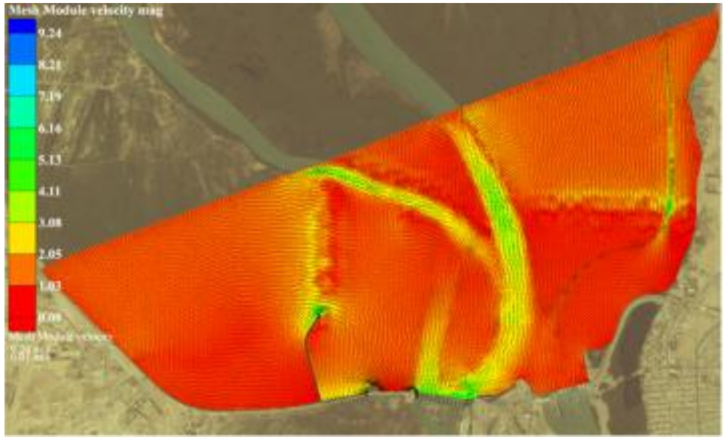

2- Existing situation with dredging channel and island

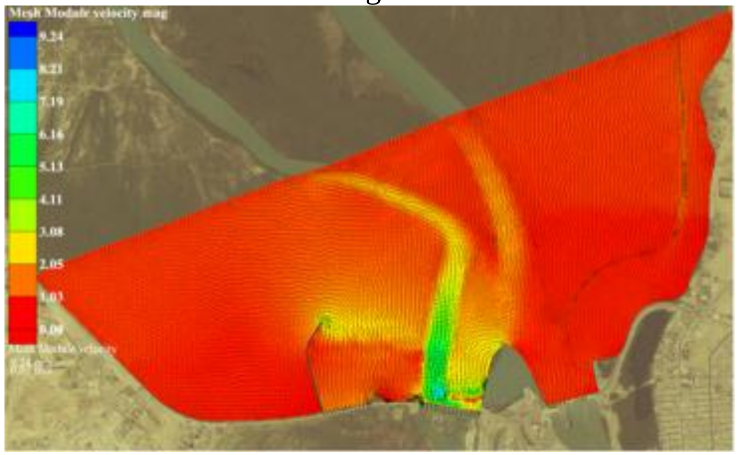

3-Constructing future guide bank

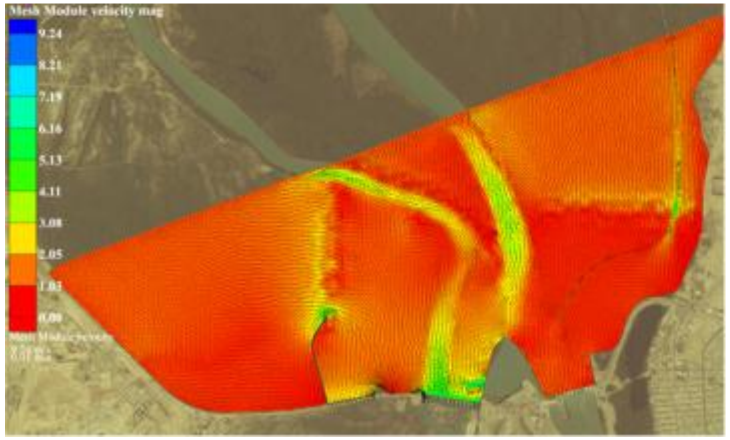

4-Constructing future guide bank with dredging channel and island

Figure 12. Distribution of velocities upstream of Samarra-Al Tharthar system for third scenario with discharge of 15060 m^3/s and new expansion Regulator of 7000 m^3/s.

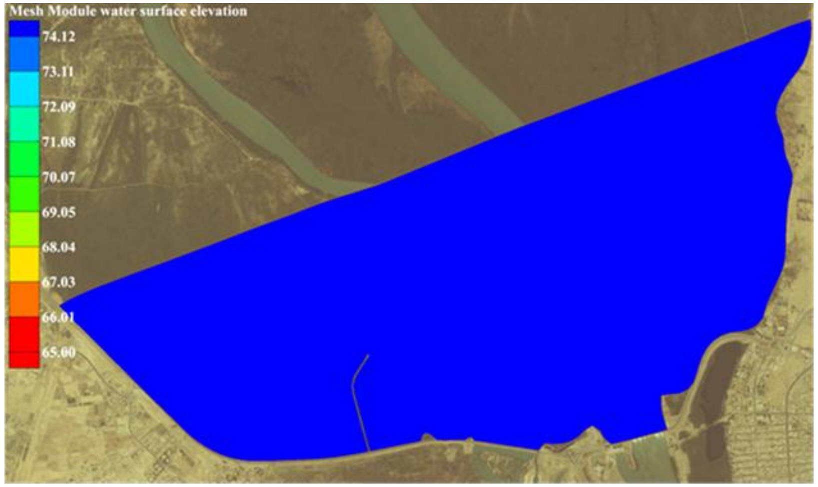

1- Existing situation

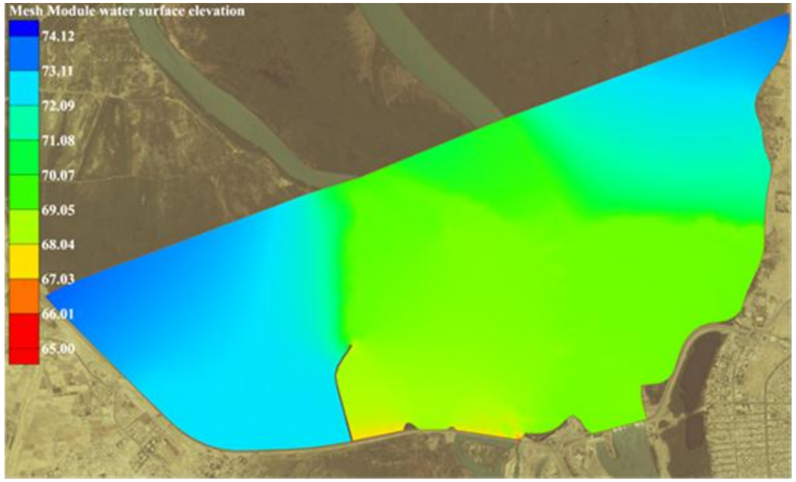

2- Existing situation with dredging channel and island

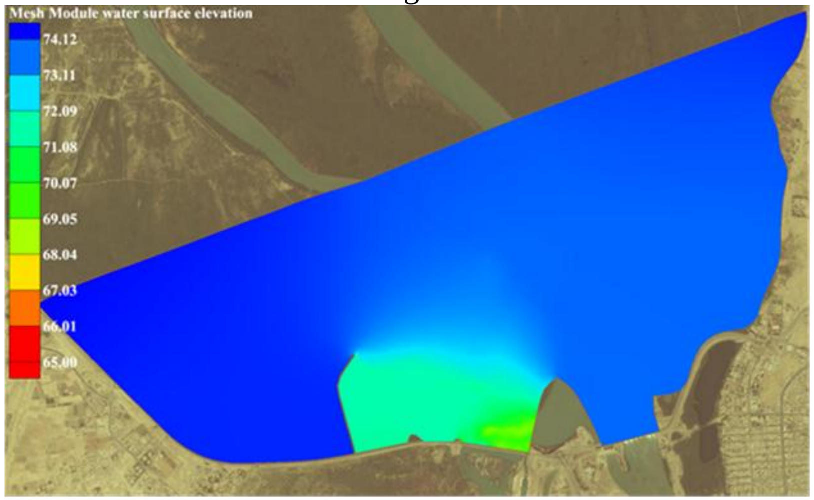

3- Constructing future guide bank

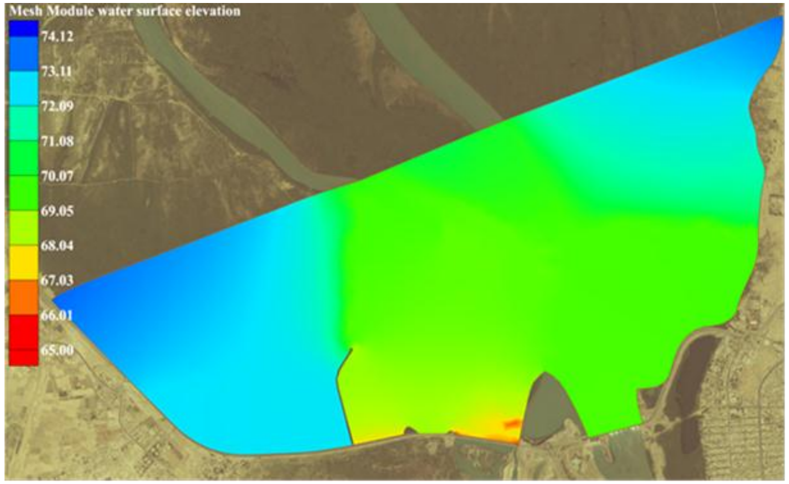

4- Constructing future guide bank with dredging channel and island

Figure 13. Water surface elevation upstream of Samarra-Al Tharthar system for third scenario.

Table 3. Summary of the RMA-2 software results of velocity distribution and water depth for Samarra-Al Tharthar System of the adopted cases in the third scenario with a discharge of 15060 m^3/s.

case	**Upstream Samarra Barrage**	**Upstream Al Tharthar Regulator**	**Upstream Expansion of Al Tharthar Regulator**
	Velocity, m/s		
	Depth of water, m		
Existing situation	0.00-0.75	0.50-1.50	0.50-0.80
	20.40	14.00-17.00	15.60
Existing situation with channel and island dredging.	**0.17-0.80**	**0.50-1.50**	**2.00-2.40**
	10.00-10.50	**5.50-7.40**	**6.25**
Constructing of future guide bank	0.14-1.50	2.00-7.40	1.00-1.16
	10.00-15.00	2.00-10.00	8.00-10.00
Constructing of future guide bank , dredging channel and Island	0.20-1.00	1.00-5.00	1.40-2.00
	7.50-11.00	4.00-8.00	4.00-6.00

Table 4. Summary of the RMA-2 software results of water surface elevation for Samarra-Al Tharthar System of the adopted cases in the 3rd scenario with a discharge of 15060 m^3/s for new regulator of capacity 4000 and 7000 m^3/s.

S	**Description**	**Capacity of the new regulator, m^3/s**	**Water surface elevation, m.a.m.s.l.**		
			Upstream New Al Tharthar Regulator	**Upstream Al Tharthar Regulator**	**Upstream Samarra Barrage**
3-5	Existing situation	7000	78.30	78.26	78.40
3-6	Existing situation with dredging channel and Island.		**66.90**	**67.10**	**68.50**
3-7	Constructing of future guide bank		70.95	69.00	73.19
3-8	Constructing of future guide bank with dredging channel and Island		**67.10**	**66.60**	**68.90**

Rotating Ceramic Water Filter Discs System for Water Filtration

Dr. Riyadh Z. Al Zubaidy
Professor
College of Engineering
University of Baghdad
azzubaidi@hotmail.com

Dr. Mahmoud Al-Khafaji
Assistant professor
department of Building and Construction
University of Technology
mahsal74@yahoo.com

Riyadh J. M. Al-Saadi
Assistant lecturer
College of Engineering
University of Karbala
riyadhj62@yahoo.com

ABSTRACT

This work aimed to design, construct and operate a new laboratory scale water filtration system. This system was used to examine the efficiency of two ceramic filter discs as a medium for water filtration. These filters were made from two different ceramic mixtures of local red clay, sawdust, and water. The filtration system was designed with two rotating interfered modules of these filters. Rotating these modules generates shear force between water and the surfaces of filter discs of the filtration modules that works to reduce thickness of layer of rejected materials on the filters surfaces. Each module consists of seven filtration units and each unit consists of two ceramic filter discs.

The average measured hydraulic conductivity of the first module was 13.7mm/day and that for the second module was 50mm/day. Results showed that the water filtration system can be operated continuously with a constant flow rate and the filtration process was controlled by a skin thin layer of rejected materials. The ceramic water filters of both filtration modules have high removal efficiency of total suspended solids up to 100% and of turbidity up to 99.94%.

Key words: ceramic filters, filtration system, water filtration, water purification.

منظومة اقراص مرشحات الماء الخزفية الدوارة لترشيح المياه

أ.د. رياض زهير الزبيدي
كلية الهندسة/جامعة بغداد

أ.م.د. محمود صالح الخفاجي
قسم هندسة البناء والانشاءات/الجامعة التكنولوجية

م.م. رياض جاسم محمد السعدي
كلية الهندسة/جامعة كربلاء

الخلاصة

هدف هذا العمل هو تصميم وانشاء وتشغيل منظومة جديدة بمقياس مختبري لترشيح المياه. استخدمت هذه المنظومة لفحص كفاءة اثنين من المرشحات الخزفية كوسط لترشيح المياه. تم تصنيع هذه المرشحات الخزفية من اثنين من الخلطات الخزفية من الطين الاحمر المحلي مع نشارة الخشب والماء. صممت منظومة الترشيح باثنين من وحدات ترشيح متداخلة ودوارة من هذه المرشحات. يعمل تدوير هذه الوحدات على توليد قوة قص بين الماء وسطوح اقراص الترشيح التي تعمل على تقليل سمك طبقة المواد المرفوضة على سطوح المرشحات. تتألف كل وحدة من سبعة مفردات من المرشحات، وكل مفردة تتألف من اثنين من اقراص المرشحات الخزفية.

كان معدل الايصالية الهيدروليكية المقاسة للوحدة الاولى 13.7 ملم/اليوم وللوحدة الثانية 50 ملم/اليوم. بينت النتائج ان منظومة ترشيح المياه لها القابلية على العمل باستمرار بمعدل تصريف ثابت وان عملية الترشيح محكومة بطبقة رقيقة من المواد المرفوضة المتراكمة على اسطح المرشحات. تمتلك مرشحات الماء الخزفية لكل من وحدتي الترشيح كفاءة عالية في ازالة المواد العالقة الكلية تصل الى 100% وفي ازالة العكورة تصل الى 99.94%.

1. INTRODUCTION

Availability of fresh and safe water for human consumptions is becoming scarce due to the increasing population, deficit in water sources, and contaminations being released into these sources. Governments, several civilian community organizations, universities, scientific research centers, and other institutions are working to get rid of these problems by supporting studies, researches, and activities in the fields of improving the water quality and increasing the water uses efficiencies. One of the fields of concerns is to supply safe water with low cost systems.

Ceramic is one of the common materials that had been used to produce water filters for a safe drinking water. The ceramic filters offer many advantages over other filters made of other materials. The ceramic filters are efficient in raw water filtration, of low cost, environmentally friendly, and a simple technology is needed to produce them.

Many studies and researches were performed on ceramic filters to improve the water quality by using and developing different mixtures and techniques to increase the efficiency of removing the suspended materials. **Jassim, 2010**, studied the evolution of water purifier cartridge made from Iraqi local ceramic materials. The main conclusion of this study was that all of the tested ceramic filters produced using four types of additives have excellent removal efficiencies of suspended materials and have good efficiencies in adsorption of some cations and anions. **Musa, 2010**, studied the performance of ceramic water filters made from selected two types of clays, sawdust and water for point-of-use. A linear relation between filters porosity and the percentage of the added sawdust was obtained. A quadratic relation was found between the percolation rate of water and the filters porosity. Moreover, a nonlinear polynomial relation of third degree was obtained between the percolation rate and the filters thickness. The results of the study showed that the filters made of both clay types have good removal efficiency of turbidity and total coliform. **Plappally, et. al, 2011**, conducted a field study on the use of ceramic water filters of frustum shaped and influences on the general health. These filters were made from different percent of local clay and sawdust. The results showed that the filters made from the mix ratio of clay: sawdust of 50:50 by volume has better efficiency in microbial filtration and better field service than the other ratios. In laboratory part of a study on the hydraulic performance ceramic pot water filters, **Peabody, 2012**, tested the comparison of hydraulic properties of the Filter Pure (FP) and Potters for Peace (PFP) ceramic pot filters. The FP filters was made from a mixture of clay, sawdust, water, and colloidal Silver. The PEP filter was made from the same mixture of the filter FP except of colloidal silver which was used as coated layer on the surface of PEP filter. The results showed that the filter FP has hydraulic performance better than the PEP filter. In the study of **Sharhan, 2013,** ceramic filter discs were produced from different Iraqi local materials to test their hydraulic performance. A laboratory scale bioreactor for municipal wastewater treatment with rotating ceramic discs was designed and constructed in order to examine the quality of water filtrated by using these ceramic discs. The obtained results showed that the mixture of red clay soil and sawdust as an additive has a maximum hydraulic conductivity over other additives. The results indicated that the bioreactor system can be used efficiently to treat municipal wastewater. The removal efficiency of the bioreactor system was related inversely to the hydraulic conductivity of the ceramic filters and was proportionally related to the hydraulic detention time. **Subriyer, 2013**, studied the treatment of domestic water using ceramic filter made from natural clay, fly-ash, and iron powder. In this study, the content of heavy metal in water was minimized by using a simple method of filtration technology. The analysis showed that the filtration system has good ability to decrease dissolved solids in permeates. It was found that the flow rate has no significant influence on the reduction of dissolved solids. The study showed that these filters have high efficiency in producing good quality of permeate due to removing the iron and zinc by more than 99% and 96% respectively. **Yakub, et. al, 2013**, conducted the research on the filtration characteristics of frustum-shaped ceramic water filters. These filters were made from red clay and sawdust in three different proportions by volume. It was found that filters produced with 50% of sawdust have an optimum flow rate and high efficiency of E. coli removal. The study concluded that the filtration efficiency did not change significantly with volume fraction of sawdust. Moreover, the removal of E. coli was referred in general to the geometrical clogging resulted by micro-pores and totally may be by a high adsorption due to the increasing of tortuosity. **Zair, 2013**, carried out a research on development of the performance of ceramic candle filters for water purification using mixing of different percent of Iraqi locally materials. It was found that the filters made from a mixture by weight of 25% activated kaolin clay, 35% coal, and 40% porcelanite have good performance of water purification. **Abiriga**, and **Kinyera, 2014**, studied the purification of water by ceramic filters in double filtration system. The ceramic filters were made from different mixes of ball clay, hardwood sawdust and grog. This filtration system has two ceramic disc fixed one over other with a specified distance between them. The results showed that the double filtration discs produced from mix ratios 5:1:2 and 4:2:1 by volume of clay, sawdust, and grog respectively for each have best efficiency of E. coli removal.

The above mentioned studies are some examples and there are many other studies that encourage efforts for more studies to develop new ceramic filter having different geometric shapes with high performance in purifying of water and to apply new design of water filtration systems that use this type of filtration material.

Generally, this study aims to produce two different ceramic filters with a disc shape manufactured from local materials. These disc filters are assembled to form two different filtration modules that are used in a designed and constructed laboratory scale water filtration system. The modules filters are rotated within the system to reduce accumulation of rejected materials on the surfaces of the filters.

2. CERAMIC FILTERS MODULES

Two different ceramic filters modules were prepared, FM1 and FM2. Each module consists of fourteen ceramic disc filters. Ceramic filter discs in each module have approximately the same properties. The filters used in these two modules were produced from two mixtures of local raw materials. These mixtures have different ratios of red clay, and sawdust as an additive. The ratios of the raw materials in addition to the pressure used to form these discs and the firing temperature are the key parameters that affect the filtration properties of the filters. **Table.1** presents the ratios of raw materials used in each mixture, in which all the presented ratios are by weight. The percentage of water added to the mixtures was 10% by weight. Semi dry pressing method was used to form the disc shape of these filters. Details of this method can be found in **Hammer, 1975**. A special steel mold was used and press pressures of 40, and 20MPa were applied to prepare the ceramic filters of FM1 and FM2, respectively. The mold was designed to produce ceramic filters of 12cm in diameter and a thickness of 2.5mm. The ceramic filters were fired inside a programmable electrical kiln according to a time schedule program of firing. The final firing temperature of 1070˚C was used to produce both filters discs. This firing temperature was found suitable to give efficient filter disc, **Sharhan, 2013**. **Fig. 1** shows samples of the produced ceramic filters discs. Each of the filtration module, **Fig. 2**, consists of seven ceramic filter units. The filter unit is constructed from two discs separated by PVC ring of 3mm width as shown in **Fig. 3**. A pipe with holes at each filter unit is used to fix these units and to collect the filtered water from each unit. This pipe is of 20mm outer diameter and 12mm inner diameter.

The produced ceramic filters of the two modules were tested for their hydraulic conductivity and are presented in **Table 2**. The measured hydraulic conductivity of the filters of FM1 ranged between 10 and 17mm/day with an average of 13.7mm/day. The hydraulic conductivity of FM2 ranged between 46 and 55mm/day with an average of 50mm/day.

3. WATER FILTRATION SYSTEM

A laboratory scale water filtration system was prepared by using the ceramic filter modules. **Fig. 4** shows a schematic diagram of this system and **Fig. 5** shows the filtration system installed in the laboratory. The system consists of a storage tanks, filtration tank, two ceramic filtration modules, backwash tank, two treated water storage tanks, peristaltic pump, and an electrical control board. All units are fixed on a steel frame of three floors. The dimensions of the storage tank were 34cm width, 66cm length, and 34cm depth with 60l net volume. The tank is supplied by raw water through a pipe of 12mm inner diameter located at the left hand side at a distance 2cm from the top edge of the tank. This pipe is controlled by an electrical float valve used to preserve 30cm of raw water depth. This tank supplies raw water to the filtration tank. The filtration tank is the main unit of filtration system that consists of the filtration modules. The tank has the outer dimensions of 32cm width, 81cm length, and 52cm depth with 96l net volume. A mechanical float valve was used to control the inflow to the filtration tank. Four submersible water pumps were used to circulate raw water in order to prevent settling of the suspended materials. A drain pipe of 50mm fixed at the bottom of filtration tank was controlled by a mechanical valve to wash or empty the filtration tank and also used for taking samples. The two ceramic filtration modules were installed inside the filtration tank in a way shown by **Fig. 2.** The distance between the two filter modules is 75mm center to center with an interference of about 20% between the surface areas of each of the filtration units of the two modules. A motor is used to rotate these modules at rate of 15rpm. The reason behind rotating the ceramic filtration modules is to provide a shear force between these discs by water filling the gap between the filters. This force provides unsuitable environment for micro-organism growth and reduces the thickness of the accumulated rejected materials by the filters. Backwashing with clear water is necessary to remove the rejected material within and over the ceramic filter during operation. The backwash tank has a square base of 32×32cm and a depth of 28cm with 20l net capacity. Fresh water is supplied to this tank through an inlet pipe of 12mm diameter controlled by a mechanical float valve. The backwash process is carried out by a pump that operates at a maximum rate of 20l/min and a minimum rate of 8l/min. The filtration system was supplied by two treated water storage tanks of 17.5cm width, 21cm length, and 16cm depth. The capacity of each tank is 4l. Each tank receives treated water from one filtration modules. Each tank has a tap of 12mm diameter that is used for water sampling. A peristaltic pump with two heads was used to pump water from each filtration modules to the treated water storage tanks. The rotating speed of this peristaltic pump is ranged between 60 and 600rpm. Four sizes of silicon tubes can be used to pump water with a range vary between 6 and 180l/hr. Two pressure gauges were installed at the section side of each head of the peristaltic pump.

3.1 Design of Experiment Runs

A total of twenty experiment runs was carried out by using raw water with five different total suspended solids, TSS, concentrations. These experiments were grouped in five sets. Each set consists of four experiments that were carried out with a specific concentration of TSS of the water to be filtered by using the filtration system. The concentrations of TSS were 500, 1000, 3000, 5000, 7000 mg/l. These concentrations were achieved by adding red clay as weight percentage to the volume inside the filtration tank. Properties of raw water that was used in the experiments are summarized in **Table 3**. The first experiment run of each set was conducted without using peristaltic pump and without using backwash. In this case, the water flows through the ceramic filters to the treated water storage tank by gravity. Other three experiments were conducted by using peristaltic pump and backwash with different discharge and backwash time.

The discharge of the peristaltic pump in the second to the fourth experiments of each set is selected to be one and half, three and six times the higher value of the steady state flow rate obtained from the two modules.

A total of thirty tests of temperature, pH, electrical conductivity, turbidity, total dissolved solids and total suspended solids of raw water were carried out before starting each set of experiment run. Four hundred and eighty physical tests were carried out on the effluent of the filtration system including turbidity and total suspended solids. One hundred and eighty negative suction pressure readings of the two pressure gauges were recorded during all runs when using the peristaltic pump. Sixty water flow rate measurements of treated effluent discharge were carried out during experiment runs without using the peristaltic pump.

3.2 Water Filtration System Operation Procedure

Each set of experiments is executed according to the following procedure:

1. Tap water is filtrated before it was added to the storage tank by one-micron cotton filter. Then, the filtration tank is filled with the filtered potable water via the storage tank.
2. The water filtration system is operated without using peristaltic pump and backwash pump. The flow rate of treated filtrating water from each of the two filtration modules is measured by volumetric test using graded vessel with time watch. The flow rate is measured every one hour until reaching the steady state of flowing for each module. This run is too important in order to be sure that all trapped air and probable residue of ceramic incineration have been removed from filter pores.
3. The required concentration of TSS for raw water is prepared by adding a calculated amount of red clay slurry to the filtered tap water inside the filtration tank. The slurry of the red clay is prepared by adding amount of clay to about 15l of water in a container and is mixed well. This slurry is then gradually added with a good mixing to the filtration tank.
4. The samples of raw water are collected by using clean plastic bottles. These samples are to be tested for pH, EC, TSS, TDS, and turbidity.
5. The first experiment is carried out without using peristaltic pump and backwash pump. At the beginning, the flow rate from each filtration module is measured volumetrically as water flow by gravity. Then the flow rate is measured each hour of five hours running.
6. Samples of water filtered by each filtration module are collected from the treated water storage tanks. These samples are to be tested for TSS and turbidity only. The temperature of water is measured each time of the water samples collection.
7. All filtrated water during the experiment is continuously returned back to the storage tank in order to maintain the concentration of raw water and the constant head in the filtration tank.
8. At the end of operation, the filtration tank is drained out and the accumulated rejected materials on the filters are removed during the backwashing by using distilled water for a duration of twelve seconds on and off for a period of half hour. Moreover, tap water is poured gently on the outer faces of filters. Finally, the filtration tank is well cleaned by potable water and is then completely drained.
9. The filtration tank is filled with tap water in the same way as in the first step mentioned above. The water filtration system is then kept running without peristaltic pump by using tap water. The effluent of filtration water from the modules was monitored until it reached the steady state flow rate.

10. The filtration system is operated with the use of peristaltic pump and backwash pump. The flow rate of peristaltic pump is selected to be one and half of the maximum steady state flow rate resulted from step number 9 mentioned above. The backwash pump is operated when the negative suction pressure gauge reading being less than about -0.4bars and stop when the reading of pressure becomes higher than -0.4bars. The system is kept running for five continuous hours. Samples of filtrated water are collected from each of filtration modules to be tested for TSS and turbidity t the starting time and at each hour of operation.
11. Steps 7 to 10 are then repeated two times. These represent experiment number three and four. But in step number 10, the flow rate of the peristaltic pump is selected to be three and six times the maximum steady state flow rate for experiment number three and four, respectively.

4. RESULTS ANALYSIS

Tests results of the five sets of experiments are presented in **Table 4 to Table 8** under different concentration of TSS of 500, 1000, 3000, 5000, and 7000mg/l, respectively. The calculated removal efficiencies during these experiments are presented in **Table 9**. **Figs. 7** and **8** show the time variation of effluent of FM1 and FM2 during the first experiment of each set, respectively. The relation between the steady state effluent of filtration modules and the used TSS concentration during the first experiment of each set are presented in **Fig. 9**. The time variation of suction pressure gauge readings of the two modules for all TSS of raw water that were recorded during the experiments is presented in **Figs. 10** to **15**.

The steady state potable water flow rate of FM1 and FM2 when the filters are virgin was 125ml/min and 175ml/min, respectively. All other examined flow rates with potable water of FM1 and FM2 during other experiments reach a steady state flow rate of 100ml/min and 150ml/min, respectively. These steady flow rates are achieved after approximately three hours of the test start. This change in steady state flow rate is probably due to clogging of some pores inside the body of the filter discs. The steady flow rate of FM1 is less than that of FM2 by about 29%. This is due to the use of less percentage of sawdust and high pressing pressure in the production of FM1 compared to that of FM2.

In general, in all experiment with raw water of different concentrations of TSS, a thin layer of rejected materials was formed on the surfaces of ceramic filters. This layer increased with time until they reached a steady state thickness. This thickness is a function of the concentration of TSS and the shear resulted between the filters units due to their rotation. This layer is controlling the filtration process instead of the ceramic filters medium.

In the first experiment of all sets, the results showed that the effluent water from modules FM1 and FM2 is decreasing gradually until it reached a steady state effluent rate. The rate of this decrease and the value of the steady state depend on the concentration of the TSS of the water being treated. The overall percentage of decrease in the effluent of modules FM1 and FM2 is 20% and 14%, respectively. The maximum percentage of this decrease is 28% and 19% for FM1 and FM2, respectively, that was recorded during experiment with 7000mg/l TSS concentration of raw water. While, its minimum value of 12% and 9% for FM1 and FM2, respectively, which was recorded during the experiment with TSS concentration of 1000mg/l. It is expected that the minimum decrease to be recorded when the concentration of TSS is 500mg/l, which is during the first experiment of the first set. But in this experiment, the filter has never been subjected to raw water before and the initial effluent rate was 125 and 175ml/min for FM1 and FM2, respectively. While in all other experiment, the initial effluent rate was 100 and 150ml/min for FM1 and FM2, respectively. This may explain why the minimum reduction in the effluent rate was not in the first experiment of the first set. At the end of the first run of experiment of the first set, some of the pores of the filter media were clogged by the suspended particles that cannot removed by backwashing and this clogging being permanent. In these experiments, the steady state effluent rate is reached after approximately three hours. The values of steady state effluent of FM1 were 100, 88, 83, 77, and 72ml/min that was recorded during the first experiment of the five sets, respectively, and that for FM2 were 150, 136, 133, 128, and 122ml/min. The variation in values of the steady state effluent with the variation in the concentration of TSS may be referred to the nature of formation of the thin layer of the rejected materials on the filters surfaces. This formation depends on the concentration of the TSS and the shear between the filter surfaces due to the rotation of filtration modules. As the concentration of the TSS increased, the rate of accumulation of this layer is increased also, but the shear at the filter surface attempts to reduce the thickness of this layer until a steady state relation between the thickness formation and the shear is reached so that a specific thickness is achieved. This specific thickness of the rejected material is proportionally related to the concentration of the TSS.

In all experiments, the results showed that the values of TSS concentration and turbidity of the effluent for both FM1 and FM2 start to decrease during all runs and then reach a constant value. This may be referred to formation of the thin layer of rejected material on the surface of the filters. The particles of this layer have smaller pores than that of the filter and are forming a skin filter on the original filter media.

The overall average of TSS concentration of the effluent of FM1 is 1.3mg/l, while that for FM2 is 1.2mg/l. This difference in TSS concentration between both modules FM1and FM2 is referred to the smaller pores of module FM1 compared to that of Module FM2 as a result of using less percentage of sawdust and high press pressure in the production of FM1 compared to that of FM2.

The maximum recorded value of the TSS concentration of the effluent of the both modules FM1 and FM2 was 4mg/l that was recorded at the beginning of test number two of set number one. This was expected during the first run of using the peristaltic pump with TSS concentration of 500mg/l that forces fine particles to penetrate inside the filters pores at the beginning of this run and cannot be removed by the subsequent backwash. No TSS concentration in the effluent of FM1 and FM2 was recorded after three hour of test number four of set number one. This may be due to temporarily clogging of more filter pores during the second and third runs and accumulation of more fine partials on the surface of the filters.

The behavior of turbidity of effluent water is completely like that of TSS concentration for all runs of all experiments sets because turbidity reflects the same index of total suspended solids in the water. The turbidity of effluent water for both modules FM1 and FM2 is generally less than 5NTU. This turbidity is within the requirements of the Iraqi water quality and the world health organization standard of turbidity in drinking water, **WHO, 2004; Iraqi Central Organization for Standardization and Quality Control, 2001**.

The results of experiments showed that the ceramic water filters discs of both filtration modules FM1 and FM2 have high removable efficiency of the TSS and turbidity. The range of removal efficiency of TSS varies from 99.20% to 100% for filtration module FM1 and from 99.40% to 100% for filtration module FM2. The range of removal efficiency of turbidity was from 97.12% to 99.94% for filtration module FM1 and from 97.70% to 99.94% for filtration module FM2. These results indicated that the removal efficiencies of the two filtration modules are approximately the same.

The negative gauge pressure measured at the suction side of the peristaltic pump was recorded during each run of the experiment sets that were carried out with the peristaltic pump. The results of these runs showed that the negative suction gauge pressure for modules FM1 and FM2 is decreased with time until it reaches a steady state value at about the third hour of running. Moreover, the results showed that the suction pressure for both modules FM1 and FM2 decreased when increasing the discharge of peristaltic pump. The negative suction pressure for both modules FM1 and FM2 was decreased with the increasing of TSS concentration of influent raw water. The minimum value of negative suction gauge pressure was -0.52bar for FM1 and -0.50bar for FM2 that were recorded during the second hour of run number four of experiments set number five. The decreasing in the pressure with time is due to clogging of filter pores during time with suspended solids of raw water and reaching the steady state suction pressure is due to effect of the thin layer of the rejected materials on the filters surfaces that was kept at a final constant thickness due to the action of the shear force.

Therefore, filters of module FM2 is better than of module FM1 because filters of module FM2 have hydraulic conductivity about three times greater than that of module FM1.

5. CONCLUSIONS

The salient issues obtained from this study to test the filtration efficiency of ceramic filter discs by using the laboratory scale water filtration system are as follows:

1. The water filtration system showed excellent performance in water purification.
2. The water filtration system can be continuously operated with a constant flow rate.
3. A thin layer of rejected materials was formed on the surfaces of ceramic filters during all runs. This thickness is a function of the concentration of TSS and the shear resulted between the filters units due to their rotation.
4. The filtration by using water filtration system is controlled by a skin thin layer of rejected materials which was formed during system operation.
5. When the FM1 and FM2 are virgin and when using potable water, the steady state effluent was 125ml/min and 175ml/min, respectively. In all other experiments with potable water, the examined effluent of flow of FM1 and FM2 reach a steady state of 100ml/min and 150ml/min, respectively.
6. The effluent water from modules FM1 and FM2 during the first experiment of all sets is decreased gradually until it reached a steady state effluent rate. The rate of this decrease and the value of the steady state depend on the concentration of the TSS of the water being treated. The overall percentage of decrease in the effluent of modules FM1 and FM2 is 20% and 14%, respectively.
7. The maximum decreasing percentages in the effluent of the modules FM1 and FM2 was 28% and 19%, respectively, occurred at the first run of experiments set using 7000mg/l TSS concentration of raw water.
8. The minimum percentages of decreasing the effluent of the modules FM1 and FM2 was 12% and 9%, respectively, occurred at the first run of experiments set using 1000mg/l TSS concentration of raw water.
9. The overall average TSS concentration of the effluent of FM1 is 1.3mg/l, while that for FM2 is 1.2mg/l.
10. The turbidity of effluent water for both modules FM1 and FM2 is within the requirements of the WHO and Iraqi standards of turbidity in drinking water which is 5NTU.
11. There is no significance difference of removal efficiencies of TSS and turbidity between ceramic filter discs of both filtration modules. Therefore, from the hydraulic conductivity point of view, the FM2 is better than FM1 because filters of module FM2 have hydraulic conductivity about three times greater than that of module FM1.
12. The removal efficiencies of TSS and turbidity were increased with time during the operation of water filtration system for both of filtration modules FM1 and FM2.

13. The negative suction gauge pressure for both modules FM1 and FM2 was decreased with increasing of the discharge of the peristaltic pump. As well as, the negative pressure for both modules FM1 and FM2 was decreased by increasing of TSS concentration of the raw water. The lower value of suction pressure was -0.52bar for FM1 and -0.50bar for FM2 occurred at the second hour of run number four of experiments set number five.

REFERENCES

- Abiriga, F., and Kinyera, S., O., 2014, Water Purification by Double Filtration Using Ceramic Filters, Environment and Natural Resources Research; Vol. 4, No. 2: 92-101.

- Hammer, F., 1975, The Potters Dictionary of Materials and Techniques, 1st edition, Pitman Publishing, London, UK.

- Iraqi Central Organization for Standardization and Quality Control, 2001, Drinking Water Standards, No. 417.

- Jassim, S., Abdul-Razak, 2010, Evaluation of Water Purifier Cartridge Made of Local Ceramic Materials, Ph.D. dissertation, Department of Water Resources Engineering, College of Engineering, University of Baghdad, Iraq.

- Musa, K., 2010, Performance of Ceramic Water Filters Made from Selected Uganda Clays for Point-of Use, M.Sc. thesis, The Graduate School, Makerere University, Uganda.

- Peabody, D., 2012, Field and Laboratory Comparison of the Hydraulic Performance of Two Ceramic Pot Water Filters, M.Sc. thesis, Department of Civil and Environmental Engineering, College of Engineering, University of South Florida, USA.

- Plappally, A., Chen, H., Ayinde, W., Alayande, S., Usoro, A., Friedman, K. C., Dare, E., Ogunyale, T., Yakub, I., Leftwich, M., Malatesta, K., Rivera, R., Brown, L., Soboyejo, A., and Soboyejo, W., 2011, A Field Study on the Use of Clay Ceramic Water Filters and Influences on the General Health in Nigeria, Journal of Health Behavior and Public Health, Vol. 1, No. 1.

- Sharhan, F., A., 2013, A Bio-Reactor with Rotating Hollow Ceramic Discs Filter for Municipal Wastewater Treatment, Ph.D. dissertation, Department of Water Resources Engineering, College of Engineering, University of Baghdad, Iraq.

- World Health Organization, WHO, 2004, Guidelines for Drinking Water Quality, Vol.1 Recommendations, 3rd edition, Geneva.

- Yakub, I., Plappally, A., Leftwich, M., Malatesta, K., Friedman, K. C. , Obwoya, S., Nyongesa, F., Maiga, A. H., ASCE, M., Soboyejo, A. B. O., Logothetis, S. and Soboyejo, W., 2013, Porosity, Flow, and Filtration Characteristics of Frustum-Shaped Ceramic Water Filters, ASCE, Journal of Environmental Engineering, July, Vol. 139.

- Zair, Z. R., 2013, Developement the Performance of Ceramic Candle Filters for Water Purification Using Locally Materials, The Iraqi Journal For Mechanical And Material Engineering, Vol.13, No.1.

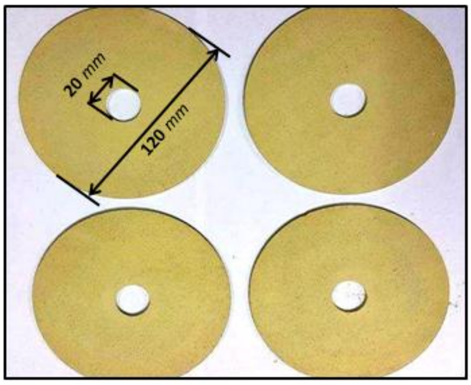

Figure 1. Samples of the produced ceramic filter discs.

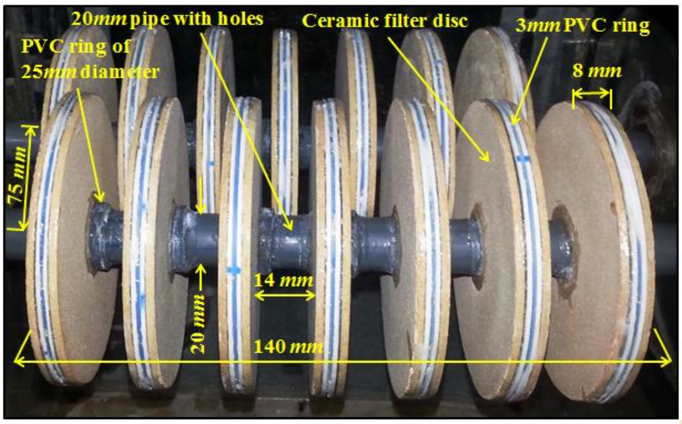

Figure 2. The filtration modules.

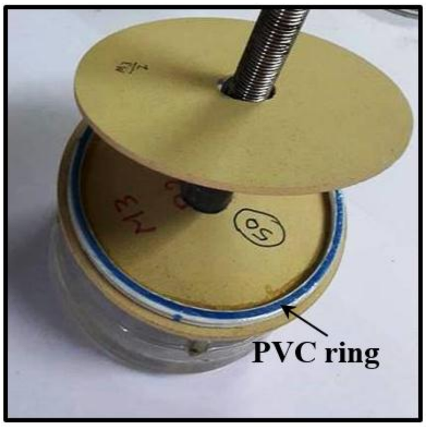

Figure 3. The filter unit.

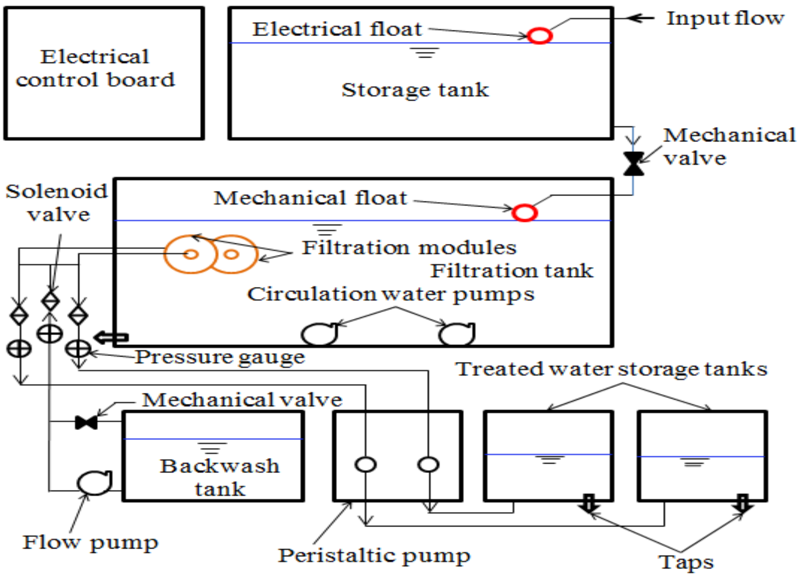

Figure 4. A schematic diagram of the water filtration system.

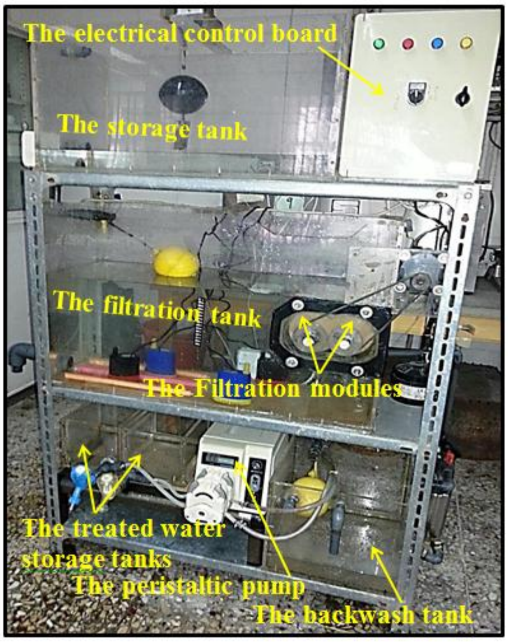

Figure 5. The water filtration system installed in the laboratory.

Table 1. Different mixtures of red clay and sawdust.

Filters Set	**Red Clay**, %	**Sawdust**, %	**Particle size of sawdust,** µm
S1	95	5	75 - 425
S2	92.5	7.5	

Table 2. Measured hydraulic conductivity of the filtration modules

Filtration module FM1				**Filtration module FM2**			
Filter unit no.	**Ceramic filter disc no.**	**Hydraulic conductivity** mm/day		**Filter unit no.**	**Ceramic filter disc no.**	**Hydraulic conductivity** mm/day	
		Ceramic disc	**Filter unit**			**Ceramic disc**	**Filter unit**
1	1	13	13.5	1	1	52	50
	2	14			2	48	
2	3	15	14	2	3	52	50
	4	13			4	48	
3	5	17	13.5	3	5	53	49.5
	6	10			6	46	
4	7	14	14	4	7	55	50.5
	8	14			8	46	
5	9	14	14	5	9	50	50
	10	14			10	50	
6	11	14	13.5	6	11	50	50
	12	13			12	50	

7	13	16	13.5	7	13	50	50
	14	11			14	50	
Mean hydraulic conductivity			13.7	Mean hydraulic conductivity			50

Table 3. Physical properties of raw water used for water filtration system tests.

Run set no.	**TSS** mg/l	**TDS** mg/l	**Turbidity** NTU	**EC** µs/cm	**pH**	**Temperature** ˚C
1	500	524	174	874	8.42	20
2	1000	554	326	924	8.30	16
3	3000	562	1235	936	8.27	16
4	5000	610	1751	1017	8.12	15
5	7000	652	3194	1086	7.85	15

Table 4. The results of water filtration system tests with TSS concentration of 500mg/l.

Raw water		**Run case**	**Run no.**	**Time** hr	**Effluent water**						**Suction pressure** bar	
Turbidity NTU	**TSS** mg/l				**Turbidity** NTU		**TSS** mg/l		**discharge** ml/min			
					FM1	**FM2**	**FM1**	**FM2**	**FM1**	**FM2**	**FM1**	**FM2**
174	500	Without using peristaltic pump	1	0	4	4	3	3	125	175		
				1	4	3	3	2	122	171		
				2	3	2	2	1	118	165		
				3	2	2	1	1	112	159		
				4	2	2	1	1	100	150		
				5	2	2	1	1	100	150		
		With using peristaltic pump	2	0	5	5	4	4	263		0	0
				1	3	3	2	2			-0.04	-0.01
				2	2	2	1	1			-0.07	-0.01
				3	2	2	1	1			-0.08	-0.02
				4	2	2	1	1			-0.08	-0.02
				5	2	2	1	1			-0.08	-0.02
			3	0	3	3	2	2	450		0	0
				1	3	3	2	2			-0.11	-0.05
				2	2	2	1	1			-0.12	-0.06
				3	2	2	1	1			-0.13	-0.07
				4	2	2	1	1			-0.13	-0.07
				5	2	2	1	1			-0.13	-0.07
			4	0	2	2	1	1	900		0	0
				1	2	2	1	1			-0.2	-0.15
				2	2	2	1	1			-0.23	-0.18
				3	1	1	0	0			-0.25	-0.2
				4	1	1	0	0			-0.25	-0.2
				5	1	1	0	0			-0.25	-0.2

Table 5. The results of water filtration system tests with TSS concentration of 1000mg/l.

Raw water		Run case	Run no.	Time hr	Effluent water						Suction pressure bar	
Turbidity NTU	TSS mg/l				Turbidity NTU		TSS mg/l		Discharge ml/min			
					FM1	FM2	FM1	FM2	FM1	FM2	FM1	FM2
326	1000	Without using peristaltic pump	1	0	2	2	1	1	100	150		
				1	2	2	1	1	98	147		
				2	2	2	1	1	94	142		
				3	2	2	1	1	88	136		
				4	2	2	1	1	88	136		
				5	2	2	1	1	88	136		
		With using peristaltic pump	2	0	2	2	1	1	225		0	0
				1	2	2	1	1			-0.06	-0.01
				2	2	2	1	1			-0.08	-0.03
				3	2	2	1	1			-0.10	-0.05
				4	2	2	1	1			-0.10	-0.05
				5	2	2	1	1			-0.10	-0.05
			3	0	3	3	2	2	450		0	0
				1	3	3	2	2			-0.14	-0.1
				2	3	2	2	1			-0.16	-0.13
				3	2	2	1	1			-0.18	-0.16
				4	2	2	1	1			-0.18	-0.16
				5	2	2	1	1			-0.18	-0.16
			4	0	4	3	3	2	900		0	0
				1	4	3	3	2			-0.22	-0.17
				2	3	3	2	2			-0.27	-0.22
				3	3	2	2	1			-0.28	-0.26
				4	2	2	1	1			-0.28	-0.26
				5	2	2	1	1			-0.28	-0.26

Table 6. The results of water filtration system tests with TSS concentration of 3000mg/l.

Raw water Turbidity NTU	Raw water TSS mg/l	Run case	Run no.	Time hr	Effluent water Turbidity NTU FM1	Effluent water Turbidity NTU FM2	Effluent water TSS mg/l FM1	Effluent water TSS mg/l FM2	Effluent water Discharge ml/min FM1	Effluent water Discharge ml/min FM2	Suction pressure bar FM1	Suction pressure bar FM2
1235	3000	Without using peristaltic pump	1	0	3	3	2	2	100	150		
				1	3	3	2	2	96	145		
				2	2	2	1	1	90	139		
				3	2	2	1	1	83	133		
				4	2	2	1	1	83	133		
				5	2	2	1	1	83	133		
		With using peristaltic pump	2	0	2	2	1	1	225		0	0
				1	2	2	1	1			-0.07	-0.03
				2	2	2	1	1			-0.09	-0.04
				3	2	2	1	1			-0.11	-0.06
				4	2	2	1	1			-0.11	-0.06
				5	2	2	1	1			-0.11	-0.06
			3	0	2	2	1	1	450		0	0
				1	2	2	1	1			-0.17	-0.14
				2	2	2	1	1			-0.18	-0.15
				3	2	2	1	1			-0.19	-0.17
				4	2	2	1	1			-0.19	-0.17
				5	2	2	1	1			-0.19	-0.17
			4	0	2	2	1	1	900		0	0
				1	2	2	1	1			-0.31	-0.29
				2	2	2	1	1			-0.35	-0.32
				3	2	2	1	1			-0.35	-0.32
				4	2	2	1	1			-0.35	-0.32
				5	2	2	1	1			-0.35	-0.32

Table 7. The results of water filtration system tests with TSS concentration of 5000mg/l.

Raw water Turbidity NTU	Raw water TSS mg/l	Run case	Run no.	Time hr	Effluent Turbidity NTU FM1	Effluent Turbidity NTU FM2	Effluent TSS mg/l FM1	Effluent TSS mg/l FM2	Discharge ml/min FM1	Discharge ml/min FM2	Suction pressure bar FM1	Suction pressure bar FM2
1751	5000	Without using peristaltic pump	1	0	4	3	3	2	100	150		
				1	2	2	1	1	89	139		
				2	2	2	1	1	83	133		
				3	2	2	1	1	77	128		
				4	2	2	1	1	77	128		
				5	2	2	1	1	77	128		
		With using peristaltic pump	2	0	4	4	3	3	225		0	0
				1	3	3	2	2			-0.1	-0.07
				2	2	2	1	1			-0.12	-0.08
				3	2	2	1	1			-0.14	-0.11
				4	2	2	1	1			-0.14	-0.11
				5	2	2	1	1			-0.14	-0.11
			3	0	3	3	2	2	450		0	0
				1	2	2	1	1			-0.20	-0.18
				2	2	2	1	1			-0.21	-0.19
				3	2	2	1	1			-0.22	-0.20
				4	2	2	1	1			-0.22	-0.20
				5	2	2	1	1			-0.22	-0.20
			4	0	3	2	2	1	900		0	0
				1	3	2	2	1			-0.34	-0.32
				2	2	2	1	1			-0.36	-0.34
				3	2	2	1	1			-0.36	-0.34
				4	2	2	1	1			-0.36	-0.34
				5	2	2	1	1			-0.36	-0.34

Table 8. The results of water filtration system tests with TSS concentration of 7000mg/l.

Raw water Turbidity NTU	Raw water TSS mg/l	Run case	Run no.	Time hr	Effluent Turbidity NTU FM1	Effluent Turbidity NTU FM2	Effluent TSS mg/l FM1	Effluent TSS mg/l FM2	Effluent discharge ml/min FM1	Effluent discharge ml/min FM2	Suction pressure bar FM1	Suction pressure bar FM2
3194	7000	Without using peristaltic pump	1	0	4	3	3	2	100	150		
				1	3	3	2	2	83	133		
				2	3	2	2	1	77	128		
				3	2	2	1	1	72	122		
				4	2	2	1	1	72	122		
				5	2	2	1	1	72	122		
		With using peristaltic pump	2	0	3	3	2	2	225		0	0
				1	3	3	2	2			-0.2	-0.17
				2	2	2	1	1			-0.24	-0.21
				3	2	2	1	1			-0.25	-0.22
				4	2	2	1	1			-0.25	-0.22
				5	2	2	1	1			-0.25	-0.22
			3	0	3	3	2	2	450		0	0
				1	3	2	2	1			-0.30	-0.28
				2	3	2	2	1			-0.32	-0.30
				3	2	2	1	1			-0.32	-0.30
				4	2	2	1	1			-0.32	-0.30
				5	2	2	1	1			-0.32	-0.30
			4	0	3	2	2	1	900		0	0
				1	3	2	2	1			-0.47	-0.45
				2	2	2	1	1			-0.52	-0.5
				3	2	2	1	1			-0.52	-0.5
				4	2	2	1	1			-0.52	-0.5
				5	2	2	1	1			-0.52	-0.5

Table 9. Removal efficiency of TSS and Turbidity from raw water by using filtration modules FM1 and FM2.

Raw water		Run no.	Filtration module code	Removal efficiency% of TSS			Removal efficiency% of Turbidity		
TSS mg/l	Turbidity NTU			Max.	Min.	Ave.	Max.	Min.	Ave.
500	174	1	FM1	99.80	99.40	99.60	98.85	97.70	98.28
			FM2	99.80	99.40	99.60	98.85	97.70	98.28
		2	FM1	99.80	99.20	99.50	98.85	97.12	97.99
			FM2	99.80	99.60	99.70	98.85	98.28	98.57
		3	FM1	99.80	99.60	99.70	98.85	98.28	98.57
			FM2	99.80	99.60	99.70	98.85	98.28	98.57
		4	FM1	100	99.80	99.90	99.43	98.85	99.14
			FM2	100	99.80	99.90	99.43	98.85	99.14
1000	326	1	FM1	99.90	99.90	99.90	99.39	99.39	99.39
			FM2	99.90	99.90	99.90	99.39	99.39	99.39
		2	FM1	99.90	99.90	99.90	99.39	99.39	99.39
			FM2	99.90	99.90	99.90	99.39	99.39	99.39
		3	FM1	99.90	99.80	99.70	99.39	99.10	99.25
			FM2	99.90	99.80	99.70	99.39	99.10	99.25
		4	FM1	99.90	99.70	99.80	99.39	98.77	99.08
			FM2	99.90	99.80	99.70	99.39	99.10	99.25
3000	1235	1	FM1	99.97	99.93	99.95	99.84	99.76	99.80
			FM2	99.97	99.93	99.95	99.84	99.76	99.80
		2	FM1	99.97	99.97	99.97	99.84	99.84	99.84
			FM2	99.97	99.97	99.97	99.84	99.84	99.84
		3	FM1	99.97	99.97	99.97	99.84	99.84	99.84
			FM2	99.97	99.97	99.97	99.84	99.84	99.84
		4	FM1	99.97	99.97	99.97	99.84	99.84	99.84
			FM2	99.97	99.97	99.97	99.84	99.84	99.84
5000	1751	1	FM1	99.98	99.94	99.96	99.90	99.80	99.85
			FM2	99,98	99.96	99.97	99.90	99.83	99.87
		2	FM1	99.98	99.94	99.96	99.90	99.80	99.85
			FM2	99.98	99.94	99.96	99.90	99.80	99.85
		3	FM1	99.98	99.96	99.97	99.90	99.83	99.87
			FM2	99.98	99.96	99.97	99.90	99.83	99.87
		4	FM1	99.98	99.96	99.97	99.90	99.83	99.87
			FM2	99.98	99.98	99.98	99.90	99.90	99.90
7000	3194	1	FM1	99.99	99.96	99.98	99.94	99.87	99.91
			FM2	99.99	99.97	99.98	99.94	99.91	99.93
		2	FM1	99.99	99.97	99.98	99.94	99.91	99.93
			FM2	99.99	99.97	99.98	99.94	99.91	99.93
		3	FM1	99.99	99.97	99.98	99.94	99.91	99.93
			FM2	99.99	99.97	99.98	99.94	99.91	99.93
		4	FM1	99.99	99.97	99.98	99.94	99.91	99.93
			FM2	99.99	99.99	99.99	99.94	99.94	99.94

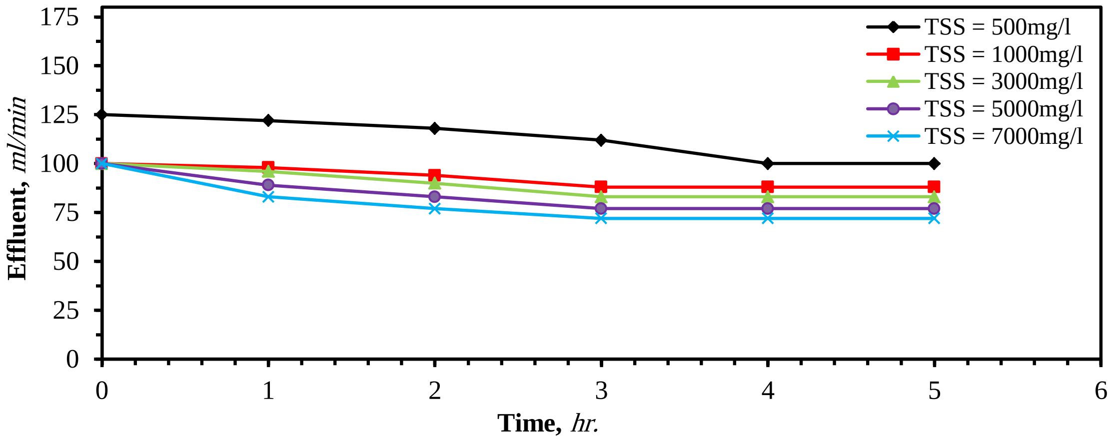

Figure 7. The time variation of effluent of FM1during runs without using peristaltic pump.

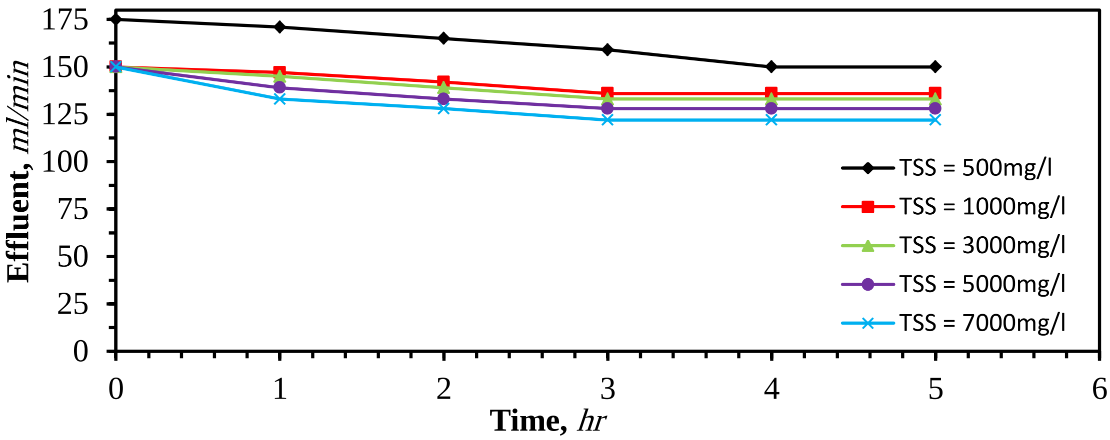

Figure 8. The time variation of effluent of FM2 during runs without using peristaltic pump.

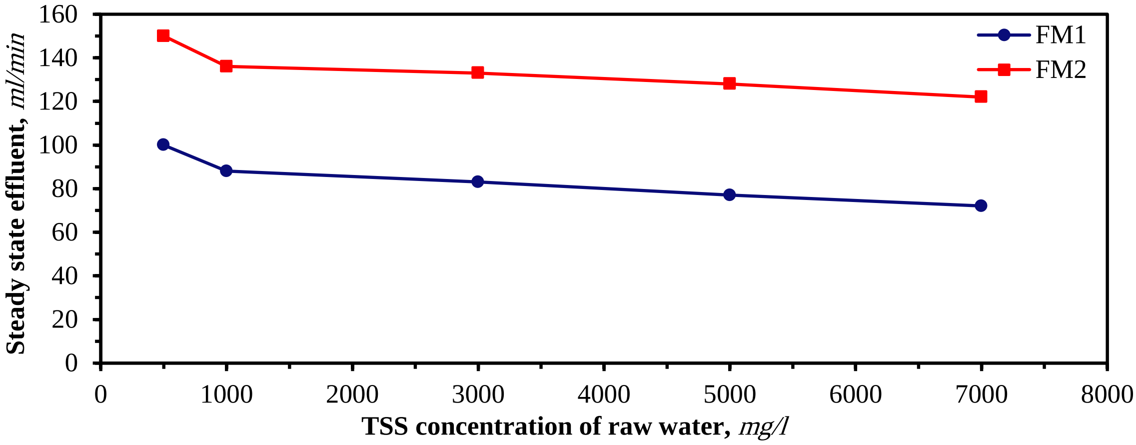

Figure 9. Relation between the steady state effluent of modules and the TSS concentration of raw water without using peristaltic pump.

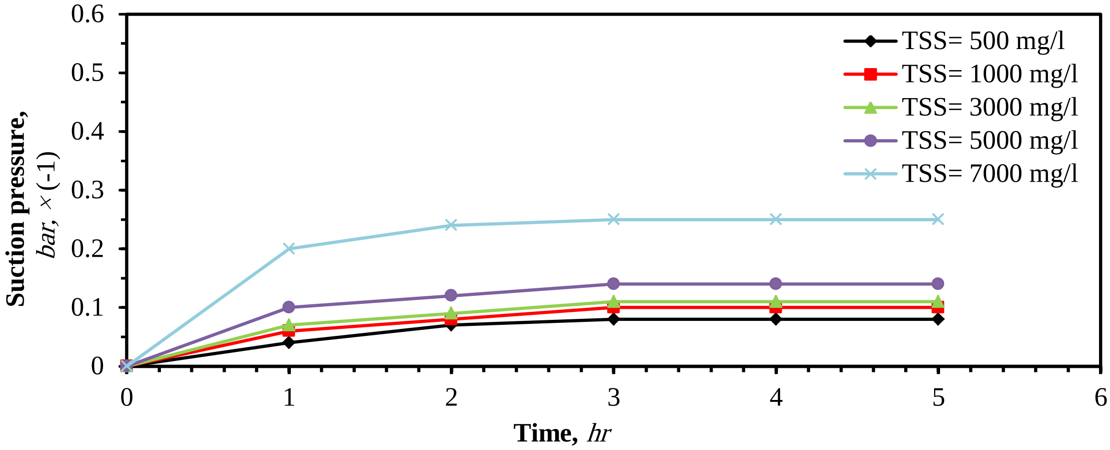

Figure 10. Comparison of time variation of the suction pressure gauge reading of FM1, discharge of peristaltic pump= 225ml/min except for TSS= 500mg/l was = 263ml/min.

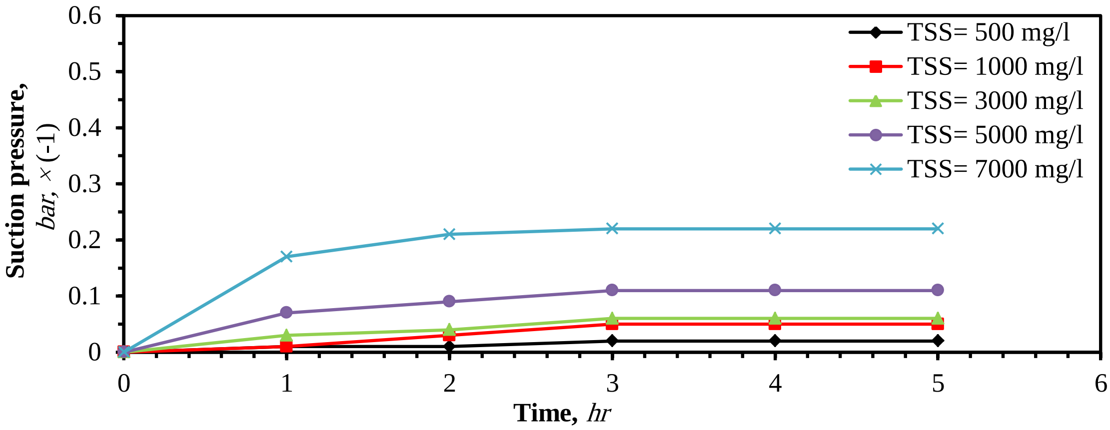

Figure 11. Comparison of time variation of the suction pressure gauge reading of FM2, discharge of peristaltic pump= 225ml/min except for TSS= 500mg/l was = 263ml/min.

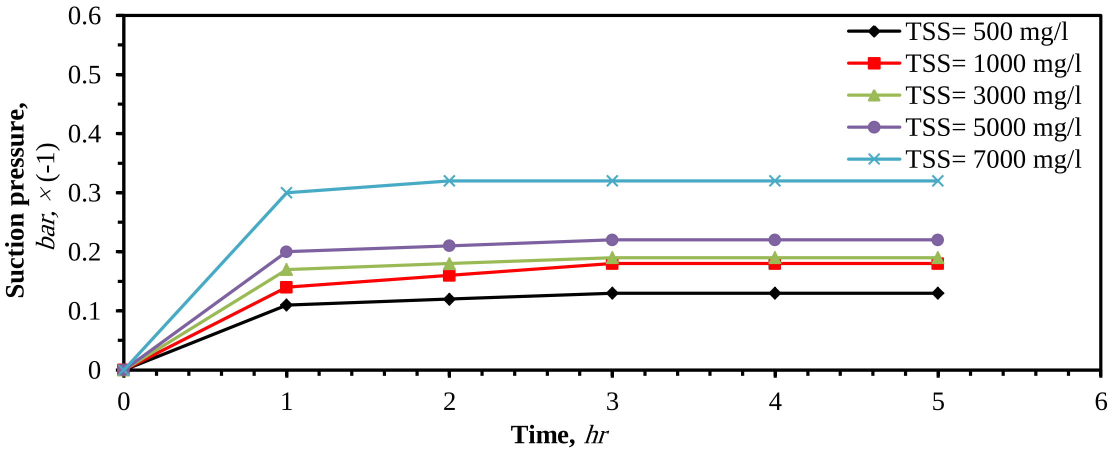

Figure 12. Comparison of time variation of the suction pressure gauge reading of FM1, discharge of peristaltic pump= 450ml/min.

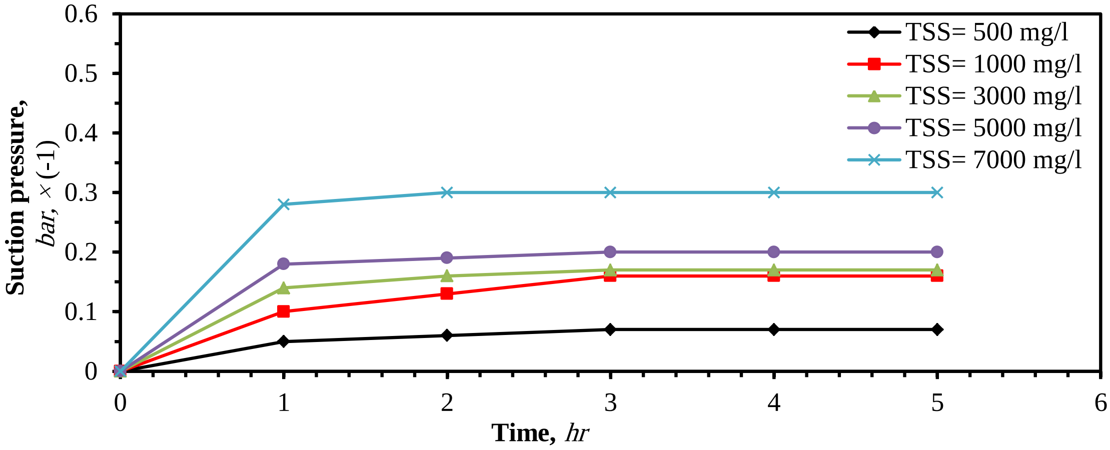

Figure 13. Comparison of time variation of suction pressure gauge reading of FM2, discharge of peristaltic pump= 450ml/min.

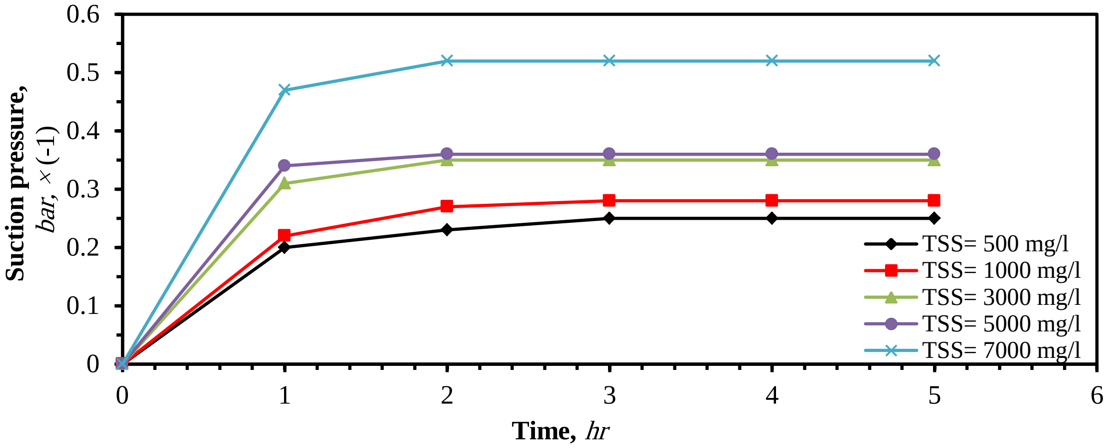

Figure 14. Comparison of time variation of suction pressure gauge reading of FM1, discharge of peristaltic pump = 900ml/min.

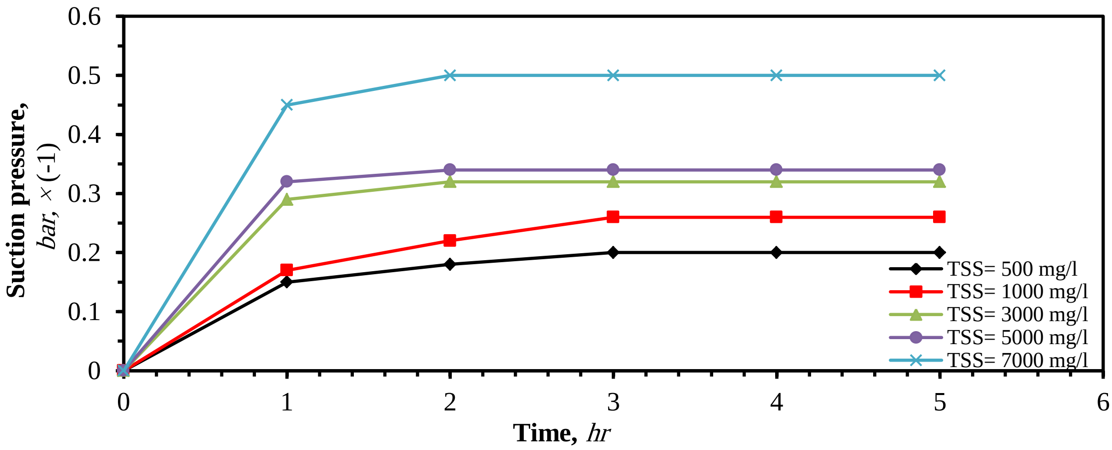

Figure 15. Comparison of time variation of suction pressure gauge reading of FM2, discharge of peristaltic pump = 900ml/min.

Evaluation the Mechanical Properties of Shot Peened TIG Welded Aluminum Sheets

Ahmed Ameed Zain Al-Abideen
Lecturer
Material Eng. Dept.-University of Technology
Email: ahmed_ameed@yahoo.com

Jabbar Hussein Mohmmed
Lecturer
Material Eng. Dept.-University of Technology
Email: jabbaraljanaby@yahoo.com

Najmuldeen Yousif Mahmood
Assistant Lecturer
Mechanical Eng. Dept.-University of Technology
Email: najmuldeen.uot@gmail.com

ABSTRACT

A tungsten inert gas (TIG) welding is one of the most popular kinds of welding used to join metals mainly for aluminum alloys. However, many challenges may be met with this kind of joining process; these challenges arise from decay of mechanical properties of welded materials. In the present study, an attempt was made to enhancing the mechanical properties of TIG weld joint of 6061-T6 aluminum alloy by hardening the surfaces using shoot peening technique. To optimize the shoot peening process three times of exposure (5, 10, and 15) min. was used. All peened and unpeened, and welded and unwelded samples were characterized by metallographic test to indicate the phase transformation and modification in microstructure occurring during welding process. Tensile test and Vickers micro-hardness measurements were performed for all samples to investigate the effect of shoot peening on mechanical properties of welded aluminum. The results indicated a significant improvement in properties for peened welded and unwelded samples compared with those unpeened one. Also, the results showed that the tensile and micro-hardness properties were increased with increasing the time of exposure to 15 min. due to generation of compressive residual stresses at surface.

Key words: shot peening, TIG welding, aluminum alloy 6061 -T6.

تقييم الخواص الميكانيكية لصفائح الالمنيوم الملحومة بطريقة قطب التنكستن المحمي بالغاز الخامل والمعاملة بطريقة القذف بالكرات

احمد عميد زين العابدين
مدرس
قسم هندسة المواد-الجامعة التكنولوجية

جبار حسين محمد
مدرس
قسم هندسة المواد-الجامعة التكنولوجية

نجم الدين يوسف محمود
مدرس مساعد
قسم الهندسة الميكانيكية-الجامعة التكنولوجية

الخلاصة

تعتبر عملية اللحام بقطب التنكستن المحمي بالغاز الخامل (TIG) من اكثر انواع اللحام انتشارا والمستخدمة لربط المعادن وخصوصا سبائك الالمنيوم. رغم هذا فهناك العديد من التحديات والتي ممكن مواجهتها عند استخدام هذا النوع من عمليات

الربط. هذه التحديات ناشئة من انخفاض الخواص الميكانيكية للمواد الملحومة. في الدراسة الحالية تم عمل محاولة لتحسين الخواص الميكانيكية لوصلة من سبائك الالمنيوم (6061-T6) ملحومة بطريقة اللحام بقطب التنكستن المحمي بالغاز الخامل (TIG) من خلال تصليد السطح باستخدام تقنية القذف بالكرات. وللوصول الى الاسلوب الامثل في عملية القذف بالكرات تم استخدام ثلاث ازمان للتعرض (5,10,15) دقيقة. تم توصيف جميع العينات المعاملة بالقذف بالكرات وغير المعاملة، الملحومة وغير الملحومة من خلال فحص سطح المعدن لبيان التحولات الطورية والتغيرات الحاصلة خلال عملية اللحام. تم اجراء فحص الشد وقياس صلادة فيكرز المجهرية لجميع العينات لدراسة تاثير القذف بالكرات على الخواص الميكانيكية لملحومات الالمنيوم. بينت النتائج تحسن ملموس في خواص العينات المعاملة بالقذف بالكرات الملحومة وغير الملحومة مقارنة بالعينات الغير معاملة. بينت النتائج ايضا ان خواص الشد والصلادة المجهرية قد ازدادت مع زيادة زمن التعرض الى 15 دقيقة نتيجة لتوليد مستويات اعلى من اجهادات الضغط المتبقية عند السطح.

1. INTRODUCTION

Aluminum alloys (Al6061) are preferred engineering material for many application in fields of construction (building and high way construction), automobile, aerospace, and various high performing components owing to their lower weight, excellent corrosion resistance, and high thermal conductivity **Kaufman, 1999, Narsimhachary, 2014**. But when joining these materials, there are many difficulties raised. These difficulties are associated with the high thermal conductivity and high coefficient of thermal expansion of aluminum, the existence of tenacious oxide layers, shrinkage, and high solubility of hydrogen in molten state **Narsimhachary, 2014**, **Nandan, 2010**. In addition to, problems associated with phase transformation and softening of the alloys due to heating during welding operation which results in reducing the mechanical properties of alloys **Kumar, et al., 2013**. The welded joints are involved in wide range of components and being used in critical load bearing structures. Therefore, it is important to study techniques or methods that can alleviate these negative effects of welding process and enhance the mechanical properties of welded components. One of these techniques is hardening the surface by shot peening method. Shot peening is a metal working process in which small spherical balls with velocities of 20-120 m/s are fired toward the surface of a part. Shot peening is usually used to produce a continuous layer of compressive stress at the surface of parts **Salman, et al., 2015**. The compressive stress produced by shot peening depends upon several factors; material properties being shot peened, prior processing, and the specific peening parameters (velocity, time exposure, ball diameter) **Mehmood,** and **Hammouda, 2007**.

Many papers were published in this field. The effects of surface hardening by shot peening on fatigue properties for low carbon steel (1020 AISI) were studied by **Abbass, 2008**. She found a significant improvement in the fatigue strength of shot peened welded parts. Similarly, **Salman, et al., 2015** investigated the mechanical properties for welded joint of aluminum alloy 6061 and influence of shot peening of welded parts. Also, the modifying the surface of friction stir welded 7075 aluminum alloy samples by using laser peening and shot peening was analyzed by **Hatamleh, et al., 2007**.

A TIG welding was used in present work to weld 6061 aluminum alloy specimens. TIG welding is one of the most popular methods used to join metals mainly for aluminum alloys. With this method the electric arc, created between a continuously fed filler wire electrode and the metal, provides thermal energy to melt the work piece as well as the filler material **Weman, 2003**.

In this work, shot peening was used to introduce compressive residual stresses into TIG AA-6061-T6. An attempt was involved in this study to optimize the shot peening parameters in order to get the best enhancement of mechanical properties of welded Al6061 specimens. Hence, varying time exposure (5, 10, and 15) was used for shot peening process. The mechanical properties (yield strength and elongation) of unpeened and shot peened TIG welded specimens were investigated also in this work and compared to the base unpeened material.

2. EXPERIMENTAL WORK

2.1 Sample Preparation

The samples used for welding process were rectangular plates (100mm×50mm with a thickness of 3mm) of aluminum alloy (Al6061-T6) and wire type ER4043 used as a filler, their chemical compositions are shown in Table 1. The sample surface was peroxided by stainless steel brush and whipped with acetone solution to remove scale, rust and dirt. **Table 2** illustrates different categories of used samples.

2.2 TIG Welding Process

Cleaned and brushed samples with dimension (100 x 50 x 3) mm were joined by using TIG welding to yield butt joints TIG welding using ER4043 as filler metal and argon as shielding gas. The other parameters were as follows: current 133A, flow rate 33 cfh, gap 1mm, filler diameter 3mm, voltage 20V. The welded samples were then inspected visually by using dye penetrating and magnetic inspections. The inspections revealed there were no defects in welded samples.

2.3 Shot Peening Treatment

All specimens (welded and as received (unwelded samples)) were shot peened with steel ball (1.25 mm mean diameter) for varying time (5, 10, and 15) min. The angle of nozzle inclination was shifted by 10^o with respect to vertical axis to avoid medium collision. A constant distance about 120 mm was maintained between specimen and nozzle.

2.4 Tests and Inspection

2.4.1 Metallographic Practice

Metallographic samples with dimensions (30mm x 20mm x 3mm) were cut from the welded sheets in perpendicular to the welding direction. The as-received and welded samples were prepared by mounting, grinding, polishing and then etched to analyze the microstructure, and observe the change in grain structure. Wet grinding was performed by emery paper of SiC with particle size sequentially (320, 500, 800, 1000, and 1200) and water was used as a coolant and lubricant to facilitate hand grinding. Polishing stage was carried out by using special polishing cloth and diamond paste to obtain mirror polished surface. Finally, etching was performed by immersing the prepared specimen in Keller's Reagent (15 ml HF, 45 ml HCl, 15ml HNO_3 and 25 ml H_2O) for (15-20 sec) and washing by water, then the samples were dried by exposing to stream of warm air. Optical microscope was used to perform this test.

2.4.2 Micro-hardness Measurement

The micro-hardness of the samples was measured with a Vickers micro-hardometer model (HVS-1000). The micro-hardness test was taken using an indentation load of 500 g for 15 seconds at different regions across the surface of the weld. In order to obtain a reliable statistical data, the micro-hardness was evaluated by taking two indentations on each point and averaging of these values.

2.4.3 Tensile Test
The tensile properties for all samples were characterized by using Instron tensile testing machine 3710-016 according to ASTM 638. The orientation of the samples was with the weld in the center of the sample and the load was applied perpendicular to the weld direction. A cross head speed of 10 mm/min was used and all tests were performed at room temperature.

3. RESULTS AND DESCUSSION

3.1 Metallographic
Different regions of the weld were shown in **Fig. 1,** where **1-a** illustrates the microstructure of base metal. While, **Fig. 1-b&c** illustrate the microstructure of weld and the transition area for base metal and weld zone. It is clear from **Fig. 1** that the base metal consists of uniformly distributed and equi-axed grains which are significantly coarser as compared with those of weld zone. Also, it can be noticed that there are some precipitates, represented by dark particles, that are spread uniformly in base metal and their amount are larger than those in weld zone. This may explain the higher strength of base metal. Moreover, it can be shown the dendritic structure in weld zone that may be attributed to the fast heating in welding process of base metal and fast cooling for molten metal as it gets lesser time for solidification.

3.2 Micro-Hardness
Fig. 2 and **Table 3** illustrate the micro-hardness measurement at different locations across the weld zone. There are three areas in which micro-hardness values show significant change, the weld zone; fusion boundary and heat affected zone (HAZ). The largest value of micro-hardness was at base metal 90 HV. The lowest value was recorded at HAZ and weld center. As it moves from the HAZ the micro-hardness values increase at fusion boundary and then return to decrease at near and at weld line due to softening effects. Micro-hardness value varies at a range of 90 HV to 56 HV from base metal to weld center. The variations in micro-hardness values may be correlated to the microstructure developed after the welding process. The low level in micro-hardness at base metal can be explained by coarsening grain size structure which reduces the effect of precipitation elements. The higher value of micro-hardness at fusion boundary may be attributed to recrystallization process occurring at this region due to high temperature during the thermal cycle of the TIG welding which yielded fine grain size. Moreover, it may be due to precipitation of intermetallic phase and thermal cycles. The same findings were observed by **Kumar, et al., 2013, and Abbass, at el., 2013**. They reported that this variation in micro-hardness values is due to phase transformation induced by fusion weld metal effect of heat input.

3.3 Tensile Properties
Fig. 3 and Table 4 summarize the results of tensile test for all samples. These results indicate that the highest tensile properties was for unwelded samples (as received or peening treated sample) as compared with other TIG weld samples in all cases. These are revealing that the effects of softening occurred due to high temperature involved in welding process. The microstructure test shows the phase transformation was taking place in weld zone. It is also observed that the location of fracture was at or near the weld line. As reported previously **Suzuki,** and **Hasegawa, 2007**, there is relation between surface hardness and tensile properties, and it was clarified that

the surface hardness is one of the main factors for determining the tensile, tensile, and fatigue strength. **Fig. 2** shows that the HAZ region and weld center have the lowest micro hardness area because the recrystallization process occurs in this region due to high temperature and the decreasing in participates particles left in the material. **Hatamleh, et al., 2007**, found the similar results and reported in his article the effect of laser and shot peening on fatigue life that "this area of the weld will be relatively ineffective in inhibiting dislocation motion and the strain localization in the softened area of the weld will result in a degradation of the mechanical properties".

On the other hand, an improvement in tensile strength and elongation was recognized with shot peening treated samples in all conditions. Moreover, it is noticed that there is significant effect of shot peening time on magnitude of this improvement in tensile and elongation properties. The improving properties were increased with shot peening time 5 and 15 min. while decreased for 10 min. This variation may be caused by the quantity of residual compressive stress generated at the surface and its values and distribution. Compared to tensile strength of unpeened samples of about (300) MPa, the tensile strength of shot peened samples for 5, and 15 min was about (334 and 332) MPa respectively. The increase of about 11% was recognized. The same trend was observed with TIG weld samples, where the tensile properties of shot peened TIG weld samples exhibited higher values than unpeened TIG weld samples in all cases. The specimens processed with shot peening indicated around 11.2% increase on average in tensile strength when compared to the unpeened TIG weld samples. In the same manner, it is noticed also from the results that the properties were changed as a result of changing the shot peening exposer time. The tensile properties were enhanced in about 5.5 % with shot peening 15 min as compared with (5 and 10) min.

4. CONCLUSIONS

It can be concluded from the results above the following points:

- Properties of weld zone are greatly affected by microstructure and softening effects.
- Shot peening is effective way to improve the properties of welded structures. It improved the yield strength in about 11.2%.
- The effect of shot peening on the improvement of time exposure properties is apparent and more obviously at time of 15 min and in lesser level at time 5 min.

REFERENCES

- Abbass, M. K., Abd, H. H., 2013, *A Comparison Study of Mechanical Properties between Friction Stir Welding and TIG Welded Joints of Aluminum Alloy (Al 6061-T6)*, Eng. & Tech. Journal, Vol. 31, Part (A), No. 14.

- Abbass, M. K., 2008, *Effect of Shot Peening on Fatigue Strength of Welded Joints For Low Carbon Steel* , Eng. & Tech. Journal, Vol. 26, No.3.

- Hatamleh, O. , Lyons J., and Forman R., 2007, *Laser Peening and Shot Peening Effects on Fatigue Life and Surface Roughness of Friction Stir Welded 7075-T7351 Aluminum*, Fatigue & Fracture of Engineering Materials & Structures, Vol. 30, No. 2, pp. 115-130.

- Kaufman, J. G., 2002, *Properties of Aluminum Alloys; Tensile, Creep, and Fatigue Data at High and Low Temperatures*, the Aluminum Association Inc. and ASM International, Washington, USA

- Kumar, P., Anoop, C. A., and Kumar, S., 2013, *Study of Heat Input for GTA Welded Aluminium Alloy 7039*, International Journal of Engineering Science and Innovative Technology (IJESIT), Vol. 2, No. 5.

- Mehmood, A., and Hammouda M. M. I., 2007, *Effect of Shot Peening on the Fatigue Life of 2024 Aluminum Alloy*, Failure of engineering materials & structures, Code 02, pp.1-12.

- Nandan S. J., 2010, *Double-Sided Arc Welding of AA5182 Sheet in the Lap-Joint Configuration*, Master Thesis, University of Waterloo, Canada.

- Narsimhachary, D., 2014, *Effect of Laser Welding Parameters on 6061 Aluminium Alloy*, Master Thesis, National Institute of Technology, Rourkela.

- Salman, H. K., Abbass M. K., and Mohammed, A. H., 2015, *Effect Of Shot Peening On The Mechanical Properties For Welded Joints of Aluminium Alloy 6061 -T6*, NDMRP, Vol. 2, pp. 43-56.

- Suzuki, H., and Hasegawa, M., 2007, *Effect of Shot Peening on Fatigue Strength of Friction Welded Joint with Flash under the Condition of the Various Carbon Steel for Machine Construction*, Quarterly Journal of the Japan Welding Society, Vol. 27, No. 2, pp. 381-385.

- Weman, K., 2003, *Welding Process Handbook*, Cambridge, England.

Table 1. Chemical Analysis of the used materials 6061 - T6 and Filer wire ER 4043.

Element	Cr	Cu	Fe	Mg	Mn	Si	Ti	Al
Measured Value	0.04-0.35	0.15-0.4	Max 0.7	0.8-1.2	Max 0.15	0.4-0.8	Max 0.15	balanced
Standard Value	0.25	0.35	0.55	1	0.15	0.4	0.12	balanced
Filer Metal	0.15	0.3	0.45	0.9	0.15	0.45	0.12	balanced

Table 2. Test samples classification

No.	Symbol	Conditions
1	$A_{\circ}$	As received (unwelded samples)
2	A_1	As received + shot peening 5 min.
3	A_2	As received + shot peening 10 min
4	A_3	As received + shot peening 15 min
5	$B_{\circ}$	TIG Weld Process
6	B_1	TIG Weld + shot peening 5 min
7	B_2	TIG Weld + shot peening 10 min
8	B_3	TIG Weld + shot peening 15 min

Table 3. Micro-hardness values across the TIG weld A6061-T6 sample**.**

Distance	-12	-11	-10	-9	-8	-7	-6	-5	-4	-3	-2	-1	0 Weld line
Micro-hardness Value	90	88	73	66	57	56	61	59	78	80	63	57	56
Distance	1	2	3	4	5	6	7	8	9	10	11	12	....
Micro-hardness Value	66	75	74	56	58	61	65	68	76	79	88	89	.....

Table 4. Tensile test results of all samples

Sample	Yield Strength MPa	Elongation %
$A_{\circ}$	300	17
A_1	334	21.7
A_2	304	21.9
A_3	332	21.7
$B_{\circ}$	140	7.2
B_1	151	9.7
B_2	150	9.3
B_3	158	12

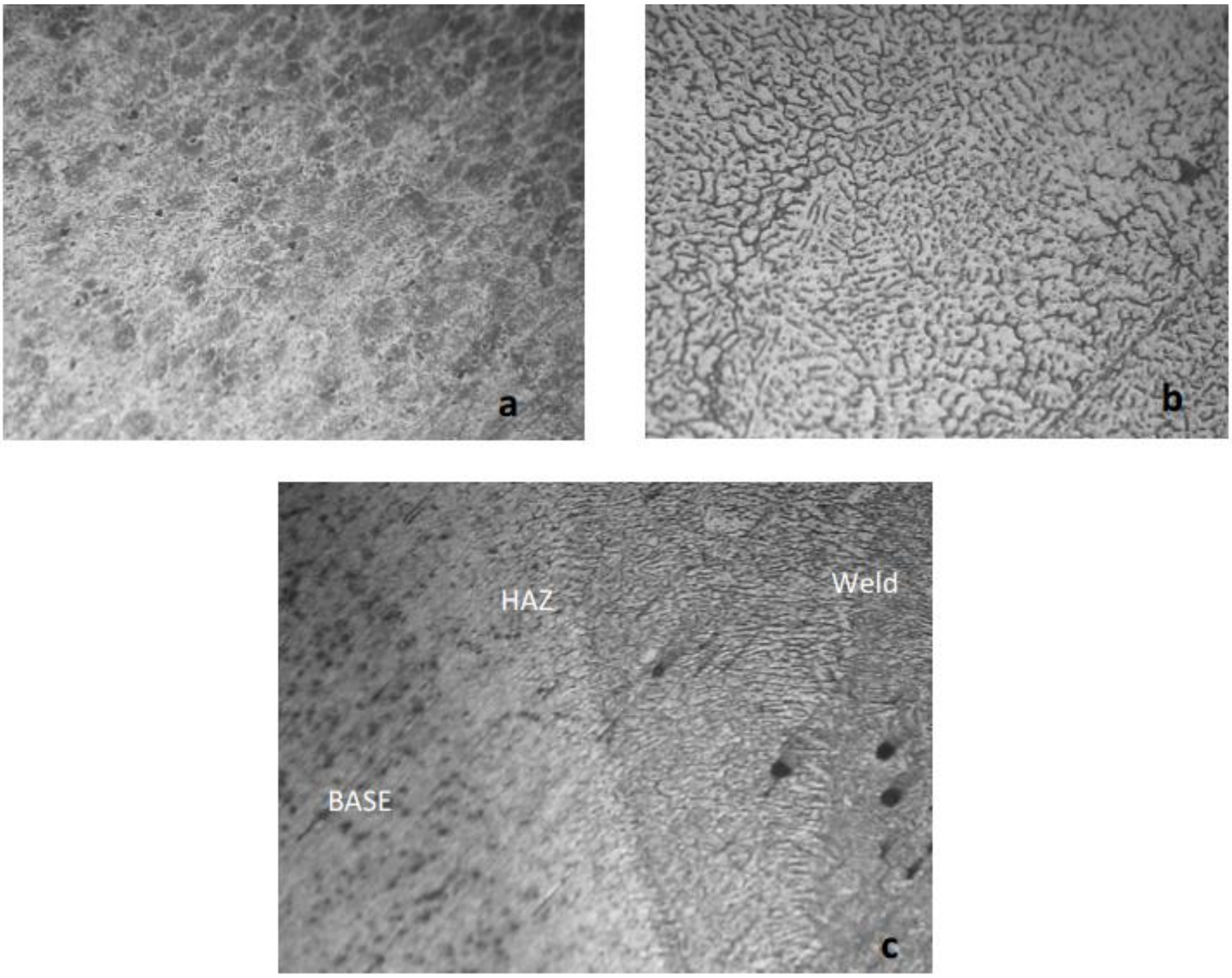

Figure 1. Microstructure of samples a- base metal, b- weld zone, c- base metal, HAZ, and weld zone interface. (20X).

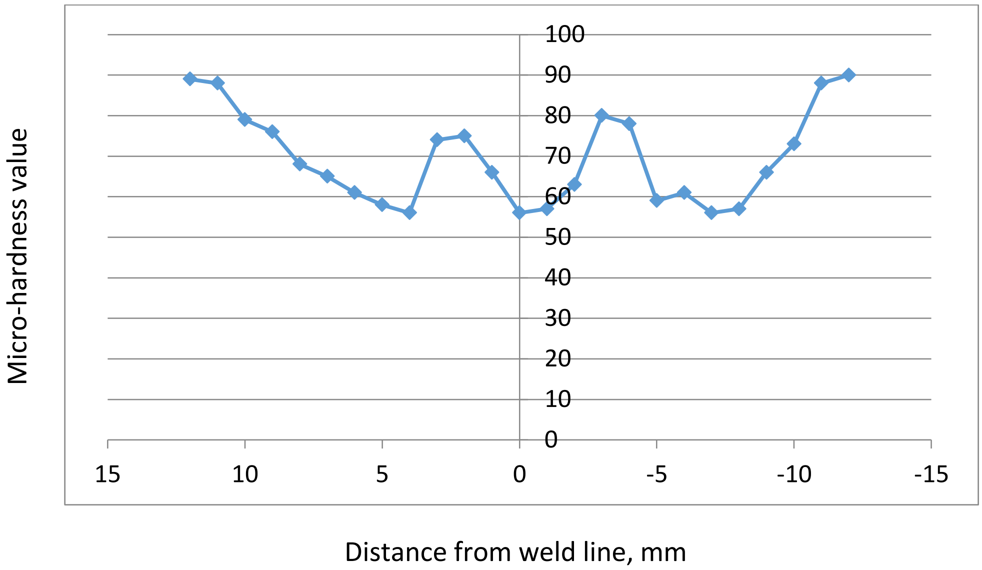

Figure 2. Micro-hardness distribution across the TIG weld A6061-T6 sample

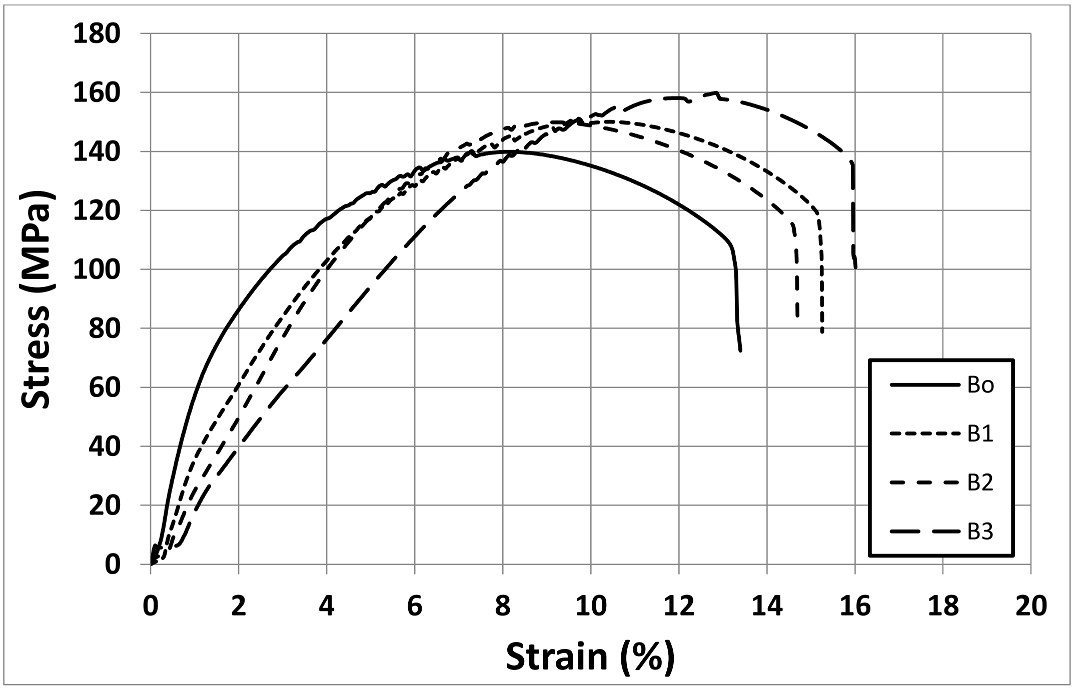

Figure 3. Stress-strain curves of all samples

Thermo-Physical and Mechanical Properties of Unsaturated Polyester /Cobalt Ferrite Composites

Lamees Salam Faiq
Assistant Lecture
Materials Engineering Department,
University of Technology
Email:lameessalam@yahoo.com

Zahraa Fadyal Attiyah
atyahzahraa@yahoo.com

ABSTRACT

Unsaturated polyester was used as a matrix which was filled with different percentages of cobalt ferrite using hand lay-up method. Cobalt ferrite was synthesized using solid state ceramic method with reagent of CoO and Fe_2O_3. Mechanical properties such tensile strength, Young's modulus and shore D hardness of the composite have been studied. All these properties have increased by 10% with increasing cobalt ferrite contents. Also the thermal properties such thermal conductivity and specific heat capacity are highly increased as the ferrite content increased, while the thermal diffusivity increased by 22 %. On the other hand dielectric strength of composite has been measured which increased by 50% by increasing the cobalt ferrite content.

Keywords: cobalt ferrite, thermal conductivity, thermal diffusivity, specific heat capacity, tensile strength, dielectric strength.

الخواص الفيزو حرارية والميكانيكية لمتراكب بولي استر الغير مشبع/ كوبلت فرايت

لميس سلام فائق
مدرس مساعد
قسم هندسة المواد- الجامعة التكنولوجية

زهراء فاضل عطية

الخلاصة

استخدم البوليستر غير المشبع كمادة اساس وذلك بتدعيمها بنسب مختلفة من فرايت الكوبلت ، تم تحضير المتراكبات بالطريقة اليدوية. أستخدمت طريقة الحالة الصلبة السيراميكية وهي احدى الطرق التقليدية في تحضير فرايت الكوبلت .

درست الخواص الميكانيكية مثل متانة الشد ، معامل يونك وصلادة شور دي. كل هذه الخواص تأثرت باضافة فرايت الكوبلت حيث تزداد هذه الخواص مع زيادة نسبة الكوبلت فرايت.

اما الخواص الحرارية مثل التوصيلية الحرارية والنفاذية الحرارية والسعة الحرارية النوعية فقد تم دراستها وايضا تأثرت باضافة فرايت الكوبلت حيث ازدادت بصورة بسيطة. ايضا تم دراسة متانة العزل لهذا المتراكب وازدادت بزيادة محتوى فرايت الكوبلت.

الكلمات الرئيسية: كوبلت فرايت، التوصيلية الحرارية، الانتشارية الحرارية، السعة الحرارية النوعية، مقاومة الشد، مقاومة العزل الكهربائي.

1. INTRODUCTION

The importance of polymer is mainly still regarded as a cheap alternative material that is manufactured easily. The intensive use of polymer in broad use has led to the development of materials for specific applications namely composite. One of these polymers is unsaturated polyester which characterized by vinyl unsaturation in the polyester backbone which is thermosetting polymer unsaturated polyester resins are most widely used in systems, particularly in marine industry. By for the majority of dinghros, yachts and workboat built in composite make use of the resin system **Han and Soon, 2001**.

Ferrite with spinel structure represents the importance class of magnetic materials which are ferromagnetic oxides consisting of ferric oxide and metals oxides. The spinel ferrites having the chemical formula MFe_2O_4 (where M is a divalent metal ions such Co, Ni, Mn , etc.) **Mukta, et al., 2009**.

Among the different spaniel ferrites cobalt ferrites $CoFe_2O_4$ are promising magnetic materials because of their moderate saturation magnetization, high electrical properties, high magnetic-crystalline anisotropy, good mechanical properties and chemical stability **Mukta, et al., 2009**.

Magnetic polymer composites are a subclass of composite materials which have attracted the attention of the researchers and scientists due to their unique properties, which render their use to be important in various applications such as high capacity information storage device, integral circuits, micro sensors, cell separation, bioprocessing, medical diagnosis and controlling drug delivery **Gomez-Del et al., 2014, Gardea and Lagoudas 2014**.

Adding small amounts of ferrite particles into polymers is one of the major research challenges because they can substantially improve the quality of composite materials in the terms of mechanical, thermal and electrical properties **Andrei et al., 2006**.

Haifel et. al. have studied the thermal conductivity and dynamic mechanical analysis of ferrite particles filled thermoplastic natural rubber composite **Haifel et al., 2013**.

Many works have been done on polymer based composites filled with magnetic materials in micrometer- size such as barium ferrite **Li et al., 2007**. NiZn ferrite **Nakamuca et al., 1994** and Fe_3O_4- Yag **Yusof et al., 2007**. Faiq and Attiyah have studied the effect cadmium ferrite on the epoxy resin. The mechanical properties and thermos- physical properties have affected with incorporated the ferrite content **Faiq and Attiyah, 2016**.

The main objective of the research is to study the effect of cobalt ferrite on the mechanical and thermal properties and dielectric strength of polyester.

2. EXPERIMENTAL PART

2.1 Materials Used:

Cobalt ferrite was synthesized from reagent grade of CoO and Fe_2O_3 using solid state ceramic method.

The unsaturated polyester resin is used as the matrix in the preparation of ferrite- polymer composite. It is provided from the Saudi Arabia (SIR) Company in the form of transparent viscous liquid at room temperature which is a thermally hardened polymer (thermosets) with a density of (1.255 gm / cm^3). MEKP is stable organic peroxide that decomposes rapidly in the presence of certain metallic carboxylate salts. MEKP is used as hardener Table 1 shows the characteristics of unsaturated polyester used in the research.

2.2 Procedures:

The synthesis of cobalt ferrite starting from stoichiometric mixture of CoO and Fe_2O_3 subjected to a combination of mechanical mixing and ball milled grinding and then sintered at 1200°C for 4 hrs.

The unsaturated polyester was in the form of viscous liquid, transparent pink color at room temperature.

The resin converts from a liquid to solid state by adding hardener which is manufactured by the company itself; a methylethylketon peroxide symbolized by (MEKP) in the form of a transparent liquid is added to resin by rate 2% room temperature and increasing the speed of hardened by stirring for 2 hrs. The most basic fabrication method for thermoset composite is hand lay-up which is typically consisted of laying polymer layer by hand on to a tool to form a laminate stack. A good mixing between polymer and its hardener is done to form a matrix. Cobalt ferrite powder with different percentages(2,5,8,10,15)% mixed with matrix and stirred for one hour to avoiding any bubbles occur.

The mixture was poured into a mould. Finely composite plates were cut into different shape and dimensions for each test according to international standard. The casting time occurred overnight at room temperature.

2.3 Characterization:

2.3.1 Tensile test

The tensile test was performed according to (ASTM D638) at room temperature with capacity (20KN) applied load and strain rate of (0.5 mm/min) by using the machine type WDW-200E. **Fig. 1** shows the tensile machine and **Fig. 2** shows standard and experimental specimens for tensile test.

2.3.2 Hardness test

The hardness test is performed by using hardness (Shore D) and according to (ASTM DI-2242) standard. Samples have been cut into a diameter of (40mm) and a thickness of (5mm). **Fig.3** shows the hardness machine.

2.3.3 Thermal and dielectric properties test

To study the thermal properties test, two samples with the same dimensions have been prepared according to the standard specifications of instrument (3x2)mm, one of the most precise and convenient techniques for studying thermal transport properties is the transient plane source (TPS) method. It is a modern technique, yielding information on thermal conductivity, thermal diffusivity as well as specific heat per unit volume of material under study. The dielectric strength is performed by the impedance analyzer device. The optimization of polymer/ ferrite filler interfacial interaction is significant for the enhancement of thermal transport of polymer/ ferrite composite. The most important thermos- physical properties of a material that are needed for heat transfer calculations are: thermal conductivity, thermal diffusivity and specific heat. **Fig.4** shows thermal properties machine and **Fig. 5** shows thermal properties specimens. The dielectric strength is performed by the impedance analyzer device.

3. RESULTS AND DISCUSSION:

X- ray diffraction (XRD) was carried out at room temperature to determine the crystallinity of cobalt ferrite. All the diffraction peaks in the XRD pattern were compared with JCPDS (standard values cards) with nearly no impurities respect to cobalt ferrite pattern. It shows that the cobalt ferrite formed well defined spinel phase as shown in **Fig. 6.** The tensile strength at break for ferrites composite with variation of ferrite contents are demonstrated in **Fig. 7.** It can be seen from the graph that at 10% ferrite content the tensile strength shows remarkable increasing with the highest value of 27 MPa. As the content of ferrite continually increased the tensile strength of composite slightly increased. The lowest value of 14 MPa is for pure polymer.

The incorporation of cobalt ferrite as filler loading actually is associated with the improvement of tensile strength. The effect of good interface between cobalt ferrite particles and polyester resin is very important to the composite to stand the strength. When load is applied the matrix will distribute the forces to cobalt ferrite, which carry most of the applied load. The same behavior was for the Young's modulus of the composite, the modulus increased slightly with the ferrite content having the highest value at 10% with 2.93 GPa Young's modulus after that it decreased as shown at **Fig.8**.

Fig.9 represents the effect of ferrite content on the shore D hardness of the composite which again is increased as the ferrite content increased having a high value at 10% with value of 85.3 and then decreased while the hardness of pure polyester is 74. Most mechanical properties may be due to the flaw acts as stress concentration and causes the bond between the filler content and the matrix to break. The filler will act as physical and chemical cross-linking points and restricts the movement of polymer chain. It is a sign of the materials flexibility, which shows that the addition of cobalt ferrite creates a stronger but yet brittle composite **Surata et al., 2014**.

Fig. 10 reveals the thermal conductivity measured at different content of cobalt ferrite. It can be observed that the thermal conductivity of the composite with 10% cobalt ferrite is larger than pure polyester or other present thermal transport in the ferrite composite includes phonon diffusion in the matrix and ballistic transportation in the filler. The improving of thermal conductivity in this composite may stem from the improved percolation because of better dispersion and formation of a network **Jin et al., 2007**. This indicates that the thermal properties of the composite are mainly dominated by the interface thermal transport between cobalt ferrite /matrix interface **Kumar et al., 2007**.

The thermal diffusivity is an important property in all problems involving a non-steady state heat transfer. **Fig. 11** represents the effect of ferrite content on thermal diffusivity of the composite having the highest value at 15% cobalt ferrite which increased slightly with the increasing content of ferrite. The thermal diffusivity of the composite cannot be explained solely by the differences in the properties of the ferrite content. This indicates that the real quality determined in this study was so-called apparent thermal diffusivity **Sivakumar et al., 2007**. The obtained values of thermal diffusivity are affected by some factors e.g heat losses as a temperature dependent thermo-physical property. It depends too much on density of the used materials while the specific heat capacity has much effect on thermal diffusivity.

Fig. 12 represents of the heat capacity of the composite which is affected by cobalt ferrite content, again the same behavior occurs having the specific heat capacity with high value at 10% cobalt ferrite which increased as the content of ferrite increased but it decreased slightly after 10% cobalt ferrite.

Fig.13 demonstrates the dielectric strength of the composite against the ferrite content. As shown in the figure the pure polymer has a good dielectric strength which is 8.29KV/mm, but when adding the ceramic material (cobalt ferrite) which has a high strength because it is good insulator. The dielectric strength increased with increasing ferrite content having the highest value at 15% **Hasselman and Donaldson, 1990**.

4. CONCLUSIONS

From the work done on the synthesis of cobalt ferrite and the polymer/ ferrite composite the following conclusions can be drawn

1- Solid state ceramic method is a good method for synthesis cobalt ferrite.

2- All the mechanical properties increased with cobalt ferrite content at 10% and then decreased.

3- The thermal properties are affected by the incorporation of cobalt ferrite powder which increased slightly with the ferrite content.

4- Dielectric strength of the composite was affected by the ferrite content.

4. REFERENCES

- Andrei, G., Dima, D., Andres, L., 2006, *High Weight Magnetic Composite for Aircraft Applications* of Optoelectronic, Adu.M.Vol. 81, PP. 726-730.
- Faiq, L.S. and Attiya, Z.F., 2016, *The Effect of Ferrite Content on the Thermomechanical properties and Dielectric Strength Properties of Epoxy* Composite, J.Eng. and Technology Vol. 34, Part (A), No.1.
- Gardea , F. and Lagoudas , D., 2014, *Characterization of Electrical and Thermal Properties of Carbon Tube / Polymer Composite*, Composite, Part B, Eng.Vol 56, PP. 611-620.
- Gomez-Del, T., Rodriguze , J. and Pearson, R., 2014, *Compression Properties of Modified Polymer Resin at Different Strain Rates*, Composite, Part B, Engineering, Vol.57,PP.173-179.
- Haifel, M., Ahmed, S., Harsan, A., Bahr, S., Tarawneh, M. and Jue L. r, 2013, *Composite,Part B*, PP. 334-339.
- Han, M. and Soon , S., J., 2001, *Polyesters and Their Applications*, Appl.Polym.Sci., Vol. 82,PP2760.
- Hasselman, D. and Donaldson, K., 1990, *Effect of Detector Nonlinearity and Specimen Size on the Apparent Thermal Diffusivity of NIST8425 Graphite*, International Journal of thermoplastic, Vol. 1113, PP. 573-588.
- Jin, J., Park, Y. and Yoon, K., 2007, *Rheological and Mechanical Properties of Surface Modified Multi- Walled Carbon Nanotube Filled PET Composite*, Composite Science and Technology, Vol. 6, No. 15-16, PP. 3434-3441.
- Kumar S., Alan M. and Murthy J., 2007, *Effect of percolation in thermal transport in nanotube composite*, Applied letters, Vol.90, No. 10.
- Li, B., Shen, Y., Xue, Z. and Nan, C., 2007, *Influence of Particle Size on Electromagneti Behavior or Microwave Absorption Properties of Barium Ferrite Polymer Composite*, J.Magn.Magn.Mater.Vol.313, PP.322-328.
- Mukta, L., Shashi, S., Sadgupal, D., Kuthari, R., Ajay, A. and Sulabla K., 2009, *High Coercivity of Oleic acid $CoFe_2O_4$ at Room Temperature*, J.Phys.Chem.B, Vol. 113, PP. 9670 – 9076.
- Nakamuca, T., Tsu taokaed, T., Hatakeyanea, K., 1994, *Frequency Disperses of Permeability in Ferrite Composite Materials*, J.Magn.Magn.Mater. Vol.138, PP.319-328.

- Shinde, A., 2013, *Structural and Electrical Properties of Cobalt Ferrite*, International Journ of Innorative Technology and exploring Engineering , Vol.5, Issue 4.
- Surata, W., Agunged, J., Arnis, K., *Mechanical Properties of Rice Husks Powder Reinforced Polymer Composite,* 2014, International J. of Materials, mechanic and manufacturing, Vol. 2, No. 2.
- Sivakumar, R., Guo, S., Nishimura, T. and Kagana, Y., 2007, *Thermal Properties in Multi Wall Carbon Nanotube / Silica- Based Composite*, Scripta materialia, Vol.56, No.4, PP. 265-268.
- Yusof, A., Sani, J., Abdullah, M. and Ahmed, N., 2007, *Electromagnetic and Absorption Properties of Polymer /Fe_3O_4/Yag Microwave Absorbers and Specular Absorbers Method*, *Sains Malusian*, Vol.26, PP.165-175.

Table 1 Characteristics of unsaturated polyester used in the research

Density(gm/cm^3)	Tensile strength (MPa)	Percent elongation (EL%)	Thermal conductivity w/m.c^o
1.255	70.3 -103	<2.6	0.17

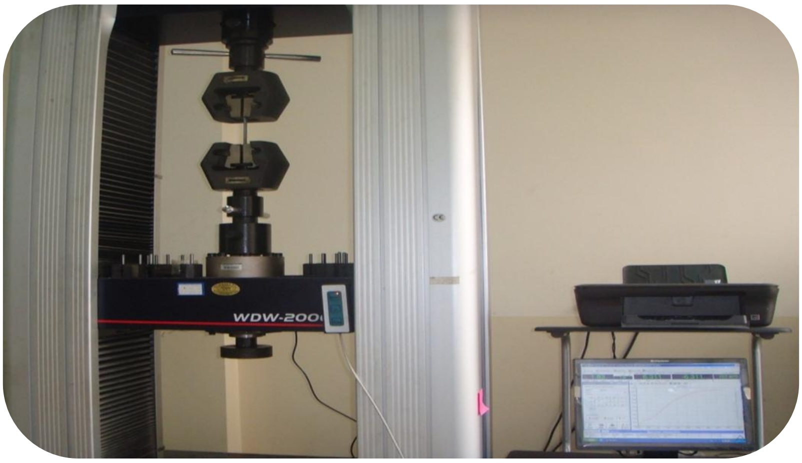

Figure1. Tensile strength machine.

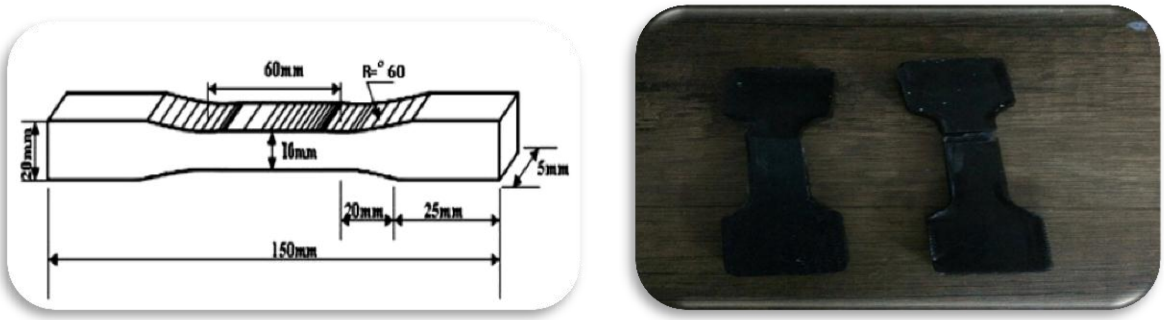

Figure2. Standard and experimental specimens for tensile test.

Figure 3. Hardness device.

Figure 4 .Thermal properties device.

Figure 5. shows thermal properties specimens.

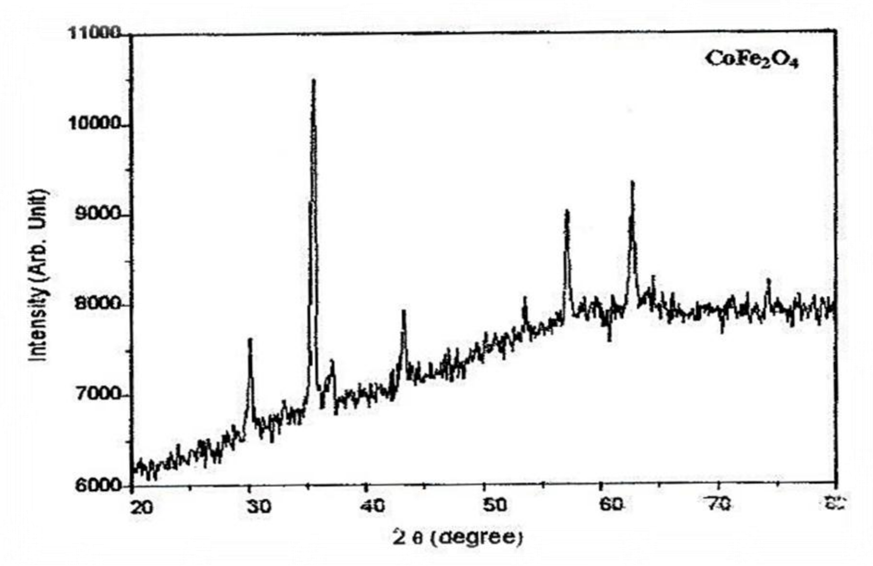

Figure 6. XRD pattern of cobalt ferrite.

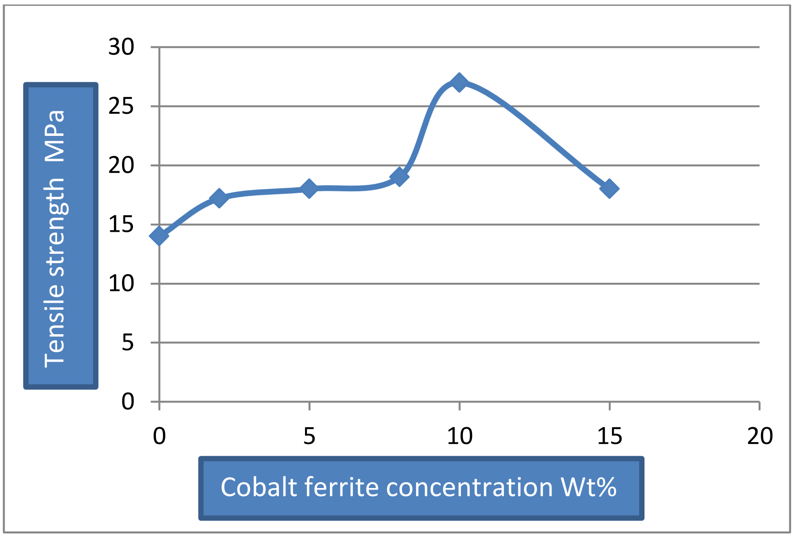

Figure 7**.** The effect of ferrite content on the tensile strength of composite.

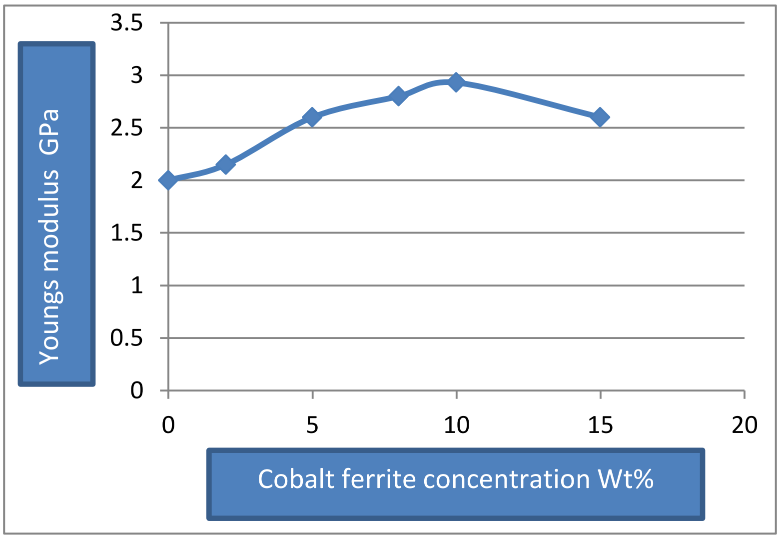

Figure 8. The effect of ferrite content on the youngs modulus of composite.

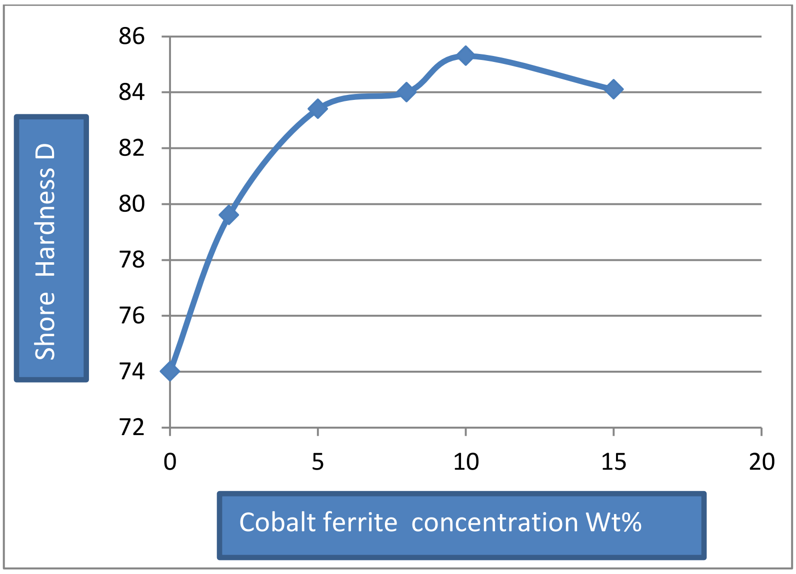

Figure 9. The effect of ferrite content on the shore hardness D of composite.

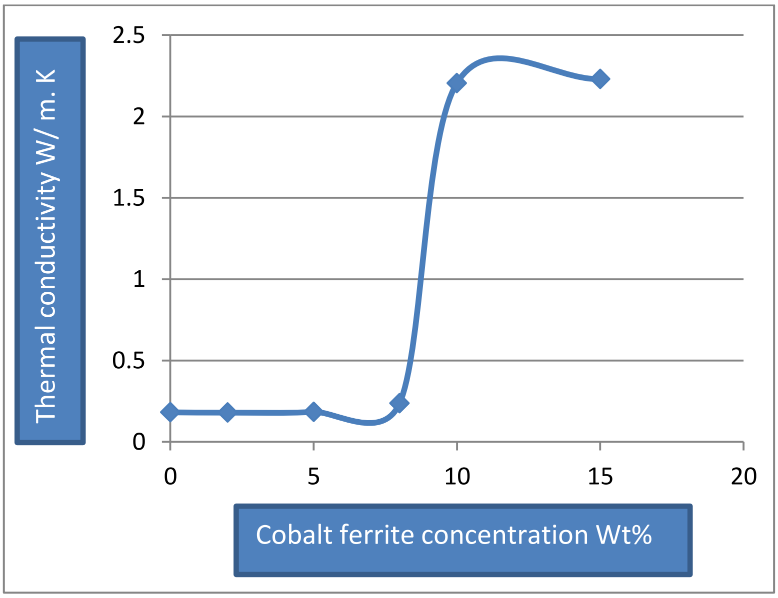

Figure 10 . The relation between cobalt ferrite content and thermal conductivity of composite.

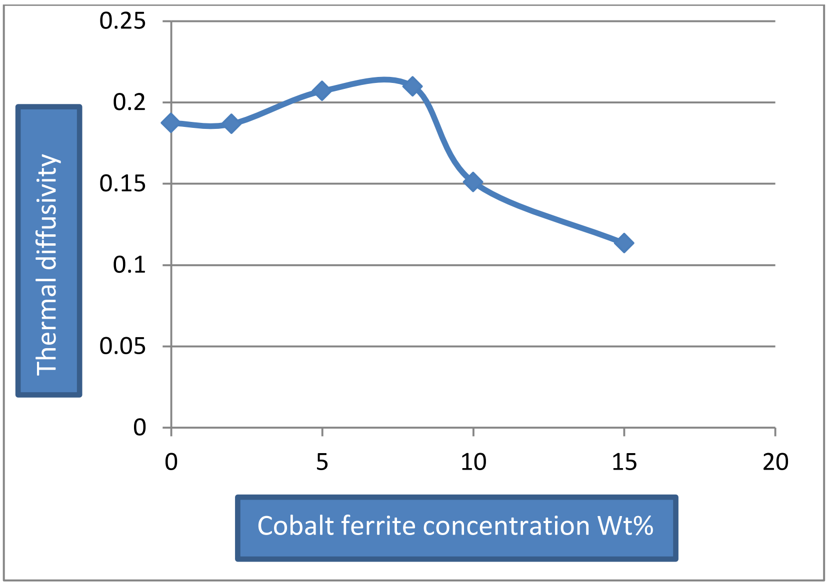

Figure 11. Thermal diffusivity vs cobalt ferrite content.

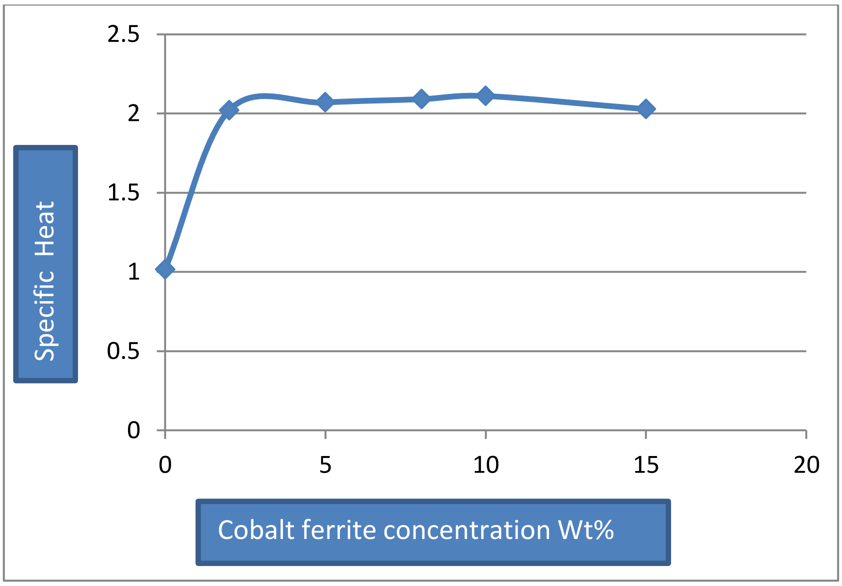

Figure 12. The relation of specific heat capacity with ferrite content of the composite.

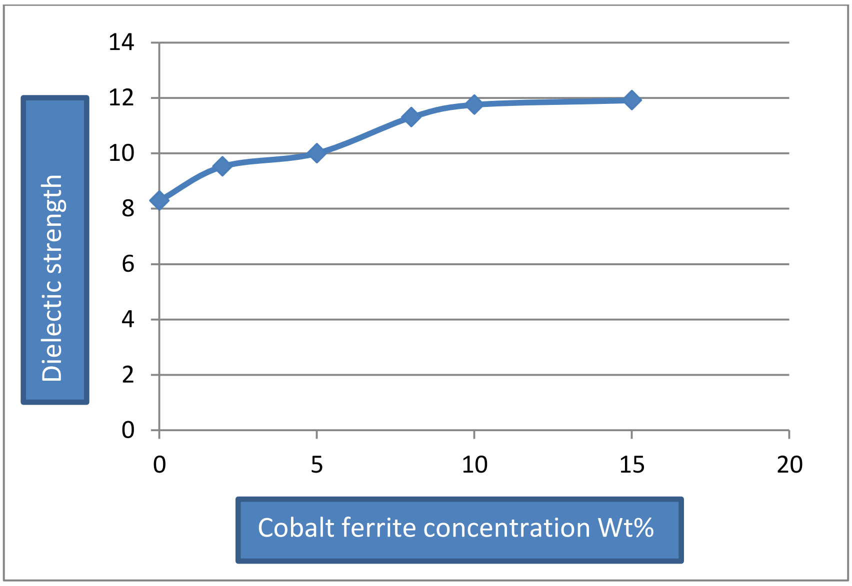

Figure 13. Dielectric strength of composite vs cobalt ferrite content.

Free Vibration Analysis of Laminated Composite plates with General Elastic Boundary Supports

Dr.Wedad Majed Ibrahim
Assisant proffesor
College of Engineering-University of Baghdad
email: wedad_majeed@yahoo.com

Rafat Assad Ghani
Msc student
College of Engineering-University of Baghdad
email-rafat_eng90@yahoo.com

ABSTRACT

In this investigation, Rayleigh–Ritz method is used to calculate the natural frequencies of rectangular isotropic and laminated symmetric and anti-symmetric cross and angle ply composite plate with general elastic supports along its edges. Each of the admissible functions here is composed of a trigonometric function and an arbitrary continuous function that is introduced to ensure the sufficient smoothness of the so-called residual displacement function at the edges. Perhaps more importantly, this study has developed a general approach for deriving a complete set of admissible functions that can be applied to various boundary conditions. Several numerical examples are studied to demonstrate the accuracy and convergence of the current solution with considering some design parameters such as boundary conditions, aspect ratio, lamination angle, thickness ratio, orthotropy ratio, also these results are compared with other researchers and give a good agreement .

Key words: free vibration, Rayleigh–Ritz method, general boundary condition, composite laminated plate

تحليل الاهتزازالحر لصفيحة مركبة مع اسناد حافات مرنة وعامة

أ.م.د وداد مجيد ابراهيم
مساعد بروفيسور
جامعة بغداد-كلية الهندسة
قسم الهندسة الميكانيكية

رأفت أسعد غني
طالب ماجستير
جامعة بغداد-كلية الهندسة
قسم الهندسة الميكانيكية

الخلاصة

في هذة الدراسة ، تستخدم طريقة Rayleigh–Ritz لأيجاد التردد الطبيعي للصفيحة الموحدة الخواص والمركبة المستطيلة ذات الزوايا المتعامدة والمائلة ،المتماثلة والغير متماثلة مع ظروف اسناد لحافاتها مختلفة . والدوال المستخدمة في هذا البحث يمكن ان تمثل بدوال مثلثية و دوال عشوائية مستمرة و ذلك لضمان السلاسة المطلوبة لعمل الدالة الرئيسية . ولعل الأهم من ذلك، ان هذه الدراسة قد طورت اسلوب عام لاشتقاق مجموعة كاملة من الدوال المقبولة التي يمكن تطبيقها لشروط اسناد الحافات المختلفة. لقد تم دراسة عدة امثلة عددية لاثبات دقة وتقارب نتائج الحل الحالي مع الاخذ بنظر الاعتبار تغيير في بعض معايير التصميم مثل شروط الحدود، نسبة الارتفاع، وزاوية التصفيح، ونسبة سماكة، ونسبة الـ orthotropy ،حيث تم مقارنة النتائج مع باحثين اخرين واعطت تقارب جيد جدا .

الكلمات الرئيسية: نظرية القص ذات الرتبة العالية ، الالواح الطبقية المركبة ، التحليل الاستاتيكي .

1. INTRODUCTION:

Composite materials are so necessary in many engineering applications, as vehicles parts industry, aero structures industry and medical devices industry. With the wide use of composite plate in the modern industry, static and dynamic analysis of plate structure under different types of loads and different boundary condition become a main part in design procedure. In the past few years, many researchers resorted to the development of many theories to clearly predict the response of laminated plate composite material. It is necessary to know the theories of laminated composite plates, because it is not possible to provide accurate analysis without knowledge of theories. These theories can be classified in to three type's single layer theories, layer-wise theories and continuum based 3D elasticity theories.

Many researchers had studied Vibration analysis of rectangular plates with general elastic boundary supports by classical plate theory (CLPT), and other researchers have studied the natural frequency of composite plates with all boundary conditions. **Pervez, Al-Zebdeh, and Farooq, 2010**

W.L. Li ,2004. used Rayleigh–Ritz method to determine the modal characteristics of a rectangular isotropic plate with general elastic supports alone its edges. Each of the admissible functions here is composed of a trigonometric function and an arbitrary continuous function. He firstly investigated the convergence of his function then he studied many different cases of isotropic plate such as different aspect ratio and different values of elastic restraint constant (k,K). **Y.F. Xing** and **B. Liu ,2009.** solved new exact solutions for free vibrations of thin orthotropic rectangular plates by using a novel separation of variables. The exact normal eigenfunctions and eigenvalue equations for the boundary condition combinations SSCC, SCCC and CCCC are obtained through the mode formulation and boundary conditions. **Henry Khov, Wen L. Li** and **Ronald F. Gibson ,2009.**presented an accurate solution method for the static and dynamic deflections of orthotropic plates with general boundary conditions. The displacement function is expressed as a 2-D Fourier cosine series supplemented with several terms in the form of 1-D series. Thus, a classical solution can be derived by letting the series exactly satisfy the governing differential equation at every field point and all the boundary conditions at every boundary point, respectively**. W.L. Li, X.Zhang, J.Du** and **Z.Liu ,2009.** studied an exact series solution for the transverse vibration of rectangular isotropic plates with general elastic boundary supports. An analytical method is developed for the vibration analysis of rectangular plates with elastically restrained edges. The displacement solution is expressed as a two-dimensional Fourier series supplemented with several one-dimensional Fourier series. Thus, an exact solution can be obtained by letting the series simultaneously satisfy the governing differential equation and the boundary conditions on a point-wise basis. **H.DAL** and **O.K.MORGUL,2011.** studied vibrations of elastically restrained rectangular isotropic plates. Vibrations of plates with boundary conditions were elastic along full edges. Deflections function was expressed as the combination of a Fourier sine series and an auxiliary polynomial. Solution function as employed by **Li**

2002. has been adopted for plates with fully elastic edges. Frequency parameters of plate were calculated for different plate parameters. **H.T.Thai , S.E.Kim ,2012.** obtained Levy-type solution for free vibration analysis of orthotropic plates based on two variable refined plate theory. The theory, which has strong similarity with classical plate theory in many aspects, accounts for a quadratic variation of the transverse shear strains across the thickness, and satisfies the zero traction boundary conditions on the top and bottom surfaces of the plate without using shear correction factors. **Kookhyun Kim, B. Kim, T.Choi and D.Cho ,2012.** presented free vibration analysis of rectangular isotropic plate with arbitrary edge constraints using characteristic orthogonal polynomials in assumed mode method. Natural frequencies and their mode shapes of the plate are calculated by solving an eigenvalue problem of a multi-degree-of-freedom system matrix equation derived by using Lagrange's equations of motion. Characteristic orthogonal polynomials having the property of Timoshenko beam functions which satisfies edge constraints corresponding to those of the objective plate are used. **A. Pagani ,2014.** extended free vibration analysis of composite plates by higher-order 1D dynamic stiffness elements based on Carrera Unified Formulation (CUF) and experiments. The principle of virtual displacements is then used to derive the equations of motion and the natural boundary conditions, which are subsequently expressed in the frequency domain by assuming a harmonic solution. After the resulting system of ordinary differential equations of second order with constant coefficients is solved, the frequency dependent DS matrix of the system is derived. Finally the algorithm of Wittrick and Williams is applied to extrapolate the free vibration characteristics of laminated composite plate. **Wan-You Li, W.Li, B. Lv, H. Ouyang, J. Du,H. Zhou, and D. Wang ,2014.** presented a Hybrid Finite Element-Fourier Spectral Method for Vibration Analysis of Structures with Elastic Boundary Conditions. A novel hybrid method, which simultaneously possesses the efficiency of Fourier spectral method (FSM) and the applicability of the finite element method (FEM), is used for the vibration analysis of structures with elastic boundary conditions. The computational domain of general shape is divided into several subdomains firstly, some of which are represented by the FSM while the rest by the FEM. Then, fictitious springs are introduced for connecting these subdomains. Numerical examples of a one-dimensional Euler-Bernoulli beam and a two-dimensional rectangular plate show that the present method has good accuracy and efficiency. Further, one irregular-shaped plate which consists of one rectangular plate and one semi-circular plate also demonstrates the capability of the present method applied to irregular structures. **Firas Hamzah Taya,2014.** presented free vibration and buckling behavior of laminated composite thin plates subjected to in-plane uniform, parabolic, and linear distributed loads is studied using classical laminated plate theory (CLPT). Different functions were used for different boundary conditions applying Ritz method to get homogeneous set of equations and solved as Eigen value problems of buckling load solution for laminated plate. The boundary conditions considered in this study are (SSSS, CCCC, CSCS, SFSF, and CFCF). **G. Jin, T. Ye,** and **S. Shi ,2015.** presented Three-Dimensional Vibration Analysis of Isotropic and

Orthotropic Open Shells and Plates with Arbitrary Boundary Conditions. Vibration characteristics of the shells and plates have been obtained via a unified three-dimensional displacement-based energy formulation represented in the general shell coordinates, in which the displacement in each direction is expanded as a triplicate product of the cosine Fourier series with the addition of certain supplementary terms were introduced to eliminate any possible jumps with the original displacement function and its relevant derivatives at the boundaries. All the expansion coefficients are then treated equally as independent generalized coordinates and determined by the Rayleigh-Ritz procedure.

In present work the function proposed by **W.L. Li ,2004.** is used for laminated symmetric and antisymmetric cross and angle ply composite plate with general elastic supports along its edges.

2. THEORETICAL ANALYSIS:

2.1 Classical Laminated Plate Theory:

The equivalent single layer ESL laminated plate theories are those in which a heterogeneous laminated plate is treated as a statically equivalent single layer having a complex constitutive behavior, reducing the 3-D continuum problem to a 2-D problem. The ESL theories are developed by assuming the form of the displacement field or stress field as a linear combination of unknown functions and the thickness coordinate: **J.N. REDDY,2004.**

$$\psi\_i(x,y,z,t) = \sum_{j=0}^{N} (z)^j \, \psi_i^j(x,y,t) \tag{2.1}$$

where ψ_i is the component of displacement or stress, (x,y) is the in-plane coordinates, z is the thickness coordinate, t is the time, and ψ_i^j are functions to be determined. When ψ_i displacements, then the equations governing are ψ_i^j are determined by the principle of virtual displacements (or its dynamic version when time dependency is to be included)

$$0 = \int_0^T (\delta\Pi + \delta W - \delta E_c)\, dt \tag{2.2}$$

where $\delta\Pi$, δW, and δE_c denote the virtual strain energy, virtual work done by external applied forces, and the virtual kinetic energy, respectively. These quantities are determined in terms of actual stresses and virtual strains, which depend on the assumed displacement functions, and their variations.

The simplest laminated plate theory is the classical laminated plate theory (or CLPT), which is an extension of the Kirchhoff (classical) plate theory to laminated composite plates. It is based on the displacement field

$$u(x,y,z,t) = u_o(x,y,t) - z\frac{\partial w_o}{\partial x}$$

$$v(x,y,z,t) = v_o(x,y,t) - z\frac{\partial w_o}{\partial y}$$

$$w(x,y,z,t) = w_o(x,y,t) \qquad (2.3)$$

where (u_o, v_o, w_o) are the displacement components along the (x, y, z) coordinate directions, respectively, of a point on the midplane (i.e., z = 0).

The governing differential equation for the free vibration of laminated thin plate is given by: **Henry Khov,2009.**

$$D_{11}\frac{\partial^4 w}{\partial x^4} + D_{22}\frac{\partial^4 w}{\partial y^4} + 2(D_{12} + 2D_{66})\frac{\partial^4 w}{\partial x^2 \partial y^2} + 4D_{26}\frac{\partial^4 w}{\partial x \partial y^3} + 4D_{16}\frac{\partial^4 w}{\partial x^3 \partial y} - \rho h \omega^2 w(x,y) \qquad (2.4)$$

2.2 Total Mechanical Energy:

The first law of thermodynamics or the principle of conservation of energy serves as the foundation for energy-based methods employed in the analysis of structures, including plates. In the absence of energy dissipation and other non-conservative forces, i.e. if the forces acting on the system are conservative, this principle is reduced to the principle of stationery total energy, **Victor Birman ,2011.**

The total mechanical energy (defined as the sum of its potential and kinetic energies) of a particle being acted on by only conservative forces is constant, **Robert G. Brown ,2007.**

$$E = E_c + \Pi = Constant \qquad (2.5)$$

where E: Total mechanical energy of a system

E_c: Total kinetic energy of the system

Π: Total potential energy of the system

In static problems, the principle of stationary total energy reduces to the principle of minimum total potential energy implying that the virtual work of forces acting on the system in equilibrium is equal to zero **Victor Birman,2011.** so that:

$$\Delta E=0 \text{ OR } E= Constant \qquad (2.6)$$

Where

$$\Pi = \frac{1}{2}\int_0^b \int_0^a \left[D_{11}\left(\frac{\partial^2 w}{\partial x^2}\right)^2 + D_{22}\left(\frac{\partial^2 w}{\partial y^2}\right)^2 + 4D_{66}\left(\frac{\partial^2 w}{\partial x \partial y}\right)^2 + 2D_{12}\frac{\partial^2 w}{\partial x^2}\frac{\partial^2 w}{\partial y^2}\right] dx\, dy +$$
$$\frac{1}{2}\int_0^b \left[k_{x0}w^2 + K_{x0}\left(\frac{\partial^2 w}{\partial x^2}\right)^2\right]_{x=0} dy + \frac{1}{2}\int_0^b \left[k_{x1}w^2 + K_{x1}\left(\frac{\partial^2 w}{\partial x^2}\right)^2\right]_{x=a} dy +$$
$$\frac{1}{2}\int_0^a \left[k_{y0}w^2 + K_{x0}\left(\frac{\partial^2 w}{\partial y^2}\right)^2\right]_{y=0} dx + \frac{1}{2}\int_0^b \left[k_{y1}w^2 + K_{y1}\left(\frac{\partial^2 w}{\partial x^2}\right)^2\right]_{y=b} dx \qquad (2.7)$$

and

$$E_c = \frac{1}{2}\omega^2 \iint I_o w_o^2 dx\, dy \qquad (2.8)$$

2.3 Boundary Conditions:

In terms of the flexural displacement, the bending and twisting moments and transverse shearing forces can be expressed as, **Henry Khov ,2009.**

$$M_x = -D_{11}\frac{\partial^2 w}{\partial x^2} - D_{12}\frac{\partial^2 w}{\partial y^2} \qquad (2.9)$$

$$M_y = -D_{22}\frac{\partial^2 w}{\partial y^2} - D_{12}\frac{\partial^2 w}{\partial x^2} \qquad (2.10)$$

$$M_{xy} = -2D_{66}\frac{\partial^2 w}{\partial x \partial y} \qquad (2.11)$$

$$Q_x = -D_{11}\frac{\partial^3 w}{\partial x^3} - (D_{12} + 4D_{66})\frac{\partial^3 w}{\partial y^2 \partial x} \qquad (2.12)$$

$$Q_y = -D_{22}\frac{\partial^3 w}{\partial y^3} - (D_{12} + 4D_{66})\frac{\partial^3 w}{\partial x^2 \partial y} \qquad (2.13)$$

The boundary conditions for an elastically restrained rectangular plate are

$k_{x0}w = Q_x \quad K_{x0}\frac{\partial w}{\partial x} = -M_x$ ....*at x=0* (2.14-15)

$k_{x1}w = -Q_x \quad K_{x1}\frac{\partial w}{\partial x} = M_x$ ....*at x=a* (2.16-17)

$k_{y0}w = Q_y \quad K_{y0}\frac{\partial w}{\partial y} = -M_y$ ....*at y=0* (2.18-19)

$k_{y1}w = -Q_y \quad K_{y1}\frac{\partial w}{\partial y} = M_y$ ....*at y=b* (2.20-21)

where k_{x0} and k_{x1}(k_{y0} and k_{y1}) are the linear spring constants, and $K_{x0}$and K_{x1} (K_{y0} and K_{y1}) are the rotational spring constants at x =0 and a (y = 0 and b), respectively. Eqs. (14)–(21) represent a set of general boundary conditions from which, for example, all the classical homogeneous boundary conditions can be directly obtained by accordingly setting the spring constants equal to an extremely large or small number **Fig 2**

From Eqs. (9–21), the boundary conditions can be finally written as:

$$k_{x0}w = -D_{11}\frac{\partial^3 w}{\partial x^3} - (D_{12} + 4D_{66})\frac{\partial^3 w}{\partial x \partial y^2} \qquad (2.22)$$

$$k_{x1}w = D_{11}\frac{\partial^3 w}{\partial x^3} + (D_{12} + 4D_{66})\frac{\partial^3 w}{\partial x \partial y^2} \quad (2.23)$$

$$K_{x0}\frac{\partial w}{\partial x} = D_{11}\frac{\partial^2 w}{\partial x^2} + D_{12}\frac{\partial^2 w}{\partial y^2} \quad (2.24)$$

$$K_{x1}\frac{\partial w}{\partial x} = -D_{11}\frac{\partial^2 w}{\partial x^2} - D_{12}\frac{\partial^2 w}{\partial y^2} \quad (2.25)$$

2.4 Admissible functions

Admissible functions play a critical role in the Rayleigh–Ritz method. For plate problems, the products of the beam functions are often chosen as the admissible functions and the displacement function can be accordingly expressed as, **W.L. Li ,2004.**

$$w(x, y) = \sum_{m,n=1} A_{mn}\, X_m(x) Y_n(y) \quad (2.26)$$

where $X_m(x)$ and $Y_n(y)$ are the characteristic functions for beams that have the same boundary conditions in the x- and y-direction, respectively.

Although beam functions can be generally obtained as a linear combination of trigonometric and hyperbolic functions, they include some unknown parameters that have to be determined from the boundary conditions. Consequently, each boundary condition basically leads to a different set of beam functions. In real applications, this is clearly inconvenient, not to mention the tediousness of determining the characteristic functions for a generally supported beam. In order to avoid this difficulty, an improved Fourier series method have been proposed for beams with arbitrary supports at both ends in which the characteristic functions are sought in the form of, **W.L. Li,2000.**

$w(x) = \sum_{m=0}^{\infty} a_m \cos\lambda_{am} x + p(x) \quad (\lambda_{am} = m\pi/a)\,, \quad 0 \le x \le a \quad (2.27)$

The function $p(x)$ in Eq. (27) represents an arbitrary continuous function that, regardless of boundary conditions, is always chosen to satisfy the following equations:

$p^{```}(0) = w^{```}(0) = \alpha_0 \;, \quad p^{```}(a) = w^{```}(a) = \alpha_1$ (2.28-29)

$p^{`}(0) = w^{`}(0) = \beta_0 \;, \quad p^{`}(a) = w^{`}(a) = \beta_1$ (2.30-31)

As explained in Ref. **W.L. Li ,2000.** the function $p(x)$ is here introduced to take care of the potential discontinuities of the (original) displacement function and its derivatives at the end points. Accordingly, the Fourier series now simply represents a residual displacement function, $\acute{W}(x) = W(x) - p(x)$; that is periodic continuous and has at least three continuous derivatives over the entire x-axis. Mathematically, it is already known that the smoother a periodic function is, the faster its Fourier expansion converges. Therefore, the addition of the function $p(x)$ will have two immediate benefits: (1) the Fourier series expansion is now applicable to any boundary conditions, and (2) the Fourier series solution can be drastically improved regarding its accuracy convergence.

So far, $p(x)$ has only been understood as a continuous function that satisfies Eqs. (28)–(31), its form is not a concern with respect to the convergence of the series solution. Thus, the function $p(x)$ can be selected in any desired form. As a demonstration, suppose that $p(x)$ is a polynomial function

$$p(x) = \sum_{n=0}^{4} c_n p_n\left(\frac{x}{a}\right) \tag{2.32}$$

where c_n is the expansion coefficient and $p_n(x)$ is the Legendre function of order n. It is obvious that the function $p(x)$ needs to be at least a fourth order polynomial to simultaneously satisfy Eqs. (28)–(31). Substituting Eq. (32) into Eqs. (28)–(31) results in

$$c_3 p_3'''(0) + c_4 p_4'''(0) = a^3 \alpha_0 \tag{2.33}$$

$$c_3 p_3'''(1) + c_4 p_4'''(1) = a^3 \alpha_1 \tag{2.34}$$

$$c_1 p_1'(0) + c_2 p_2'(0) + c_3 p_3'(0) + c_4 p_4'(0) = a\beta_0 \tag{2.35}$$

$$c_1 p_1'(1) + c_2 p_2'(1) + c_3 p_3'(1) + c_4 p_4'(1) = a\beta_1 \tag{2.36}$$

From the above equations, the coefficients, c_n (n = 1, 2, 3, 4), are directly obtainable in terms of the boundary constants, α_0, α_1 , β_0 and β_1. Since the constant c_0 does not actually appear in Eqs. (33)–(36), it can be an arbitrary number theoretically. For instance, c_0 is here selected to satisfy

$$\int_0^a p(x)\, dx = 0 \tag{2.37}$$

The final expression for the function $p(x)$ can be written as

$$p(x) = \zeta_a(x)\bar{\alpha} \tag{2.38}$$

Where $$\bar{\alpha} = \{\alpha_0\ \alpha_1\ \beta_0\ \beta_0\ \} \tag{2.39}$$

and $$\zeta_a(x)^T = \begin{Bmatrix} -(15x^4 - 60x^3 + 60a^2x^2 - 8a^4)/360a \\ (15x^4 - 30a^2x^2 + 7a^4)/360a \\ (6ax - 2a^2 - 3x^2)/6a \\ (3x^2 - a^2)/6a \end{Bmatrix} \tag{2.40}$$

The results in Eqs. (38)–(40) were previously derived from a more straightforward but less general approach, **W.L. Li,2004 .**

In order to determine the unknown boundary constants, α_0, α_1, β_0 and β_1, substitution of Eqs. (27) and (38) into the boundary conditions Eqs. (22)–(25) results in

$$\bar{\alpha} = \sum_{m=0}^{\infty} H_a^{-1} Q_{am} a_m \tag{2.41}$$

Where

$$H_a = \begin{bmatrix} 1+\frac{8k_{x0}a^3}{360D_{11}} & \frac{7k_{x0}a^3}{360D_{11}} & \frac{-k_{x0}a}{3D_{11}} & \frac{-k_{x0}a}{6D_{11}} \\ \frac{7k_{x1}a^3}{360D_{11}} & 1+\frac{8k_{x1}a^3}{360D_{11}} & \frac{-k_{x1}a}{6D_{11}} & \frac{-k_{x1}a}{3D_{11}} \\ \frac{a}{3} & \frac{a}{6} & \frac{K_{x0}}{D_{11}}+\frac{1}{a} & \frac{-1}{a} \\ \frac{a}{6} & \frac{a}{3} & \frac{-1}{a} & \frac{K_{x1}}{D_{11}}+\frac{1}{a} \end{bmatrix} \tag{2.42}$$

and

$$Q_{am} = \left\{ (-1)\frac{k_{x0}}{D_{11}} \quad (-1)^m \frac{k_{x1}}{D_{11}} \quad -\lambda_{am}{}^2 \quad (-1)^m \lambda_{am}{}^2 \right\}^T \tag{2.43}$$

It should be mentioned that the matrix Ha will become singular for a completely free beam. However, this problem can be overcome to a certain extent by artificially attaching one or more springs with very small stiffness to the ends of a beam. It has been shown in **W.L. Li ,2002.** that although the matrix may be ill-conditioned in such a treatment, the natural frequencies can still be accurately calculated for a completely free beam.

Nevertheless, the characteristic functions are well known for this particular case and can be readily used as the admissible functions in the Rayleigh–Ritz method.

Making use of Eqs. (38) and (41), Eq. (27) can be rewritten as

$$w(x) = \sum_{m=0}^{\infty} a_m \varphi_m^a(x) \tag{2.44}$$

Where $$\varphi_m^a(x) = cos\lambda_{am}x + \zeta_a(x)H_a^{-1}Q_{am} \tag{2.45}$$

Mathematically, Eq. (44) indicates that each of the beam functions can be viewed as a function in the functional space spanned by the basic functions $\{\varphi_m^a(x)$; m = 0, 1, 2,.......}. Thus, Eq. (26) can be accordingly rewritten as

$$w(x,y) = \sum_{m,n=0}^{\infty} A_m \varphi_m^a(x)\varphi_n^b(y) \tag{2.46}$$

Where $$\varphi_n^b(y) = cos\lambda_{bn}y + \zeta_b(y)H_b^{-1}Q_{bn} \tag{2.47}$$

The expressions for $\zeta_b(y)$, H_b and Q_{bn} can be, respectively, obtained from Eqs. (40), (42) and (43) by simply replacing the x-related parameters by the y-related.

2.5 Determination of Natural Frequency:

Consider an orthotropic laminated plate, the material directions of which coincide with the plate directions. This plate is subjected to free vibration along the edges x = 0-a and y = 0-b.

Where the transverse displacement (w) is substituted in the total mechanical energy as mentioned in section 2.4. To calculate the natural frequency ω. Performing the required mathematical processes (differentiations and then integrations) of eqs. (2.7) and (2.8) and then putting the mechanical energy in the following equation:

$$\frac{\partial E}{\partial A_{mn}} = 0 \tag{2.48}$$

eq. 2.48 will lead to a set of linear homogeneous algebraic equations as follow:

$$f(A_{mn}, \omega) = 0 \quad for\ vibration \tag{2.49}$$

Solving the last equation as an Eigen-value problem to get the following form:

$$\begin{bmatrix} a_{1,1} & \cdots & a_{1,(m*n)} \\ \vdots & \ddots & \vdots \\ a_{(m*n),1} & \cdots & a_{(m*n),(m*n)} \end{bmatrix} \begin{Bmatrix} A_{11} \\ \vdots \\ A_{mn} \end{Bmatrix} = 0 \tag{2.50}$$

where a_{ij} are the coefficients of the nonzero unknowns A_{mn}. Finding the determinant of the first term of eq. (2.50) and equating it to zero will lead to get the natural frequency ω. When M and N are more than 1, the natural frequency ω are determined by solving Eigen value problem. For different arbitrary boundary conditions and M & N are greater than 1, the solution becomes more difficult and needs computer programming to determine the natural frequency ω. In this work, Matlab R2013a is used to solve the Eigen-value problem.

3-RESULT AND CONCLUSIONS

3-1-Results

The natural frequency of isotropic and composite laminated plate with elastic boundary condition is analyzed and solved using MATLAP version13 programming. To examine the validly of the derived equations and performance of computer programming for vibration analysis of composite laminated plate, numerical results of isotropic plate are compared with those obtained by **W.L. Li ,2004.** and **Hüseyin DAL ,2011.** as shown in **Tables (1,2)** which give very close results for different boundary conditions. While present results for laminated composite plate with different boundary conditions give good agreement when compared with **Henry (2009)** and those obtained by numerical program **ANSYS** as shown in **Table 3.** and figures (3) and (4), also present work results are compared with those obtained by **Reddy** for ssss cross ply plate with different orthotropy ratio as shown in **table(4).**

Also cross ply scheme (symmetric and non-symmetric) with different layer number was studied as shown in **Table 5.** where the frequency parameter for symmetric ply is more than that for non-symmetric because the stiffness of the rare is larger than symmetric ply as proved by many researchers, while the other presented scheme is angle ply scheme (symmetric and non-symmetric) with different layer number as shown in **Table6.** where the frequency parameter for symmetric angle ply have no great change than that for non-symmetric because the stiffness of the two type are close to each other as proved by many researchers Also we study isotropic scheme in **Tables (7,8)** which give very close results for different boundary conditions and aspect ratio with **Wen le 2004**, it can be noted that when the aspect ratio increases the frequency parameter increases for same boundary condition .

While the other presented scheme is laminated cross ply scheme (symmetric and non-symmetric) with different boundary conditions and aspect ratio as shown in **Table 9.** where the frequency parameter decreases when the aspect ratio increases, and the largest frequency parameter for clamped boundary at all edges of the symmetric cross-ply plate. The next presented scheme is laminated angle ply $[45 \ \ -45]_2$ as shown in **Table10.** where the frequency parameter decreases when the aspect ratio increases. Also the next presented scheme is laminated angle ply $[30 \ \ -30]_2$ as shown in **Table11.** where the frequency parameter decreases when the aspect ratio increases. It can be noted that in **Tables (10,11)** the largest frequency parameter for SSCC boundary conditions for square plate .

The thickness ratio schemes of laminated plate with different boundary conditions are changed, once symmetric cross ply and $[45 \ \ -45]_s$ schemes are studied with different boundary conditions and thickness ratio as shown in **Table12.** where the frequency parameter decreases when the thickness ratio increase (reduces the thickness) for same boundary condition and the largest frequency parameter for clamped boundary at all edges because it has largest stiffness. The next presented scheme is angle ply $[30 \ \ -30]_s$ as shown in **Tables 13.** Where the frequency parameter decreases when the thickness ratio increase (reduces the thickness) for same boundary condition and the largest frequency parameter for clamped boundary at all edges because it has largest stiffness.

Rotational restraint along edges of laminated and isotropic plate with different boundary conditions are changed, consider plates are elastically restrained along edges. The first one involves a simply supported square isotropic plate with a uniform elastic restraint against rotation along each edge, that is, $K_{x0}a/D$=$K_{x1}a/D = K_{y0}a/D = K_{y1}a/D = Ka/D$, in **Table 14**. the first six frequency parameters are shown for a few different stiffness values. Because of the symmetries about the x- and y-axis, the second and third frequency parameters are identical. The fifth and sixth frequency parameters are also the same for $Ka/D = 0$. However, they become slightly different for other stiffness values. The frequency parameter increases when the stiffness values increases, when it zero the behavior of the frequency parameter like a simply supported along all edge , but when the stiffness values equal to infinity the behavior of the frequency parameter like a clamped along all edge. **Table 15** shows the frequency parameter of a simply supported square laminated plate $[0\ 90]_2$with a uniform elastic restraint against rotation along each edge, that is, $K_{x0}a/D_{22}$ =$K_{x1}a/D_{22} = K_{y0}a/D_{22} = K_{y1}a/D_{22} = Ka/D_{22}$, the first four frequency parameters are shown for a few different stiffness values. Because of the symmetries about the x- and y-axis, the second and third frequency parameters are identical.

The frequency parameter increases when the stiffness values increases, when it is zero the behavior of the frequency parameter is like a simply supported along all edge, but when the stiffness values is equal to infinity the behavior of the frequency parameter like a clamped along all edge.The orthotropy ratio schemes of laminated plate with different boundary conditions are changed, **Fig.5** shows the frequency parameter of non-symmetric cross ply with different boundary conditions and orthotropy ratio , where the frequency parameter increases when the orthotropy ratio increases, the largest frequency parameter for CFCF boundary conditions and then less in SSSS and smallest in SFSF boundary conditions. **Fig6** shows the frequency parameter of angle ply$[60 \ \ -60]_2$, where the frequency parameter increases when the orthotropy ratio increases, the largest frequency parameter for SSSS boundary conditions and then less in CFCF and smallest in SFSF boundary conditions .

3.2. Conclusions

This study presented investigations for free vibration of a composite laminated plate. Some assumptions are made to solve the vibration problems and determine the results desired for this paper.

The results are determined mainly by analytic method and compared with numerically found results, and with obtained by other researchers; the comparison showed high agreement between them.

The vibration results lead to the following conclusions:

1- The number of half wavelengths affects the natural frequency, where the increasing aspect ratio requires larger number (M & N) to get more accurate results where the error is found 4.71% for cccc isotropic plate a/b=2.5 at ($m = n = 3$).

2- The boundary conditions affect the fundamental natural frequency. Clamped edges conditions offer high stiffness, results in high natural frequency. Clamped boundaries make the plate holds larger frequency than simply supported boundaries, where the fundamental natural frequency for SSSS cross ply, is less by 47.3% than fundamental natural frequency of CCCC cross ply, while for angle ply, is less by 58.21%,and the fundamental natural frequency for SSSS isotropic plate, is less by 55.28% than of CCCC plate.

3- The aspect ratio is inversely proportional to the frequency parameter $\Omega = \omega b^2/\pi^2\surd(\rho h \ / \ D22)$ of the orthotropic plate and frequency parameter $\Omega = \omega b^2/\pi^2\surd(\rho h \ / \ D)$ of the isotropic plate.

4- Rotational restraint along edges of laminated and isotropic plate affects the natural frequency, where the value of (Ka/D) and (Ka/D_{22}) is zero the behavior of the natural frequency like a (SSSS) boundary conditions, but when the value is infinity the behavior of the natural frequency like a (CCCC) boundary conditions.

5- The orthotropy ratio is directly proportional with the frequency parameters, $\Omega = \omega a^2/h\surd(\rho \ / \ E_2)$ of the orthotropic plate.

6- The increasing of the lamination angle is inversely proportional with frequency parameters, $\Omega = \omega b^2/\pi^2\surd(\rho h \ / \ D22)$ of the orthotropic plate.

7- The thickness ratio is inversely proportional with the natural frequency of the orthotropic plate.

NOMENCLATURE

Symbol	Discretion	Units
a	Length of a plate	m
b	width of a plate	m
h	Plate thickness	m
A	vector of the expansion or Rayleigh–Ritz coefficients	
A_{mn}	expansion or Rayleigh–Ritz coefficients	
a_m	expansion or Rayleigh–Ritz coefficient	
D_{ij}	flexural rigidity	-
E_1 , E_2, E_3	Elastic modulus components	Gpa
$G12, G23, G13$	Shear modulus components	Gpa
M,N	numbers of expansion terms used in x- and y-direction, respectively	
M_x , M_y , M_{xy}	Moment result per unit length	N.m/m
Q_x , Q_y	Transverse shear force result	N
K_{x0} , K_{x1}	rotational stiffnesses at x = 0 and a, respectively	Rad.N/m
K_{y0} , K_{y1}	rotational stiffnesses at y = 0 and b, respectively	Rad.N/m.
k_{x0} , k_{x1}	translational stiffnesses at x = 0 and a, respectively	N/m
k_{y0} , k_{y1}	translational stiffnesses at y = 0 and b, respectively	N/m
$P(x)$	a simple polynomial function	
x,y,z	Cartesian coordinate system	m
E, E_c	Total mechanical and kinetic energies of a system	N.m
Π	Total potential energy of the system	N.m
U	Strain energy of deformation	N.m
V_c	the elastic potential energy	N.m
$\epsilon_x, \epsilon_y, \epsilon_z$	Strain components	
γ_{xz} , γ_{yz}	Transverse shear strain	
ν_{12}	Poisson’s ratio components	-
σ_{xx} , σ_{yy} , σ_{xy} , σ_{yz}	Stress components	Gpa

σ_{xz}		
u, v, w	Displacements in x, y, z directions	m
u_o, v_o, w_o	Displacements of the reference surface in the x, y, z directions	m
$W(X)$	flexural displacement of a beam	m
$w(x,y)$	flexural displacement of a plate	m
$X_m(x)$, $Y_n(y)$	beam characteristic function	
α_1 , α_0	$=w'''(a), w'''(0)$	
β_1, β_0	$=w'(a), w'(0)$	
λ_{am}	$\frac{m\pi}{a}$	-
λ_{bn}	$\frac{n\pi}{b}$	-
ρ	Density of material	Kg/m^3
$\varphi_m^a(x)$	admissible functions in x-direction	-
$\varphi_n^b(y)$	admissible functions in y-direction	
ω	Natural frequency	Cycle/sec

REFERENCES:

- Autar K. Kaw, 2006, *Mechanics of Composite Materials*, 2nd ed., CRC Press, Taylor & Francis Group, 2006.
- *A*. Pagani , 2014, *Free vibration analysis of composite plates by higher-order 1D dynamic stiffness elements and experiments*, Composite Structures 118 (2014) 654–663
- *C*.B. Kim, H. S.Cho and H.G.Beom, 2012, *Exact solutions of in-plane natural vibration of a circular plate with outer edge restrained elastically*, Journal of Sound and Vibration 331 (2012) 2173–2189
- Eduard Ventsel & Theodor Krauthammer, 2001 *Thin Plates and Shells: Theory, Analysis, and Applications*, The Pennsylvania State University, University Park, Pennsylvania,.
- Firas Hamzah Taya, 2014, *Buckling and Vibration Analysis of Laminated Composite Plates* , University of Baghdad.
- G. Jin, T. Ye, and S. Shi ,2015 ,*Three-Dimensional Vibration Analysis of Isotropic and Orthotropic Open Shells and Plates with Arbitrary Boundary Conditions*, International journal of scientific world,Vol 3,pp12-17.
- Henry Khov, Wen L. Li and Ronald F. Gibson, 2009, *an accurate solution method for the static and dynamic deflections of orthotropic plates with general boundary conditions*, Composite Structures 90, 474–481

- H.DAL and O.K.MORGUL, 2011, *Vibrations of elastically restrained rectangular isotropic plates*, Scientific Research and Essays Vol. 6(34), pp. 6811-6816, 30 December.
- H.T.Thai , S.E.Kim , 2012, *Levy-type solution for free vibration analysis of orthotropic plates based on two variable refined plate theory,* Applied Mathematical Modelling 36, 3870–3882
- J.N. REDDY, 2004, *Mechanics of Laminated Composite Plates and Shells: Theory and Analysis*, 2nd ed., CRC Press LLC.
- Jean-Marie Berthelot, 2010, *Mechanics of Composite Materials and Structures*, ISMANS, Institute for Advanced Le Mans, Materials and Mechanics, France.
- J.K.Ahmed,Agarwal, P.Pal, V. Srivastav , 2013, *Static and Dynamic behavior of Composite Laminated Plate*, IJITEE, Vol 3,pp 2278-3075
- Kookhyun Kim, B. Kim, T.Choi and D.Cho , 2012, *Free vibration analysis of rectangular isotropic plate with arbitrary edge constraints*, Inter J Nav Archit Oc Engng 4:267-280
- L. Aszlo P. Kollar and George S. Springer, *Mechanics of Composite Structures*, Cambridge University Press, 2003.
- Lorenzo Dozio , 2010, *Free in-plane vibration analysis of rectangular plates with arbitrary elastic Boundaries,* Mechanics Research Communications 37, 627–635
- P. Jana and K. Bhaskar, 2006, *Stability Analysis of Simply-Supported Rectangular Plates under Non-Uniform Uniaxial Compression Using Rigorous and Approximate Plane Stress Solutions*, Thin-Walled Structures 44, 507–516.
- Robert G. Brown, 2007, *Introductory Physics I: Elementary Mechanics*, Duke University Physics Department.
- Victor Birman, 2011, *Solid Mechanics and Its Applications: Plate Structures*, Springer Science+Business Media B.V.
- W.L. Li , 2004, *Vibration analysis of rectangular plates with general elastic boundary supports*, Journal of Sound and Vibration 273, 619–635
- W.L. Li, X.Zhang, J.Du and Z.Liu , 2009 , *An exact series solution for the transverse vibration of rectangular isotropic plates with general elastic boundary supports*, Journal of Sound and Vibration 321, 254–269
- Wan-You Li, B. Lv, H. Ouyang, J. Du,H. Zhou, and D. Wang , 2014, *A Hybrid Finite Element-Fourier Spectral Method for Vibration Analysis of Structures with Elastic Boundary Conditions,* Hindawi Publishing Corporation Mathematical Problems in Engineering, Article ID 834834, 11 pages
- W.L. Li, M. Daniels, 2002, *A Fourier series method for the vibrations of elastically restrained plates arbitrarily loaded with springs and masses,* Journal of Sound and Vibration 252, 768–781.

- W.L. Li, 2000, *Free vibrations of beams with general boundary conditions*, Journal of Sound and Vibration 237, 709–725.

- Y.F. Xing and B. Liu , 2009, *New exact solutions for free vibrations of thin orthotropic rectangular plates*, Composite Structures 89, 567–574
- Zhou Ding,1996, *an approximate solution for calculating eigen frequencies of transverse vibration of rectangular isotropic plates elastically restrained against rotation along edges,Appliad mathematics and mechanics*,Vol.17,No 5,May.
-

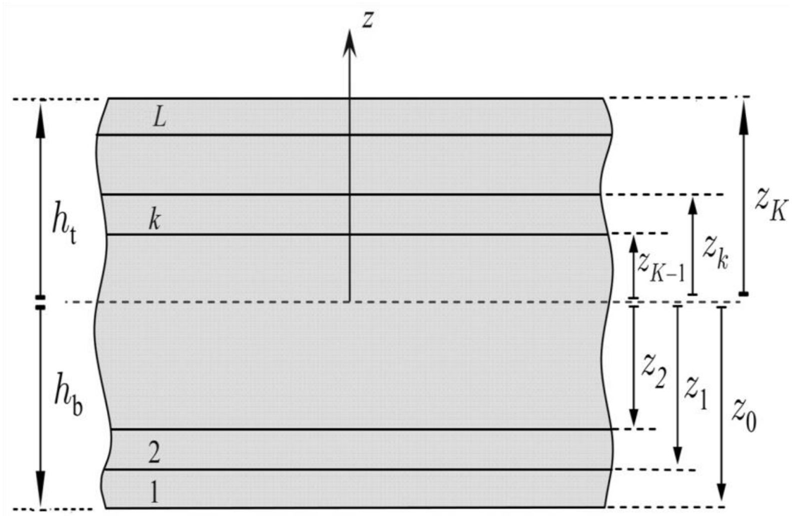

Figure 1 Distances from the reference plane.

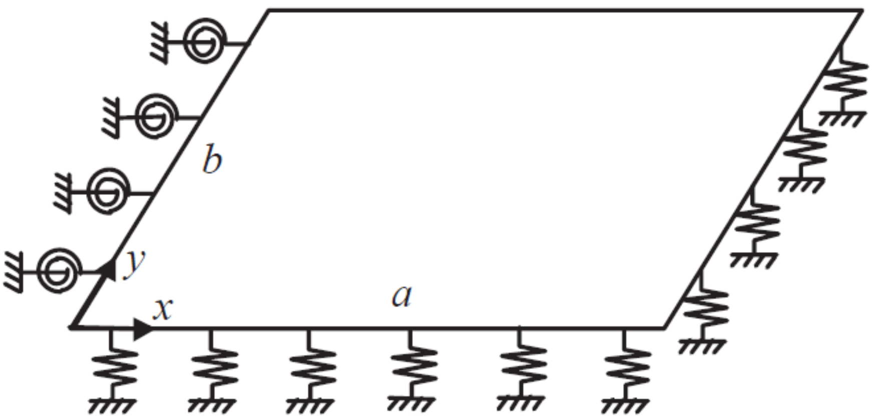

Figure 2 A rectangular plate elastically restrained along edges.

Table 1. Frequency parameters, Ω= ω$a^2\sqrt{(\rho h\ /\ D)}$, for all clamped boundary conditions (cccc) plate with ($\frac{a}{b} = 2.5$). For $m = n = 1,2,3$.

M=N	mod 1	mod2	mod 3	mod 4	mod 5
1	147.43	172.60	395.47	419.39	--------
2	147.87	172.54	220.33	394.94	419.39
3	146.87 $(147.8)^a$ 0.62%	172.52 $(173.8)^a$ 0.73%	220.33 $(221.4)^a$ 0.48%	293.49 $(291.7)^a$ -0.61%	387.85 $(384.4)^a$ -0.89%

a : **Wen le 2004 .**

Tabel 2. Frequency parameters, Ω= ω$a^2\sqrt{(\rho h\ /\ D)}$, for squar plates of different boundary conditions

B C S		mod 1	mod2	mod 3	mod 4	mod 5	mod 6
ssss	present	19.67	49.14	49.14	78.04	98.37	98.38
	H. DAL	19.72	49.32	49.32	78.88	98.56	98.56
	Diff %	0.25	0.36	0.36	1.06	0.19	0.19
	Wen le 2004	19.74	49.35	49.35	78.96	98.70	98.70
	Diff %	0.35	0.42	0.42	1.16	0.33	o.33
cscs	present	28.71	54.18	68.73	92.2	101.36	128.55
	H.DAL	28.91	54.64	69.37	93.91	102.04	128.58
	Diff %	0.69	0.84	0.92	1.82	0.66	0.02
	Wen le 2002	28.95	54.74	69.32	94.61	102.23	129.09
	Diff %	0.82	1.02	0.85	2.54	0.85	0.41
Ssfs	present	11.82	27.92	41.55	59.22	63.28	91.09
	H. DAL	11.58	27.68	41.11	59.20	62.93	90.42
	Diff %	-2.07	-0.86	-1.07	-0.03	-0.55	-0.74
	Wen le 2002	11.68	27.79	41.23	59.24	62.37	90.51
	Diff %	-1.19	-0.46	-0.77	0.03	-1.45	-0.64

Table 3. Natural frequencies (Hz) of graphite–epoxy plates consisting of 12 plies oriented at 0 under different boundary conditions (E1=127.9Gpa , E2 =10.27Gpa , G12=7.312Gpa , υ12=0.22)

Mod	ssss				ccfc			
	Ansys	Henry 2009	Present	Diff %	Ansys	Henry 2009	Present	Diff %
1	108.10	108.7	108.82	-0.11	70.63	70.96	71.01	-0.07
2	170.09	171.4	171.91	-0.29	166.96	167.5	169.35	-1.10
3	292.84	294.8	297.55	-0.93	215.69	219.7	219.88	-0.08
4	384.97	388.4	390.52	-0.54	294.77	298.1	298.8	-0.23
5	429.83	435.0	437.27	-0.52	314.51	314.8	323.27	-2.69

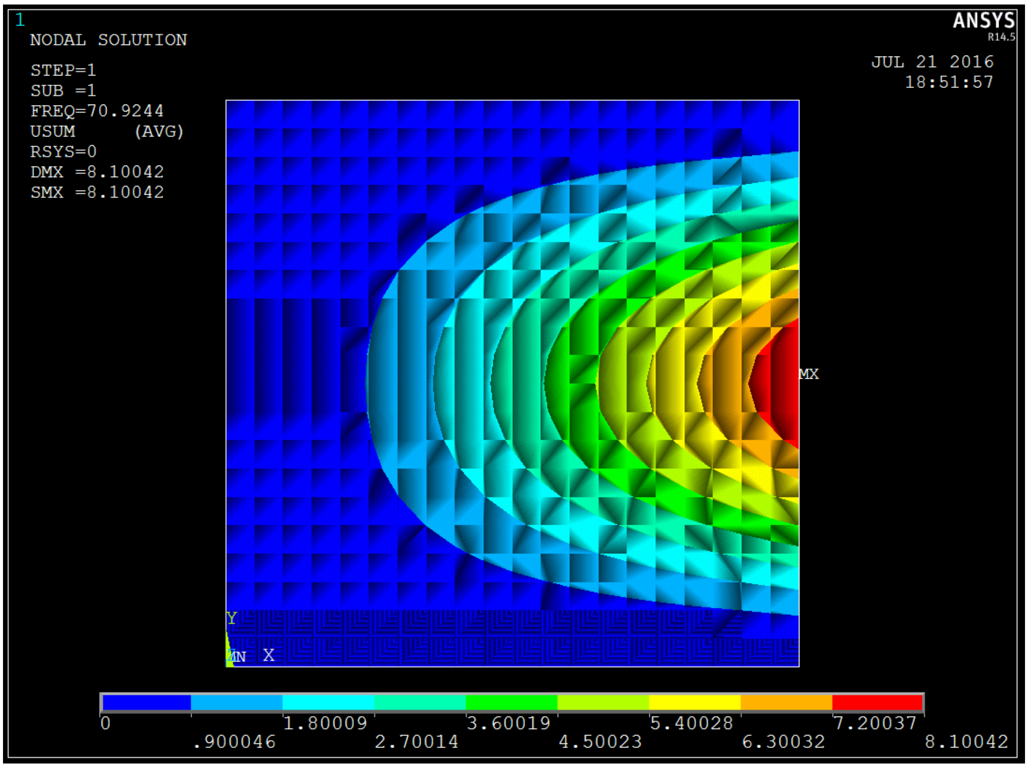

Figure 3 . First Mode shape for free vibration of a CCFC orthotropic square plate.

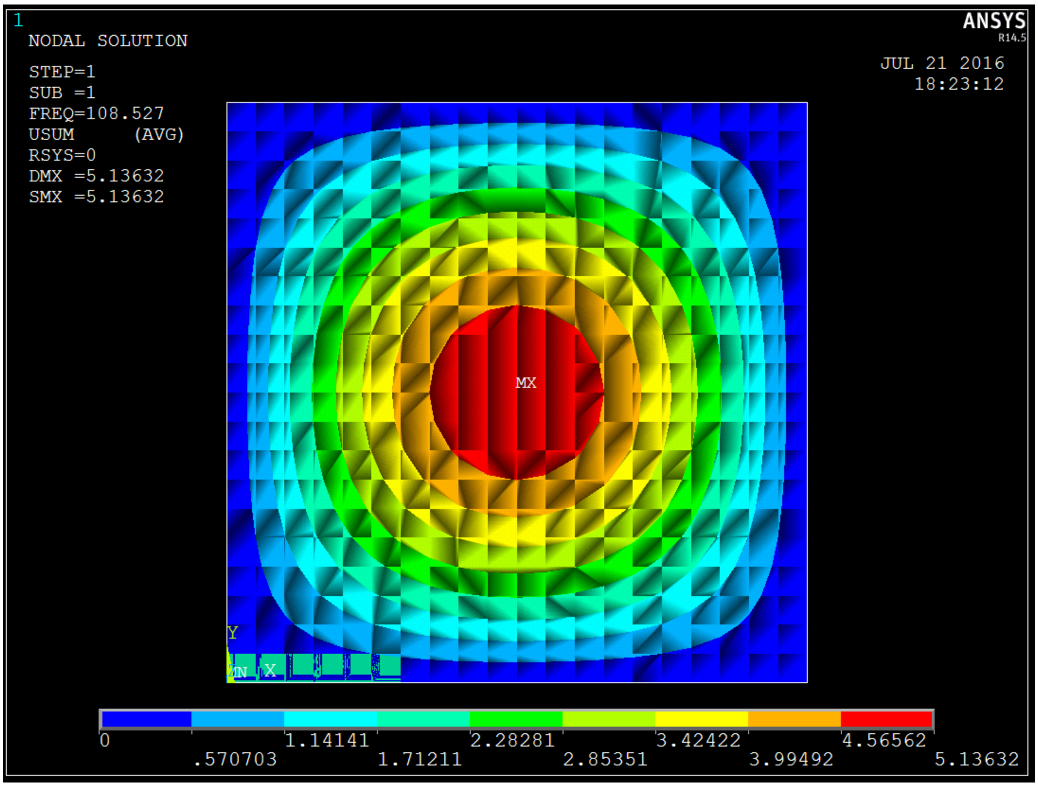

Figure 4 . First Mode shape for free vibration of a SSSS orthotropic square plate.

Table 4. Frequency parameters, Ω= $\omega a^2/h\sqrt{(\rho / E_2)}$, for s-s-s-s squar plates and (a/h=10, G12=0.6E2, υ12=0.25).

E_1 $/E_2$	[0 90 90 0]		
	Present	Reddy	Diff %
3	7.53	7.47	-0.80
10	10.65	10.56	-0.85
20	13.95	13.83	-0.86
30	16.61	16.47	-0.85
40	18.90	18.73	-0.90

Table 5. Frequency parameters, Ω= $\omega b^2/\pi^2\sqrt{(\rho h\ /\ D22)}$, of a square plate of various laminations and boundary conditions. (E1/E2=10, G12=0.6E2, υ12=0.25)

Angle Ply Orientations		ssss	cccc	cscs	cfcf
[0 90]s	present	2.56	5.37	4.93	4.65
	Firas	2.55	5.35	4.91	4.63
	Diff %	-0.39	-0.37	-0.40	-0.43
	Ansys	2.55	5.31	4.91	4.63
[0 90 0 90]	present	1.58	3.33	2.606	2.27
	Firas	1.58	3.33	2.606	2.26
	Diff %	0	0	0	-0.44
	Ansys	1.60	3.39	2.58	2.31
[0 90 0]s	present	2.04	4.28	3.73	3.45
	Ansys	2.03	4.31	3.72	3.43
$[0\ 90]_3$	present	1.59	3.33	2.61	2.27
	Ansys	1.58	3.24	2.55	2.19

Table 6. frequency parameters, Ω= $\omega b^2/\pi^2\sqrt{(\rho h\ /\ D22)}$, of a square plate of various laminations and boundary conditions. (E1/E2=10, G12=0.6E2, υ12=0.25).

Angle Ply Orientations		ssss	cccc	cscs	cfcf
[45 -45]s	present	2.52	4.09	3.38	2.27
	Firas	2.51	4.12	3.39	2.26
	Diff %	-0.39	0.78	0.29	-0.44
	Ansys	2.72	4.49	3.15	1.98
[45 -45 45 -45]	present	2.52	4.09	3.38	2.27
	Firas	2.51	4.12	3.39	2.26
	Diff %	-0.39	0.78	0.29	-0.44
	Ansys	2.31	4.01	3.24	2.25
[30 -30]s	present	3.40	5.84	5.30	4.32
	Ansys	3.17	5.76	5.14	4.12
[30 -30 30 -30]	present	3.40	5.84	5.30	4.32
	Ansys	3.30	5.62	5.04	4.09
[45 -45 45]s	present	2.52	4.09	3.38	2.27
	Ansys	2.43	4.08	3.31	2.16
$[45\ \ -45]_3$	present	2.52	4.09	3.38	2.27
	Ansys	2.48	3.98	3.30	2.14

[30 -30 30]s	present	3.40	5.84	5.30	4.32
	Ansys	3.31	5.84	5.23	4.19
$[30\ -30]_3$	present	3.40	5.84	5.30	4.32
	Ansys	3.36	5.79	5.18	4.13

Tabel 7. Frequency parameters, Ω= $\omega a^2\sqrt{(\rho h\ /\ D)}$, for all clamped boundary conditions(cccc) plates with different aspect ratios.

a/b		mod 1	mod2	mod 3	mod 4	mod 5	mod 6
1	present	35.58	72.44	72.44	104.48	130.18	131.44
	Wen.le	35.99	73.4	73.4	108.2	131.6	132.2
	Diff %	1.13	1.30	1.30	3.43	1.07	0.57
1.5	present	60.31	93.05	148.28	149.88	176.38	225.82
	Wen.le	60.76	93.84	148.8	149.7	179.6	226.8
	Diff %	0.74	0.84	0.34	-0.12	1.79	0.43
2	present	97.67	126.24	178.75	251.68	256.46	278.91
	Wen.le	98.31	127.3	179.1	253.3	255.9	284.3
	Diff %	0.65	0.83	0.19	0.63	-0.21	1.89
2.5	present	146.87	172.52	220.33	293.49	387.85	413.81
	Wen.le	147.8	173.8	221.4	291.7	384.4	394.3
	Diff %	0.62	0.73	0.48	-0.61	-0.89	-4.94

Table 8. Frequency parameters, Ω= $\omega a^2\sqrt{(\rho h\ /\ D)}$, for CSSF plates with different aspect ratios .

a/b	Reference	mod 1	mod2	mod 3	mod 4	mod 5	mod 6
1	present work	16.88	31.18	51.67	65.19	67.27	100.31
	Wen.le	16.87	31.14	51.64	64.03	67.64	101.2
	Diff %	-0.05	-1.27	-0.05	-1.81	0.54	0.87
1.5	present work	18.68	50.62	54.14	89.09	110.64	130.16
	Wen.le	18.54	50.43	53.72	88.78	108.2	126.10
	Diff %	-0.75	-0.37	-0.78	-0.34	-2.25	-3.21
2	present work	20.89	56.83	77.54	113.13	117.81	176.94
	Wen.le	20.65	56.54	77.33	111.3	117.3	176.0
	Diff %	-1.16	-0.51	-0.27	-1.64	-0.43	-0.53
2.5	present work	23.41	60.46	112.14	117.19	153.89	196.47
	Wen.le	23.07	59.97	111.9	115.1	153.1	189.6
	Diff %	-1.47	-0.81	-0.21	-1.18	-0.51	-3.62

Table 9. show Frequency parameters, Ω= $\omega b^2/\pi^2\sqrt{(\rho h\ /\ D22)}$, of effect of aspect ratio and boundary conditions. (E1/E2=10, G12=0.6E2, υ12=0.25).

a/b		[0 90 0 90]			[0 90]s		
		ssss	cccc	cffc	ssss	cccc	cffc
1	present	1.58	3.33	0.583	2.56	5.37	0.94
	Firas	1.58	3.33	0.592	2.55	5.35	0.95
	Diff %	0	0	1.52	-0.39	-0.37	1.05
1.5	present	1.19	2.55	0.435	1.57	3.24	0.579
2	present	1.09	2.38	0.393	1.27	2.67	0.467
2.5	present	1.052	2.32	0.377	1.16	2.48	0.421

Table 10. Frequency parameters, Ω= $\omega b^2/\pi^2\sqrt{(\rho h\ /\ D22)}$, for (45/-45/45/-45) plates of different aspect ratios and boundary conditions ,(E1/E2=10, G12=0.6E2, υ12=0.25).

	Type of boundary conditions				
a/b	ssss	sscc	ssff	ccff	ccfc
1	2.52	3.239	0.496	0.854	2.581
1.5	1.77	2.326	0.329	0.596	2.405
2	1.467	1.998	0.246	0.494	2.347
2.5	1.313	1.844	0.196	0.444	2.321

Table 11. Frequency parameters, Ω= $\omega b^2/\pi^2\sqrt{(\rho h\ /\ D22)}$, for (30/-30/30/-30) plates of different aspect ratios and boundary conditions,(E1/E2=10, G12=0.6E2, υ12=0.25).

	Type of boundary conditions				
a/b	ssss	sscc	ssff	ccff	ccfc
1	3.404	4.502	0.633	1.166	2.818
1.5	2.194	2.862	0.422	0.754	2.499
2	1.723	2.291	0.316	0.589	2.396
2.5	1.486	2.027	0.252	0.507	2.351

Table 12. Natural Frequency ω(rad/sec) , of effect of thickness ratio for squar plate (E1/E2=10, G12=0.6E2, υ12=0.25) .

	[0 90 90 0]			[45 -45 -45 45]		
a/t	cccc	ssss	cscs	cccc	ssss	cscs
20	1.11	0.532	1.025	1.09	0.67	0.90
40	0.55	0.266	0.513	0.545	0.335	0.45
100	0.223	0.106	0.205	0.218	0.134	0.18

Table 13. Natural Frequency ω(rad/sec), effect of thickness ratio for square plate (E1/E2=10, G12=0.6E2, υ12=0.25) (30/-30/-30/30).

a/t	Type of boundary conditions				
	cccc	ssss	cscs	cfcf	sfsf
20	1.097	0.638	0.995	0.811	0.356
40	0.548	0.319	0.497	0.405	0.178
100	0.219	0.127	0.199	0.162	0.071

Table 14. Frequency parameters, Ω= $\omega a^2\sqrt{(\rho h\ /\ D)}$, for SSSS square plate with different uniform rotational restraint along edges.

K a/D	Reference	mod 1	mod2	mod 3	mod 4	mod 5	mod 6
0	present work	19.67	49.14	49.14	78.04	98.38	98.38
	Wen.le 2004	19.74	49.35	49.35	78.96	98.70	98.70
	Diff %	0.35	0.42	0.42	1.16	0.32	0.32
10	present work	28.50	60.52	60.52	90.97	112.82	113.07
	Wen.le 2004	28.50	60.22	60.22	90.81	111.20	111.40
	Diff %	0	-0.49	-0.49	-0.17	-1.45	-1.49
20	present work	31.08	64.68	64.68	95.97	118.83	119.25
	Wen.le 2004	31.08	64.31	64.31	95.82	116.80	117.20
	Diff %	0	-0.57	-0.57	-0.15	-1.73	-1.74
100	present work	34.67	71.27	71.27	104.61	129.69	130.36
	Wen.le 2004	34.67	70.78	70.78	104.50	127	127.60
	Diff %	0	-0.69	-0.69	-0.10	-2.11	-2.16
∞	present work	35.58	72.44	72.44	104.48	130.18	131.44
	Wen.le 2004	35.99	73.40	73.40	108.20	131.60	132.20
	Diff %	1.13	1.30	1.30	3.431	1.07	0.57

Table 15. Frequency parameters, $\Omega = \omega b^2/\pi^2\sqrt{(\rho h \,/\, D22)}$,for SSSS square plate [0 90 0 90] with uniform rotational restraint along edges.

$K\,a/\,D22$	mod 1	mod2	mod 3	mod 4
0	1.59	4.39	4.39	6.39
10	2.60	5.61	5.61	7.80
20	2.86	6.04	6.04	8.34
100	3.21	6.69	6.69	9.19
∞	3.33	6.95	6.95	9.54

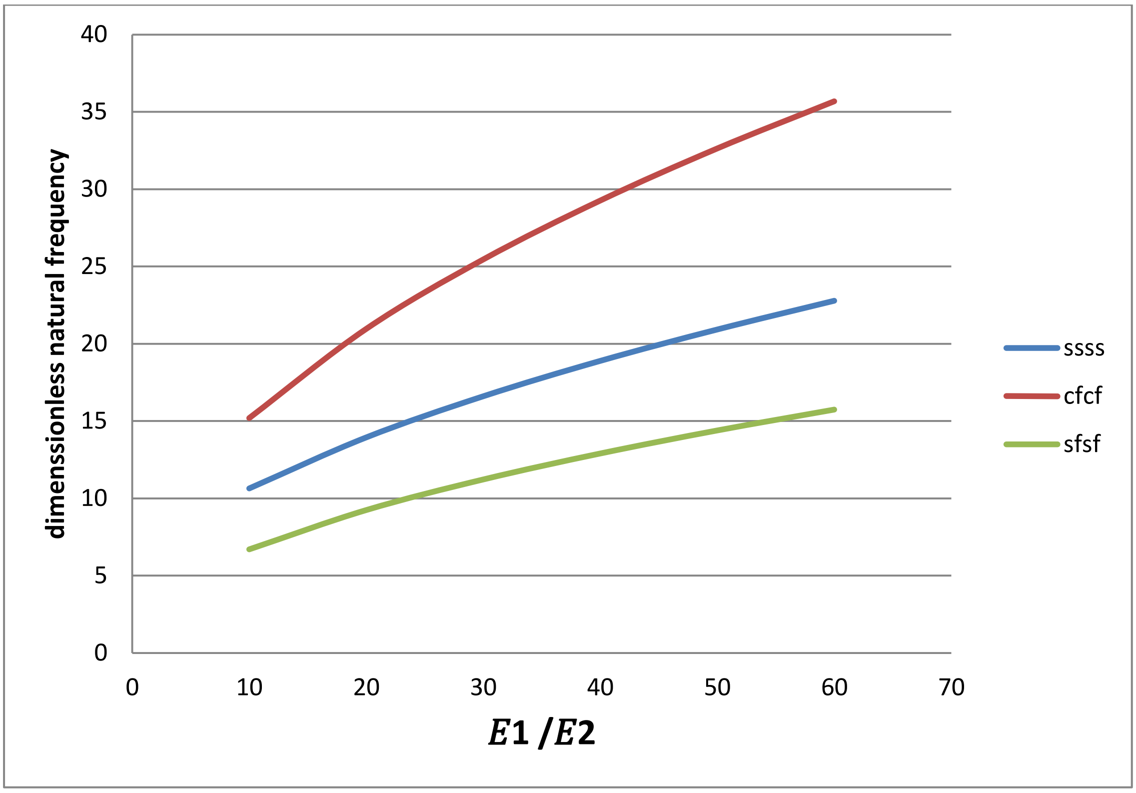

Figure 5. Frequency parameters, $\Omega = \omega a^2/h\sqrt{(\rho \,/\, E_2)}$, for square plates with different orthotropic ratio, (a/h=20, G12=0.6E2, υ12=0.25) (0/90/0/90).

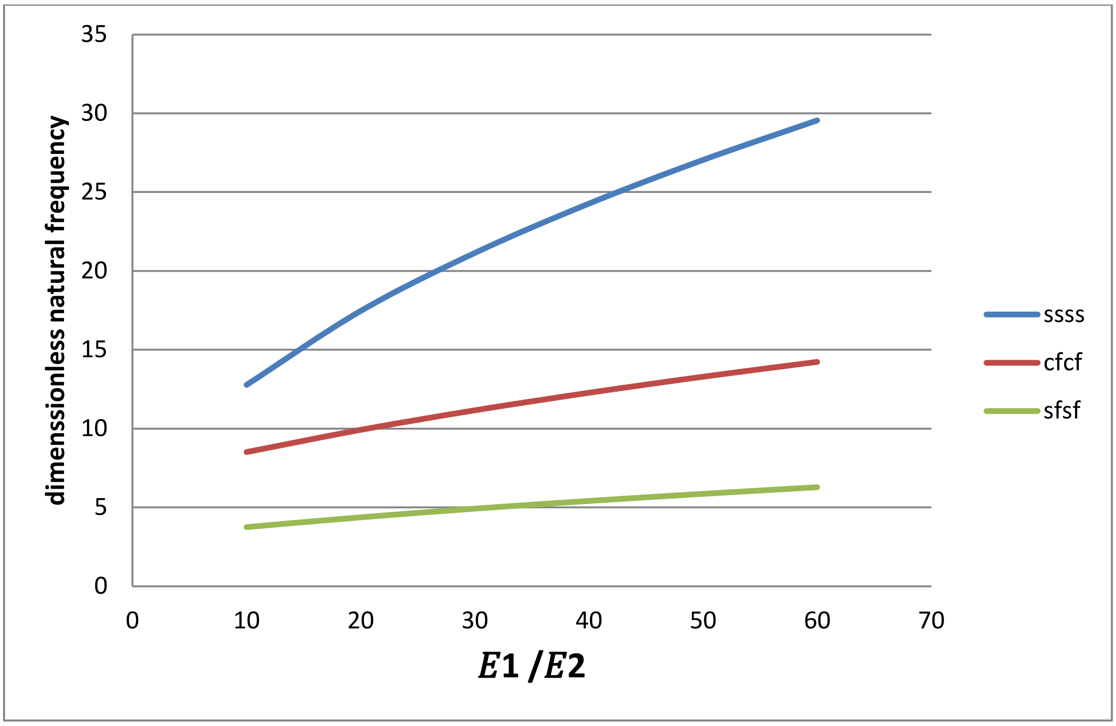

Figure 6. Frequency parameters, $\Omega = \omega a^2/h\sqrt{(\rho\ /\ E_2)}$, for square plates with different orthotropic ratio, (a/h=20, G12=0.6E2, υ12=0.25) (60/-60/60/-60).

Aerodynamic Characteristics of a Rectangular Wing Using Non-Linear Vortex Ring Method

Anmar Hamid Ali
Lecturer
Engineering College-Baghdad University
aha_has@yahoo.com

ABSTRACT

The aerodynamic characteristics of general three-dimensional rectangular wings are considered using non-linear interaction between two-dimensional viscous-inviscid panel method and vortex ring method. The potential flow of a two-dimensional airfoil by the pioneering **Hess & Smith** method was used with viscous laminar, transition and turbulent boundary layer to solve flow about complex configuration of airfoils including stalling effect. Viterna method was used to extend the aerodynamic characteristics of the specified airfoil to high angles of attacks. A modified vortex ring method was used to find the circulation values along span wise direction of the wing and then interacted with sectional circulation obtained by **Kutta-Joukowsky** theorem of the airfoil. The method is simple and based mainly on iterative procedure to find the wings post stall aerodynamic results. Parametric investigation was considered to give the best performance and results for the rectangular wings. Wing of NACA 0012 cross sectional airfoil was studied and compared with published experimental data for different speeds and angle of attacks. Pressure, skin friction, lift, drag, and pitching moment coefficients are presented and compared good with experimental data. The present method shows simple, quick and accurate results for rectangular wings of different cross-section airfoils.

Key words: lifting line method, Viterna method, potential flow, viscous-inviscid panel method

خصائص الديناميكا الهوائية لجناح مستطيل باستخدام طريقة الدوامة الحلقية غير الخطية

انمارحامد علي
مدرس
كلية الهندسة – جامعة بغداد

الخلاصة

تمت دراسة الخصائص الايروديناميكية للاجنحة الثلاثية الابعاد المستطيلة الشكل باستخدام التاثير اللاخطي المتبادل بين طريقة الالواح لزج-غير لزج ثنائية البعد وطريقة الدوامة الحلقية .ان الجريان الكامن لجنيح ثنائي البعد بطريقة Hessو Smith البدائية قد استخدم مع الطبقة المتاخمة الطباقية ،الانتقالية والمضطربة لحل الجريان حول اشكال معقدة من الجنيحات متضمنا تاثير الانهواء فيها .طريقة فيترنا استخدمت لتمديد الخواص الايروديناميكية للجنيح الى زوايا هجوم عالية .طريقة الدوامة الحلقية المعدلة استخدمت لايجاد قيم التدوير على طول امتداد الجناح وايجاد تاثيرها مع التدورة المقطعي الماخوذة من نظرية **Kutta-Joukowsky** للجنيح. الطريقة بسيطة وتعتمد اساسا على عملية التاثير المتبادل لايجاد النتائج الايروديناميكية الاجنحة ما بعد الانهواء. تمت دراسة العوامل التي تعمل على اعطاء افضل اداء ونتائج للمسالة . الجناح ذو مقطع مطيار NACA 0012 تمت دراسته ومقارنته مع البيانات العملية المنشورة لمختلف السرع وزوايا الهجوم. معامل الضغط، الاحتكاك، الرفع، الممانعة، و عزم التارجح قد تم عرضها ومقارنتها جيدا مع البيانات العملية. ان الطريقة الحالية تظهر بساطة، سرعة ودقة النتائج للجناح المستطيل ولمختلف مقاطع الجنيحات.

1. INTRODUCTION

The conceptual design of aircraft requires numerous representative calculations to a large number of aircraft configurations. Fast methods to find the aerodynamic characteristics have been of great interest. The Navier-Stockes equations results are too complex calculations during aircraft design phase, in other hand Lifting line, vortex lattice and panel methods are still used today as a tool to find the aerodynamic characteristics of aircrafts. The potential methods have the same assumptions irrotational, incompressible and discretization at the wing and body of the aircraft. These methods are simple, fast, and need small computer memory to solve them.

In lifting line and vortex methods, the airfoil shape is not a part of solution and this may cause errors when calculating the configurations have un-conventional airfoils. These errors could be obtained due to the assumption of no stalling characteristics, and then no profile drag could be estimated (only induced drag). Moderate to high angle of attacks during take-off, landing and military aircraft manoeuvring have inclusion of non-linear aerodynamic characteristics. Accurate predictions of the flow in those conditions are needed during design phases especially in structure modelling.

Two–dimensional airfoil data lift, drag and pitching moment are available from the experimental, Navier-Stockes solutions and even by panel method interacted with boundary layer solution as in **Eppler,** and **Somers, 1980, Drela, 1989,** and **Ali, 2014**. Various methods were available to solve two-dimensional airfoil sectional characteristics (lift, drag and pitching moment) which used as input data to calculate three-dimensional aerodynamic characteristics of wings. The solution is simple, fast and less hardware demanding as compared with CFD computations.

An early method was presented in **Sivells**, and **Neely, 1947**; the local lift coefficient for NACA 4-series airfoil was interacted with lifting-line method. The vortex strengths along the span of a wing were solved using iteration method. The induced drag with final span wise circulation distribution were presented and discussed with previous experimental works. The drawback of the method is the limitation of lifting line method for large aspect ratio and small swept wings. A two-dimensional steady incompressible flow was calculated for NASA GA(W)-1 airfoil characteristics using linear vortex panel method interacted with boundary layer laminar, transition and turbulent regions for attached and separated flow had been presented in **Piszkin** and **Levinsky, 1976**. Lifting line method was used to calculate flow in three-dimensional wing using the characteristics of two-dimensional airfoil lift curve. Only distributed load and wake shape of the rectangular wing were showed.

Dropped and un-dropped leading edge wing in post stalling region were studied by **Anderson, et al., 1980,** to find non-linear post stall behaviour of a rectangular wing. Experimental airfoil characteristics of dropped and un-dropped shape were incorporated with prandtle lifting line method to solve the problem. The accuracy of the results was 20% as compared with the experimental works. No pressure or shear stresses distribution presented in the work.

The quick aerodynamic characteristics predictions for high lift module during conceptual design stages of an aircraft was made by coupling a non-linear lifting surface method (modified **Weissinger** method) with two-dimensional viscous characteristics of aircraft to calculate three-dimensional wing of the designed aircraft was presented in **Van Dam, et al., 2001**. Semi-empirical equations for two-dimensional high lift airfoils were utilized based on the computational fluid dynamic (CFD) and experimental data for different configurations. The method provided necessary accuracy and fast enough for the design stage.

Multiple wings aerodynamic characteristics prediction method for post stall flight condition was shown in **Mukherjee,** and **Gopalarathnam, 2003**. De-cambering approach was developed in each section of wing to consider viscous effect at high angle of attack. The results were presented to lift coefficient as a function of angle of attack and load distribution along span wise direction of the aircraft.

Different approaches were used to find the interaction between potential solution and two-dimensional viscous effects at high angle of attack. Most of the models were developed based on the two-dimensional lift-angle of attack curve at moderate to high ranges experimentally as shown in **de Vargas,** and **de Oliveira, 2006, Pakalnis, Lasauskas,** and **Stankunas, 2005**, and **Spalart, 2014**.

The most important notes about all the previous considerations are that, the presented results were restricted to lift, drag coefficients and load distribution along span wise direction of the wing of the aircraft only. This may be attributed to the information used as input (two-dimensional airfoil lift and drag curves) to solve the characteristics of the wing. The pressure and boundary layer characteristics distributions along upper and lower surfaces were not consisted in the results. So that, in the present work the aerodynamic characteristics with pressure and boundary layer parameters will be studied and demonstrated using vortex ring method which was discussed in **Ali, 2010** to solve the potential linear behaviour of a rectangular wing and then coupled with the two-dimensional viscous-inviscied interaction method of multi-element airfoil in ground effects illustrated by **Ali, 2014**. Viterna method **Tangler,** and **Kocurek, 2005** was used to extrapolation the lift and drag forces of the wing sectional airfoil without need for extra solution of a large angle of attacks. Iteration method will be used to find the circulations along the span wise direction of rectangular wings.

The presentation of a non-linear vortex ring method will be discussed in theory of the method section, which illustrates the iterative procedure used to include airfoil distribution characteristics data to the wing calculation of circulation distribution along span wise direction and the results are discussed. Parametric investigation and results verification are done by comparing with the experimental published data. Last conclusions and future work are stated.

2. THEORY OF THE METHOD

For small to moderate angles of attack, linear aerodynamic characteristics can be modelled for most aircrafts wings, but at high angles of attack a non-linear behaviour of forces and moment are produced. Panel methods are linear solution, so it cannot take into account the non-linearity of the stall effects. In the present method the non-linearity effects of un-swept to moderate swept wings the vortex ring method of **Ali, 2010** is modified to account the stalling effects.

2.1 Two Dimensional Airfoil Characteristics

A general method for inviscid-viscous boundary layer interaction method is used to calculate flow about multi-element airfoil in ground effect which was described in details by **Ali, 2014**. Two-dimensional **Hess,** and **Smith, 1967** panel method with constant source and vortex distribution is used to find the potential flow around complex configurations of multi-elements airfoils like slats and flaps high lift elements. Each elements of the configuration are discretized using flat panels on the upper and lower side of the airfoil. Constant source strength is assumed at control point of the panel with constant vortex strength for the whole airfoil. Boundary condition of zero normal velocity is applied at the control points with kutta condition at the trailing edge of the airfoil. The linear equations which are obtained from influence each panel by the other are solved to determine the unknown strengths of the main airfoil and its elements. The boundary layer growths along the upper and lower sides of multi-element airfoils are calculated by using the pressure and velocity of the potential flow which were solved previously. The boundary layer regions are solved by using the method of **Thewait's** for laminar flow, n^9- or **Micheal's** methods for transition point and **Head's** method for turbulent flow along upper and lower surfaces of the airfoil. Iterative scheme with transpiration method is used for each control point to investigate the viscous effect in the boundary condition of panel method of the airfoil. Ground effect is considered by imaging the configuration around ground x-axis. Wake shape is relaxed optionally to give more realism to the calculations.

Direct and inverse methods are used to calculate linear and non-linear (separating flow) behaviour of the aerodynamic characteristics around MEA in ground effects. The program is presented and discussed for different cases and tested in **Ali, 2014**. Comparisons were showed good agreement between the theoretical and experimental results for low to moderate angles of attack.

Non-linear behaviour characteristics of an airfoil can be obtained for small to moderate angles of attack by using previous method, but at higher angles or even in negative angles of attack the convergence is not reached. Viterna method **Tangler**, and **Kocurek**, **2005**, was developed to extrapolate lift and drag coefficients to extreme angles using flat plate theory and empirical assumptions obtained from experimental data for losses in BEM. In present method, the forces and moments are evaluated through Viterna method for post stall angles, but pressure and boundary layer properties are restricted to the method of interaction presented previously. Single element airfoil is considered in the present analysis.

2.2 Three Dimensional Wing Characteristics

In a vortex ring method, a non-planar finite wing is descretized into number of sections where for each section only one quadrilateral panel in chord wise directions is represented. A vortex ring shape placed at quarter chord line for each panel to satisfy the boundary condition of zero normal velocity of the wing using Biot-Savart law of vorticity. The wake behind the wing is descretized using single long element (about 2-3 times span length **Katz**, and **Plotkin**, **1991**) or multiple elements along wake length (optionally to calculate wake shape effects) for each section as shown in **Fig. 1**. The two-dimensional discretization of the cross-sectional airfoil geometry into finite number of element in a clockwise direction beginning from the trailing edge lower surface to the upper surface trailing edge and in span wise direction to form the surface elements are shown in **Fig. 2**. Kutta condition at the trailing edge is used to calculate the strengths of the wake elements. The flow tangency boundary condition is satisfied at three-quarter chord point for each panel (centre point of the vortex ring). Linear sets of influence coefficients equations are solved using Gauss's elimination method to find the strengths of vortices of the panels. Optionally the wake may be relaxed to be a stream line starting from the trailing edge. Different test cases are presented and discussed in **Ali, 2014**. The wing discretization in the present study is limited to one element in the chord wise direction because the final circulation distribution of the wing will be related to the sectional two-dimensional airfoil characteristics calculated previously. The potential solution of rectangular wing using vortex ring method for different angle of attack and aspect ratio will be showed and discussed in the results section.

2.3 Method of interaction

The extension of the linear potential vortex ring method to the non-linear viscous post stalling characteristics at high angle of attack is presented in this section. Kutta-Joukowsky theorem of lift is the main idea of this method. The sectional circulation of the wing (vortex strength at each section of wing by using vortex ring method) is related to the circulation obtained from two-dimensional airfoil data which was investigated and stored for each section. The induced angle of attack is calculated at each section from vortex ring method at load points (centre point of bound vortex segment). The induced angle simply represents the angle between the down wash velocities divided by free stream velocity. The effective angle of attack is then evaluated by subtracting induced angle from geometrical angle of attack at each section. Two-dimensional airfoil lift coefficient is evaluated at the effective angle of attack of each section. The circulations for three- and two-dimensional analysis are compared and damped by using iterative procedure to find new value. The following steps are used to calculate the non-linear vortex ring method,

1- Geometric and operational conditions parameters are defined starting from root to tip which consists of (airfoil geometric coordinates, tip coordinates of the wing, chord length, geometric angle of attack, number of span wise sections, wake options for root and tip sections).
2- Two-dimensional airfoil aerodynamic characteristics are calculated for the root and tip airfoils by using viscous-inviscid interaction method of the multi-element airfoil in ground effects for angle of attack range (-10 to 20^{o}) as discussed in the section 2.1.
3- Viterna method is used to extrapolate the airfoil characteristics (lift and drag coefficient) to extreme ranges of angles of attack as discussed in the section 2.1.
4- The airfoil results (pressure, forces, moment, boundary layer characteristics, etc) are stored.
5- The wing and wake are discretized into number of sections. Cosine low is used to distribute the sections along the span of the wing.
6- Linear interpolation of the airfoils characteristics between the root and tip sections (intermediate sections), is applied.
7- Initial bound vortex distribution along the span of the wing is calculated from linear solution of the vortex ring method as discussed in the section 2.2. The linear solution consists of computing the influence coefficients of the bound and trailing vortices at each control point as illustrated in **Fig. 1**. Tangency boundary condition is applied at the three-quarter chord point of the wing element to solve the linear equations.
8- Induced angle of attack at each span wise station is then calculated from the down wash velocity at the load centre,

$$\alpha_i(y) \approx -\frac{w(y)}{V_\infty} \quad (1)$$

where w is the down wash velocity.

9- Effective angle of attack α_{eff} is calculated by subtracting induced angle from geometric angle of attack.

$$\alpha_{eff}(y) = \alpha_g - \alpha_i(y) \quad (2)$$

10- Sectional lift coefficient can be determined from known airfoil data at effective angle of attack.
11- The new circulation distribution can be calculated by using ,Kutta-Joukowski theorem as;

$$\Gamma(y)_{2\mathrm{D}} = \frac{cl(y)\, V_{\infty} c}{2} \tag{3}$$

12- The new circulation distribution is determined by the following equation;

$$\Gamma_{\mathrm{new}} = \Gamma_{\mathrm{old}} + \mathrm{D}(\Gamma(y)_{2\mathrm{D}} - \Gamma_{\mathrm{old}}) \tag{4}$$

where D is the damping factor.

13- Step (2-11) is repeated until the difference between the old and new circulation distribution are within the given accuracy (1.0 e^{-5}).
14- The aerodynamic characteristics and boundary layer properties are calculated based on the final characteristics data obtained from 2-D airfoil characteristics at effective angle of attack and from 3-D vortex ring forces and moments.

3. RESULTS AND DISCUSSION

The results of the potential solution of the rectangular using are presented and discussed in the following sub sections.

3.1 Validation Results

In order to verify the results with other conventional methods like vortex lattice method and experimental data obtained from published works, three test cases for accuracy are considered in the present work,

1- Accuracy of two-dimensional airfoil results as compared with experimental data.
2- Parametric considerations of the present method which includes (no. of span wise elements, damping factor, convergence tolerance).
3- Accuracy of nonlinear vortex ring method as compared with the published theoretical and experimental data.

The results presented in this work were programmed and executed using **Matlab 7.6** on a personal computer Dell Core i3 of (2.4) GHz. All the accuracy test cases are restricted to the rectangular or straight geometrical wing of cross-sectional airfoil NACA 0012, aspect ratio (6) and taper ratio (1).

Fig. 3 and **4** show the aerodynamic characteristics of two-dimensional NACA 0012 airfoil at Reynolds number $3\text{x}10^6$. The Viscous-Inviscid panel method (VIP) shows good accuracy as compared with **Abbot**, and **Von Doenhoff**, **1949** experimental data except at the stalling region. The discrepancy with them may be attributed to the multiple parameters of boundary layer separation like wall roughness, pressure variation along normal direction in the separation region, position of the transition point, etc. **Fig. 3** shows a delay separation angle. **Fig. 4** shows good drag coefficient prediction because it depends on the semi-empirical equation at the tailing edge as illustrated in **Ali, 2014**. The number of panels to represent the airfoil surface is 160 which are sufficient to give good accuracy as discussed in **Ali, 2014** with many accuracy considerations about VIP method. The pressure and shear stress distribution along the airfoil upper and lower surfaces are stored in files for next wing calculations. **Fig. 5** and **6** show Viterna results of lift and drag coefficients which extended the airfoil characteristics to high angle of attacks. Positive and negative angle of attacks are extended to 180^o and plotted in the figures to show the behaviour of the aerodynamic characteristics at these angles. For lift coefficient in positive angles is not symmetric with negative angles due to range of exactly lift coefficient calculations (-10^o to 20^o), other this range represents the prediction results which are not bad at all. The lift coefficient at angle 90^o is approximately zero and the drag coefficient shows the maximum value at a right angle to flow direction. These characteristics are also stored in the programs for next calculation.

Three important accuracy parameters are considered in the present method number of span wise elements, damping parameter and convergence parameter. These parameters are discussed separately to evaluate the quick and efficient solution. For the basic calculation the previous parameters are setting to the following values (20, 0.8, 1e-4) respectively.

Fig. 7 and **8** show the effect of span wise number of elements on the lift and drag coefficients respectively for the wing geometry discussed previously at Reynolds number 3x10^6. The number of elements is selected 10, 20 and 40. The differences between lift coefficients for different number of elements are very small as shown in **Fig. 7**. Same results are found for total drag coefficient of the wing as illustrated in **Fig. 8**. It is clear that, when increasing the number elements of the wing, the execution time will be increased. So that, choosing 20 elements can give reasonable results and fast execution time.

The damping factor is considered in **Table 1** where the aerodynamic coefficients are investigated for the wing at 10^o angle of attack. The damping factor is listed in table as 0.1, 0.5 and 0.8. The table shows that 0.8 damping factor is good choice for solution because it decreases the number of iteration and the execution time of the problem. No effects are noticed on the aerodynamic coefficients (lift and total drag) due to damping factor and stable solution is indicated for these ranges.

Table 2 lists four different factors of convergence at angle of attack 10^o. The iteration number and execution time are affected by the convergence tolerance. The iteration and time are increased as the tolerance decreased (accuracy increased). It is clear that the 1x10^{-4} represents a good choice to solve the problem.

The parametric consideration discussed previously shows the optimum solver conditions for rectangular wing at high angle of attack. Other consideration is required for different wing configuration. Generally, the non-linear results can be divided in to two branches. The first is the distributed coefficients (pressure, shear stress, span wise lift, transition line, etc) of the wing and the second is the aerodynamic characteristics (lift, total drag, pitching moment, centre of pressure, and aerodynamic centre) of the wing. The airfoil NACA 0012 is considered in the present analysis, which is symmetric airfoil. The results are compared with available published experimental data obtained in **Long**, and **Gury**, **1976** for pressure distribution and lift coefficient. The wing geometric and flow characteristics are illustrated in **Table 3**.

The pressure coefficient distribution on the upper and lower surfaces at different wing sections are shown in **Fig. 9** for dynamic pressure 2.87 kPa and 6.75^o angle of attack. As shown, the comparisons with experimental data are good for different sections of the wing. There are some discrepancy for the tip section y/c=0.99 due to highly viscous tip vortex especially near trailing edge of the wing section. Linear interpolation is used to find the pressure coefficient for the in between sections. Frictional shear stress coefficients for sections are also presented in **Fig. 10**. The frictional shear stress coefficient shows no separation along the span of the wing at this angle which indicated by a negative value of the skin friction coefficient.

Fig. 11 shows the surface pressure distribution for different angle of attack at q_∞=2.87 kPa. The angle of attacks are started from 6^o to 25^o, separation is noticed as expected at high angle of attacks 25^o. Also, the trailing edge is the first separated region on the wing a shown in the figure with red colour. The peak negative values of pressure coefficient are noticed at the leading edge of the wing. **Fig. 12** shows the skin friction drag coefficient distributed on the wing for different angle of attacks at q_∞=2.87 kPa. The flow separation is cleared at wing tips due to trailing vortex and at the trailing edge due to high angle of attack.

The present method lift coefficient for the wing is in good accuracy as compared with experimental data at q_∞=2.87 kPa obtained in **Long**, and **Gury**, **1976** as shown in **Fig. 13**. The drag polar and pitching moment coefficients are shown in **Fig. 14** and **15** respectively. Also, the span wise load distribution is shown in **Fig. 16** and compared with experimental data. The results show high accuracy of about 5% error by the present method as compared with the experimental data.

4. CONCLUSIONS AND RECOMMENDATIONS

The aerodynamic characteristics of rectangular wing either distributed (pressure and frictional stress coefficients) or total coefficients (lift, drag and pitching moments) are considered in the present work using a coupled method between two-dimensional characteristics of the airfoil at high angle of attack with help of Viterna method which extended the aerodynamic characteristics to high angles and that modified vortex ring method to find span wise circulation strength of the wing. Iterative method with specified accuracy is used to find the final circulation distribution along span wise direction of the wing. Two-dimensional airfoil results show good agreement with experimental data for intermediate angle of attack. To include high angles, Viterna method was used to find the aerodynamic coefficients at these angles. Parametric investigations were considered to have effective performance for the present method. The number of sections, convergence accuracy and damping factor were limited for rectangular wings. The wing of NACA 0012 airfoil section were solved and compared with published experimental data. The comparison shows excellent agreement and the accuracy reached to 5% with experiments.

The present method shows to be fast and simple to solve non-highly swept wings with different cross sectional airfoil configuration. More tests cases are required to investigate this method and more accurate solver for the two-dimensional airfoil are required like CFD to give more accurate results in 3-dimensional wing.

5. REFERENCES

- Abbot, I. H. and Von Doenhoff, A. E., 1949, *Theory of Wing Sections*, Dover Publications, Inc., New York, NY.
- Ali, A. H., 2014, *Aerodynamic Characteristics of Multi-Element Airfoil System with Ground Effects*, Ph.D. Thesis, Baghdad University.
- Ali, A. H., 2010, *Wake Roll-Up Behind Wings With Ground Effect*, Iraqi Journal of Mechanical and Material Engineering, Babylon University, Vol. 10, Issue 2, P.P. 181-202.
- Anderson, J. D., Corda, S., and Van Wie, D. M., 1980, *Numerical Lifting Theory Applied to Drooped Leading Edge Wings Below and Above Stall*, Journal of Aircraft, Vol. 17, No. 12, P.P. 898-904.
- Drela, M., 1989, *XFOIL, an Analysis and Design System for Low Reynolds Number Airfoils;* Massachusetts Institute of Technology, Department of Aeronautics and Astronautics, Cambridge, MA.
- Eppler, R., and Somers, D.M., 1980, *A Computer Program for the Design and Analysis of Low-Speed Airfoils*, NASA-TM-8021.
- Hess, J. L., Smith A. M. O., 1967, *Calculation of Potential Flow About Arbitrary Bodies*, Progress in Aeronautical Sciences, Vol. 8, P.P. 1-138.
- Katz, J. and Plotkin, A., 1991, *Low Speed Aerodynamics*, Cambridge University Press, Cambridge, England, UK.
- Long, P. Y., and Gury, L. S., 1976, *Pressure Distributions on a 1- By 3- Meter Semi-Span Wing at Sweep Angles From 0^o to 40^o in Subsonic Flow*, NASA-TN-8307.
- Mukherjee, R., Gopalarathnam, A., 2003, *An Iterative Decambering Approach for Post-Stall Prediction of Wing Characteristics Using Known Section Data*, AIAA 2003-1097.
- Piszkin, S. T., and Levinsky, E. S., 1976, *Non-Linear Lifting Line Theory for Predicting Stalling Instability on Wings of Moderate Aspect Ratio, CASO-NSC-76-001.*
- Sivells, J. C., and Neely, R. H., 1947, *Method for Calculating Wing Characteristics by Lifting Line Theory Using Non-Linear Section Lift Data*, NACA-TN-1269.
- Tangler, J. L. and Kocurek, J. D., 2005, *Wind Turbine Post-Stall Airfoil Performance Characteristics Guidelines for Blade-Element Momentun Methods*, NREL/CP-500-38456, AIAA/NREL.
- Van Dam, C. P., Vander Kam, J. C., and Paris, J. K., 2001, *Design-Oriented High-Lift Methodology for General Aviation and Civil Transport Aircraft*, Journal of Aircraft, Vol. 38, No. 6.
- de Vargas, L. A. T. and de Oliveira, P. H. I. A., 2006, *A Fast Aerodynamic Procedure for a Complete Aircraft Design Using the Know Airfoil Characteristics*, SAE Technical Paper 2006-01-2818.
- Pakalnis, E., Lasauskas, E., and Stankunas, J. 2005, *Convergence of lift force calculation of a tapered wing using non-linear section data*, Mechanika, No. 1, pp. 61 – 5.
- Spalart, P. R., 2014, *Prediction of Lift Cells for Stalling Wings by Lifting-Line Theory*, AIAA Journal, Vol. 52, pp. 1817–1821.

NOMENCLATURE

c	chord length	m
cl	lift coefficient	
D	damping factor	
q_∞	dynamic pressure $0.5\rho_\infty v_\infty^2$	Pa
V_∞	free stream velocity	m/s
w	down wash velocity	m/s
y	y-axis (span wise)	m
α_{eff}	effective angle of attack	Deg
α_g	geometric angle of attack	Deg
α_i	induced angle of attack	Deg
Γ_{2D}	2-dimensional circulation value	m^2/s
Γ_{new}	newer circulation value	m^2/s
Γ_{old}	previous circulation value	m^2/s

Table 1. Effect of damping factor on the numerical stability at $\alpha = 10^o$.

Damping Factor	Number of Iteration	Execution time, Sec.	Lift Coefficient	Drag Coefficient
0.1	550	3.86	0.8027	0.0448
0.5	115	0.714	0.8026	0.0447
0.8	53	0.363	0.8026	0.0447

Table 2. Effect of convergence tolerance on the numerical stability at $\alpha = 10^{o}$.

Convergence Tolerance	Number of Iteration	Execution time, Sec.	Lift Coefficient	Drag Coefficient
$1x10^{-3}$	44	0.394	0.8027	0.0447
$1x10^{-4}$	53	0.363	0.8026	0.0447
$1x10^{-5}$	66	0.461	0.8026	0.0447
$1x10^{-6}$	88	0.579	0.8026	0.0447

Table 3. Geometric and flow field characteristics of the wing.

Wing Aspect Ratio	5.9
Sweep Angle	0
Root Airfoil Section	NACA 0012
Tip Airfoil Section	NACA 0012
Span	5.9 m
q_{∞}	2.87 kpa
α , β	2.75^{o} , 0^{o}

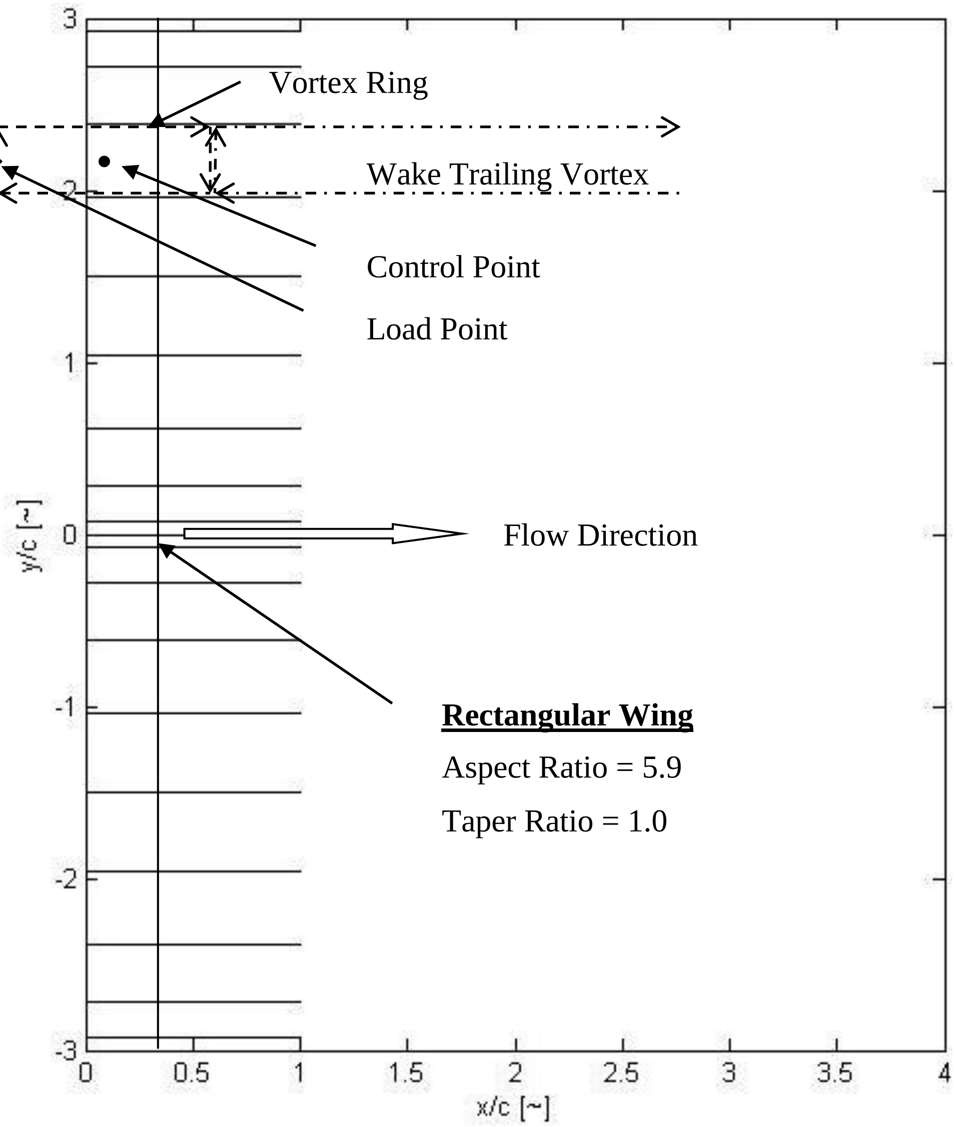

Figure 1. Discretization of the vortex ring method for rectangular wing (top view).

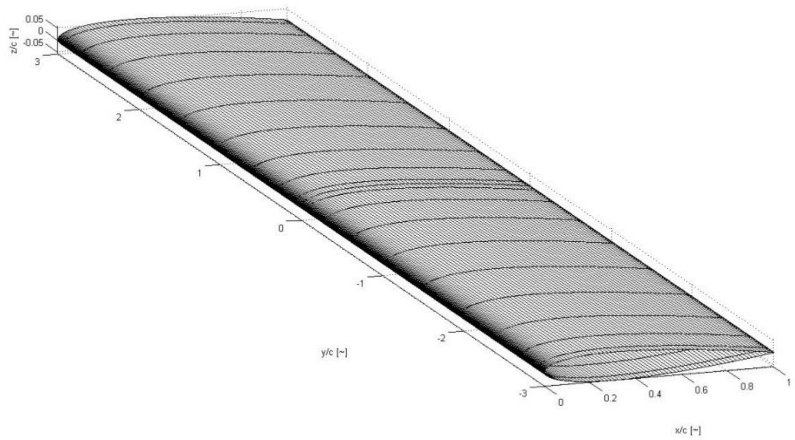

Figure 2. Two and three-dimensional descretization conjunction for a rectangular wing.

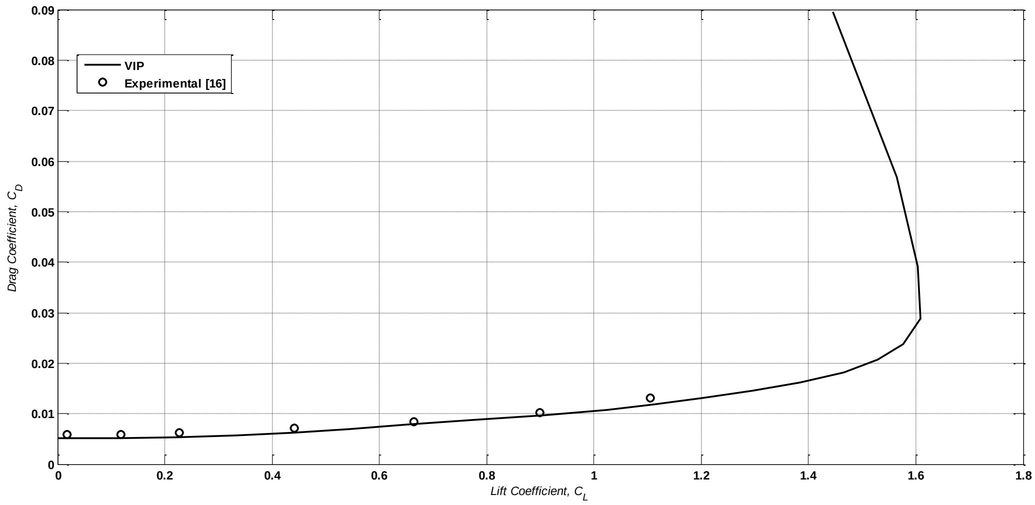

Figure 3. Two-dimensional lift coefficient for NACA 0012 airfoil at Re=3x10^6.

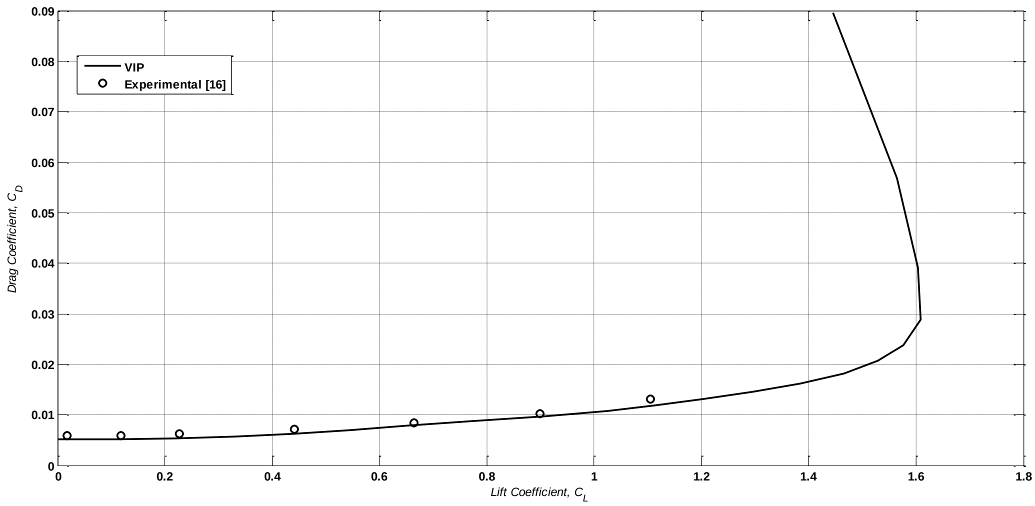

Figure 4. Two-dimensional drag coefficient for NACA 0012 airfoil at Re=3x10^6.

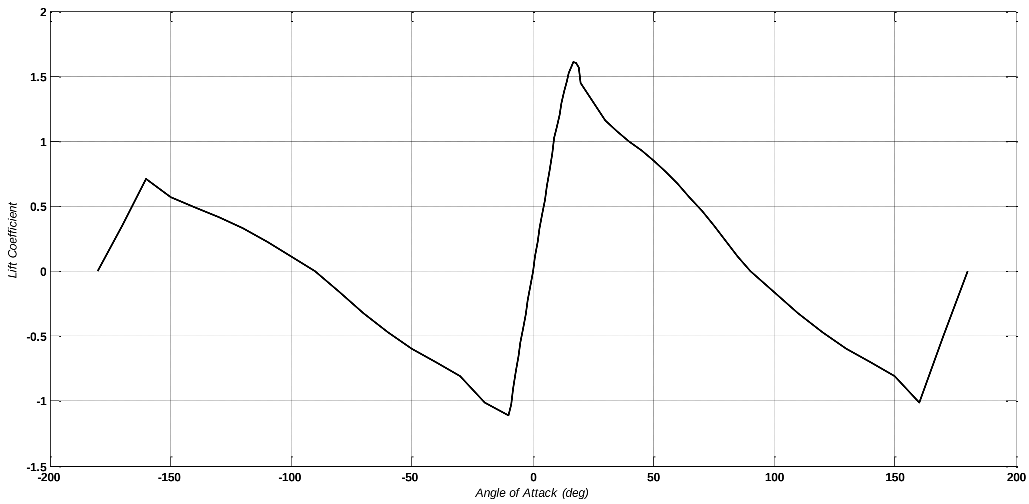

Figure 5. Viterna method to find lift coefficient of NACA 0012 airfoil at high AoA.

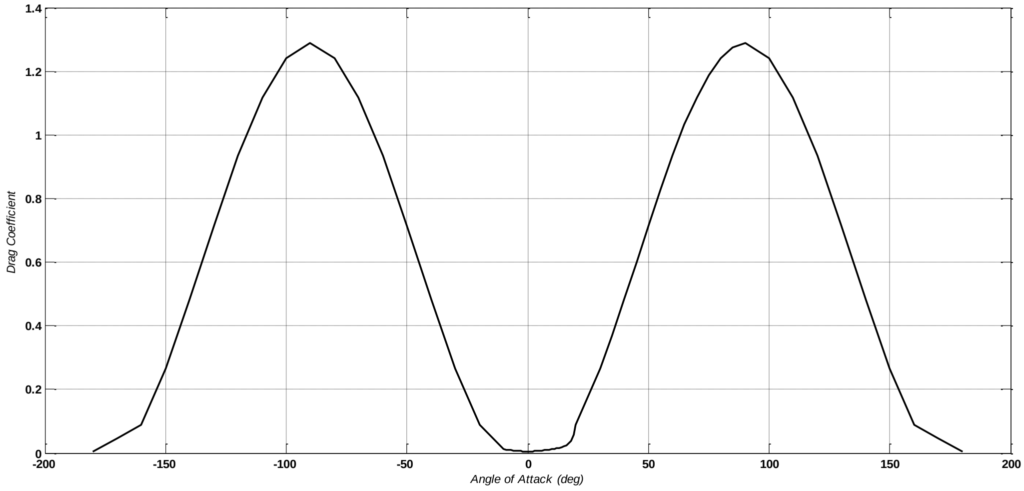

Figure 6. Viterna method to find lift coefficient of NACA 0012 airfoil at high AoA.

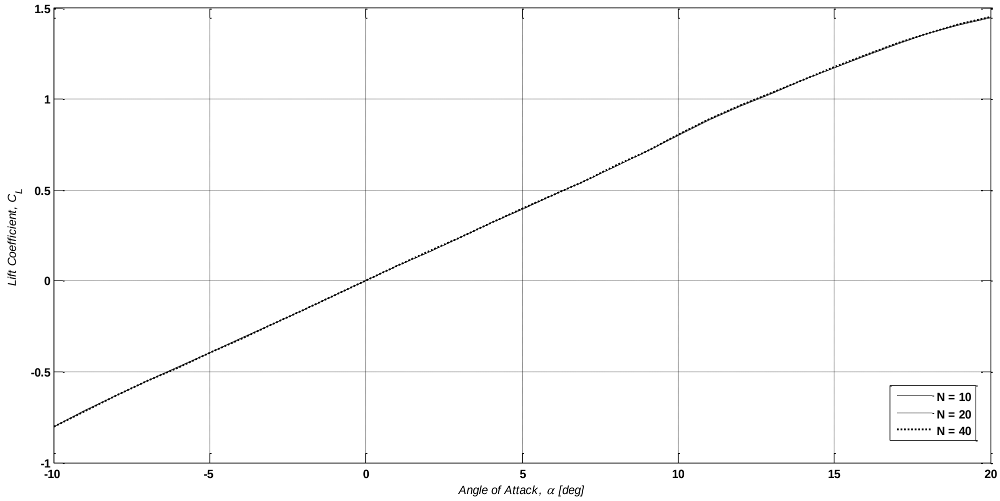

Figure 7. Lift coefficient of the wing affected by number of sections for Re=3x10^6.

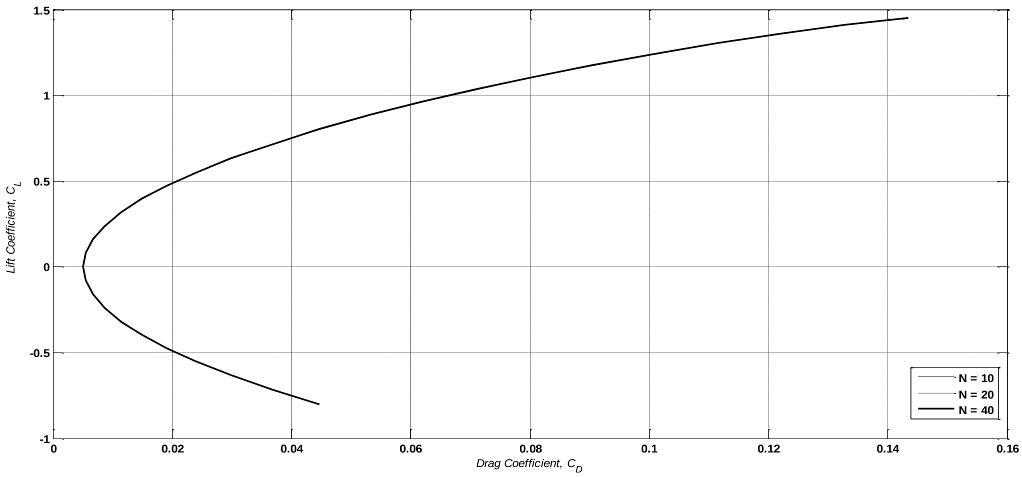

Figure 8. Lift coefficient of the wing affected by number of sections for Re=3x10^6.

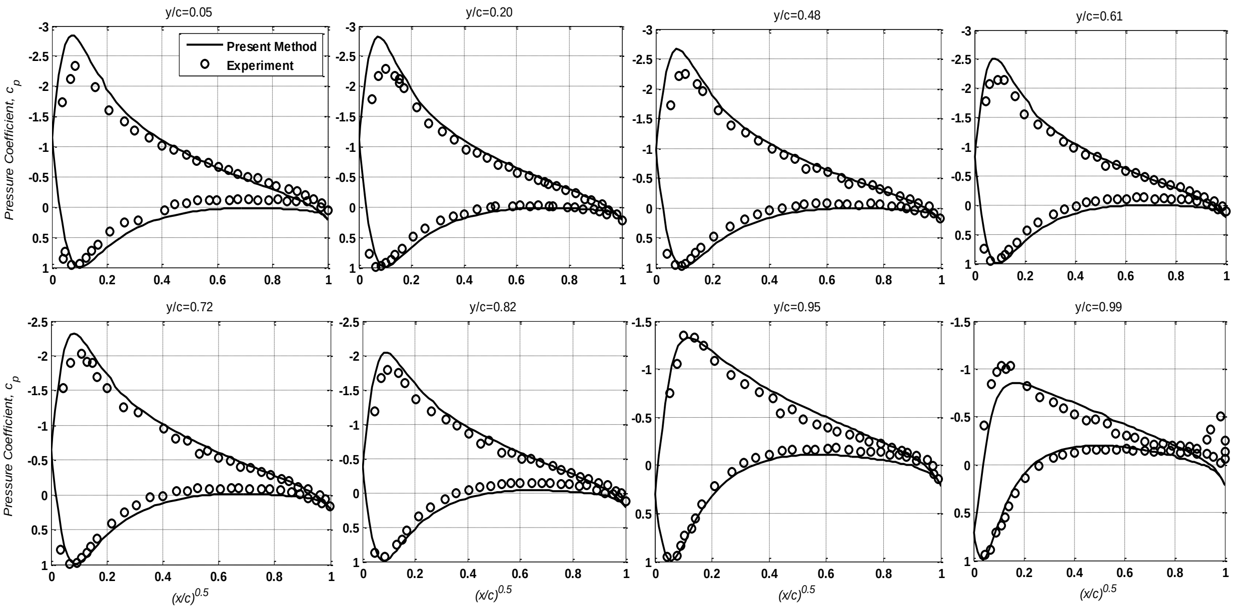

Figure 9. Pressure Distribution for different sections of the wing at α= 6.75^o and q_∞=2.87 kPa where – theory & o experiment.

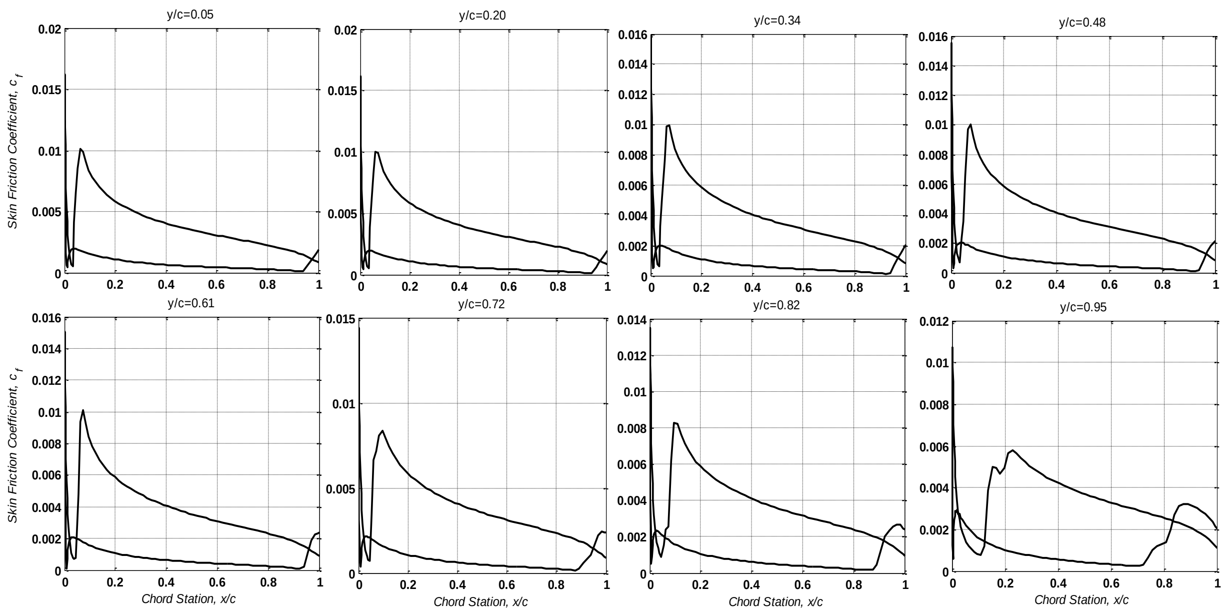

Figure 10. Frictional shear stress distribution for different sections of the wing at α= 6.75^o and q_∞=2.87 kPa where – theory & o experiment.

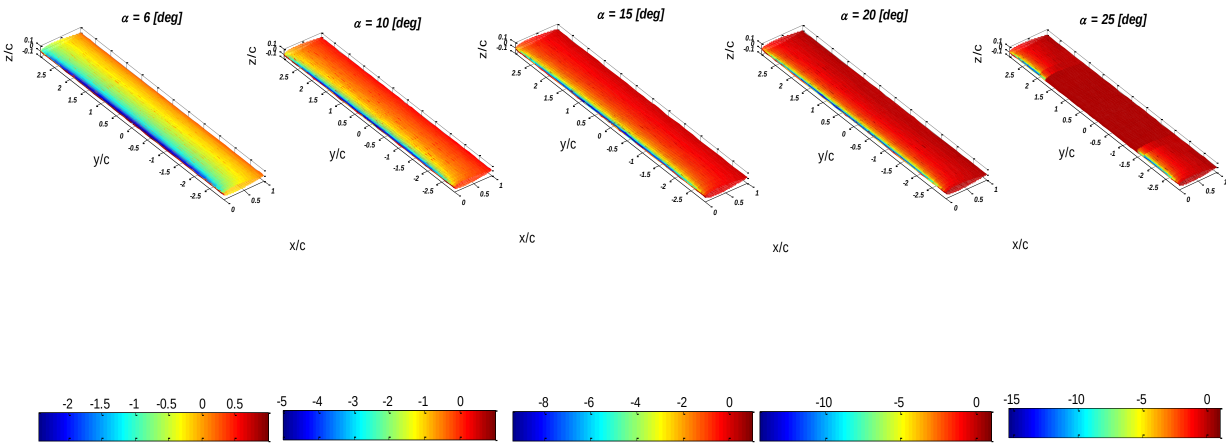

Figure 11. Wing surface pressure coefficient distribution at q_∞=2.87 kPa.

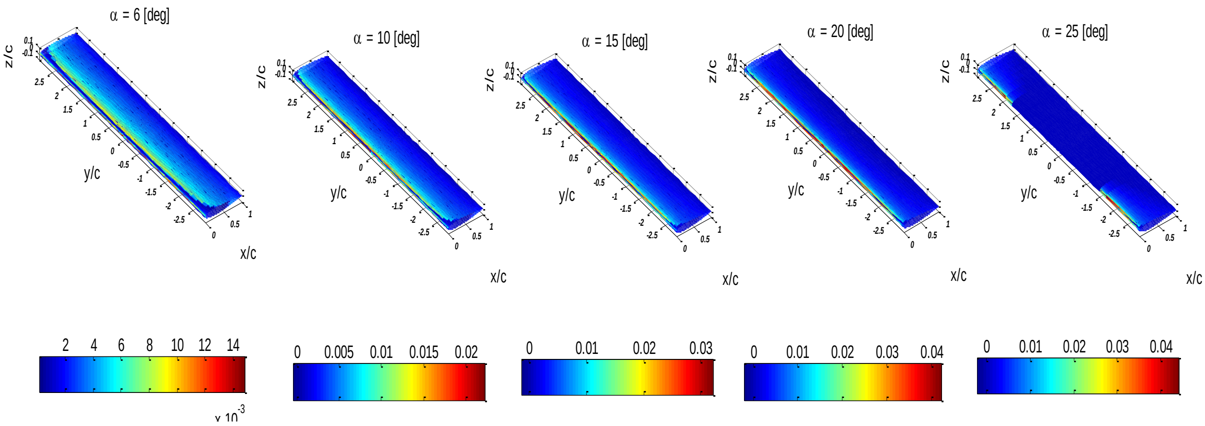

Figure 12. Wing skin friction coefficient distribution at q_∞=2.87 kPa.

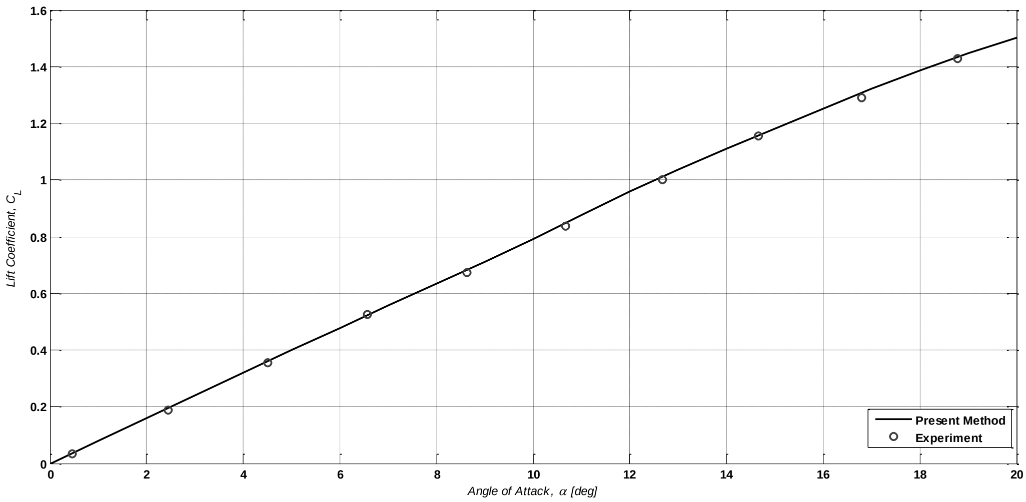

Figure 13. Lift coefficient for wing of NACA 0012 airfoil section at q_∞=2.87 kPa.

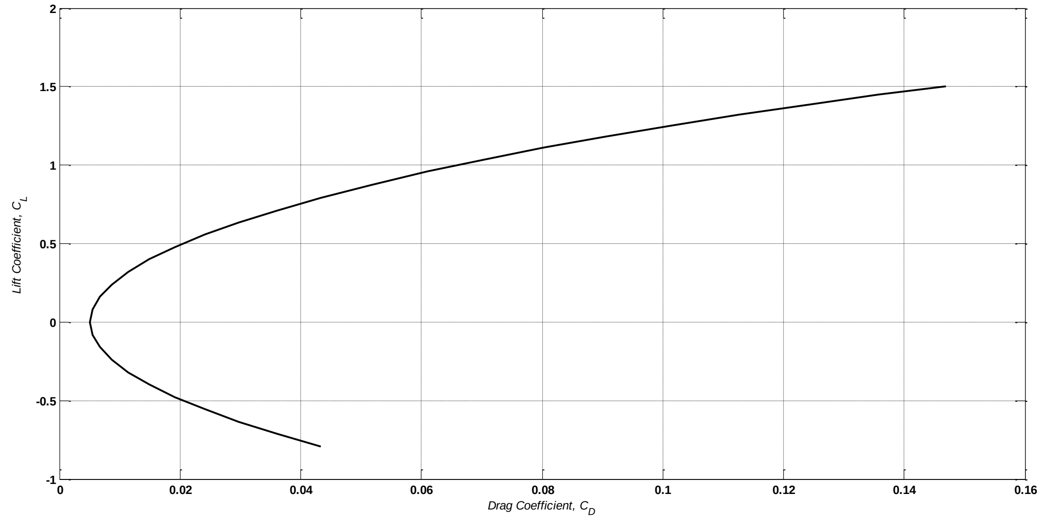

Figure 14. Drag polar for wing of NACA 0012 airfoil section at q_∞=2.87 kPa.

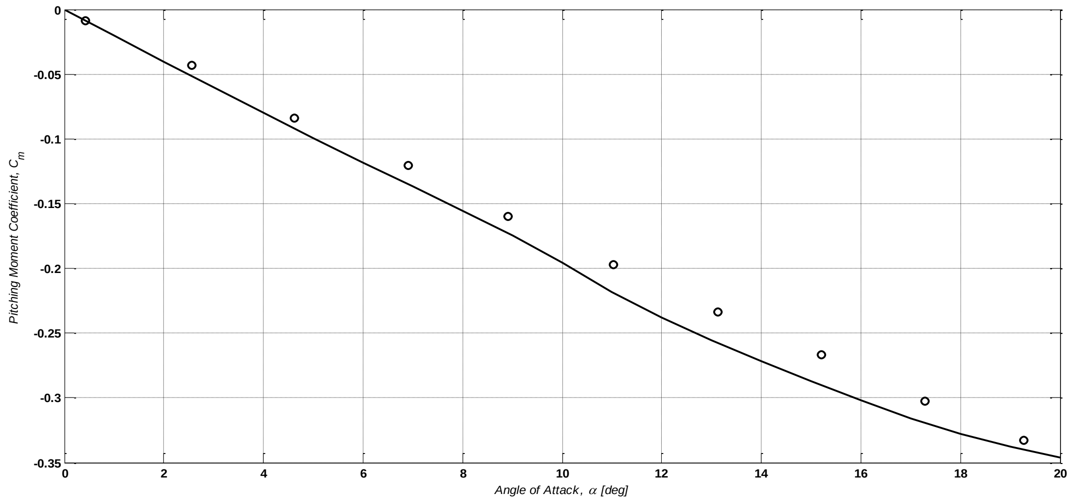

Figure 15. Pitching moment coefficient for wing of NACA 0012 airfoil section at q_∞=2.87 kPa.

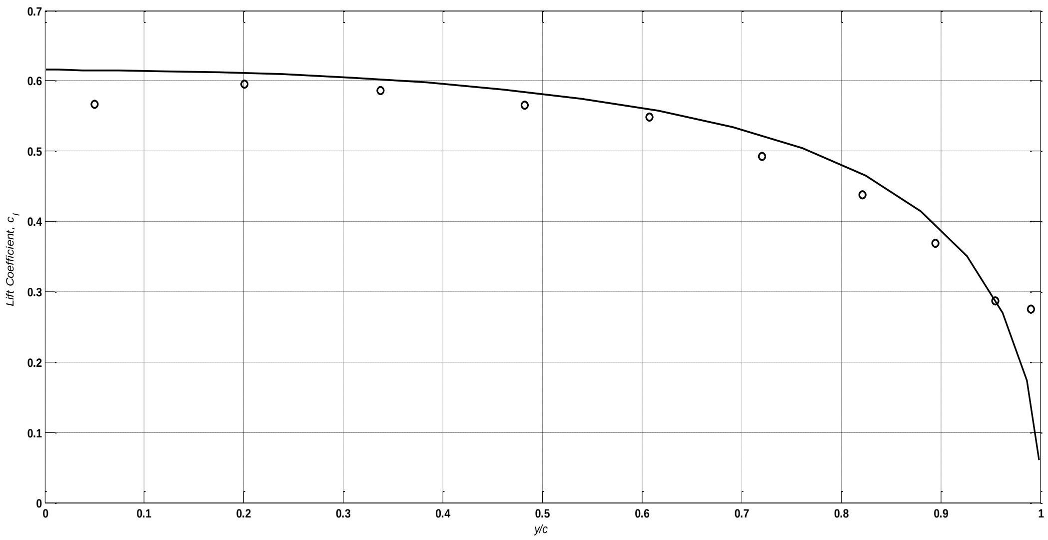

Figure 16. Span wise lift coefficient distribution of the wing at α= 6.75^o and q_∞=2.87 kPa.

Experimental Measurements of Viscosity and Thermal Conductivity of Single Layer Graphene Based DI-water Nanofluid

Prof. Dr. Najdat N. Abdulla
Department of Mechanical Engineering
University of Baghdad
E mail: najdat_abdulla@yahoo.co.uk

Hussein A. Ibrahim
Department of Mechanical Engineering
University of Baghdad
E mail: hussain1983ali@gmail.com

ABSTRACT

Experimental measurements of viscosity and thermal conductivity of single layer of graphene based DI-water nanofluid are performed as a function of concentrations (0.1-1wt%) and temperatures between (5 to 35ºC). The result reveals that the thermal conductivity of GNPs nanofluids was increased with increasing the nanoparticle weight fraction concentration and temperature, while the maximum enhancement was about 22% for concentration of 1 wt.% at 35ºC. These experimental results were compared with some theoretical models and a good agreement between Nan's model and the experimental results was observed. The viscosity of the graphene nanofluid displays Newtonian and Non-Newtonian behaviors with respect to nanoparticles concentration and temperature, and about 111% enhancement was obtained compared to the base fluid with GNPs weight fraction concentration of 1wt.% at 35ºC. Based on the experimental data, correlations were developed for predicting thermophysical properties of the GNPs based DI-water nanofluid.

Key words: Graphene, Nanofluid, Thermal conductivity, Viscosity, Experimental measurements

القياسات التجريبية للموصلية الحرارية واللزوجة لمائع نانوي احادي الطبقة (كرافين - ماء)

أ.د. نجدت نشأت عبدالله
قسم الهندسة الميكانيكية
جامعة بغداد

حسين علاوي ابراهيم
قسم الهندسة الميكانيكية
جامعة بغداد

الخلاصة

قياسات اللزوجة والموصلية الحرارية للمائع النانوي احادي الطبقه (كرافين- ماء) اجريت وفقا لكل من التراكيز 0.1- (1wt%) ودرجة حرارة (5 to 35ºC). اظهرت النتائج ان الموصلية الحرارية للمائع النانوي (كرافين- ماء) تزداد بزيادة تركيز الجزيئات النانوية للكرافين ودرجة حرارة المائع وكان الحد الأقصى للتعزيز حوالي 22% لتركيز (1% wt) في (35ºC).

هذه النتائج التجريبية قورنت مع بعض النماذج النظريه ورصد اتفاق جيد بين نموذج نان والنتائج التجريبية. اللزوجة للمائع النانوي (كرافين- ماء) يبدي سلوك نيوتيني وغير نيوتيني اعتمادا على تركيز الجزيئات النانوية ودرجة الحرارة، ونحو

%111زيادة مقارنه مع السائل الأساسي مع تركيز (1wt %) ودرجة حرارة 35ºC. استنادا إلى البيانات التجريبيه ، تم ايجاد علاقات ترابطيه للتنبوء بالخصائص الحراريه للمائع النانوي كرافين-ماء.

الكلمات الرئيسية: كرافين، مائع نانوي، الموصلية الحرارية، اللزوجة، القياسات العملية.

1. INTRODUCTION

Most heat transfer applications use conventional fluids like ethylene glycol (EG), DI-water and engine oil as heat transfer working fluids. The efficiency of these fluids is often limited by their low heat transfer capacities so the efficiency of the conventional fluids can be enhanced by improving the heat transfer properties and thermal conductivity. These heat transfer fluids have low thermal conductivity with respect to solid materials. Therefore, solid particles with high thermal conductivity are generally added to traditional heat transfer fluids to increase their thermal conductivity. However, the addition of micrometer or millimeter particles sized can cause problems as sedimentation and agglomeration. **Choi, 1995,** avoided these problems by introducing a new kind of heat transfer medium referred to nanofluid where the nanoparticles size less than (100 nm) are dispersed in base fluids like EG, water and oil.

The benefits of nanofluids technologies are expected to be large due to the heat transfer characteristic of cooling devices or heat exchangers in many applications. For example, the thermal transport industry requires minimizing the weight and size of thermal systems of vehicles and nanofluids can enhance thermal transport of lubricants and coolants. The nanoparticles when properly dispersed in base fluid, nanofluids can show many advantages besides the abnormal high effective thermal conductivity. These advantages involve, reduction in pumping power, improving heat transfer and stability, miniaturizing systems, micro channel cooling without clogging and savings cost and energy **Murshed, 2008**.

Many different nanoparticale materials are used for preparation nanofluids, such as metals (Cu, Al, Au, Fe and Ag), metal oxide (CuO, Al_2O_3, MgO), carbide ceramics (SiC, TiC), Semiconductors (SiO_2, TiO_2) and Carbon nanostructures as (graphite, diamond, carbon nanotube, graphene, graphene oxide). Carbon nanostructures materials are utilized due to their extremely high thermal conductivity (k) in the axial directions, low density and large surface area compared with metals or metal oxides materials.

Base fluids mostly used in the producing of nanofluid are the conventional fluid such as ethylene glycol, water and oil.

Recently, several investigations were devoted to study the thermal properties such as viscosity and thermal conductivity of the nanoparticles based nanofluid prepared from different carbonic structures, like single-wall, multiwall carbon nanotubes, graphite nanoparticles, and diamond nanoparticles, graphene oxide, graphene. Among all of these structural forms, single layer graphene is a 2-D material with one carbon atom thickness layer was discovered **by Novoselov** in **2004**. It has unique thermal characteristics due to large specific surface area and high thermal conductivity compared with other carbonic forms. However, according to literature, experimental and theoretical studies on the heat transfer thermal properties like viscosity and thermal conductivity of graphene based nanofluids are scarce.

Ramaprabhu, 2010, carried out experimental study on thermal, electrical conductivities and heat transfer characteristics for hydrogen exfoliated graphene nanosheets dispersed in DI-water and EG-based nanofluids for different temperatures and volume fractions. The results of 0.05% volume concentration of hydrogen exfoliated graphene dispersed in DI-water based nanofluid was shown an improvement in thermal conductivity of around, 75%, 16% at 50°C and 25°C respectively.

Xie, 2011, investigated experimentally the thermal conductivity of graphene EG-based nanofluid. The result of 5.0% volume fraction of graphene dispersion showed significant improvement in the thermal conductivity of nanofluid up to 86%. The stiffness and 2D structure of graphene oxide and graphene helped to enhance the thermal conductivity of the nanofluids. The results of thermal conductivities of graphene oxide and graphene EG-based nanofluid were around ~4.9 and 6.8 W/m K, respectively.

Rashidi, 2013, studied the thermal conductivity and stability behavior of graphene based water nanofluid. The Thermal conductivity of graphene versus temperature and time for various weight concentrations were determined. Alkaline method was utilized to functionalize without any additives or surfactant. This method was successfully dispersed of graphene in water. Results suggested that there was an augmentation in thermal conductivity by increasing temperature and graphene weight fraction concentration. The best result showed augmentation of thermal conductivity about 14.1% with 0.05 wt.% of alkaline functionalized Graphene (AFG) with respect to water at 25 °C and 17% at 50 °C.

Dey, 2013, prepared a well dispersed and stable fictionalized graphene (f-HEG) base (distilled water and ethylene glycol) nanofluids with volume concentration between 0.041 to 0.395%.

Measurements of viscosity and thermal conductivity were performed at different volume concentrations and temperature between 10 to 70 ºC. The results showed thermal conductivity enhancement about ~15% for a volume fraction of 0.395 vol.%. Viscosity of the nanofluids and base fluid showed non Newtonian behavior with the appearance of shear thinning and about 100% increment compared to the base fluid (ethylene glycol distilled water) with volume fraction of 0.395.%.

Rashidi, 2014, investigated the effects of graphene oxide (GO/water) nanofluid concentration and temperature on the thermal conductivity. Result indicated thermal conductivity of (GO/water) nanofluid higher than thermal conductivity of base fluid. Thermal conductivity depended strongly on the graphene oxide concentration and enhanced with increasing it. When the nanosheet weight fraction was 0.25wt.%, the enhancement ratio was 33.9% at 20°C and when the temperature increased up to 40°C the enhancement ratio up to 47.5%.

The aim of the present work is to measure experimentally viscosity and thermal conductivity of GNPs based DI-water nanofluid for various weight fraction concentrations and temperatures.

2. EXPERIMENTAL SET-UP

2.1 Viscosity Measurements

The viscosity of the GNPs based DI-water nanofluids at a different weight frictions concentrations (1, 0.9, 0.8, 0.7, 0.6, 0.5, 0.4, 0.3, 0.2 and 0.1wt%) were measured by using a rotational kind low viscosity DV-I prime digital model viscometer from (Laboratories of Brookfield Engineering Inc.) at convective heat transfer laboratory of Texas A&M University. The maximum torque rating for this model is 0.06737 m.N and a accuracy is ±1%.The viscometer was calibrated by using a Brookfield's viscosity standard test fluid. **Fig. 1** shows the DV-I prime viscometer.

A combination of cylindrical spindle and sample container referred as UL adapter was utilized for taking measurements at low viscosity. This type of spindle can be used to measure viscosities of both non Newtonian and Newtonian fluids. The viscous drag experienced by the spindle in UL adapter was manufactory calibrated to offer percentage of maximum torque and dynamic viscosity by using Eqs. (1) and (2). on a digital output screen. **Operating Instructions Manual, 2014.**

$$\dot{\gamma}=\frac{2R_c^2}{(R_c^2-R_{sp}^2)}\omega \quad (1)$$

$$\tau=\frac{M}{2\pi R_{sp}^2 L} \quad (2)$$

$$\mu=\frac{\tau}{\dot{\gamma}} \quad (3)$$

$$\omega=\frac{2\pi N}{60} \quad (4)$$

where R_c, R_{sp}, ω, M, L, μ, and N are radius of the sample container, radius of the spindle, angular speed of the spindle, torque input by the viscometer, effective length of the spindle, dynamic viscosity and rotational speed of the spindle, respectively as shown in **Fig. 2**.

Measurements are taken at different shear rates and temperatures range from (5, 10, 15, 20, 25, 30 and 35°C) and were repeated four times for each experiment to obtain accurate results.

The DV-I prime viscometer has been calibrated by using standard test fluid viscosity of (9.6cP) at temperature 25ºC which provided by the Laboratories of Brookfield Engineering Inc. Its precision was found to be +/- 0.6%.

2.2 Thermal Conductivity Measurements

Thermal conductivity is one of the most effective parameters which has important effect on augmentation of heat transfer coefficient. Thermal conductivity of GNPs based DI-water nanofluids with six various weight fraction concentrations (1, 0.8, 0.6, 0.4, 0.2, 0.1 wt%) at temperatures range from (5-35ºC) is measured by using a KD2 Pro instrument from (Decagon devices, Inc. USA). The measurements were taken under different temperature conditions by using a temperature-controlled container connected with chiller to maintain constant temperature of sample as shown in **Figs. 3** and **4**. These figures illustrate the experimental setup to measure thermal conductivity by using KD2 Pro instrument. The experimental set-up consists of: **1)** KD2 Pro microcontroller **2)** chiller **3)** probe needles 4**)** temperature-controlled path.

The instrument working is based on the fundament of a transient hot wire method and has accuracy of about 5%. A KD2 Pro consists of a sensor probe needles and handheld microcontroller. The sensor probe needle is of stainless steel 60mm length and 1.3mm diameter and includes both a thermistor and a heating element. The controller module includes a microcontroller of 16-bit /AD converter, a power control circuitry, and battery.

The measurements of thermal conductivities are based on the following assumptions: (i) the medium is both isotropic and homogeneous (ii) the long source of heat can be considered as an infinitely long heat source. Though these hypotheses are not correct in the strict sense, they are sufficient for precise measurements of thermal properties. This method is achieved by measuring the response of temperature/time of the probe to a sudden electrical pulse. Thermometer and heater are both used by probe at the same time. A derivation of temperature data and Fourier's law are used to estimate the thermal conductivity.

Thermal conductivity is estimated by controller at the end of the reading by change the temperature (ΔT) with the time as

$$k=\frac{q''(\ln t_2-\ln t_1)}{4\pi(\Delta T_2-\Delta T_1)} \tag{5}$$

whereΔT_1 and ΔT_2 are the changes in the temperature at t_1 and t_2 times respectively, q'' is the applied constant heat rate to a small and an infinitely long (line) source.

2.2.1 Working of KD2 Pro

A 30 second equilibration time for each measurement cycle, 30 second for cool and a 30 second for heat time were used. Measurements of temperature are made during 1 second intervals for cooling and heating. These measurements are then fit with functions of exponential integral utilized a nonlinear least squares procedure. During the measurement, the temperature of the sample changes to correct a linear drift term, to optimize the precision of the readings. A microprocessor and a thermo-resistor are used to measure and control the conduction in the probe. Before measurement, for ensuring the thermal equilibrium between nanofluid sample and sensor needle, the temperature of the samples was kept fixed for 30 min by using the temperature-controlled container. Five separate measurements were repeated and the average value of thermal conductivity was taken. The experiments were considered only when a mean value of data has square correlation coefficient (R^2) value more than 0.9995 **KD2 pro user guide, 2014**.

Different techniques were tried to improve the KD2 Pro instrument accuracy during the measurements of thermal conductivity of nanofluid and are as follows:

1) The needle probe is taken out and cleaned after each measurement to avoid the agglomeration and sedimentation of nanoparticles of graphene upon it.

2) The sensor needle probe was immersed fully into the nanofluid, oriented vertically by fixing it through thick plastic cover for the container and centrally inside the container to avoid touching with walls side of the container. This vertical orientation of the needle probe insertion through the nanofluid will reduce the errors from free convection. Because a slight inclination of the needle from its vertical position will produce a large error.

3) Several other precautions were taken such as avoiding vibrations during measurement by placing the instrument on an optical table and switching off the chiller during the measurement. The KD2 pro instrument has been calibrated by measuring thermal conductivity of glycerol and DI-water at 20ºC. The values of measuring glycerol and DI-water were 0.282 and 0.607 W/mK, which are in good agreement with the values from (**NIST, webbook**) of 0.285 and 0.598 W/mK, respectively, within ± 5% accuracy.

3. RESULTS AND DISCUSSION

3.1 Results of Viscosity

Viscosity of fluids is one of the most significant parameters, which estimates the heat transfer fluid quality. In the absence of any prior data on the viscosity of GNPs based DI-water nanofluids in the literature, it is most significant to confirm whether they show Newtonian or non-Newtonian behavior as a function of both weight fraction concentrations and temperature of nanofluid.

3.1.1 Effect of Shear Strain on Viscosity

The viscosity of DI- water and GNPs based DI-water has been examined with various weight fractions (0.1–1wt %) and temperatures range of (5–35)ºC. **Figs. 5 and 6** show the relationship between the viscosity and shear strain rate at temperature 5ºC and 35ºC, respectively. These figures show that the viscosity of the DI-water remains constant when the shear rate is increased. It is obviously that the DI-water displays a Newtonian behavior. Otherwise, the GNPs nanofluid displays Newtonian and Non-Newtonian behavior depends on the weight fraction concentration and temperature. From figures the viscosity of the GNPs based DI-water nanofluid for a concentration (0.1wt%) decreases with increasing the shear strain rate and this refers to the GNPs nanofluid behave as non-Newtonian fluid until reaches specific value of shear strain (80 s^{-1}). After this value the viscosity remains constant when the shear strain increases. That indicates the nanofluid works as Newtonian fluids. However, it is clear that the shear thinning (non-Newtonian) behavior become more prominent with increasing the GNPs weight fraction concentration and decreasing the temperature of nanofluid.

The reason of this shear thinning (non-Newtonian) behavior of GNPs based DI-water nanofluid can be clarified commonly as follows. When the spindle rotates in the fluid, at low shear rates, the structure of molecules fluid changes gradually and temporarily align themselves with the increasing of shear rates direction. It generates less resistance and that causes a lowering in viscosity of nanofluid. The amount of shear ordering attained maximum, when the shear strain is high, and that causes to break down the aggregates to small sizes, hence the viscosity of nanofluid is decreasing **Alvardo, 2009.** If the shear rate increases more, it will not make unchanged on the viscosity. Because of large surface area and small size of the nanoparticles and there is a possibility for structuring at low shear strain rates and a restriction and deformation at high value of shear strain rates.

3.1.2 Effect of the Temperature on the Viscosity

Fig.7, shows reduction in the viscosity of the DI-water and GNPs nanofluid when the temperature is increasing. This due to that, when the temperature is rising, that causes the weakening of the adhesion forces for inter-particles intermolecular and that reduces the average forces of intermolecular. Subsequently, the viscosity reduces when the temperature increases. This is noticed for the most kinds of nanofluids **Elias, 2014**. **Figs. 8 and 9** show the maximum increment in viscosity of GNPs based DI-water is 111% at 1 wt% weight concentration and temperature 35 ºC compared with base fluid.

The correlation is developed to calculate the viscosity of GNPs nanofluid depending on the experimental results with the limit of the temperature (5–35ºC) and weight fraction (0.1–1%) as shown in **Fig. 10**. It can be expressed as:

$$\mu_{nf} = (aT^2+bT+c) \tag{6}$$

where a, b, and c are the fitting parameter as shown in **Table 1**.

Unfortunately, theoretical formulations to predict the temperature dependence of viscosity of GNPs nanofluids are practically absent **Ijam, 2015.**

3.1.3 Effect of Concentration on Nanofluid Viscosity

The viscosity of the GNPs based DI-water nanofluid is examined with various weight fraction concentrations, as shown in **Fig. 11**. It shows the viscosity of GNPs increment with increasing the weight fraction concentration. This is because the large surface area of the GNPs nanoparticles in contact and increasing the base fluid molecules resistance with increasing the weight fraction of GNPs nanoparticles.

The experimental data were compared with theoretical models that are proposed by other authors at 25ºC temperature as shown in **Fig. 11**.

It can be seen from this figure that these theoretical models failed to calculate the viscosity of GNPs based water nanofluids. This may be due to variation in surface chemistry, morphology, shear rate and measurement technique, etc.

3.2 Results of Thermal Conductivity

Thermal conductivity of the GNPs nanofluids with various weight fraction concentrations and temperature ranging from (5 to 35°C) are shown in **Fig. 12**. It is clear from this figure that the thermal conductivity enhancement was obtained with increasing weight concentrations and temperature. **Fig. 13** shows the thermal conductivity enhancement ratio.

$$((k_{nf} - k_{bf}) / k_{bf})\times 100 \qquad (7)$$

where k_{bf} and k_{nf} were the thermal conductivities of base fluid and nanofluid, respectively.

The maximum enhancement ratio in thermal conductivity for 1 wt% of GNPs was 22% at 35 ºC and 10% for 0. 1 wt % concentration compared with base fluid.

The conventional theoretical models that have been developed to calculate nanofluids thermal conductivity, such as the Hamilton-Crosser model and the Maxwell model, considered only nanoparticles volume fraction and base fluid thermal conductivities, while particle shape, size, and motion and dispersed particles distribution do not show considerable effect on thermal conductivity improvement. Hence, the results of the experiments cannot be compared with the values correlated by these traditional theoretical models. These models showed weakness in estimating the thermal conductivities of nanofluids which drove to suggest different new mechanisms. Many researchers **Choi, 2003, Kole, 2013, and Mehrali, 2014** indicated the Brownian motion of nanoparticles as an important factor for figure out the improvement. Recently, widely accepted idea leads the presence of nanolayer at liquid–solid interface and nanoparticles aggregation of may frame the prime contributing mechanisms for improvement of thermal conductivities in nanofluid. The liquid molecules close to nanoparticles surfaces forms layered structures and conduct as a solid.

GNPs have the largest surface area compared with spherical and nanotube shape of nanoparticles based nanofluids because it has two-dimensional structures. This mean that the GNPs will have considerable larger contact area/interface with the molecules of base fluid. Hence the resistance of contact (Kapitza resistance) will be reduced for the GNPs nanofluid interface considerably and that will assist to enhance the effective thermal conductivity of the GNPs nanofluid. This illustrates why the thermal conductivity of GNPs nanofluid is high.

Researchers from various organizations completed a benchmark research on the thermal conductivity of GNP nanofluids, and the data referred that the results of experiments were in better agreement with Nan's model. Accordingly to **Nan's model,1997**, the GNPs nanofluid thermal conductivity can be estimated as below:

$$k_{nf}=k_{bf}\frac{3+\varphi v[2\beta_{11}(1\text{-}L_{11})+\beta_{33}(1\text{-}L_{33})]}{3\text{-}\varphi v(2\beta_{11}L_{11}+\beta_{33}L_{33})} \tag{8}$$

where φv and L_{ii} are the volume fraction and the geometrical factor of nanoparticles, respectively. β_{ii} is defined as

$$\beta_{ii}=\frac{k_p-k_{bf}}{k_{bf}-L_{ii}(k_p-k_{bf})}$$

where k_{bf}, k_p are the thermal conductivities of base fluid and nanoparticles respectively. The aspect ratio of GNPs is very high, therefore $L_{11}=0$ and $L_{33}=1$. Thermal conductivity estimated by Nan's model took into account the matrix additive interface contact resistance. The predicted thermal conductivity of composite in Eqs. (8), is very sensitive to the change in the nanoparticles thermal conductivity of. Furthermore, the theoretical estimation confirmed that the graphene thermal conductivity of can be affected by the dimensions of nanoparticles, defect density and edge roughness. **Fig. 14** displays the thermal conductivity of GNPs nanofluid improvement at temperature of 30°C and as a function of weight fraction concentration. The results indicate that, data can be obtained by using Nan's model to predict thermal conductivity with a good accuracy.

The correlation is developed to estimate the GNPs based DI-water nanofluid thermal conductivity based on the experimental result with the limitation of the weight concentrations range of (0.1–1)% and temperature range of (5–35)ºC as shown in **Fig. 15**. It can be expressed as the following equation:

$$k= (a\,T^2+ bT + c) \tag{9}$$

where a, b, and c are the fitting parameter as given in **Table 2**.

4. COMPARISON WITH PUBLISHED WORK

The comparison of the present experimental results of GNPs based DI-water nanofluid with the published work, of **Mehrali, 2014** and **Mehrali, 2015**, are shown in **Fig. 16** for thermal conductivity and **Fig. 17** for viscosity. These comparisons show a reasonable agreement with an error not exceeding 11%, 13% and respectively.

5. CONCLUSIONS

The thermophysical properties like thermal conductivity and viscosity of the suspensions of GNPs based DI-water nanofluid were examined for different weight fraction concentrations and temperatures. From this study it can be concluded that:

1. The thermal conductivity is increased with increasing the temperature of the GNPs nanofluid and nanoparticles weight concentrations, and maximum enhancement in thermal conductivity was around 11.9% to 22.2% with concentration of (φ_m=1wt%) and temperature range from 5 to 35ºC.
2. The GNPs based DI-water nanofluid displayed a Newtonian and non- Newtonian behavior with respect to nanoparticles concentration and temperature. The viscosity of the nanofluid decreased with increasing the temperatures, and their increment was 80−111% compared with DI-water when the temperature increased from 5 to 35 ºC.

3. The traditional models were not able to predict the viscosity and thermal conductivity of the GNPs based DI-water nanofluid. Therefore, correlations were suggested to evaluate the thermophysical properties based on the experimental results.

REFERENCE

- Brookfield Engineering Labs Inc., 2014," *Model DV-I PRIME Operating Instructions* "Manual No. M/07-022.
- Brookfield Engineering Labs, Inc., 2005, "*More Solutions to Sticky Problems*".
- Batchelor G.K., 1977,"*The effect of Brownian motion on the bulk stress in a suspension of spherical particles*", J. Fluid Mech. Vol.83, P.97–117.
- Brinkman H.C., 1952,"*The viscosity of concentrated suspensions and solutions*", J. Chem. Phys. Vol.20, P.571.
- Choi S., and Eastman A., 1995,"*Enhancing thermal conductivity of fluid with nanoparticles*", in: D.A. Siginer, Developments and Applications of Non-Newtonian Flows, Vol.66, PP.99–105.
- Dey T. K. and Kole M., 2013,"*Investigation of thermal conductivity, viscosity, and electrical conductivity of graphene based nanofluids*" Journal Of Applied Physics,Vol.113, PP.084307-1.
- Einstein A., 1956,"*Investigations on the Theory of the Brownian Movement*", Courier Dover Publications.
- Elias M., Mahbubul I., Saidur R. and Sohel M., 2014,"*Experimental investigation on the thermophysical properties of Al2O3 nanoparticles suspended in car radiator coolant*" International communications in Heat Mass Transfer Vol.54, PP.48–53.
- Ijam A., Saidur R., Ganesan P. andGolsheikh A., 2015,"*Stability, thermo-physical properties, and electrical conductivity of graphene oxide deionized water/ethylene glycol based nanofluid*", International Journal of Heat and Mass Transfer, Vol.87, PP.92–103.
- Murshed S.M.S, and Yang C., 2008,"*Thermophysical and electrokinetic properties of nanofluids*" – A critical review, Vol.28, PP.2109-2125.
- Mehrali M., Sadeghinezhad E., Latibari S., Kazi1 S., 2014,"*Investigation of thermal conductivity and rheological properties of nanofluids containing graphene nanoplatelets*", Nanoscale Research Letters, 9:15.
- Mehrali M., Sadeghinezhad E. and Rosenc A., 2015, "*Heat transfer and entropy generation for laminar forced convection flow of graphene nanoplatelets nanofluids in a horizontal tube*", International Communications in Heat and Mass Transfer Vol.66, PP.23–31.
- National institute of standards and technology (NIST), 2015. http://webbook.nist.gov/chemistry/fluid

- Nan Ce-Wen and Birringer R., 1997,"*Effective thermal conductivity of particulate composites with interfacial thermal resistance*", Journal of Applied Physics, Vol.81 PP.6692-6699.
- Novoselov K., Geim A., Morozov S., Dubonos S. and Firsov A., 2004,"*Electric field effect in atomically thin carbon films*", Science Vol.306, PP. 666.
- Ramaprabhu S.and Baby T., 2010,"*Investigation of thermal and electrical conductivity of graphene based nanofluids*", Journal oF Applied Physics Vol.108, PP.124308.
- Rashidi A., M.Ghozatloo A. and Shariaty-Niasar M., 2013,"*Preparation of nanofluids from functionalized Graphene by new alkaline method and study on the thermal conductivity and stability*" International Communications in Heat and Mass Transfer Vol.42, PP.89–94.
- Rashidi A., Hajjar Z., and Ghozatloo A., 2014,"*Enhanced thermal conductivities of graphene oxide nanofluids*" International Communications in Heat and Mass Transfer Vol.57, PP.128–131.
- Wang X., Xu X. and ChoiS., 1999,"*Thermal conductivity of nanoparticle-fluid mixture*", J. Thermophys. Heat Transfer Vol.13, P.474–480.
- Yu W., Xie H., , Wang X., Wang X.,2011,"*Significant thermal conductivity enhancement for nanofluids containing graphene nanosheets*", Physics Letters A Vol.375, PP.1323-1328.

NOMENCLATURE

AFG alkaline functionalized Graphene

EG ethylene glycol

f-HEG fictionalized graphene

GO graphene oxide

GNPs single layer Graphene

NIST National Institute of Standards and Technology

$\dot{\gamma}$=shear strain, N/m^2.

τ=shear stress, N/m^2.

M=torque input by the viscometer, N/m^2.

μ=dynamic viscosity, kg/m.s.

μ_{nf}=dynamic viscosity of nanofluid, kg/m.s.

μ_{bf} =dynamic viscosity of base fluid, kg/m.s.

ω=angular speed of the spindle

R_c=radius of the sample container, m

R_{sp}=radius of the spindle,m

N=rotational speed of the spindle

L=effective length of the spindle,m

k=Thermal conductivity, W/m.K

k_p=Thermal conductivity of particle, W/m.K

k_{bf}=Thermal conductivity of base fluid, W/m.K

k_{nf} =Thermal conductivity of nanofluid, W/m.K

q''= heat flux,W/m^2

T=temperature, ˚C.

t =time, second.

L_{ii}=geometrical factor, dimensionless

φv=particle volume faction, dimensionless

φm=mass fraction of the particles, dimensionless

ρ_p=density of the nanoparticle, kg/m^3.
ρ_b=density of base fluid, kg/m^3.

Table 1. Values of factors for viscosity of GNPs nanofluid.

φ_m	a	b	c	R^2
0 wt%	0.00052	-0.04695	1.73063	0.9993
1 wt%	0.00047	-0.05921	3.01429	0.9977
0.9 wt%	0.00052	-0.05995	2.88714	0.9988
0.8 wt%	0.00059	-0.06348	2.79571	0.9993
0.7 wt%	0.00066	-0.0654	2.70429	0.9989
0.6 wt%	0.00086	-0.07298	2.65571	0.9978
0.5 wt%	0.00083	-0.06683	2.41857	0.9982
0.4 wt%	0.00045	-0.0479	2.14429	0.9989
0.3 wt%	0.0005	-0.04795	2.02857	0.9992
0.2 wt%	0.00047	-0.0462	1.93071	0.9989
0.1 wt%	0.0062	-0.05048	1.87143	0.9973

Table 2. Values of factors for thermal conductivity of GNPs nanofluid.

φ_m	a	b	c	R^2
0 wt%	0.00001	0.001757	0.5628	0.9985
1 wt%	0.00006	0.00173	0.6294	0.9983
0.8 wt%	0.00005	0.00177	0.6198	0.9964
0.6 wt%	0.00005	0.00145	0.6168	0.9901
0.4 wt%	0.00005	0.00106	0.6151	0.9812
0.2 wt%	0.00007	0.00022	0.614	0.995
0.1 wt%	0.00005	0.000829	0.592	0.9939

Figure 1. Brookfield DV-I Prime Viscometer.

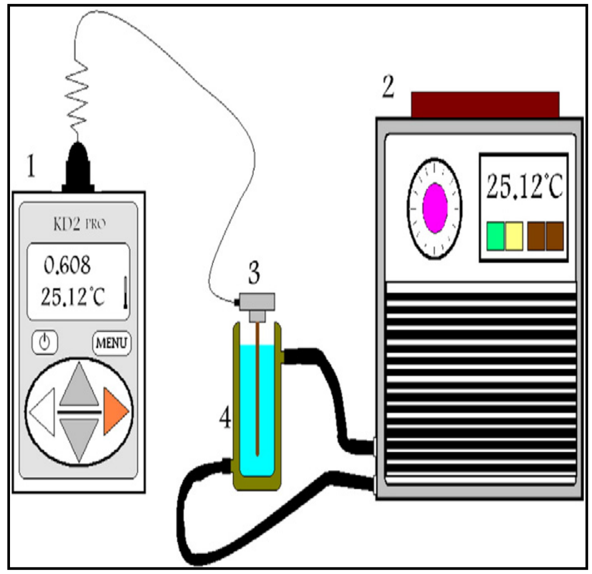

Figure 2. Scheme of experimental set-up to measure thermal conductivity.

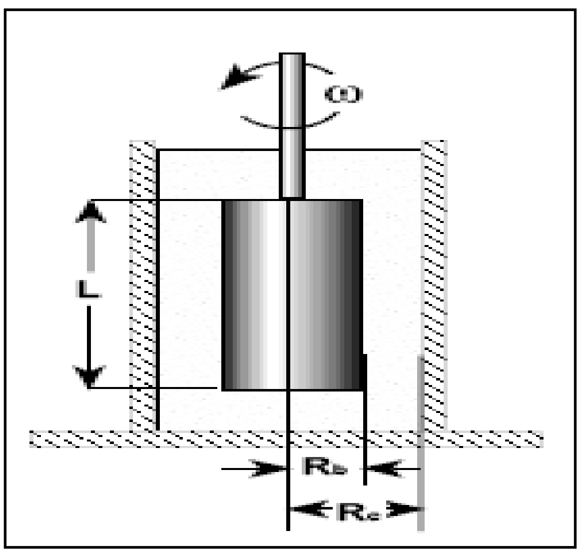

Figure 3. Diagram to explain the dimension parameters.

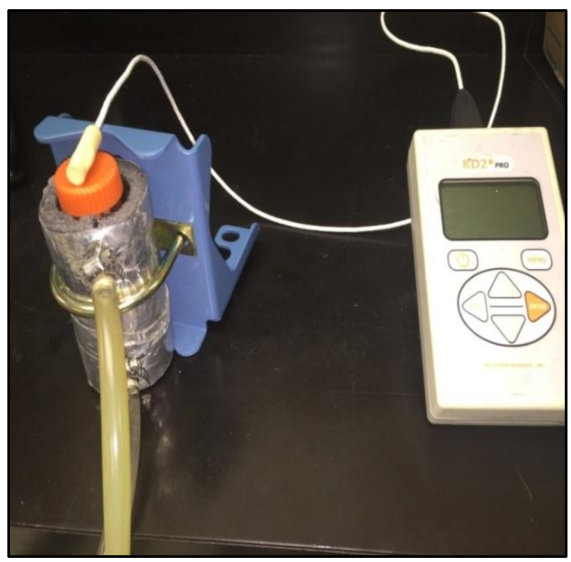

Figure 4. Set-up of experiment to measure thermal conductivity.

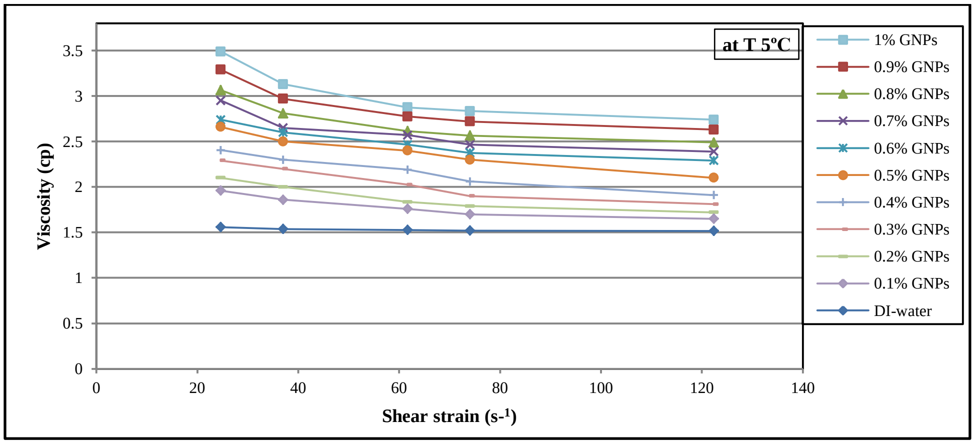

Figure 5. Effect of shear rate on viscosity of GNPs nanofluid with different weight concentrations.

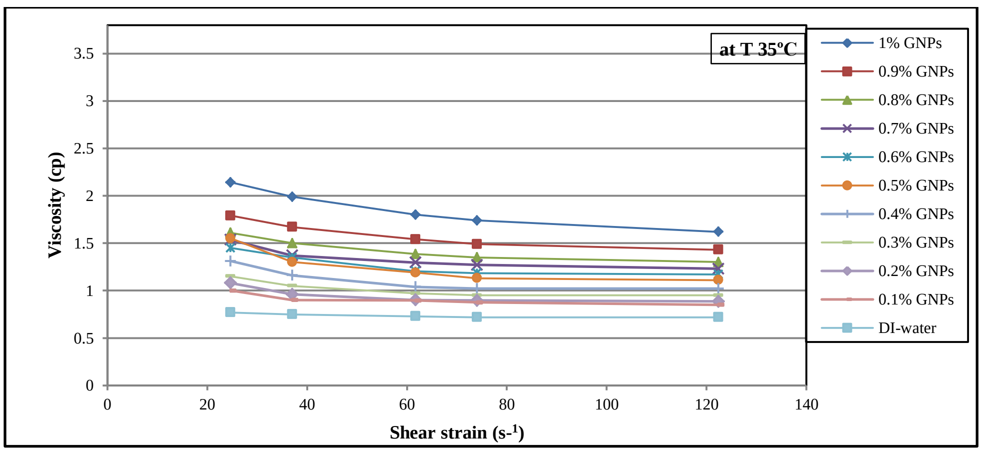

Figure 6. Effect of shear rate on viscosity of GNPs nanofluid with different weight concentrations.

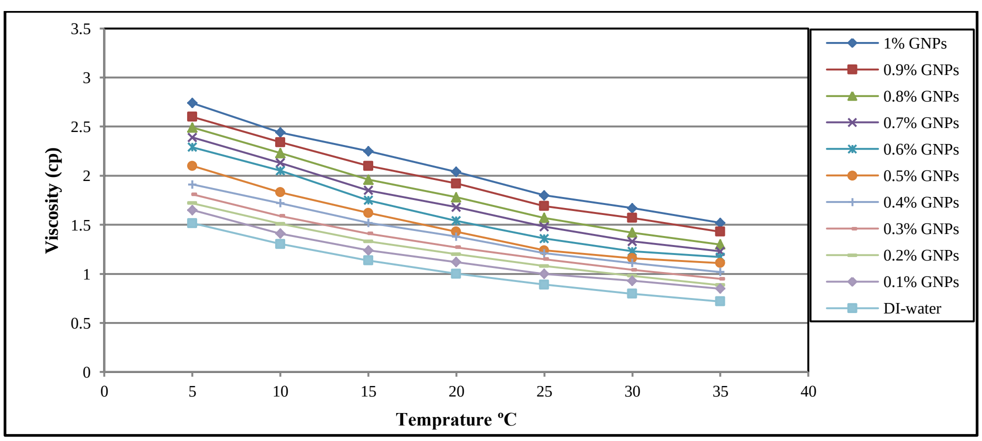

Figure 7. Effect of temperature on viscosity of GNPs nanofluid with different weight concentrations.

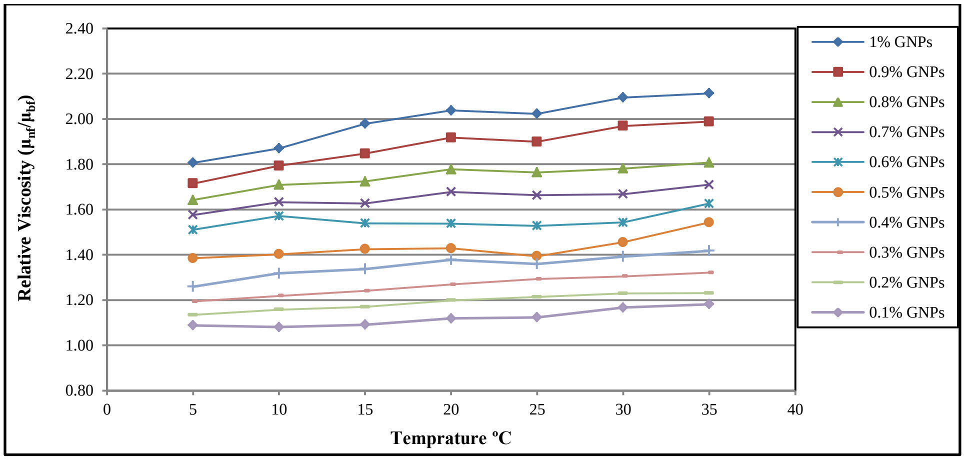

Figure 8. Effect of temperature on relative viscosity of GNPs nanofluid with different weight concentrations.

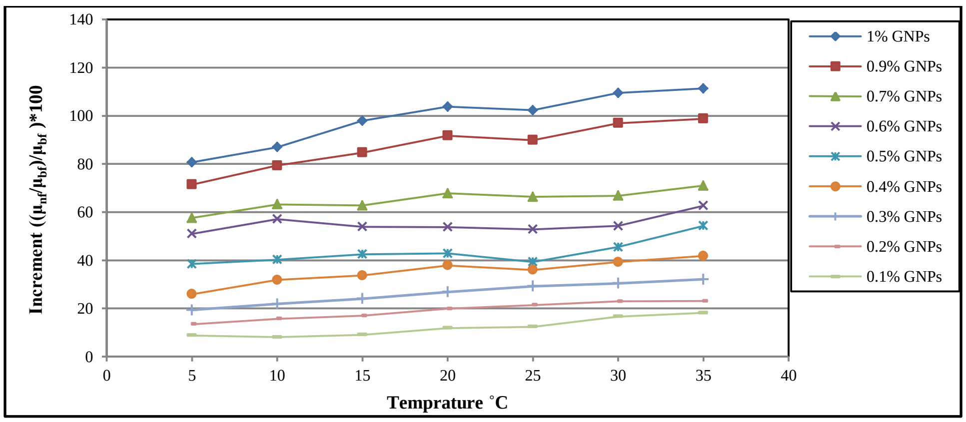

Figure 9. Effect temperature on increment of viscosity of GNPs nanofluid at different concentrations.

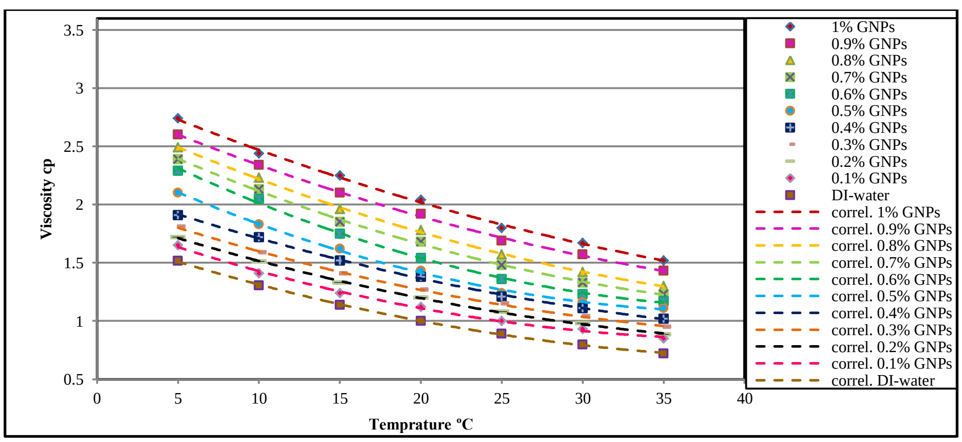

Figure 10. Correlation of experimental results of viscosity for GNPs nanofluid at different temperatures and concentrations.

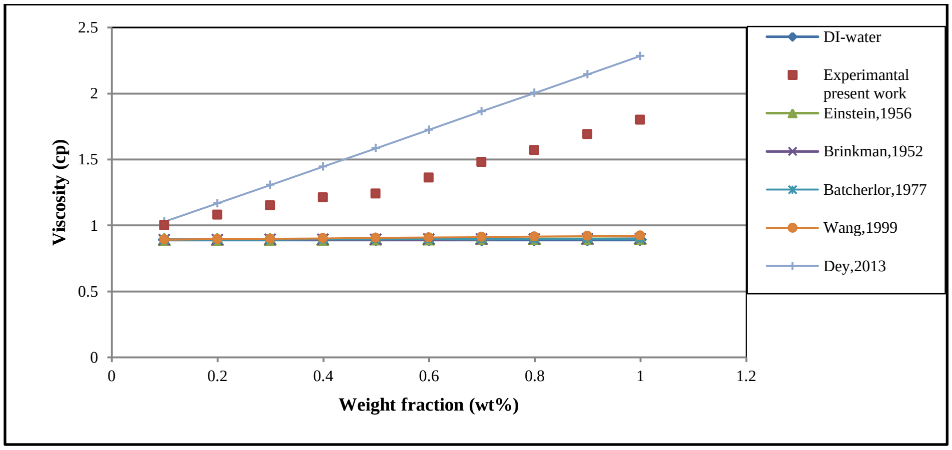

Figure 11. Effect of weight fraction concentration on viscosity of GNPs nanofluid at (35ºC) with other references.

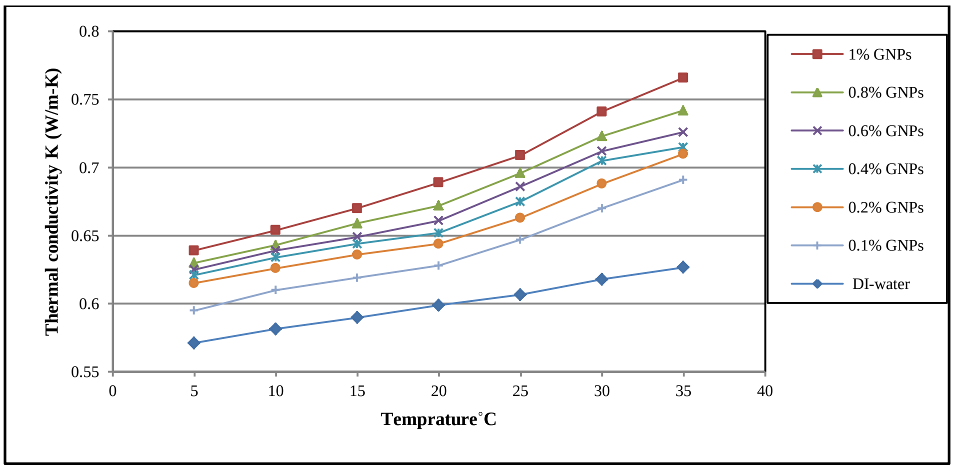

Figure 12. Effect of temperature on thermal conductivity of GNPs with different weight concentrations.

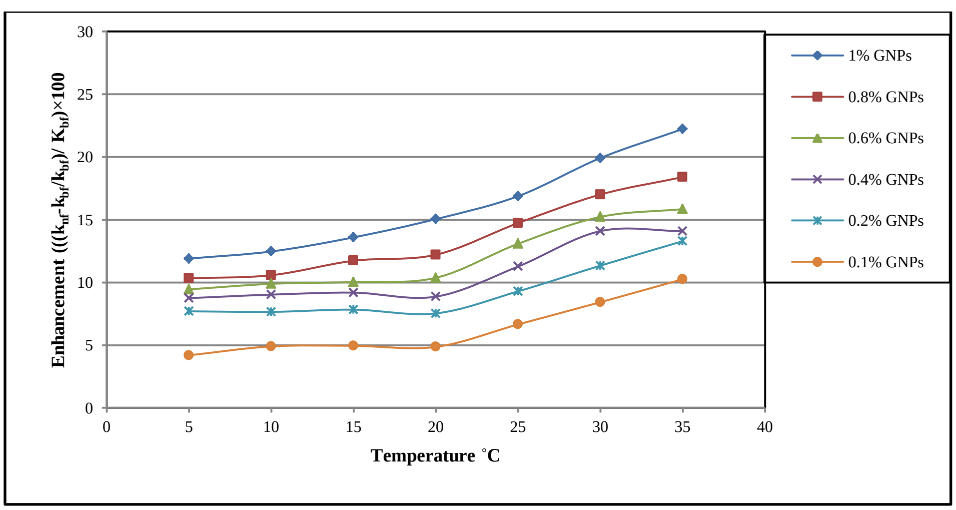

Figure 13. Effect of temperature on thermal conductivity enhancement percentage compared with DI-water.

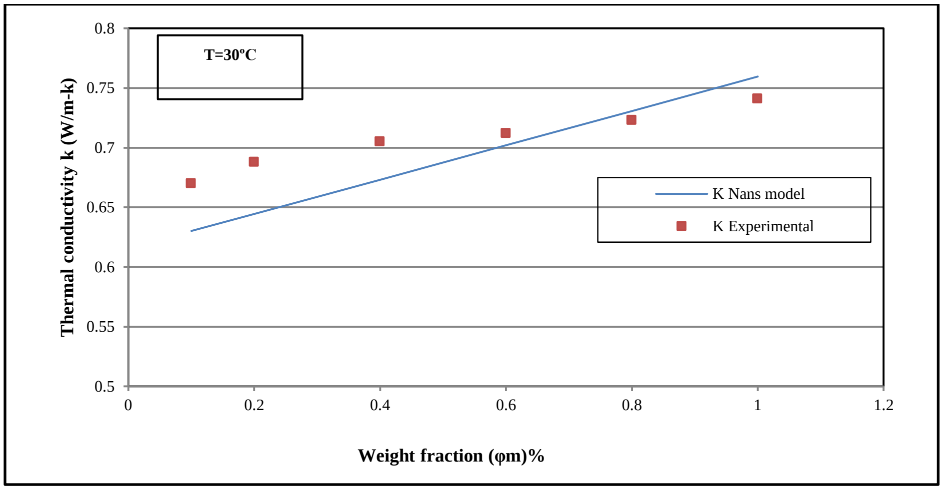

Figure 14. Comparison of experimental thermal conductivity results of GNPs nanofluid with Nan's model.

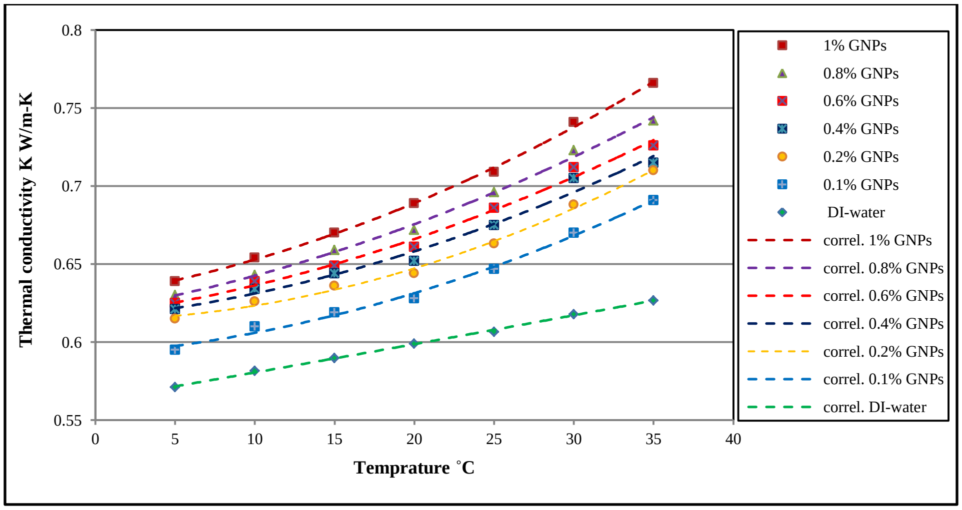

Figures 15. Correlation of experimental results of thermal conductivity for GNPs nanofluid at different temperatures and concentrations.

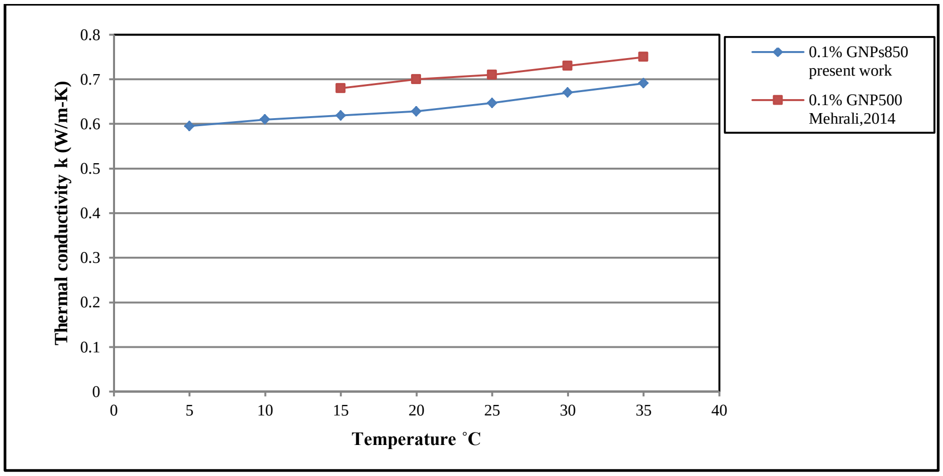

Figure 16. Comparison of experimental results of thermal conductivity for present work with the published data of **Mehrali, 2014**.

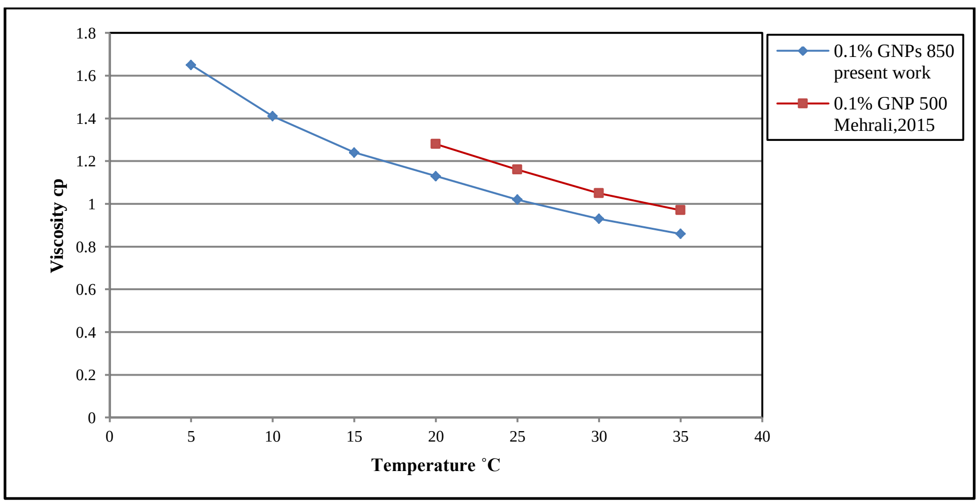

Figure 17. Comparison of experimental results of viscosity for present work with the published data of **Mehrali, 2014**.

Openness and the Degree of Impact on Engagement Learner
Department of Architecture Case Study

Dr.Asmaa M.H Al-Muqaram
Assistant Professor
University of Technology /Baghdad
E-mail: asmaamh1@yahoo.com

Riyam Rajab Fanjan Al-Amara
Instructer
University of Technology /Baghdad
E-mail: riyam.r8785@yahoo.com.au

ABSTRACT

This paper concerns with openness concept in contemporary learning environment, which ranges from physical characters to its relation with learning efficiency and its output**.** Previous literatures differ to clear the effect of openness on the engagement between learner within themselves, and with this kind of spaces. Engagement means: active participation, the ability of making dialogue, self-reflection and the ability to explore and communicate with them and within learning space. Research roblem was: The lack of knowledge about the effect of Openness on learner engagement with learning spaces. The two concepts were applied on three types of learning spaces in the Department of the Architecture in the University of Technology, according to their measurements. The research found that there are two types of engagment, positive and negative, that effect of openness in learning space, as increasing of the openness in learning space as more of the positive engagement of the learner, offset by a decrease in the negative engagement which cause conditions of the boredom and loss of concentration and scattering the learner mind - within this kind of space.

Key words: Openness, engagement, learning space, learning environment.

الانفتاحيــة ودرجة تأثيرها على أندماجية المتعلم ضمن فضاء التعلم
أقسام هندسة العمارة كحالة دراسية

أسماء محمد حسين عبد الرزاق المقرم
أستاذ مساعد
الجامعة التكنلوجية/قسم الهندسة المعمارية

ريام رجب فنجان الامارة
باحثة – طالبة ماجستير
الجامعة التكنلوجية/قسم الهندسة المعمارية

ارتبطت خاصية الانفتاحية بفضاءت التعلم المعاصرة . مرة بارتباطها بالجوانب الفيزيائية ومرة بعلاقتها بكفاءة التعلم وتحسين مخرجاته. تباينت المعرفة السابقة في طرح علاقاتها بتفاعل وسلوك واندماجية المتعلمين ضمن هذه الفضاءات ، والتي تعني المشاركة الفعالة للمتعلم،والقابلية على النقاش والحوارية، والتفكير الذاتي والقدرة على الاستكشافية للمعلومات والتواصل معها ضمن فضاء التعلم. بهذا الجانب تركزت مشكلة البحث في" **غياب التصور الكافي عن تأثير انفتاحية فضاءات البيئة التعليمية على درجة أندماجية المتعلمين ضمن هذة البيئات وتفاعلهم مع بعضهم البعض**" . تم تحديد اسلوب القياس وطريقته وطُبق على ثلاثة انماط مختلفة من فضاءات التعلم ضمن قسم العماره–الجامعة التكنلوجية. توصل البحث الى وجود نوعين من الاندماجية:أيجابيه وسلبية تقابل الانفتاحية المادية في للفضاء التعليمي، اذ تزداد لاندماجية الايجابية المتعلم بزيادة الانفتاحية بالفضاء التعليمي، يقابله تناقص في الاندماج السلبي المتمثل بحالة الملل وفقدان التركيز وتشتت ذهن المتعلم ضمن الفضاء.

الكلمات المفتاحية:الانفتاحية ، الاندماجية ، فضاء التعلم ،بيئة التعلم

1- المقدمـــــــــــة

تهتم التوجهات المعاصرة بكيفية تحقيق الانفتاحية العالية في الفضاءات، بما يخدم المناهج التعليمية المعاصرة القائمة على كيفية جعل التعلم متمحورا حول المتعلم وليس حول المعلم، من خلال تحقيق فضاءات ذات أتصالية وتواصلية عالية مع الفضاءات التعليمية الاخرى ضمن المبنى التعليمي، مع الابتعاد عن النماذج التقليدية التي قد تحد من درجه تفاعلية الطالب ومدى تقلبه للمعلومات، لكي يصبح هو المسؤول والمتحكم في عملية التعلم تلك بمساعدة الكادر التدريسي.

يحاول هذا البحث تسليط الضوء على تلك الخاصية من الناحية المادية للفضاء التعليمي وكيفية التي يؤثر بها على مدى أندماج ومشاركة المتعلم في عملية التعلم، وتقبلة للمعلومات ، وكيف يمكن لخاصية الانفتاح المادي في الفضاء أن تؤثر على تلك النواحي النفسية والاجتماعية للمتعلم.

2- مفهوم البيئات التعليمية

عُرفت البيئة التعليمية بأنها "ذلك المكان الذي يقوم على تقديم الخدمات التربوية والتعليمية للمتعلمين وفق أهداف محددة"،كما عرفت على أنها "تمثل الجوانب المادية والمعنوية التي تحقق التشاركية لأفرادها داخل منظومة معينة" http://tec-edu8.blogspot.com. بدأت بيئات التعلم بالتغير مؤخرا ردا على المواقف الاجتماعية الحالية من مجموعات من الفصول الدراسية المعزولة إلى بيئات التعلم والمعلومات المفتوحة، إذ ساعدت تكنولوجيا المعلومات والاتصالات الآونة الأخيرة من اجراء التغييرات في العناصر الهيكلية والمادية في المباني التعليمية ، التي أثرت على الديناميات الاجتماعية في المدارس التي جاءت انعكاسا على التغير في طبيعة الدراسة. تم التوصل الى ان تجربة التعلم في العالمين الفعلي والافتراضي، دعمت عملية التعلم وكذلك رفعت من قدرة طلبة المدارس المعاصرة من التواصل بين المجتمعات المحلية والعالمية (Benjamin,2011:p266).

3- مفهوم الانفتاحية

- **مفهوم الانفتاح في اللغة:** مصدر الفعل الخماسي "أنفتح"، ويعني في اللغة " الانكشاف" ،إذ قال أبن منظور : " كل ما أنكشف عن الشئ"، " فقد أنفتح"، وهو ضد الانغلاق (معجم لسان العرب). أما الانفتاح في الاصطلاح: .إمكانية تفهُّم شيء أو اتساع الفكر له ،"يمتاز بانفتاحه على كلِّ جديد" ، " نعيش الآن عصر انفتاحات علميّة واقتصاديّة" (المعجم :اللغة العربية المعاصر). إنفتح الباب" صار غير مغلق" ،"إنفتح الشيء عن الشيء " انكشف عنه" (المعجم :الرائد). كما يعني عدم وجود قيود أو محددات، عدم أخفاء شي، تقبل تغيير في فكرة معينه https://en.oxforddictionaries.com

كما ارتبط بالامتداد والانبساط ،أنفتحت الزهرة وبدأت رائحتها تعبق، أوراقها تفتحت أنبسطت وتمددت. "أنفتح ذهنة عن الاشياء التي كان يجهلها"،"عرف تطورا وأنتعاشا" (المعجم: الغني). فالانفتاح كمفهوم هو أحد المفاهيم الجديدة في النظم الاجتماعية الحديثة . وعُد كمفهوم جديد مواكب لمتطلبات عصر جديد لمجتمعات تسعى نحو الانطلاق المعرفي والتقني العالمي http://gaha.ba7r.org/t19754-topic. أما مفهوم الانفتاح على مستوى الممارسة فتمثل بكون المشاركة مع المعلمين اصبحت أكثر انكشافا ومرئية، كما أن تبادل الأفكار والمهارات تعمل مع بعضها البعض بشكل وثيق، والتي تعتبر كدافع أساسي في تغيير البيئة الصفية المادية (Campbell et al., 2013; Hill & Epps, 2009; Lieberman & Mace, 2010).

بذلك فان مفهوم الانفتاح لغويا واصطلاحا يعني، (الانكشاف، عدم الانغلاق ، المشاركة ، أتساع الفكر ، الوضوح والابتعاد عن الغموض ، التفاعل، مواكبة متطلبات العصر).

4- الانفتاحية في الفضاء التعليمي

تَشارك المعلمين والمهندسين المعماريين– من منتصف 1960 و حتى عام 1980 – في التفكير في تنظيم المدارس اجتماعيا (socially organized) ومكانيا (spatially configured) وطرح حلول مبتكرة لذلك، مايقارب عقدين من الزمن وكانت الفكرة تتركز ليس فقط في طرح رؤى جديدة حول المناهج المدرسية والتربية والتقييم، وانما أيضا في تصميم المباني المدرسية المعاصرة.

يعد الصف الدراسي خلال الثورة الصناعية وقبل منتصف 1960 الوحدة التنظيمية الأساسية للمدرسة. جاءت بعد ذلك وانطلاقا من التعليم والاصلاحات الاجتماعية ،محاولة كبيرة لتغيير الطبيعة المادية للتعليم ، تبعه تطوير المباني التعليمية كمنظومات مفتوحة خلال 1960 و1970. في هذا الوقت، دعا الأكاديميون والتربويين الى طرق تدريس تدعم التعلم الفردي والتي تتطلب مساحات جديدة ومفتوحة ، تساعد على تحسين التفاعل بين المعلمين والطلاب (1998,Lackney).كما ظهرت فلسفات تربوية تتعلق بالخبرة والتعليم الديمقراطي التي بلغت ذروة من الابتكار، مثل تلك التي ينادي بها شخصيات تعليمية بارزة ک ديوي[1] (1966، 1971) وفريري[2] (1970، 1973). امتاز بذلك الفضاء التعليمي المفتوح بقابلية على المشاركه والتواصل مع فضاءات تعليمية اخرى من خلال: (توفر فرصة للمراقبة الذاتية – التعلم من الاخرين – امكانية الملاحظة الذاتية – توفر فرصة للوصول الى مايتعلمة المتعلمين في فضاءات تعليمية أخرى) . أما ([3]Mark) فقد دعا الى اقتراح فضاءات تستكمل وتعزز التعلم (learning) والتدريس (teaching) في آن واحد (Mark,2013,P4).

5– الدراسات السابقة التي تناولت مفهوم الانفتاحية في البيئات التعليمية

طُرحت خاصية الانفتاحية في المعرفة السابقة من عدة جوانب منها ماركز على: الانفتاحية وسلوك المتعلم ومنها الانفتاحية ودرجة تفاعل المتعلم، واخرى على الانفتاحية وأستقلالية المتعلم، والانفتاحية ودرجة التمتع بعملية التعلم، واخيرا على الانفتاحية ومخرجات التعلم:

–**الانفتاحية وسلوك المتعلم:**أرتبطت ابحاث كل من (Barker and Gump) بعلاقات السلوك في المباني ، اذ طوروا وفقا لها أستخدام نظرية السلوك لتقييم تأثير البيئة على سلوك الناس، اذ توصلوا الى أن إعدادات السلوك في كلا البيئتين المفتوحة والتقليدية لا تؤدي بالضرورة إلى تغييرات في البرامج التعليمية كما كان متوقعا، ومنها توصلوا إلى أن العمارة المفتوحة تؤثر على الممارسات التعليمية بدرجة كبيرة (Barker & Gump, 1964; Gump, 1974; 1980).

– **الانفتاحية ودرجة تفاعل المتعلم:** وجد (Gump) أن البيئات التعليمية المفتوحة تعطي تفاعلية اكبر بين المتعلمين والكادر، كما تعطي أمكانية عالية لحرية الحركة مقارنه مع البيئات التعليمية التقليدية،كما ان المتعلمين يكونوا أكثر ثقة بأنفسهم في البيئات المفتوحة ، مقارنه بالبيئات التعليمية التقليدية(Gump, 1980) .

---

[1] جون ديوي (John Dewey): فيلسوف أمريكي في مجال التربية والتعليم، يعتبر من أعلام التربية، أذ عمل على في جانب التعليم بتفيرة وفقا لنظريات التعليم الحديثة وكيفية ربطها بالواقع مع عدم أهمال القيم والتقاليد الموروثة بالمجتمع المصدر : http://www.almarefh.net/

[2] باولو فريري: معلم برازيلي و صاحب نظريات ذات تأثير كبير في مجال التعليم. كان يرى في التعليم وسيلة للثورة على القهر، وصولاً إلى الحرية وإلى تمكين المقهورين من مقدراتهم. ومنهجه في تحقيق ذلك يرتكز على «الحوار» الذي يتبادل فيه المعلم والمتعلم أدوارهما، فيتعلم كل منهما من الآخر، ويصبح موضوع الحوار الذي يدور في الغالب حول أوضاع المتعلمين المقهورين الحياتية هو المدخل إلى تعليمهم القراءة والكتابة. المصدر: http://archive.aawsat.com/

[3] Mark Osborne: مستشار ودكتورا متخصص في تطوير التعليم المستقبلي، في مجالات بيئات التعلم المبتكرة، وممارسة التعلم الحديث في جامعة مالبورن(the University of Melbourne)،أذ ساعدعلى تصميم البيئات التعليمية كمنظومات ومساحات مفتوحة وتأثيرها على المعلمين في تطوير قدرتهم بكيفية الاستفادة القصوى من تلك المساحات. المصدر : http://www.core-ed.org

-**الانفتاحية وأستقلالية المتعلم:** اذ وجدت أن المتعلمين يكونوا أكثر أستقلالية وتفاعلية في البيئات المفتوحة مقارنة بالبيئات التقليدية، مع شعورهم بالرضى العالي بعملهم (Meyer ,1971). في حين أشار (Weiss and Fisher) الى ان المتعلمين في البيئات المفتوحة يكونوا اكثر أيجابية في التفاعل، مع القابلية العالية في التحكم الذاتي بقراراتهم التعليمية Weiss and Fisher ,1974).

-**الانفتاحية ودرجة التمتع بعملية التعلم:** أشار (Pritchard) أن الكادر التدريسي يكونوا أكثر متعة في عملية التعلم في البيئات المفتوحة مقارنه بالصفوف الدراسية التقليدية (Pritchard, 1971).

-**الانفتاحية ومخرجات التعلم:** أن التغييرات في الفضاءات التعليمية بين المفتوحة والمغلقة تؤثر على مخرجات التعلم، حيث أن مخرجات المتعلمين في كلا البيئتين المفتوحة والمغلقة مختلفة (Rodwell's ,1998).

يتضح مما تقدم بأن الانفتاحية ضمن بيئة التعلم خاصية مرتبطة بالعلاقات الفضائية ضمن بيئة التعلم الفيزيائية، بحثت في المعرفة السابقة من عدة جوانب غير الجوانب الفيزيائية، منها رتباطها بسلوكية التفاعل للمتعلم، او بأرتباطها بخصوصية وأستقلالية المتعلم، واحيانا أرتباطها بمخرجات التعلم لارتفاع المستوى العلمي للمتعلم أو أنخفاضة. حيث لوحظ طرح أهمية وتأثير أنفتاحية فضاءات التعلم على سلوك المتعلم وتفاعلهم مع بعضهم البعض والذي يؤدي الى تحسين مخرجات التعلم، وعلى الرغم من ذلك توضح الحاجة الى وصف اوضح لطبيعة تأثير هذة الانفتاحية للفضاءات على درجة أندماجية المتعلم مع البيئة الفيزياوية من جهة ومع بقية المتعلمين من جهة أخرى وبهذا الاتجاه تركزت مشكلة البحث.

-مشكلة البحث: غياب التصور الكافي عن تأثير انفتاحية فضاءات البيئة التعليمية على درجة أندماجية المتعلمين ضمن هذة البيئات وتفاعلهم مع بعضهم البعض

- **هدف البحث:** استكشاف وتحديد العلاقة بين خاصية الانفتاحية وعلاقتها بأندماجية المتعلم ضمن بيئات التعلم.
- **فرضية البحث:** كلما زادت الانفتاحية في فضاء التعلم زادت أندماجية المتعلم وتفاعلة مع المتعلمين أو بالعكس .
- **هيكل البحث:** يتركز منهج البحث بالمراحل الآتية:

1. بناء أطار نظري حول تعريف البيئات التعليمية المفتوحة والتقليدية، تحديد مفهوم عام وشامل للانفتاحية في الفضاءات التعليمية، وتحديد اهم مفرداتها، تحديد مفهوم الاندماجية واهم مفرداتها.
2. تحديد أسلوب القياس وطريقة تحليل البيانات. تحديد النتائج والاستنتاجات والتوصيات. الشكل (1) يبين الهيكلية المعتمد في البحث

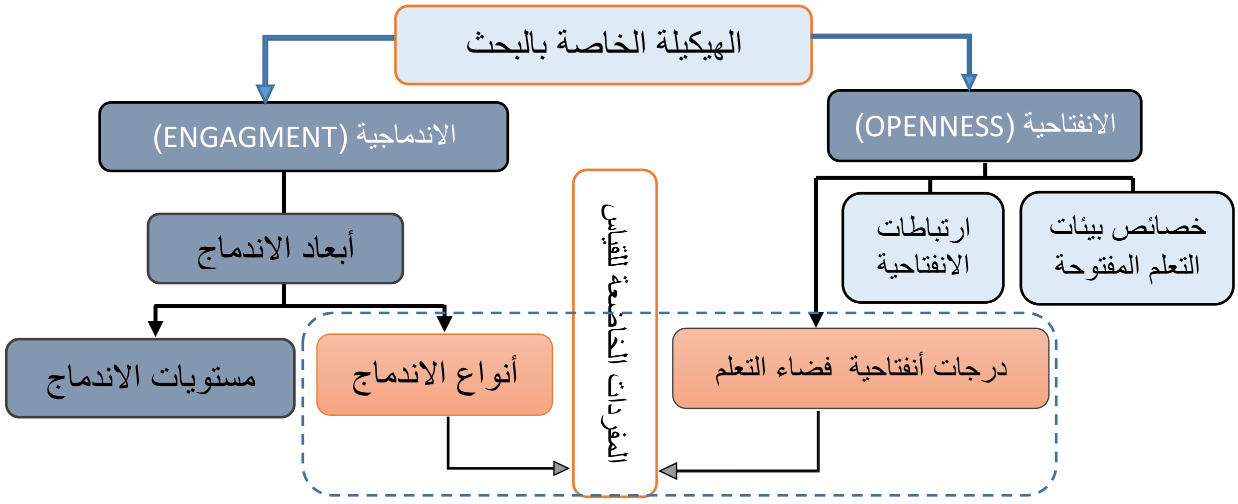

الشكل (1): المنهج المعتمد في البحث (المفردات والجوانب المطروحة لكل من خاصيتي الانفتاحية-الاندماجية)-المصدر(الباحثان)

6- الاطار النـظري: الفضاءات التعليمية المفتوحة والفضاءات التعليمية التقليدية

لغرض تحديد خصائص الانفتاحية لبيئات التعلم ينبغي توضيح مقارنه بين بيئات التعلم المفتوحة المعاصرة وبيئات التعلم التقليدية من عدة نواحي، وفي مايلي توضيح لذلك:

- **الفضاءات التعليمية المفتوحة:** وفقا الى تعريف الانفتاحية في الفضاء على انه وجود مساحة واسعة قادرة على أستيعاب أكثر من فئة واحدة ، لذا فهي قادرة على اتاحة التعليم التعاوني (Osborne, 2013). أكدت بعض آراء التربويون على كسر حدود الصفوف الدراسية وخلق مساحات تعليمية أخرى . أدى هذا الاتجاه إلى تصميم مخطط مفتوحة أو المدارس القائمة على الاستوديو (studio-based Schools). كما ظهرت تصاميم بمخططات مفتوحة ومدمجة. كانت فكرة المخطط المفتوح بطيئة القبول بالنسبة للمباني التعليمية، ففي عام (1960) تم تصميم المدارس على مبدأ "شبه المفتوحة"، التي شملت مساحات التعليم المشتركة بالإضافة إلى فصول دراسية منفصلة التقليدية. كان الهدف من هذا النموذج بناء استوديو للتركيز على أهتمامات ودوافع الطلاب من خلال التعلم النشط (active learning) ، التعلم بالممارسة (learning by doing) ، فضلا عن تطوير وتحسين المناهج الدراسية (Benjamin,2011:p200). عُدت بيئات التعلم المعاصرة بأنها أكثرا انفتاحا من البيئات التقليدية لكونها: (تمتاز بكونها اقل جدرانا عن البيئات التقليدية – اكثر أستخدام لمادة الزجاج –أستخدام فكرة التعليم المشترك الذي هو محور التعليم) (Mark,2013,P4). والاشكال الموجودة أدناة (شكل رقم 2) نماذج للفضاءات المفتوحة:

شكل2:نماذج للفضاءات المفتوحة المصدر: Department for Education and Skills,2003:P13

- **الفضاءات التعليمية التقليدية:** الفصول الدراسية التقليدية هو نتاج التربية التي تركز على المعلم ، تتأطر ضمن علاقة هرمية (framing a hierarchical) بين المعلم والطلاب مع إنغلاقية عالية عن الانشطة الأخرى وتقليل تشتتات (distractions) الطالب. اذ تعد المناهج التعليمية المتمحورة حول المتعلم مقيدة بشدة في الفصول الدراسية التقليدية،التي نشأت خلال الثورة الصناعية، والتي صممت لغرض تلقي المتعلم للمعلومات بشكل سلبي (McGregor, 2004b).

لقد أفرزت الطروحات عدة أنماط من تصميم القاعات الدراسية السائدة منها نمطين وهما (William,2011,p):

1-النمط تجميع الفصول الدراسي على جانبي الممر الوسطي ،كما في الشكل (3) .

2-نمط تجميع مركزي (قاعة مركزية) بدلا من الممر الوسطي، يسمى "مخطط الموزع المركزي (central-hall plan) ، يستخدم الموزع كقاعة للتعليم المشترك. حيث ان الجدران التي تفصل بين الفصول الدراسية والموزع تكون مزججه جزئيا لغرض السماح لرئيس المدرسة ان يرى ما يحدث داخل فصول دراسية، ويتم تغطية الجدران الزجاجية لمنح الطلبة بعض الخصوصية احيانا، (شكل رقم 4) (Seaborne, 1971, p. 27).

أتجهت المدراس في منتصف القرن التاسع عشر نحو توسيع الفصول الدراسية لزيادة عدد الطلبة ضمن الفضاء. فظهرت القاعة المركزية المفتوحة لثلاثة طوابق مع ترتيب الطلبة وفق الاعمار للطلبة ، مثل هذا توجها نحو الانفتاح في الفضاءات التعليمية (Seaborne 1971).

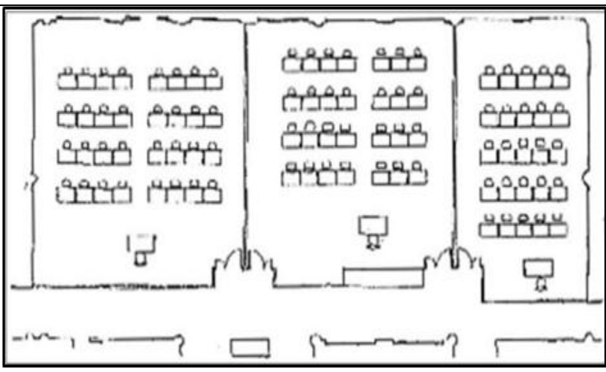

شكل 3: بيئات تعلم تقليدية متمثلة بممر وسطي (SACHSSE, 2003)

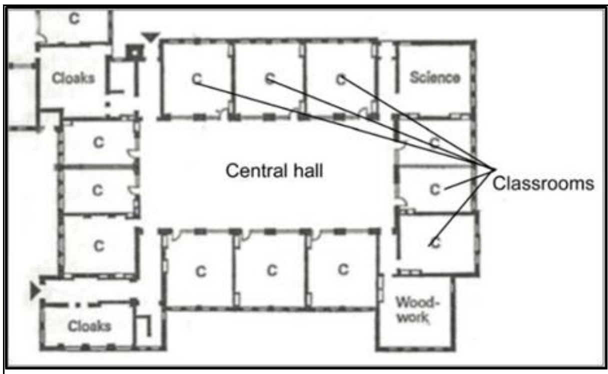

شكل 4:بيئات تعلم تقليدية متمثلة بقاعة وسطية (SEABORNE,1971)

7- خصائص بيئات التعلم المفتوحة

تتضمن هذة الفقرة جانبين، يتعلق الاول بالخصائص العامة للفضاءات التعليمية المفتوحة، والثاني بأنواع الانفتاح في الفضاءات، الجانب الثالث يتعلق بدرجات الانفتاحية

<u>الجانب الاول:</u>الخصائص العامة للفضاءات التعليمية المفتوحة: تتضمن الفضاءات التعليمية المفتوحة مجموعة من الخصائص:

- **الاتصال:** يقصد به مجموعة الاتصالات بين الافراد المنظمة الواحدة في بناية ما ، وينقسم الى نوعين اعتماد على وسائل الاتصال وهما :الاتصال بدون الحركة المكانية للافراد (المرئي او السلكي او المكتوب او الشفهي) والاتصال بواسطة الحركة المكانية للافراد (الزيارات التي يقوم بها الافراد لبعضهم البعض من نقاط تواجدهم). يتمثل الاخير بالمسافات المادية بين الناس والتي يمكن من خلالها تحقيق التفاعل والحوار مع بعضهم البعض. ظهرت مصاحبة لها بعض المفاهيم وكانت غير المسبوقة في مجال الاتصالات المكانية كمفهوم " فقاعات رد فعل الشخصية"و "مساحة شخصية" والتي جاءت انعكاسا لهذه الفكرة (http://www.ehow.com/).

- **التواصل (Communicativeness):** ناقش الناقد (بانهام) فكرة الوصل بين الفضائين من خلال الدمج الكامل بينهما ، حيث تتبع وجهة نظره من مفهوم الداخل والخارج الذي يكمل احدهما الاخر من خلال الانفتاحية ويؤكد وجوب النظر الى احداهما من خلال الاخر(بانهام،1989، ص.97) . اذ كلما قلت المساحة المفتوحة واتخذت الفتحات اشكالا اقرب الى الثقوب الصغيرة ازداد الفصل بين الفضائين ، كما ينشأ الفصل ايضا عندما تكون الفتحات التي هي نقطة الاتصال بين الداخل والخارج مقفلة فانها تنشأ روابط فضائية بصرية بين الفضائين (ching,1987,p.225).
- **الشفافية (transparency):** تعتبر خاصية الشفافية من الخصائص التي تتميز بها بيئات التعلم التفاعلية لتعبيرها عن الانفتاحية العالية في الفضاء. كما تخلق الشفافية نوع من الاتصال البصري بين الفضاءات Bethany L (Taylor,2010).

فالمفاصل الشفافة هي ادوات للمرور من خلالها وكذلك مصدر للاضاءة والتهوية، فيعد المفصل الشفاف حدا يكون من خلاله حدوث تفاعل او علاقة ما بين وسطين(جولدي،1986، ص.16)

- **الدينامية:** يمكن أن تحقق الدينامية في فضاء التعليم المعماري فهم أعمق للمقاصد والاهداف من عملية التعلم ، كما تسمح لحدوث حالة التفاعل بين عناصر البيئة الاجتماعية مع المنهج. وهذا يعني أنه ينبغي أن ينظر الى العناصر المادية على أنها قابلة للتغير باستمرار في كل من المكان والزمان وفقاً لمستخدمي الفضاء (Massey,2005).
- **المرونه (Flexibility):** تعني قابلية الفضاء على التأقلم والتناسق مع الاستعمالات المتعدده للفضاء، كما يشير هذا المفهوم الى الهياكل التي يكون لها نسبة أستخدام عالية جدا من خلال استخدام الجدران القابلة للإزالة (قابلة للطي، والانزلاق) ،وهذا يسمح لتحويلها وعكسها من بيئات تقليدية إلى مفتوحة ، وغالبا ما تتطلب هذة الفضاءات الجدران والأثاث القابلة للنقل والتحرك وفقا لنوع الفعالية التعليمية (Monahan, 2002) .

تناولت الفقرة السابقة اهم الخصائص التي تمتاز به الفضاءات التعليمية المفتوحة والتي تتمثل ب(خاصية الاتصال والتواصل بين الفضاءات والتي تمنح الطلبة فاعلية عالية في الاندماج مع بقية الطلبة) ،وخاصية المرونه والتي تجعل الفضاء التعليمي المفتوح اكثر حرية في أنشاء تنظيمات تكوينه وفقا لنوع النشاط التعليمية. الديناميكية وتتمثل بقابلية التغيير وفق الزمان والمكان.التنوع المكاني وهي ماتعطي للمتعلم بعض الخصوصية أثناء أنجازه للفعالية التعليمية وفقا لحاجته لذلك،واخيرا الشفافية التيُ تعد من اهم خصائص الانفتاحية لكونها آلية التحكم بدرجة أنفتاح الفضاء من الداخل ال الخارج وبالعكس.

<u>الجانب الثاني</u>:أرتباطات الانفتاحية: تتناول هذة الفقرة ثلاثة أرتباطات للانفتاحية الفضاء تمثلت تلك الارتباطات بـ:

أولا:أنواع الانفتاحية: حيث يوجد هنالك نوعين أساسين من الانفتاحية هما:

- الانفتاح نحو الداخل: يتمثل بنمط الفناء الداخلي في تصميم المباني التعليميه من خلال الانغلاق من الخارج وأستخدام الزجاج نحو الداخل، حيث لهذا النمط فائدتين: الاولى: تتمثل بالتأثيرات النفسية الاجابية للطالب وشعورة بالانتماء والاحتواء داخل الفضاء كما يعطي تركيز بصري عالي، اما الثانية: فتتمثل بالنواحي المناخية عن طريق توفير التهوية الجيدة (Perkins,2001:p63)
- الانفتاح نحو الخارج: تتمثل الانفتاحية نحو الخارج من خلال شفافية الفاصل بين الداخل والخارج فتكون عبارة عن مفاصل زجاجية شفافة أو نصف شفافة وهذا مايعطي درجة الانفتاحية مختلفة للفضاء. يعتمد ذلك على حجم الفتحات المستخدمة في الفضاء ،اذ كلما قلت المساحة المفتوحة واتخذت الفتحات اشكالا اقرب الى الثقوب الصغيرة ازداد الفصل بين الفضائين

،كما ينشأ الفصل ايضا عندما تكون الفتحات التي هي نقطة الاتصال بين الداخل والخارج مقفلة فانها تنشأ روابط فضائية بصرية بين الفضائين (زمن وضاء،2012:ص60).

ثانيا: التنوع في الانفتاحية: تتحقق صيغة التنوع المكاني من خلال التلاعب (manipulable) بالاثاث أو الجدران المتحركة التي تحقق خصوصية جزئية ضمن الفضاء، فقد تجد صعوبة في تحقيق جميع مستويات الخصوصية في الفضاءات التعليمية ذات الانفتاحية الكبيرة وذات الخصائص المتنوعة مكانيا ،اذ يمكن من خلال التلاعب بالشاشات والمفروشات والجدران المتنقلة تحقيق نوع من الخصوصية البصرية، أما من الناحية النفسية للمتعلم ،فيمكن تحقيق الخصوصية من خلال أنشاء فضاءات فرعية ضمن الفضاء العام ، لكن قد يصعب في مثل هذا النوع من الفضاءات تحقيق الخصوصية الصوتية(PHILIP PIPAL,1980:p40). كما في الشكل رقم (5).

ثالثا: العناصر التي تحقق الانفتاحية بين الفضاءات: تتمثل تلك العناصر بعناصر المبنى أو الفضاءات الداخلية التي تقسم الى ثلاثة أنواع :

-**أولا، العناصر التي تحدد الأماكن** :التي تتضمن مستويات العمودية والأفقية التي تخلق الفضاء.

-**ثانيا: العناصر التي تتحكم في نوعية الفضاء:** التي هي الشكل، الحجم، والنسب، والألوان، والقوام، والإضاءة.

-**ثالثا: العناصر التي تعطي مساحة ترتيب معين:** وتتمثل في الكيفية التي يتم اللاعب بها على مستوى الفضاء والتي ستؤثر على أي نوع من الفصول الدراسية تم أنشاءوها (Fatimah,2014).

يتضح مما تقدم أن ما يتحكم بدرجة أنفتاحية الفضاء على المستوى المادي هي مجموعة من العناصر المادية التي تعتمد درجة أنفتاحها على نسبة تلك المفاصل ونوعيتها كما تعتمد على درجة شفافيتها كونها الاساس في التحكم بأنفتاح الفضاء ، أذ تتمثل تلك العناصر بـ(الابواب ،النوافذ).

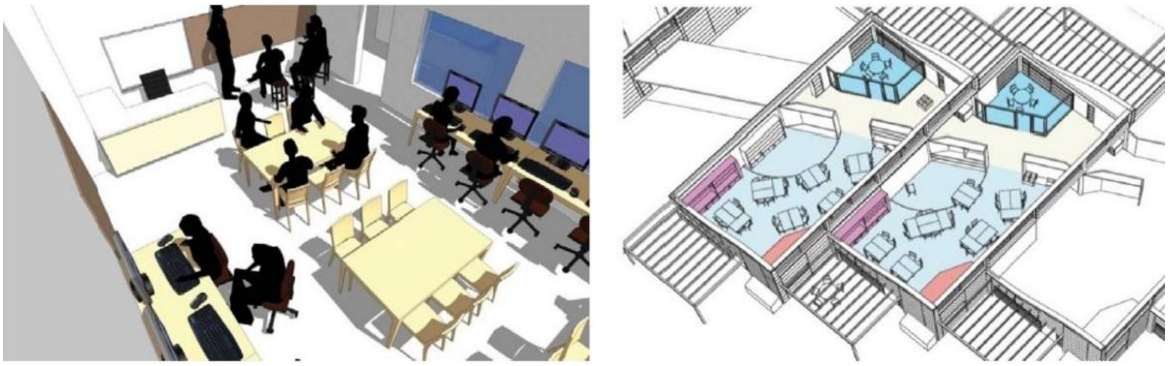

الشكل 5: نموذج مبتكر لتنظيم الفصول الدراسيةالمصدر Department Education and Skills:,2003:P13

<u>**الجانب الثالث: درجات الانفتاحية في الفضاء**</u>

أختلفت الدراسات التي تناولت موضوع الانفتاحية في البيئات التعليمية في توضيح كيفية تعريف درجات الانفتاحية، حيث قسمت الدراسات الى مستويين والتي تناولت درجات الانفتاحية من حيث العلاقة بين عرض الفضاء الى أرتفاعة:

- **المستوى الاول: كما موضح في الجدول (1) الذي يبين درجات الانفتاحية:**
- **المستوى الثاني: كما موضح بالجدول (2).**

جدول 1: درجات الانفتاحية – المصدر :(Derived from Ashihara,1970)

النسبة [4]	جودة المكانية الفضاء المفتوح
D/H<1	فضاء حميم ولكن يعطي شعور بالضيق
D/H=1	فضاء متوازن بين الانفتاح والانغلاق. فهي فضاء طبيعي
1<D/H<2	فضاء مفتوح ولكن يعطي شعور بالراحة
2<D/H	فضاء أكثر انفتاحا، حيث يصبح فضاء مكلف مع خسارة كبيرة بالفضاء

جدول 2: درجات الانفتاحية – المصدر :(Hörmann and Trieb,1977)

النسبة العرض الى الارتفاع	تعريف لفضاء
1=1	سوف ينظر الحدود فقط نصف ارتفاعها، ضيقة جدا
2=1	يمكن أن ينظر إلى ارتفاع كامل من الحدود، مكان مغلق، الشعور بالفضاء المفتوحة كفضاء ضيق
3=1	يحقق توزن بين الانفتاح والانغلاق
6=1	يعطي شعور بأن الفضاء المفتوح وواسع جدا

8- اندماجية المتعلم في الفضاء التعلم المفتوح

يتضمن هذا المحور تعريف لمفهوم الاندماجية وأنواعها ومستوياتها وأبعادها وفي مايلي تفصيل لكل جانب.

A- **مفهوم الاندماج (engagement):** يأتي المفهوم العام للاندماج كتعبير عن المشاركة الطلابية والشعور بالانتماء والمشاركة (OECD, 2000, p. 8). كما يعرف على أنها المشاركة في الممارسة التعليمية بفعالية عاليه، داخل وخارج الفصول الدراسية، والى أي مدى يمكن للمتعلمين المشاركة في الأنشطة التي تكون ذات أرتباط بجودة مخرجات التعلم (Kuh et al., 2007)،

B- **العلاقة بين البيئات التعليمية وأندماج المتعلم :**طُرحت المعرفة السابقة العلاقة بين البيئات التعليمية واندماجية المتعلم من عدة جوانب، اذ أشار (Zyngier) الى وجود أتصال عالي بين البيئات التعليمية والاندماجية كتشاركية ، موضحا أن المشاركة يجب أن لا تكون منفصلة عن الزمان والمكان والفضاء(Zyngier, 2007, p. 8). أما (Janowska and Atlay) فقد أشار الى وجود أتصال قوي بين بيئات التعلم ودرجة اندماج المتعلمين في الانشطة التعليمية، حيث استكشف تأثير مساحة مصممة خصيصا (بيئات التعلم الابداعية) على درجة أندماج المتعلم في عملية التعلم، والدافعية للاستكشاف، وتجربة والخبرة لديه وعليها فيصبحوا أكثر نشاطا، ومتعلمين أكثر أستقلالا (Janowska & Atlay, 2008, p. 271). كما وان بيئات التعلم يجب أن تكون مصممة وفقا النظم المتكاملة للتعلم التي تقوم على أساس العمل الفردي الفرد، واحد الى واحد أو مجموعة صغيرة أو المجموعة الكبيرة (Lippman ,2007; 2010). بالإضافة إلى ذلك، أشار إلى أن المتعلمين كانوا أكثر عرضة للبناء المعرفة عن أنفسهم وتبادل تفاهمات مع الآخرين وفق بيئاتهم التي تسمح لهم بالتعامل مع الانشطة التعليمية.

يمكن الاستنتاج بأن البيئات التعليمية المفتوحة ترتبط بمدى اندماجية المتعلم مع الاخرين من خلال المفردات التاليه: الدافعية العالية لدى المتعلم، التعلم بأستقلالية عالية، الاستكشافية والبحث عن المعلومات الجديدة.

[4] حيث يمثل (D) يمثل عرض الفضاء، (H) يمثل أرتفاع الفضاء

C– **أنواع الاندماج:** يقسم الاندماج الى نوعين (Benjamin William,2011):

1–أندماج أيجابي (engagement) : يعني به المشاركة الايجابية للطالب والتي ترتبط بمجموعة من المفاهيم منها: المشاركة، والتحفيز، والطاقة، والعمل، والتوجيه، والاتصال، الحكم الذاتي، والانتماء، والكفاءة ، والجهد والمثابرة الانتباه والاهتمام واستثمارية (Marks, 2000).

2–الاندماج السلبي (disengagement): يعنى به عدم الاندماج ،وارتبطت بمفاهيم مثل: الجفاء، الانفصال، التفتت والعزلة والعجز، اللامعنى، الانقطاع والملل .(Appleton et al., 2008). بالإضافة إلى ذلك، اقُترح أن مؤشرات عدم الاندماج شملت، عدم الانتباه، عدم استكمال العمل المدرسي، السلوك المضطرب، والانسحاب، التدني في التحصيل الدراسي، التغيب ورفض المدرسة ((Murray et al. (2004).

D–أبعاد الاندماج (engagement – dimensions): أن النقاش الأكاديمي حول كيفية تعريف بناء أندماج المتعلمين عملية مستمرة ، ومع ذلك، فالمعلمين والباحثين يدركون أن أندماج المتعلم في التعلم ومع الفضاء التعلم مهم للغاية لغرض تحقيق النتائج العلمية الايجابية (Zinger, 2007; Appleton et al., 2008) . ولقد حُددت عدة ابعاد للاندماجية ومن عدة باحيثن منهم:

أولا– قسم (Appleton) أبعاد الاندماج الى أربعة منها: البعد الاكاديمي (academic)، البعد السلوكي (behavioral) ، البعد المعرفي (cognitive) ، البعد النفسي (psychological) (Appleton et al. 2006)

ثانيا–بينما أشار (Fredricks) الى أنه يقسم الى ثلاثة أبعاد (Fredricks, Blumenfeld & Paris, 2004) وهي :

- البعد السلوكي (behavioral): ويرسم فكرة الاندماج السلوكي والمتمثل بالمشاركة في الأنشطة الأكاديمية والاجتماعية واللامنهجية ، ويعتبر حاسما لتحقيق نتائج إيجابية أكاديمية
- البعد المعرفي (cognitive): يشمل المشاركة العاطفي وردود الفعل الإيجابية والسلبية للمعلمين وزملاء الدراسة، والأكاديميين، والمدرسة، كما يفترض خلق روابط التي تقوم على استعداد المؤسسة للقيام بهذا العمل
- البعد الوجداني او العاطفي (emotional): تقوم على أساس التوجه نحو المشاركة المعرفي القائمة على فكرة ؛ حيث يشتمل هذا البعد على التفكير والاستعداد لبذل الجهد اللازم لفهم الأفكار المعقدة والصعبة والمهارات الرئيسية

يستنتج من اعلاه ان مفهوم الاندماجية هي الحاله التي يشعر بها المتعلم والمتمثلة بمدي قابلية على المشاركة الفعالة بالفعالية التعليمية، والتي تكون على عدة مستويات: مستوى الاندماج الذهني للمتعلم مع الفعالية، مستوى الاندماج التشاركي مع الكادر والمتعلمين ومستوى الاندماج التحفيزي بجميع الانشطة التعليمية المتمثلة بالنقاش والحوارية والملاحظة الجادة من المتعلم بأتجاه مايطرح من الكادر وبقية المتعلمين.

E– مستويات الاندماج (engagement– Levals):وضحت الطروحات المرتبطة بنظرية التعلم ثلاثة مستويات من الاندماجية وفقا لطروحات ((Lave and Wenger‘s (1991)، في ضوء رؤية (Lippman)، تتمثل هذة المستويات ب:

–المستوى الاول: الاندماج الطرفي (peripheral participation): تقوم على أساس ملاحظة وتفسير القيود المرتبطة بالنشاط.

–المستوى الثاني: الاندماج الموجه (guided participation): المحاوره والنقاش مع المتعلمين الاخرين للحصول على التفاهمات التي تخص النشاط.

–المستوى الثالث: الاندماج الكامل (full participation): كيفية أن تصبح المشاركة كاملة في النشاط بعد الحصول على تفاهمات في كيفية المشاركة في النشاط . كما في الشكل رقم (3)

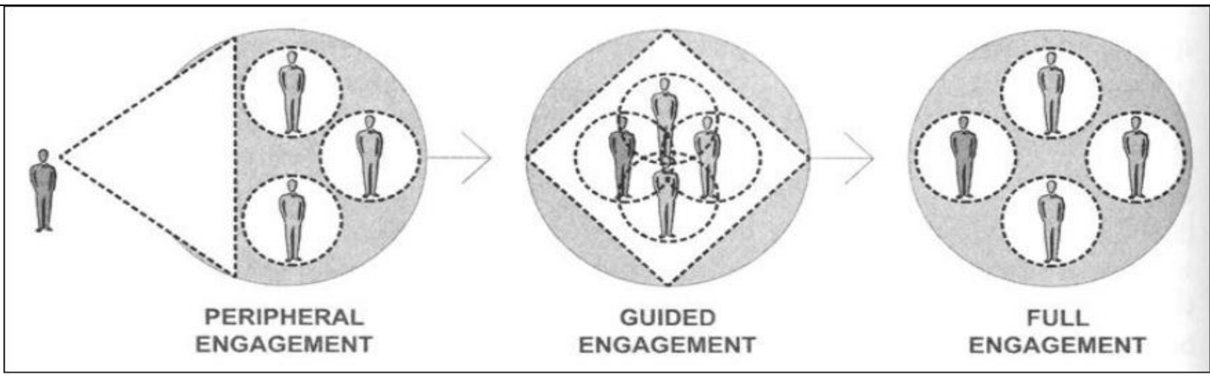

الشـــــــكل 3: مستويات الاندماج في أنشطة التعلم وفقا للنظرية البنائية (Lippman (2007; 2010

وبناء على النتائج من أبحاثه التي أجراها في الولايات المتحدة، أشار إلى أن البيئة المادية كان لها تأثير على قدرة الطلاب على التحرك من خلال هذه المستويات من المشاركة. وخلص إلى أن بيئات التعلم يجب أن تكون مصممة لتعزيز مشاركة الطرفية، والموجهة والكاملة في التعلم.

أشار (Monahan) الى أن أستخدام بعض الانماط في الترتيبات المكانية للفضاء تعطي درجة عالية من الانفتاحية في البيئات التعليمية، اذ يوفر النمط العنقودي غير المستقر بعض السيطرة المركزية التي تمنح أنفتاحية أكثر في بيئة التعلم كما تعطي أمكانية عالية في جعل فرص التعلم أكثر تنوعا (Monahan, 2005). أن نموذج البيئة المفتوحة، بما في ذلك المخطط الذي عرّف باسم استوديو التعلم، يقدم صفوف دراسية أكثر مرونة ، حيث يعمل كل فصل دراسي أو (الفضاء المسمى بأستوديو التعلم) على دمج عدد من أنشطة التعلم المختلفة (Nair & Fielding, 2007). في نفس الوقت تعتبر البيئة التعليمية المفتوحة بيئات تعليمية محفزة تدعو المتعلم للاكتشاف، والاندماج العالي في الفعاليات التعليمية من خلال أمكانية خلق تنوع عالي في تنظيم الاثاث للعمل والجلوس بما يدعم التعلم المحفز داخل الصفوف الدراسية المفتوحة (Perkins,2001:p8).

يستنتج مما سبق بأن الفضاء التعليمي له تأثيرات على أندماج المتعلم في عملية التعليم: فقد تكون تلك البيئات تحفيزية تجعله على درجة عالية من القابلية على المشاركة والتواصل العالي في الانشطه التعليمية وقد تكون لها تأثيرات سلبية تجعل المتعلم في حالة من الملل وعدم التركيز والشعور بالتشتت العالي بالافكار ، وبالتالي فأن التوجهات المعاصرة تتجه نحو جعل فضاءات التعلم أكثر أنفتاحا وتواصلية لغرض أن يتخلص المتعلم من جميع المؤثرات السلبية التي قد تتولد لديه أثناء شرح المحاضرة أو أثناء تطبيقة لعملة ضمن أستوديو التعلم

9- الدراسة العملية: سيتم في هذة الفقرة تحديد أهم مفردات القياس المرتبطة بالانفتاحية والاندماجية، وتحديد أسلوب القياس وطريقة القياس والعينه المنتخبة لغرض التطبيق.

-المفردات الخاضعة للقياس: تم أنتخاب مفردتين رئيسيتين بمؤشراتها ،مفردة (درجة الانفتاحية في فضاء التعلم) ومفردة (الاندماجية للمتعلم) بمفردتين ثانويتين هما (الاندماج الايجابي-الاندماج السلبي) ، وكما موضح بالجدول أدناه (مفردات الاطار النظري)-الجدول رقم (3) .

جدول 3: يبين مفردات الاطار النظري الرئيسية والثانوية وقيمها ، المصدر الباحثان

المفردات الرئيسية	المفردات الثانوية			القيم الممكنة	الرمز
انفتاحية الفضاء	الانفتاحية في الفضاء على أساس نسبة الارتفاع الى العرض	فضاء بدون حدود خارجية		فضاء ذا أنفتاحية عالية جدا	A1
		فضاء نسبة الارتفاع الى عرض الفضاء(1:6)		فضاء مفتوح	A2
		فضاء نسبة الارتفاع الى عرض الفضاء(1:3)		فضاء متوازن	A3
		فضاء نسبة الارتفاع الى عرض الفضاء(1:2) او أقل		فضاء مغلق	A4
	الانفتاحيه في الفضاء على أساس نسبة الزجاج المستخدمة	نوع الفواصل		شفافة	A5
				نصف شفافة	A6
				معتمة	A7
		نسبة الفواصل		نسبة الفواصل المستخدمة (75−100)%	A8
				نسبة الفواصل المستخدمة (50−75)%	A9
				نسبة الفواصل المستخدمة (0−50)%	A10
أندماجية المتعلم	اندماج أيجابي	أندماج طرفي	قابلية المتعلم على الملاحظة	التفكير الذهني	B1
				التفاعل مع الاستاذ	B2
				أندماج التفكير مع العمل اليدوي	B3
				درجة أنتباه الطالب	B4
				قابلية الطالب في التواصل مع الموضوع ضمن الفضاء	B5
		اندماج موجه	قابلة المتعلم على النقاش والحوارية	مناقشه الاستاذ	B6
				طرح الاسئلة حول الاجزاء الغامضة للموضوع	B7
				قابلية الطالب في أستكشاف المعلومات التي تفيده	B8
				البحث عن التشاركية من خلال تغيير طريقة الجلوس	B9
				درجة تفاعل المتعلم مع المعلومات التي تطرح من قبل الطلبة	B10
		أندماج كامل	المشاركة كاملة في النشاط	كتابة الملاحضات التي تطرح من الاستاذ والطلبة	B11
				مدى الاستفادة من وجهات نظر الاخرين من خلال التفكير	B12
				المتعة العالية في التفكير والمشاركة	B13
				عمل مخططات لرسم المعلومات في الذهن	B14
				البحث عن المشاركة والتحفير العالي	B15
	أندماج سلبي	التشتت بالتفكير		عالية جدا	B16
				متوسطة	B17
				منخفظة جدا	B18
		الشعور بالعزلة		عالي جدا	B19

B20	متوسط			
B21	منخفض			
B22	عالي جدا	فقدان التركيز		
B23	متوسط			
B24	منخفض			
B25	عالي جدا	الشعور بالممل العالي		
B26	متوسط			
B27	منخفض			

-**أسلوب القياس:** تم أعتماد الاسلوب الأحصائي في قياس المفردات من (A1) الى (A4) بأعتماد المعادلة (عرض الفضاء/أرتفاع الفضاء)، المعادلة ((مساحة الزجاج الكلية في الفضاء/المساحة الكلية للجدران)*100%) لغرض قياس المتغيرات من (A5) الى (A10). وأعتماد أستمارة أستبيان لقياس المتغيرات من (B1) الى (B27)

-**عينة القياس:** تم أنتخاب ثلاثة نماذج من الفضاءات التعليمية المتباينه من ناحية خصائص بيئاتها التعليمية من ناحية الانفتاحية ،وقيست على طلبة المرحلة الثالثة/الجامعة التكنولجية/قسم هندسة العمارة وفي مايلي وصف لتلك الفضاءات:

- **الفضاء الاول: قاعدة دراسية:** بأبعاد (8.8m*8m) وبأرتفاع (3.8m) خاصة بطلبة المرحلة الدراسية الثالثة، تقع في الطابق الاول للمبنى، تتألف من مدخل زجاجي بأبعاد (2.2m*3.8m)، كما تتضمن أستخدام الزجاج كنوافذ من جانب واحد وبأبعاد (2.9m*7.7m) ، الشكل (4).

– درجة انفتاحية الفضاء: تمثل هذة الخاصية وفق مستويين: أولا: وفقا لمقياس نسبة العرض / الارتفاع (2=7.9/3.8) بالتالي فأن نسبة العرض الى الارتفاع هي نسبة (2=1)،

ثانيا: وفقا لمقياس نسبة الزجاج المستخدم بالفضاء= (مساحة الزجاج الكلية في الفضاء *100)/مساحة الجدران الكلية= (23%=30m2*100/126m2)

- **الفضاء الثاني: فضاء مرسم:** بأبعاد (16.1m*7.9m) وبأرتفاع (3.8m) خاص بطلبة الرحلة الثالثة/قسم العمارة، يقع في الطابق الاول للمبنى، يضم مدخل زجاجي بأبعاد (1.5m*3.8m)، كما يتضمن أستخدام الزجاج من جانبين.

– درجة الانفتاحية في الفضاء:تمثل هذة الخاصية وفق مستويين: أولا: وفقا لمقياس العرض/الارتفاع (4=16.1/3.8)

ثانيا: وفقا لقياس نسبة الزجاج المستخدمة في الفضاء = (مساحة الزجاج الكلية في الفضاء *100)/مساحة الجدران الكلية= (63%=66.7m2*100/105.5m2) نسبة الزجاج المستخدمة في الفضاء.**الفضاء الثالث:فضاء مفتوح:** تم أختيار فضاء بدون أي حواجز مادية لعرض المحاضرة للطلبة والمتمثل بموقع عمل مفتوح ضمن الجامعة التكنلوجية، الشكل (5).

الشكل (4): يبين الفضاء المغلق (القاعة الدراسية). المصدر: الباحثان

الشكل (5): يبين الفضاء المتوازن (المرسم). المصدر : الباحثان

<u>المرحلة الثانية: تتضمن هذة المرحلة قياس سلوكي:</u> يتمثل بقياس درجة أندماجية المتعلم في الفعالية التعليميه من خلال: تنظيم أستمارة أستبيان تعد للطالب ، ويتم اعتماد عينه عشوائية من طلبة وفق عدد (15) طالب، يتم اختيار مادة تعليمية ولتكن (مادة أنشاء مباني/مرحلة ثالثة) الجامعة التكنلوجية–قسم هندسة العمارة، حيث يتم تدريس هذة المادة على ثلاثة مراحل (محاضرة نظرية في قاعة دراسية – محاضرة عملية في أستوديو التعلم– زيارات موقعة في الفضاء المفتوح)، توزيع أستمارات الاستبيان على الطلبة في كل مرحلة لقياس مدى تأثير الفضاء المادي المفتوح على مدى أندماج الطالب الذهني والعملي في الفعالية التعليمية(الملحق).

10- النتائـج:

تم التوصل الى مجموعة من النتائج الخاصة بالمحورين المحددين ببخاصيتي الانفتاحية والندماجية،وكالاتي:

- نتائج خاصية الانفتاحية للفضاءات الثلاثة: ترتبط بتقييم درجة أنفتاحية الفضاءات الثلاثة المنتخبة كما في الجدول (4)،(5).

جدول 4: يبين نتائج قياس درجة الانفتاحية للفضاءات المنتخبة، المصدر الباحثان

المتغير / انواع الفضاء	المتغير من (A1) الى (A4)	المتغير من (A5) الى (A7)	المتغير من (A8) الى (A10)
	نسبة العرض الى الارتفاع	نوع الفواصل	نسة الفواصل
الفضاء المغلق (القاعةالدراسية)	7.9/3.8=2	شفاف	23%
الفضاء المتوازن (فضاء المرسم)	16.1/3.8=4	شفاف	63%
الفضاء المفتوح	مفتوح	لايوجد أي فواصل	100%

جدول 5:نتائج تقييم درجة الانفتاحية. المصدر : الباحثان

نتائج تقييم درجة الانفتاحية للفضاءات الثلاثة					
الفضاء الاول (القاعة الدراسية)		الفضاء الثاني (المرسم)		فضاء الثالث (غير محدد)	
مغلق	23%	شبه مفتوح	63%	مفتوح	100%

- **النتائج الخاصة بخاصية الاندماجية: تتمثل هذة النتائج على ثلاثة مراحل:**

-المرحلة الاولى: قياس درجة أندماجية المتعلم من خلال أستمارة الاستبيان في القاعة الدراسية .جدول (6) يوضح النتائج -:

جدول 6: نتائج الاستبيان للقاعة الدراسية، المصدر الباحثان

ت	القيم / القاعة الدراسية	القيمة العليا	القيمة المتوسطة	القيمة الدنيا
1	المتغير (X4)- الاندماج الطرفي	27%	51%	22%
2	المتغير (X5)- الاندماج الموجه	15%	47%	38%
3	المتغير (X6)- الاندماج الكامل	1%	60%	31%
4	المتغير (X7)- الاندماج السلبي	37%	60%	3%

-المرحلة الثانية : قياس أندماجية المتعلم من خلال أستمارة الاستبيان في فضاء المرسم-جدول (7)

جدول 7: يبين نتائج الاستبيان لفضاء المرسم، المصدر الباحثان

ت	القيم / المرسم	القيمة العليا	القيمة المتوسطة	القيمة الدنيا
1	المتغير (B1-B5)- الاندماج الطرفي	43%	43%	14%
2	المتغير (B6-B10)- الاندماج الموجه	65%	29%	7%
3	المتغير (B11-B15)- الاندماج الكامل	%52	45%	2%
4	المتغير (B16-B27) الاندماج السلبي	14%	68%	18%

-المرحلة الثالثة: تتمثل في قياس أندماجية المتعلم في الفضاء المفتوح، ووفق أستمارة الاستبيان – جدول (8) المخطط رقم (1)،(2)،(3) يبين التباين في القيم بين انواع الاندماج في الفضاءات الثلاثة

جدول 8: يبين نتائج الاستبيان للفضاء المفتوح، المصدر الباحثان

ت	القيم / الفضاء المفتوح	القيمة العليا	القيمة المتوسطة	القيمة الدنيا
1	المتغير (X4)- الاندماج الطرفي	83%	34%	3%
2	المتغير (X5)- الاندماج الموجه	70.3%	29.8	0%
3	المتغير (X6)- الاندماج الكامل	48.8%	44.4%	6.6%
4	المتغير (X7) الاندماج السلبي	4.5%	63.6%	31.8%

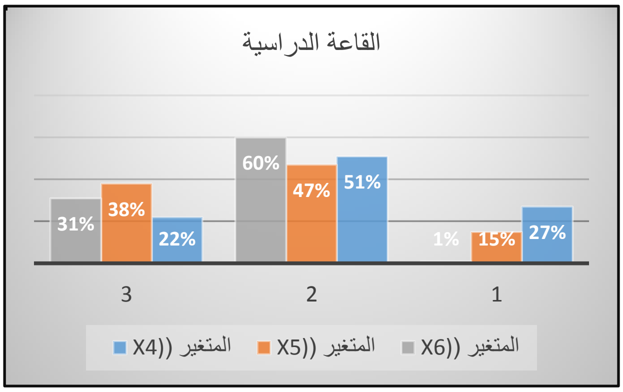

مخطط 1: يبين التباين في قيم الاندماج في القاعة الدراسية.
المصدر: الباحثان

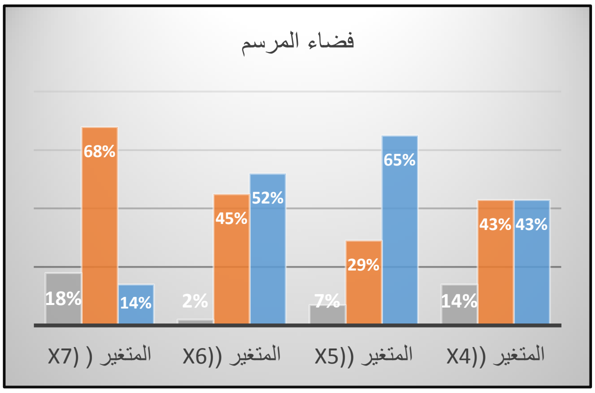

مخطط 1: يبين التباين في قيم الاندماج فضاء المرسم.
المصدر: الباحثان

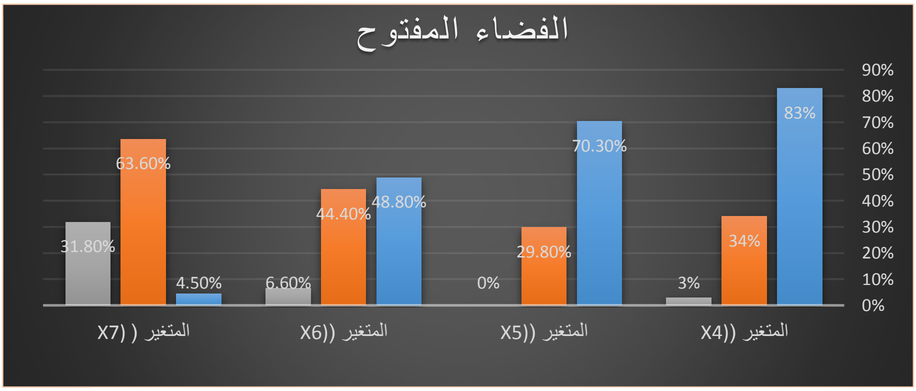

مخطط 3: يبين التباين في قيم الاندماج في الفضاء المفتوح، المصدر الباحثان

<u>مقارنه النتائج بين الخاصيتين (الانفتاحية–الاندماجية)</u>: تتناول هذة الفقرة المقارنه بين نتائج الخاصيتين (الانفتاحية–الاندماجية) والجداول رقم (9)،(10) يبين نتائج التباين بالقيم . المخطط (4)،(5) بين العلاقة بين الخاصيتين.

جدول 9: يبين نتائج الاندماج الايجابي في الفضاءات الثلاثة، المصدر الباحثان

المتغير / الفضاء	قياس الاندماج الايجابي في الفضاء التعليمي			النسبة
	المتغير (X4)	المتغير (X5)	المتغير (X6)	قيمة المتغيرات
فضاء المغلق (القاعة الدراسية)	27%	15%	1%	14%
فضاء متوازن (المرسم)	43%	65%	52%	53%
فضاء مفتوح	83%	70.3%	48.8%	67%

جدول 10: يبين نتائج الاندماج السلبي للفضاءات الثلاثة، المصدر الباحثان

المتغير / الفضاء	قياس الاندماج السلبي في الفضاء التعليمي	النسبة
	المتغير (X7)	قيمة المتغيرات
فضاء المغلق (القاعة الدراسية)	37%	37%
فضاء متوازن (المرسم)	14%	14%
فضاء مفتوح	4.5%	4.5%

ومن خلال تطبيق <u>علاقة الارتباط</u> (correlation) بين كلا الخاصيتين تم التوصل من خلال برنامج الاكسل، الى أن علاقة الانفتاحية بدرجة الاندماج تكون على نوعين:

النوع الاول:علاقة طردية: حيث تتمثل بمعامل الارتباط بينها اذ قيمه (0.97) قيمة أيجابية، أي أن زيادة درجة الانفتاحية يقابلة زيادة في درجة الاندماج الايجابي كما في المخطط رقم (5).

النوع الثاني:علاقة عكسية: حيث تتمثل بمعامل ارتباط بينهما اذ قيمة (−0.98) قيمة سالبة ،أي أن زيادة الانفتاحية يقابله أنخفاض في درجة الاندماج السلبي كما في المخطط رقم (6).

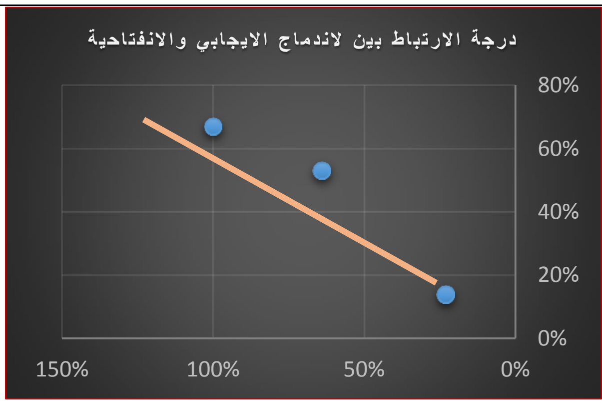

مخـــطط (4)

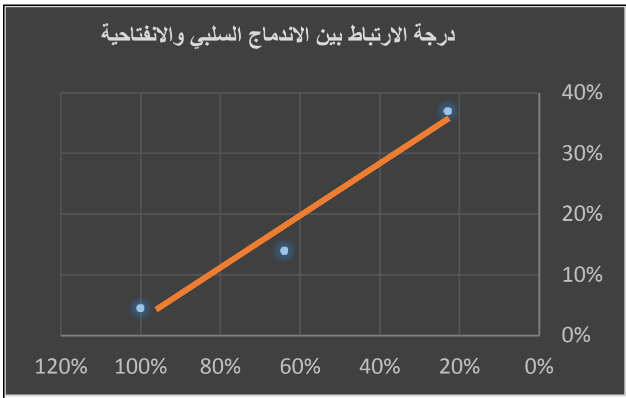

مخـطـط (5)

مخطط (4) و (5) يوضحان درجة الارتباط الإيجابي والسلبي بين خاصية الانفتاحية والاندماج الايجابي والسلبي

11- الاستنتاجات

بعد أستعراض الجانب النظري والجانب العملي فقد تم التوصل الى مجموعة من الاستنتاجات:

1-وجود علاقة ترابطية بين الانفتاح المادي للفضاء ودرجة تأثيره على أندماجية المتعلم في عملية التعلم، حيث كلما زادت الانفتاحية زادت درجة أندماج الايجابي وقلت درجة الاندماج السلبي وبالعكس. أذ تعبر الاندماجية الايجابية عن المشاركة والتفاعل والخوض في التفكير من خلال الاستفادة من وجهات نظر بقية المتعلمين، أما الاندماجية السلبية فتعبر عن حالت تشتت ذهن المتعلم وشعور بالملل وفقدان التركيز مما يقلل من حافزية المتعلم.

2-يكون المتعلمين في الفضاءات التعليمية المفتوحة أكثر تشاركية ، وهذا مايجعلهم على درجة عالية من التفاعل الاجتماعي

3-تعتبر هذة الفضاءات غير مقيدة لحركة المتعلم وحركة الكادر مما يسهل حالة التبادل والمشاركة الفعالة.

4-يمكن أن تدخل هذة الفضاءات في تطوير قدرات المتعلم العلمية والاجتماعية والبدنية، بأعتبارها مساحات واسعة تفوق مساحة الفصول الدراسية التقليدية، وبالتالي تعطي اغناء بمساعات متنوعة وممتعة للمتعلم قائمة على تنوع بالفعاليات التعليمية، تجعله في حالة تحفيزية وتفاعلية مستمرة.

6-ترفع زيادة شفافية المواد المستخدمة في واجهات تلك الفضاءات من نسبة تواصلية تلك الفضاءات مع الخارج وبالتالي زيادة الانفتاح نحو الخارج وبالاخص اذا كانت تلك الفضاءات تمتلك أرتباط مع (view) الخارجي.

7-تعطي الفضاءات المفتوحة حالة أيجابية لكلا من مستخدمي الفضاء (المتعلم-المعلم) وهذة الحالة الايجابية قد ترفع من مستوى التعلم لكل منهما.

8-توفر الفضاءات التعليمية المفتوحة للمتعلم بيئة تعليمية تختلف عن البيئة التقليدية، في قابليتها على أستيعاب أعداد مختلفة من المتعلمين والاحتياجات التعليمية المختلفة.

9-يسهم التنوع في الفضاءات التعليمية المفتوحة في تنمية قابليات المتعلمين وقدراتهم على الابداع في عملهم كما تعطي هذة الفضاءات المتعة العالية في عملية التعلم.

10-تحقيق الاندماجية في الفضاءات التعليمية المفتوحة تمنح المتعلم القابلية على المشاركة في الفعالية التعليمية على ثلاثة مستويات : مستوى الملاحظة ومستوى الحوار والنقاش ومستوى المشاركة التامة في النشاط.

11-أن نسبة عرض الفضاء الى أرتفاعة عامل مهم في زيادة سعة الفضاء وبالتالي الحصول على أنفتاحية عالية في الفضاء

12- التوصيـــــات

1-الاتجاه نحو دراسة الفضاءات التعليمية من ناحية المادية وأثرها على سلوك المتعلم ، واخذها بعين الاعتبار عند تصميم الفضاءات التعليمية.

2- التحقق من تقليل الانغلاقية (زيادة الانفتاحية) من الناحية المادية في فضاء التعلم يؤثر على أندماجية المتعلم بشكل ايجابي وتقليل شعوره بالعزلة، وهذا يرتبط بترتيب المكان وأرتفاعة وحدوده وعلاقتها بعرض الفضاء.

2- أنشاء فضاءات تعليمية مفتوحة يدعم أنشاء بيئات التعلم المحفزة للتشاركية القائمة على الحوار والنقاش بين المتعلمين بعيدا عن حالة تشتت الذهن.

3-تؤثر خاصية الانفتاحية على جوانب سلوكية أخرى للمتعلم منها خاصية الدافعية الايجابية ودعم الاستكشاف لديه.

4- يمكن تقصي خاصية الانفتاحية والجوانب المؤثره لها في فضاءات تعليمية أخرى (كالمدارس ، المراكز التعليمية ، رياض الاطفال) كتوجيهات بحثية مستقبلية

المصـــــــــــــــــادر (Reference)

أولا: المصادر العربية

- جولدي ،سنكلير ،"تذوق الفن المعماري "،ترجمة د.محمد بن حسين ابراهيم ،جامعة الملك سعود،1986.
- عبو ،فرج،"علم عناصر الفن "،الجزء الاول ،ايطاليا،1982.
- طارق، دينا نصير- ضوابط التصميم البيئي المستدام للأبنية التعليمية-رسالة ماجستير،غير منشورة جامعة بغداد-2013

ثانيا: المصادر الانكليزية

- Appleton, J. J., Christenson, S. L., Kim, D., & Reschly, A. L. (2006). Measuring cognitive and psychological engagement: Validation of the Student Engagement Instrument. Journal of School Psychology, 44(5), P427-445
- Barker, R. & Gump, P. V. (1964). Big school, small school: High school size and student behavior. Stanford: Stanford University Press.
- Benjamin William Cleveland (2011), Engaging spaces: Innovative learning environments, pedagogies and student engagement in the middle years of school
- Ching , Francis 1979, “Architecture Form , Space , Order”,VanNostrand Reinhold, London
- Campbell, M., Saltmarsh, S., Chapman, A. , & Drew, C. (2013). Issues of teacher professional learning within ‘non-traditional’ classroom environments. Improving Schools, 16(3), P209-222.
- Department for Education and Skills, “Schools for the future - exemplar designs:
- FATIMAH MOHAMMED ALSAIF-NEW ZEALAND LEARNING ENVIRONMENTS: THE ROLE OF DESIGN AND THE DESIGN PROCESS-2014

- Fredricks, J. A., Blumenfeld, P. C., & Paris, A. H. (2004). School engagement: Potential of the concept, state of the evidence. Review of Educational Research, 74(1), P59-109
- Gump, P. (1980). The school as a social situation. Annual Review of Psychology, 31, 553-582
- Jankowska, M., & Atley, M. (2007). Use of creative space in enhancing students' engagement. Innovations in Education & Teaching International, 45(3),P271-279
- Kuh, G.D., Kinzie, J., Schuh, J.H. and Whitt, E.J. (2005) Never Let It Rest: Lessons about Student Success from High-Performing Colleges and Universities. Change: The Magazine of Higher Learning. 37 (4), pp 44–51
- Lave, J. & Wenger, E. (1991). Situated learning: Legitimate peripheral participation. Cambridge: Cambridge University Press
- Lippman, P. C. (2007). Developing a theoretical approach for the design of learning environments. Paper presented at the Connected: International Conference of Design Education
- Lippman, P. C. (2010). Evidence-based design of elementary and secondary schools. Hoboken, N.J.: John Wiley & Sons
- Mark Osborne,(2013)- MODERN LEARNING ENVIRONMENTS
- Marks, H.M. (2000). Student engagement in instructional activity: Patterns in the elementary, middle and high school years. American Educational Research Journal, 37, 153-184.
- Massey, D. (2005). For space. London: Sage Publications.
- Meyer, J. (1971). The impact of the open space school upon teacher influence and autonomy: The effects of an organizational innovation. Stanford: Stanford University
- Michael A. Peters- Open Education and Education for Openness-2008
- PERKINS, BRADFORD, “BUILDING TYPE BASICS FOR elementary and concepts and ideas”, 2003
- Rodwell, G. (1998). Open-plan school architecture: a continuation of a tradition of bureaucratically imposed innovation in Australian state schools. Education Research and Perspectives, 25(2), 99-119
- Seaborne, M. (1971). Primary school design. London: Routledge & Kegan Paul
  - secondary schools” , JOHN WILEY & SONS, INC.,2001.

► Zyngier, D. (2007). (Re)conceptualising student engagement: Doing education not doing time. Teaching and Teacher Education, In press, corrected proof

ثالثا: المواقع الالكترونية

► http://gaha.ba7r.org/t19754-topic

► http://tec-edu8.blogspot.com

► http://www.ehow.com

الملحق الخاص بأستمارات الاستبيان

المرحلة الاولى:قياس أندماجية المتعلم ضمن فضاء محدد من حيث الانفتاحية والمتمثل بقاعة دراسية

القسم الاول: – مدى رؤية الطالب للفضاء كمؤثر على درجة أندماجيته

1-برأيك هل تجد نفسك في فضاء يعطيك حرية في التعبير الحر عن أرائك ومفتوح للأفكار

نعم أجده كذلك ☐ أحيانا ☐ كلا لا أجده فضاء مفتوح ☐

2-ماهو وجهة نظرك أتجاه الفضاء الخاص بالمحاضرة

فضاء يحفزني على المشاركة في المحاضرة ☐ فضاء لايعطيني اي تحفيز ويجعني غير قابل على المشاركة ☐ ارى للفضاء اي تأثير ☐

القسم الثاني:– الاسئلة التي تخص قياس مدى أندماج الطالب في المحاضرة

المفردات	ت	الاسئلة	درجات القياس		
الاندماج الطرفي	**1-**	أحاول التفكير بالموضوعات التي تطرح من قبل الاستاذ حتى أفهمها أثناء المحاضرة	بدرجة كبيرة	بدرجة متوسطة	بدرجة ضعيفة
	2-	أميل الى سؤال الاستاذ أثناء طرح المحاضرة	بدرجة كبيرة	بدرجة متوسطة	بدرجة ضعيفة
	3-	أفضل أن أندمج في تفكيري وعملي بعيدا عن بقية الطلبة	كثيرا	احيانا	لا أفضل ذلك
الاندماج الموجه	**4-**	اميل الى النقاش والحوار في المحاضرة مع الاستاذ	بدرجة كبيرة	بدرجة متوسطة	بدرجة ضعيفة
	5-	عندما تكون هناك أجزاء غامضة في المحاضرة فإنني اطلب من المدرس أن يوضحها.	بدرجة كبيرة	بدرجة متوسطة	بدرجة ضعيفة
	6-	أفضل كثيرا تغير مكان جلوسي في كل محاضرة لغرض حصولي على المشاركة بصورة عالية	كثيرا	أحيانا	نادرا
الاندماج الكامل	**7-**	اكتب ملاحظات عن المناقشات التي تمت في المحاضرة من قبل الطلبة والاستاذ	كثيرا	أحيانا	نادرا
	8-	أرى نفسي مندمج كثير في الاستفادة من وجهات نظر الطلبة حول موضوع المحاضرة	كثيرا	أحيانا	نادرا
	9-	أفضل أن أكون كثير المشاركة في المحاضرة واكثر تحفيز	كثيرا	أحيانا	نادرا
الاندماج السلبي	**10-**	أجد نفسي أحيانا منعزل في تفكيري بين مايطرح في المحاضرة وبين مدى أستجابتي للموضوع ضمن الفضا	كثيرا	أحيانا	نادرا
	11-	أثناء طرح المحاضرة يكون هناك تشتت في أفكاري	كثيرا	أحيانا	نادرا

المرحلة الثانية: اعداد أستمارة أستبيان تضم أسئلة تخص قياس الاندماج السلبي والايجابي في فضاء أكثر انفتاحية (فضاء مرسم)

المفرادات	ت	الاسئـــــــــــلة	درجات القياس		
الاندماج الطرفي	1	أرى أني أفضل اخذ المحاضرة النظرية والعملية في فضاء المرسم لانه واسع ومريح	أفضل ذلك كثير	أفضل بدرجة متوسطة	لا أفضل ذلك
	2	أرى أن تفكيري يدمج ويواصل بين المحاضرة النظرية والمحاضرة العملية	بدرجة كبيرة	بدرجة متوسطة	بدرجة ضعيفة
	3	قابليتي على لانتاج افكار مبدعة في فضاء المرسم	أنتج أفكار مبدعه	أفكر بحدود متوسطة	لا استطيع التفكير
الاندماج الموجه	4	أفضل الحركة والتنقل في الفضاء لغرض الحوار والنقاش مع زملائي	كثيرا	أحيانا	نادرا
	5	أميل أحيانا للتفكير بجميع المواضيع التي تطرح مع نفسي ومع زملائي لغرض أن أجيدها بالرسم	كثيرا	أحيانا	نادرا
الاندماج الكامل	6	أميل أحيانا الى طلب المساعدة من زملائي ومساعدتهم أثناء قيامي بالعمل في المرسم	كثيرا	أحيانا	لا أميل الى ذلك
	7	أرى ان فضاء المرسم يعطي تحفيز للقيام بالرسم والتفاعل مع الموضوع	كثيرا	أحيانا	نادرا
	8	لا أفضل الرسم مباشرة قبل التأكد من دقة المعلومات التي تخص مشروعي	أتأكد بدقة	أتأكد ولكن بصورة ليست دقيقة	أرسم مباشرة
أندماج سلبي	9	أرى أن أكمل عملي بالمنزل لاني فاقد التركيز بالمرسم	أفضل ذلك	أحيانا	لا أفضل ذلك
	10	لا يوجود مايحفزني في المرسم أثناء القيام بعملي	كثيرا	أحيانا	نادرا

المرحلة الثالثة :الفضاء المفتوح: قد يكون هذا الفضاء فضاء تجمع أجتماعي ، حيث يمتلك المتعلم الحرية الكاملة في أختيار طريقة التعلم التي يريدها.

الاندماج الطرفي	1-	أرى ان الفضاء المفتوح يعطني تفاعلية عالية في كيفية التعامل مع النموذج	بدرجة كبيرة	بدرجة متوسطة	بدرجة ضعيفة
	2-	أرى أن تفكيري يدمج ويواصل بين المحاضرة النظرية وبين ما أراه في نموذج الزيارة الموقعية	بدرجة كبيرة	بدرجة متوسطة	بدرجة ضعيفة
		ارى أن حريتي كطالب في الفضاء المفتوح يدعم عملية أندماجي في التفكير والتركيز	بدرجة كبيرة	بدرجة متوسطة	بدرجة ضعيفة
	3-	أمتلك قابلية تحكم عالية في تقييم مايفيدني من الزيارة الموقعية وفق توجيهات المحاضرة	كثيرا	أحيانا	نادرا
	4-	الفضاء يعطيني حرية في التعبير الحر عن أرائي وأفكاري بشكل حر وبأنفتاحية عالية	كثيرا	أحيانا	نادرا

		أكون لدى قابلية عالية في التفكير والحصول على الافكار الجديدة التي تدعم معلومات	كثيرا	أحيانا	نادرا
الاندماج الموجه	-5	أرى نفسي مندمج كثير في الاستفادة من وجهات نظر الطلبة حول النموذج	كثيرا	أحيانا	نادرا
	-6	أميل أحيانا للتفكير بجميع المواضيع التي تطرح مع نفسي ومع زملائي	كثيرا	أحيانا	نادرا
	-7	أكون كثير الاستكشاف حول المعلومات العلمية وأمتلك دافعية عالية في التفاعل مع نموذج الزيارة الموقعية	كثيرا	أحيانا	نادرا
الاندماج الكامل	-8	أكون دقيق جدا في طرحي للأسئلة الموجة للاستاذ حول نموذج الزيارة	كثيرا	أحيانا	لا أميل الى ذلك
	-9	عندما تكون هناك أجزاء غامضة في المحاضرة النظرية يجب أن أكون كثير الاهتمام حول فهمها وفق توجيهات الاستاذ	كثيرا	أحيانا	نادرا
	-10	أحيانا أميل الى عمل مخططات (sketch) أثناء قيامي بزيارة موقعية لغرض الاستفادة	كثيرا	أحيانا	نادرا
	-11	عمل قائمة بجميع الاسئلة التي تصعب عليه قبل القيامم بزيارة موقعة لغرض حصولي على الاجابة بدقة	كثيرا	أحيانا	نادرا
		عملية تعلمي في الفضاء المفتوح تعطي المتعة بالتعلم وليس حالة الممل	كثيرا	أحيانا	نادرا
أندماج سلبي	-12	أرى ان الفضاء المفتوح يسبب لي الكثير من التشتت وفقدان التركيز	أفضل ذلك	أحيانا	لا أفضل ذلك
	-13	لا يوجود مايحفزني أثناء التعلم في الفضاء المفتوح	كثيرا	أحيانا	نادرا

https://www.researchgate.net/journal/17264073_University_of_Baghdad_Engineering_Journal

Journal ID: 3631

ENGINEERING

College of Engineering University of Baghdad No.4 Vol. 23 April 2017

List of Contents

English Section: Page

E-ISSN 2520-3339

P-ISSN 1726-4073

Journal of Engineering

A Scientific Refereed Journal
Published by
College of Engineering
University of Baghdad

April
2017

Number 4

Volume 23

E-ISSN 2520-3339

P-ISSN 1726-4073

مجلة الهندسة

مجلة علمية محكمة تصدرها

كلية الهندسة ـ جامعة بغداد

نيسان

2017

العدد 4

المجلد 23

رقم الايداع في دار الكتب والوثائق ببغداد

2231 لسنة 2017

قـائـمـة الـمـحـتـويـات

القسم العربي: